

# **Modelling and Control of Active Suspension System for Railway Vehicle**

**A Thesis**

*Submitted in the fulfilment for the award*

*of*

**DOCTOR OF PHILOSOPHY**

*in*

*Instrumentation and Control Engineering*

**SUBMITTED BY:**

**NITISH**

**(18506002)**



**DEPARTMENT OF INSTRUMENTATION AND CONTROL ENGINEERING**

**Dr. B R AMBEDKAR NATIONAL INSTITUTE OF TECHNOLOGY,**

**JALANDHAR**

**JULY, 2024**

# **Modelling and Control of Active Suspension System for Railway Vehicle**

**A Thesis**

*Submitted in the fulfilment for the award*

*of*

**DOCTOR OF PHILOSOPHY**

*in*

*Instrumentation and Control Engineering*

**SUBMITTED BY:**

**NITISH**

**(18506002)**

*Under the esteemed guidance of*

**Dr. Amit Kumar Singh**

Assistant Professor

(Department of Instrumentation and Control Engineering)



**DEPARTMENT OF INSTRUMENTATION AND CONTROL ENGINEERING**

**Dr. B R AMBEDKAR NATIONAL INSTITUTE OF TECHNOLOGY,**

**JALANDHAR**

**JULY, 2024**



**Department of Instrumentation and Control Engineering**  
**Dr. B R Ambedkar National Institute of Technology Jalandhar**  
**Jalandhar, Punjab-144008, INDIA**

## **Certificate**

I hereby certify that the work, which is being presented in the thesis, entitled "**Modelling and Control of Active Suspension System for Railway Vehicle**" in the fulfillment of requirement for the award of degree of Doctor of Philosophy submitted in the Department of Instrumentation and Control Engineering is an authentic record of my own work carried out under the supervision of Dr. Amit Kumar Singh, Assistant Professor, Department of Instrumentation and Control, Dr. B R Ambedkar National Institute of Technology Jalandhar, Jalandhar, Punjab-144008, India.

**Nitish**

Roll. No. 18506002

---

It is certified that the above statement made by the candidate is correct to the best of our knowledge.

**Dr. Amit Kumar Singh**

Assistant Professor

Department of Instrumentation and Control  
Engineering, NIT, Jalandhar

@2024 All Right Reserved

Department of Instrumentation and Control

Dr. B R Ambedkar National Institute of Technology, Jalandhar - 14400



## Candidate Declaration


I, Nitish bearing Roll No.18506002, PhD scholar in the Department of Instrumentation and Control Engineering, I owe the full responsibility for the information, results etc. provided in this thesis titled " **Modelling and Control of Active Suspension System for Railway Vehicle** " submitted to Dr. B R Ambedkar National Institute of Technology, Jalandhar for the award of PhD degree. I hereby declare that this written submission represents my own ideas in my own words. I also declare that the other ideas which are included in thesis have adequately provided the reference from the original reported work.

I have taken care in all respect to honor the intellectual Property Right and have acknowledged the contribution of others for using them in this thesis work for academic purpose. I further declare that in case of any violation of intellectual Property Right or Copy Right, I as the candidate will be fully responsible for the same.

No content of this thesis will be published without prior approval of my Supervisor at any stage.

Date: 12/07/2024

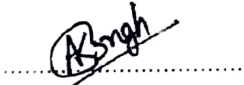
Place: Jalandhar



**Nitish**

Roll No. 18506002

It is certified that the above statement made by the candidate is correct to the best of our knowledge.



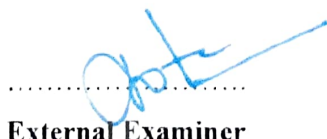
**Dr. Amit Kumar Singh**

Assistant Professor

Department of Instrumentation and Control

Engineering, NIT, Jalandhar

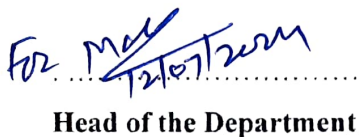
The Ph. D. Viva-Voce Examination of **Mr. Nitish**, Research Scholar has been held on 12/07/2024 and accept for the award of Ph. D. Degree.



External Examiner



Supervisor



Head of the Department



Dean Academics

## ABSTRACT

---

A high-speed railway system is one of the sustainable alternatives to other modes of transportation and may connect the most congested urban cities with minimum carbon emissions. However, the vibration intensity also increases as the train's operating speed increases, leading to a decline in both ride comfort and stability. Both passenger ride comfort and vehicle stability are the essential aspect of performance evaluation in high-speed railway vehicles, which can be accomplished by employing effective vibration control techniques. Previously, different control strategies have been adopted in this context; however, a completely effective method has not yet been revealed. Hence, the prime focus of this work is to investigate a thirty-eight-degree-of-freedom (38-DOF) dynamic model of a full-scale railway vehicle integrated with effective control strategies to reduce the railway vehicle vibrations using active suspension system. The dynamic models of the system are developed by considering the translational and rotational motion of the car body, bogies, and wheelsets. The wheel-rail contact model and the rail irregularities model are also incorporated in the analytical model.

The developed dynamic model has been translated into the two-dimensional state-space model to evaluate the effect of different track irregularities on the human ride comfort. The railway vehicle's vibration analysis is conducted at different speeds for the vertical, lateral and longitudinal directions and the critical velocity of the vehicle is evaluated. The spectral analysis techniques have been employed to analyze the output frequency response of the railway vehicle's motion. The outputs are defined in three-dimensional Power Spectral Densities under three random track irregularities: vertical profile, lateral alignment, and cross-level. Furthermore, the Sperling's method has been used to evaluate the human comfort index. For the case study, a Linke-Hofmann-Busch coach based model has been employed, and the results are validated with the experimental data of ride comfort reported by the Research Design and Standard Organization (RDSO). The simulated results of the proposed model demonstrate a remarkable alignment with the experimental data, exhibiting a small error ranging from 2.36–8.81% for vertical motion and 5.84–8.30% for lateral motion, respectively. Such promising

results offer valuable insight for the design of future coaches, ensuring enhanced ride comfort even at high speeds.

However, controlling different motions during vibration control is also an imperative criterion to achieve the desired passenger ride comfort and stability. Hence, a decentralized control structure has been developed, which performs the controlling action with five optimized Fractional Order Proportional Integral Derivative controllers that suppress the vehicle body's vertical, lateral, pitch, roll, and yaw motions. To obtain tight controller tuning parameters of the FOPID, a novel metaheuristic optimization technique named hybrid Particle Swarm Optimization-Gray Wolf Optimization has been proposed. The simulated results are compared with the passive system as well as other conventional (Z-N) and two metaheuristic optimization tuning techniques named as PSO and GWO. Moreover, the performance of the proposed control strategy is evaluated in the time and frequency domain under random track irregularities, and the results are characterized in terms of power spectral densities. The simulated results show that the hybrid metaheuristic algorithm outperforms with a significant reduction in vehicle vibration compared to other tuning methods. The percentage reduction of the vertical, lateral, pitch, rolls, and yaw accelerations is 34.83%, 29.27%, 39.17%, 24.99%, and 33.45%, respectively, ensuring enhanced vehicle ride comfort.

To better control action further, a sophisticated control strategy with the combination of an adaptive neuro-fuzzy inference system and a linear quadratic Gaussian controller tuned with equilibrium optimization has been analyzed. The effectiveness of the suggested control technique is assessed in the time and frequency domain under random track excitations. Moreover, the ride comfort enhancement capability of the proposed model is also evaluated using Sperling's methods. The simulated results are compared with passive systems and the classical tuning methods. The findings suggest that the EO-LQG controller offers a promising solution for enhancing ride comfort as the percentage reduction in RMS values for the vertical, lateral, pitch, roll, and yaw acceleration are 35.62%, 24.98%, 38.77%, 27.98%, and 35.68%, respectively. On the other hand, the active suspension system tuned with classical methods shows lower reduction capability as compared to proposed technique. Also, the ride comfort indices

for vertical motion using EO algorithms are found to be 2.482, and for lateral motion, the indices were 2.528, representing a superior level of comfort compared to that of passive and other tuning algorithms.

Eventually, despite having sound suspension systems and efficient control algorithms, the suspension system performance deteriorates with time. Hence, this work proposes a robust active vibration control system with two different robust control techniques,  $H_\infty$  and  $\mu$ -synthesis, integrated with the Kalman estimator. For analysis, a 27-degree of freedom model consisting of structured and unstructured uncertainties has been considered. The robust stability and the robust performance of the proposed control strategies have been evaluated using the structured singular values. The time and frequency domains of the closed loop perturbed responses to random track disturbances are shown. The root mean square values of the accelerations of the car bodies are used to compare the suggested control schemes to the passive system. The primary focus of this study is to examine the level of ride comfort provided by the railway vehicle in the uncertain environment. To achieve this, simulated findings are compared and verified against experimental data collected and reported by the RDSO. The observational data demonstrates that the results obtained from the suggested control methods are in close agreement with the experimental findings, with a minimal disparity ranging from 2.36% to 8.81% for lateral motion and 2.84% to 6.30% for vertical motion. Also, the percentage improvement of RMS values with the  $\mu$ -synthesis controller confirms the enhancement of the ride comfort as compared to other techniques. Some directions for the future extension of the current research work have also been identified and discussed.

## ACKNOWLEDGEMENT

---

The endless thanks to the Lord Almighty for blessing me with courage, patience, and sincerity throughout this research work. I would like to thank all those who contributed their time to complete my research and helped me with valuable suggestions for improvement. I am extremely grateful to my supervisor, Dr. Amit Kumar Singh, Department of Instrumentation and Control, Dr. B R Ambedkar National Institute of Technology Jalandhar, for his encouragement, support, valuable discussion, and guidance that enabled my work to be finished. He has guided me with his valuable suggestions and limitless patience and support to lighten the way during my darkest times. Without his guidance, it would have been impossible to complete the research work this way. I express my gratitude to Professor (Dr.) Binod Kumar Kanauiya, the Hon'ble Director of Dr. B R Ambedkar National Institute of Technology Jalandhar, and the administration for providing all necessary technical facilities required for carrying out my research work. I thank Dr. K S Nagla, Head of the Department of Instrumentation and Control Engineering, for his continuous support and encouragement. I would like to thank all my teachers that I met throughout my carrier for their guidance and support in building up my knowledge. I would also like to thank the entire faculty, especially Er. Narinder Singh, Dr. Om Prakash Verma, Dr. Karan Veer, Dr. Ashok Kumar Bagha, and the staff members of Department of Instrumentation and Control Engineering for their motivation and support during my Ph.D. work. My sincere thanks to all the editors and reviewers associated with our research work for their useful and valuable comments. I would like to thank all the researchers whose works I have cited to understand the concept used in the research. I strongly acknowledge the facilities and other technical help provided by Process Control Laboratory, Department of Instrumentation and Control Engineering, Dr. B R Ambedkar National Institute of Technology Jalandhar. I am grateful to acknowledge the funding source provided by the MHRD, Govt. of India fellowship for my Full-time Ph.D. program. My time at NIT Jalandhar was enjoyable due to my friends, and that became the best part of my life. I am fortunate to have friends like Mrs. Smita Rani Pati,

Mrs. Pooja, Mr. Sachin Kumar, Mrs. Shivani Sharma, Mr. Priyavrat Chauhan and Mr. Sunil Bodla, who have motivated and helped me many times during difficulties in my work. I am also thankful to my fellow researchers: Mr. Himanshu Gupta and Shubham Gupta for their professional favors and moral support. I would also appreciate my family friend, Mr. Anup Singh Thakur and Mrs. Ankita Thakur, been very caring and has helped me at times of trouble in some part of my life, and also to all other people who are not mentioned here but has helped in making NIT Jalandhar a very special place during these years. I would express my deep sense of gratitude and affection for the support shown to me by my family members. I dedicate this work to my parents and my family, who have made me what I am by giving consistent support and inspiring me in all dimensions of life. I owe everything to them; without their everlasting love, this thesis would never be completed. To all of you, thanks from my heart of hearts.

Nitish

NIT Jalandhar July, 2024

# TABLE OF CONTENTS

Certificate	i
Declaration	iii
Abstract	iv
Acknowledgements	vii
List of Tables	xiv
List of Figure	xv
Abbreviations	xviii
List of Symbols	xx
Chapter 1	1-18
<b>INTRODUCTION</b>	1
1.1 Introduction	1
1.2 Motivations	11
1.3 Research Gaps	13
1.4 Research Objectives	14
1.5 Research Significance	15
1.6 Thesis Outline	16
1.7 Thesis Outcomes	17
Chapter 2	19-58
<b>LITERATURE REVIEW</b>	19
2.1 Background	19
2.2 Basic building blocks of vibration control of railway vehicle	20
2.2.1 Mathematical modeling of railway vehicle and wheel-rail contact forces	21
2.2.1.1 Wheel-rail contact models	22
2.2.1.2 Modeling of railway vehicles	24
2.2.2 Types of suspensions and actuation system	28
2.2.3 Control strategies and implementations	31
2.2.3.1 Classical control	33
2.2.3.3 Optimal control law	35

2.2.3.3	Robust control	39
2.3	Conclusions	57
Chapter 3		59-86
	<b>DYNAMIC MODELING OF RAILWAY VEHICLE</b>	59
3.1	Introduction	59
3.2	General Co-ordinate system	60
3.3	Wheel-rail contact model	61
3.4	Analytical model of railway vehicle system	62
3.4.1	38-DOF dynamic model of railway vehicle	63
3.4.1.1	Vehicle body differential equations	63
3.4.1.2	Bogies differential equations ( $i=1, 2$ )	64
3.4.1.3	Wheelsets differential equations ( $i=1, 2$ , while $j=1$ ; $i=3, 4$ , while $j=2$ )	64
3.4.2	State-space formulation	66
3.5	Modeling of railway track irregularities	67
3.5.1	Periodic track irregularities	67
3.5.2	Random track irregularities	69
3.6	System response to track irregularities and vehicle velocity	70
3.7	Results and discussions	73
3.7.1	Calculation of critical velocity of the train	73
3.7.2	Car body accelerations	74
3.8	Evaluation of ride comfort using Sperling's method	80
3.9	Experimental verification of the proposed model	82
3.10	Conclusions	85
Chapter 4		87-112
	<b>SYNTHESIS OF DECENTRALIZED CONTROLLER</b>	87
4.1	Introduction	87
4.2	State-space formulation	90
4.3	Controller and optimization algorithms	91
4.3.1	FO-PID controller	91
4.4	Optimization Algorithms	93



4.4.1	Ziegler-Nichols (Z-N) Method	93
4.4.2	Particle swarm optimization (PSO) algorithm	93
4.4.3	Grey wolf optimization (GWO) algorithm	94
4.4.4	Hybrid PSO-GWO algorithm	94
4.5	System response based on a decentralized control structure	95
4.6	Results and Discussions	98
4.6.1	Tuning of decentralized controller	98
4.6.2	Simulation under periodic track irregularities	102
4.6.2.1	Time domain responses of acceleration of the body	102
4.6.3	Simulation under random track irregularities	106
4.6.3.1	Frequency domain Responses of acceleration of the body	107
4.6.3.2	Time responses of acceleration of the body	110
4.7	Conclusions	111
Chapter 5		113-138
	<b>SYNTHESIS OF CENTRALIZED CONTROLLER</b>	113
5.1	Introduction	113
5.2	A 27-DOF dynamic model of a railway vehicle	115
5.2.1	Vehicle body dynamics	115
5.2.2	Bogie dynamics (i=1, 2)	115
5.2.3	Wheel-set dynamics (i=1, 2, while j=1; i=3, 4, while j=2)	116
5.3	State-space formulation	116
5.3.1	Track irregularities model	117
5.3.2	State-space formulation for complete vehicle-track system	119
5.4	Dynamics of electro-hydraulic actuator	119
5.5	Inverse modeling of electro-hydraulic actuator	122
5.5.1	Training of ANFIS model	122
5.6	System controller based on LQG control law	124
5.7	Methods of finding the weighing matrices (Q, R and S)	125
5.7.1	Particle Swarm Optimization (PSO)	126

5.7.2	Equilibrium optimization (EO)	127
5.8	Results and Discussions	127
5.9	Simulation under random track irregularities	130
5.9.1	Acceleration responses of the vehicle body	130
5.10	Ride comfort analysis using Sperling's method	136
5.11	Conclusions	137
Chapter 6		139-162
	<b>SYNTHESIS OF ROBUST CONTROLLER</b>	139
6.1	Introduction	139
6.2	Analysis and synthesis of a robust controller for vibration control of railway vehicle	140
6.3	Mathematical formulation of Robust control strategy	141
6.3.1	Uncertain model of the railway vehicle system	141
6.3.2	Dynamics of the electro-hydraulic actuator with unstructured uncertainties	143
6.4	System controller based on robust control laws	144
6.4.1	$H_{\infty}$ Controller	146
6.4.2	$\mu$ -synthesis controller	147
6.5	Design of weighting functions	148
6.6	Results and Discussions	150
6.6.1	Robustness analysis	151
6.6.2	Simulation under random track irregularities	153
6.6.2.1	Acceleration responses of the vehicle body	153
6.7	Validation of the proposed control schemes with experimental results	157
4.7.1	Evaluation of ride comfort using Sperling's method	158
6.8	Conclusions	159
Chapter 7		163-170
	<b>CONCLUSIONS AND FUTURE SCOPES</b>	163
7.1	Conclusions	163
7.2	Future Scopes	169

REFERENCES	171-200
Appendix 1 & 2	201-205

## LIST OF TABLES

<b>Table 2.1</b>	A comparison of different actuators	32
<b>Table 2.2</b>	Summary of various mathematical modelling and control algorithms	42
<b>Table 3.1</b>	RMS value of vehicle body acceleration under high class disturbances	77
<b>Table 4.1</b>	Different Values of coefficients used in the cost function	99
<b>Table 4.2</b>	FOPID parameters and cost function values resulted from different tuning algorithms	101
<b>Table 4.3</b>	RMS values and % improvements of vehicle body accelerations under periodic track disturbances	106
<b>Table 4.4</b>	Resonance frequencies of car body	107
<b>Table 4.5</b>	RMS values and % improvement of vehicle body acceleration under random track disturbances	109
<b>Table 5.1</b>	Values of Q, R and $K_c$ calculated different from tuning techniques	130
<b>Table 5.2</b>	RMS values and % improvement of vehicle body acceleration under random track disturbances	134
<b>Table 5.3</b>	Stability margin evaluated from EO-LQG control law	138
<b>Table 6.1</b>	RMS values of car body accelerations and % improvement under random track disturbances	156
<b>Table 6.2</b>	Stability margins of proposed robust controller	161

## LIST OF FIGURES

<b>Figure 1.1</b>	Number of casualties reported in Indian railway accidents from 2011-2023	2
<b>Figure 1.2</b>	(a) Vande-bharat express (b) sub-system of railway vehicle	3
<b>Figure 1.3</b>	Types of suspension system used in railway vehicle (a) passive (b) semi-active (c) Fully- active	3
<b>Figure 1.4</b>	Semi-active dampers (a) electro-rheological (b) magneto-rheological	5
<b>Figure 1.5</b>	Flow chart for the simulation process of railway vehicle system	7
<b>Figure 2.1</b>	Various inspection areas of railway vehicle systems	20
<b>Figure 2.2</b>	The basic architecture for vibration control of railway vehicle	21
<b>Figure 2.3</b>	Normal wheel-rail contact	23
<b>Figure 2.4</b>	Tangentail forces at wheel-rail interface	23
<b>Figure 2.5</b>	Lumped parameter model of railway vehicle (a) Quarter-car (b) Half-car (c) Full-car	26
<b>Figure 2.6</b>	Electro-mechanical actuator	29
<b>Figure 2.7</b>	Electro-hydraulic actuator	29
<b>Figure 2.8</b>	Electro-pneumatic actuator	30
<b>Figure 2.9</b>	Electro-magnetic actuator	31
<b>Figure 2.10</b>	Various control strategies used for vibration control of railway vehicle	33
<b>Figure 2.11</b>	General structure of LQR and LQG control law	37
<b>Figure 2.12</b>	Standard configuration of robust control law	40
<b>Figure 3.1</b>	General co-ordinate system of railway system	60
<b>Figure 3.2</b>	(a) Pressure distribution and (b) Pressure profile at contact patch	62
<b>Figure 3.3</b>	38-DOF analytical model of a railway vehicle (a) end view (b) front view (c) top view	65
<b>Figure 3.4</b>	Track irregularities (a) vertical profile (b) Lateral alignment (c) Cross-level	68
<b>Figure 3.5</b>	PSDs and time series of track irregularities (a) vertical profile (b) lateral alignment (c) cross-level	71
<b>Figure 3.6</b>	Movement of locations of poles with respect to velocity (a) all poles of the 38-DOFs system (b) poles of the wheelsets	74
<b>Figure 3.7</b>	PSDs of vehicle body acceleration under vertical irregularities (a) vertical acceleration (b) pitch acceleration	75
<b>Figure 3.8</b>	PSDs of vehicle body acceleration under lateral irregularities (a) lateral acceleration (b) roll acceleration (c) yaw acceleration	76
<b>Figure 3.9</b>	PSDs of vehicle body acceleration under cross-level irregularities (a) lateral acceleration (b) roll acceleration (c) yaw acceleration	78

<b>Figure 3.10</b>	Time histories of vehicle body acceleration under vertical irregularities (a) vertical acceleration (b) pitch acceleration	79
<b>Figure 3.11</b>	Time histories of vehicle body acceleration under lateral irregularities (a) lateral acceleration (b) roll acceleration (c) yaw acceleration	79
<b>Figure 3.12</b>	Time histories of vehicle body acceleration under cross-level irregularities (a) lateral acceleration (b) roll acceleration (c) yaw acceleration	80
<b>Figure 3.13</b>	Ride comfort index ( $W_z$ ) of (a) vertical motion under vertical profile, (b) lateral motion under lateral alignment, (c) lateral motion under cross-level	82
<b>Figure 3.14</b>	Field test photo of (a) prototype LHB chair coach (b) sensor installation (c) data acquisition chamber	83
<b>Figure 3.15</b>	Comparison of experimental and simulation ride comfort index (a) vertical ride index (b) lateral ride index under lateral alignment (c) lateral ride index under cross-level	84
<b>Figure 3.16</b>	PSDs of longitudinal acceleration of (a) vehicle body (b) bogie (c) wheelset and pitch acceleration of (d) wheelset under cross-level irregularities	86
<b>Figure 4.1</b>	Decentralized control structure for railway vehicle	88
<b>Figure 4.2</b>	Work flow diagram of hybrid PSO-GWO	95
<b>Figure 4.3</b>	Single loop structure of regulatory feedback system	96
<b>Figure 4.4</b>	Convergence curves for (a) vertical, (b) lateral, (c) pitch, (d) roll, and (e) yaw motions	100
<b>Figure 4.5</b>	Time histories of vehicle body acceleration under periodic track disturbances (a) vertical acceleration ( $\ddot{Z}_c$ ) (b) lateral acceleration ( $\ddot{Y}_c$ ) (c) pitch acceleration ( $\ddot{\psi}_c$ ) (d) roll acceleration ( $\ddot{\Theta}_c$ ), (e) yaw acceleration ( $\ddot{\phi}_c$ )	104
<b>Figure 4.6</b>	Time histories of active force for different motions of railway vehicle (a) vertical motion ( $u_1$ ) (b) lateral motion ( $u_2$ ) (c) pitch motion ( $u_3$ ) (d) roll motion ( $u_4$ ) and (e) yaw motion ( $u_5$ )	105
<b>Figure 4.7</b>	Power spectral densities of vehicle body acceleration under random track inputs (a) vertical acceleration ( $\ddot{Z}_c$ ) (b) lateral acceleration ( $\ddot{Y}_c$ ) (c) pitch acceleration ( $\ddot{\psi}_c$ ) (d) roll acceleration ( $\ddot{\Theta}_c$ ), and (e) yaw acceleration ( $\ddot{\phi}_c$ )	108
<b>Figure 4.8</b>	Time histories of vehicle body acceleration under periodic track disturbances (a) vertical acceleration ( $\ddot{Z}_c$ ) (b) lateral acceleration ( $\ddot{Y}_c$ ) (c) pitch acceleration ( $\ddot{\psi}_c$ ) (d) roll acceleration ( $\ddot{\Theta}_c$ ), and (e) yaw acceleration ( $\ddot{\phi}_c$ )	111
<b>Figure 5.1</b>	Schematic of centralized vibration control system for railway vehicle	114
<b>Figure 5.2</b>	Hydraulic actuator (a) basic architecture (b) dynamic behavior	120
<b>Figure 5.3</b>	ANFIS modeling for inverse dynamics of electro-hydraulic actuator	123
<b>Figure 5.4</b>	Validation of ANFIS inverse model (a) force prediction (b) command current	124
<b>Figure 5.5</b>	Outputs of Kalman filter estimated different states (a) vertical (b) lateral (c)	129

	Pitch (d) roll (e) yaw	
<b>Figure 5.6</b>	Convergence curves of tuning methods	129
<b>Figure 5.7</b>	Time series and amplitude spectrums of vehicle body acceleration under random track inputs (a, b) vertical acceleration ( $\ddot{Z}_c$ ) (c, d) lateral acceleration ( $\ddot{Y}_c$ ) (e, f) pitch acceleration ( $\ddot{\psi}_c$ ) (g, h) roll acceleration ( $\ddot{\theta}_c$ ), and (i, j) yaw acceleration ( $\ddot{\phi}_c$ )	133
<b>Figure 5.8</b>	Time histories of active force for different motions of railway vehicle (a) vertical motion ( $u_1$ ) (b) lateral motion ( $u_2$ ) (c) pitch motion ( $u_3$ ) (d) roll motion ( $u_4$ ) and (e) yaw motion ( $u_5$ )	135
<b>Figure 5.9</b>	Ride comfort indices ( $W_z$ ) of (a) vertical motion (b) lateral motion	136
<b>Figure 5.10</b>	Perturbed frequency response of LQG controller	138
<b>Figure 6.1</b>	Schematic of robust vibration control system for railway vehicle	140
<b>Figure 6.2</b>	Block diagram of uncertain railway system	142
<b>Figure 6.3</b>	Uncertain model of the railway system	144
<b>Figure 6.4</b>	Robust control structure for vibration control of railway vehicles	145
<b>Figure 6.5</b>	$\mu$ -synthesis control configuration	148
<b>Figure 6.6</b>	Frequency response for $W_{per0}$ , $W_{act0}$ , and $W_{n0}$	149
<b>Figure 6.7</b>	Singular values test of $H_\infty$ controller for (a) robust stability, (b) robust performance	149
<b>Figure 6.8</b>	Singular values test of $\mu$ -synthesis controller for (a) robust stability, (b) robust performance	152
<b>Figure 6.9</b>	Perturbed frequency responses and time series of vehicle body acceleration under random track disturbances (a,b) lateral acceleration ( $\ddot{Z}_c$ ) (c,d) vertical acceleration ( $\ddot{Y}_c$ ) (e,f) pitch acceleration ( $\ddot{\psi}_c$ ) (g,h) roll acceleration ( $\ddot{\theta}_c$ ), and (i, j) yaw acceleration ( $\ddot{\phi}_c$ )	156
<b>Figure 6.10</b>	Comparison of ride comfort indices ( $W_z$ ) with different control algorithms for (a) lateral motion and (b) vertical motion	159
<b>Figure 6.11</b>	Robustness comparison of $H_\infty$ and $\mu$ -synthesis controller	161
<b>Figure 7.1</b>	Comparison of ride comfort indices ( $W_z$ ) with different control algorithms for (a) vertical motion and (b) lateral motion	168

## ABBREVIATIONS

---

ABC	Artificial Bee Colony
ACO	Ant Colony Optimization
ANFIS	Adaptive neuro-fuzzy inference system and
ARE	Algebraic Riccati Equation
ASS	Active Suspension System
AVRS	Automatic Voltage Regulator System
CC	Cohen Coon
CSA	Cuckoo Search Algorithm
CSTR	Continues Stirred Tank Reactor
DOF	Degree of Freedom
EO	Equilibrium Optimization
EH	Electro Hydraulic
ER	Electro Rheological
FA	Firefly Algorithm
FOPID	Fractional Order Proportional Integral Derivative
FPA	Flower pollination Algorithm
GA	Genetic Algorithm
GWO	Grey Wolf Optimization
LFT	Linear Fractional Transformation
LLFT	Lower Linear Fractional Transformation
LHB	Linke Hofmann Busch
LQG	Linear Quadratic Gaussian
LQR	Linear Quadratic Regulator
MIMO	Multi Input Multi Output
MR	Magneto Rheological
MSE	Mean Square Error
PID	Proportional Integral Derivative
PSD	Power Spectral Density



PSO	Particle Swarm Optimization
RDSO	Research Design and Standard Organization
RMS	Root Mean Square
Z-N	Ziegler-Nichols

## LIST OF SYMBOLS

---



---

<i>Symbols</i>	<i>Definitions</i>
$a$	Wheel base contact distance
$a_a$	Cylinder area on one side
$a_b$	Cylinder area on other side
$A_a$	Roughness coefficient of lateral alignment
$A_g$	Roughness coefficient of cross-level
$A_v$	Roughness coefficient of vertical profile
$b_1$	Vertical primary suspension spacing
$b_2$	Vertical secondary suspension spacing
$c_d$	Ram damping
$c_s$	Damping of spool-valve
$C_{1y}$	Primary lateral damping
$C_{2y}$	Secondary lateral damping
$C_{1z}$	Primary vertical damping
$C_{2z}$	Secondary vertical damping
$d_p$	Lateral primary suspension spacing
$d_s$	Lateral secondary suspension spacing
$f_{11}$	Longitudinal creep coefficient
$f_{22}$	Lateral creep coefficient
$h_1$	Vertical distance from bogie center of gravity to lateral primary suspension
$h_2$	Vertical distance from bogie center of gravity to lateral secondary suspension
$h_3$	Vertical distance from car body center of gravity to lateral secondary suspension
$J_{cx}$	Roll moment of inertial of car body
$J_{cy}$	Pitch moment of inertial of car body
$J_{cz}$	Yaw moment of inertia of car body

$J_{tx}$	Roll moment of inertia of bogie
$J_{ty}$	Pitch moment of inertia of bogie
$J_{tz}$	Yaw moment of inertia of bogie
$J_{tw}$	Yaw moment of inertia of wheel-set
$k_i$	Torque motor gain
$k_s$	Stiffness of spool-valve
$K_{1x}$	Primary longitudinal stiffness
$K_{2x}$	Secondary longitudinal stiffness
$K_{1y}$	Primary lateral stiffness
$K_{2y}$	Secondary lateral stiffness
$K_{1z}$	Primary vertical stiffness
$K_{2z}$	Secondary vertical stiffness
$K_{Gy}$	Lateral gravitational stiffness
$K_{Gz}$	Vertical gravitational stiffness
$l_b$	Distance from car body center of gravity to vertical secondary stiffness
$l_d$	Distance from bogie center of gravity to vertical primary stiffness
$m_s$	Mass of spool
$M_c$	Mass of Car body
$M_t$	Mass of bogie
$M_w$	Mass of wheel-set
$p_s$	Supply pressure
$R_1$	Vertical distance of lateral primary stiffness to track
$V_a$	Volume of cylinder on one side
$V_b$	Volume of cylinder on other side
$W$	Load per wheel-set
$Y_a$	Lateral track disturbance
$Y_c$	Lateral displacement of the car body
$Y_t$	Lateral displacement of the bogies
$Y_w$	Lateral displacement of the wheelsets
$Z_c$	Vertical displacement of the car body

$Z_t$	Vertical displacement of the bogies
$Z_w$	Vertical displacement of the wheelsets
$Z_v$	Vertical track disturbance
$\lambda_e$	Effective wheel conicity
$\sigma$	Wheel-set roll coefficient
$\beta$	Compressibility factor
$\theta_c$	Roll displacement of the car body
$\theta_t$	Roll displacement of the bogie
$\phi_c$	Pitch displacement of the car body
$\phi_t$	Pitch displacement of the bogie
$\psi_c$	Yaw displacement of the car body
$\psi_t$	Yaw displacement of the bogie
$\psi_w$	Yaw displacement of the wheelsets
$\theta_{cl}$	Cross-level track disturbance
$\Omega_c$	Truncated wavenumber
$\Omega_r$	Truncated wavenumber
$\Omega_s$	Truncated wavenumber

## CHAPTER 1

**INTRODUCTION**

---

*In the dynamic field of railway transportation, mitigating vibrations has emerged as a critical pursuit, and the integration of active vibration control systems stands at the forefront of enhancing the performance of railway vehicles. This chapter presents an overview of the dissertation that contains an introduction to the research topic, the motivation behind the proposed research work, research objectives, research significance and the outlines of the dissertation.*

**1.1 Introduction**

The beginnings of the railway system may be traced back to the early 19<sup>th</sup> century, a period of significant change in the transportation and industrial development of the world. Economic expansion and social advancement were greatly aided by the arrival of railways, which completely transformed the realm of transportation. The first public railway, the Stockton and Darlington Railway in England, opened in 1825, showcasing the potential for efficient land transportation (Smith, 2001). This event marked the beginning of an era in which steam locomotives became the primary mode of propulsion within the transportation industry. The fast expansion of the rail network across Europe, North America, and other regions was an inevitable consequence of the early railways' success (Bhatt & Kato, 2021). The transportation of raw materials, complete commodities, and people on a scale that had never been seen before was made possible due to railways, accelerating the pace of industrialization and urbanization. Over the 19<sup>th</sup> and early 20<sup>th</sup> centuries, rail transit emerged as a symbol of development (Xiao & Lin, 2021).

At present, the railway is the largest manmade transportation network in the world, which plays a vital role in sustaining the economic growth of any country. This industry employs more than 100 million people. Each year, more than 100 billion cargo and more than 1 trillion passengers are transported (Bogart & Chaudhary, 2015). So, any type of causality

is not tolerable, either in terms of infrastructure or in terms of human life. Over the past few decades, due to technological advancement, every country has adopted high-speed railway vehicle technology to reduce journey times. However, the increased speed will also raise the vibration level of railway vehicles, making the passengers' ride unpleasant. In addition to elevated speed, the presence of track irregularities further degrades the ride comfort and increases the possibility of a train derailling. In India, according to the report of the Ministry of Railways, out of 1088 accidents that happened between 2011 and 2023, 527 or 48.43 % were due to derailment and collision, in which most accidents are due to over speed or failure of rolling stocks (Indian Railways, Audit, and 2022). The number of casualties reported during this period is shown in Figure 1.1, which is in large numbers. Therefore, in order to stop these accidents, increase the service life of rails, improve ride quality, and ensure safe operation, it is necessary to build a reliable system that mitigates track vibrations even at high speed. Two approaches can be used to address these vibration issues: (1) improving the state of the railway tracks and (2) improving the vibration mitigation system. Since the track cannot be altered once built, the second strategy of improving vibration mitigation systems is more practicable.

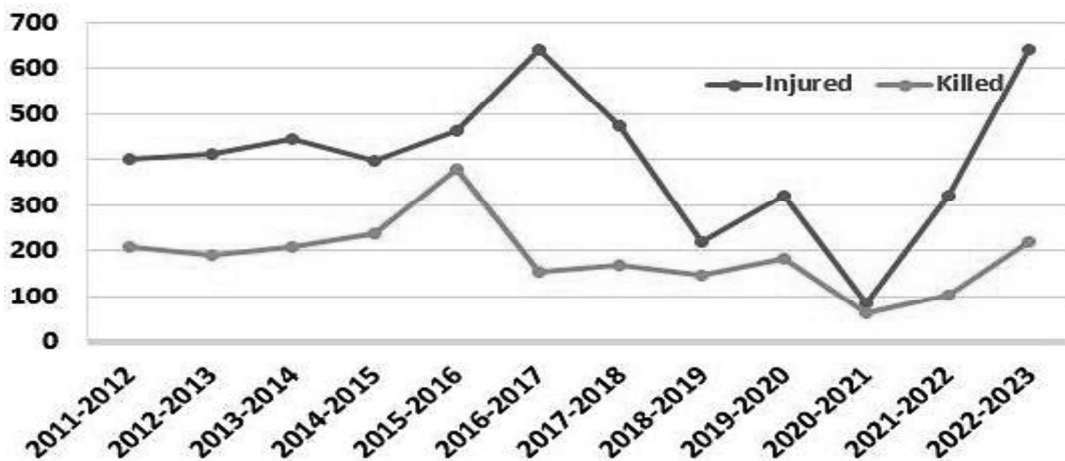


**Figure 1.1.** Number of casualties reported in Indian railway accidents from 2011-2023

In a modern railway vehicle (as shown in Figure 1.2 (a)), two types of vibration mitigation systems are generally present:

1. Primary suspension and,
2. Secondary suspension.

Primary suspension connects the wheelset to the bogie, while the bogie is connected to the car body through secondary suspensions, as shown in Figure 1.2 (b). This suspension system can be further classified into three categories: passive, semi-active, and active (Karkoub & Zribi, 2006), as depicted in Figure 1.3 (a), (b), and (c), respectively.

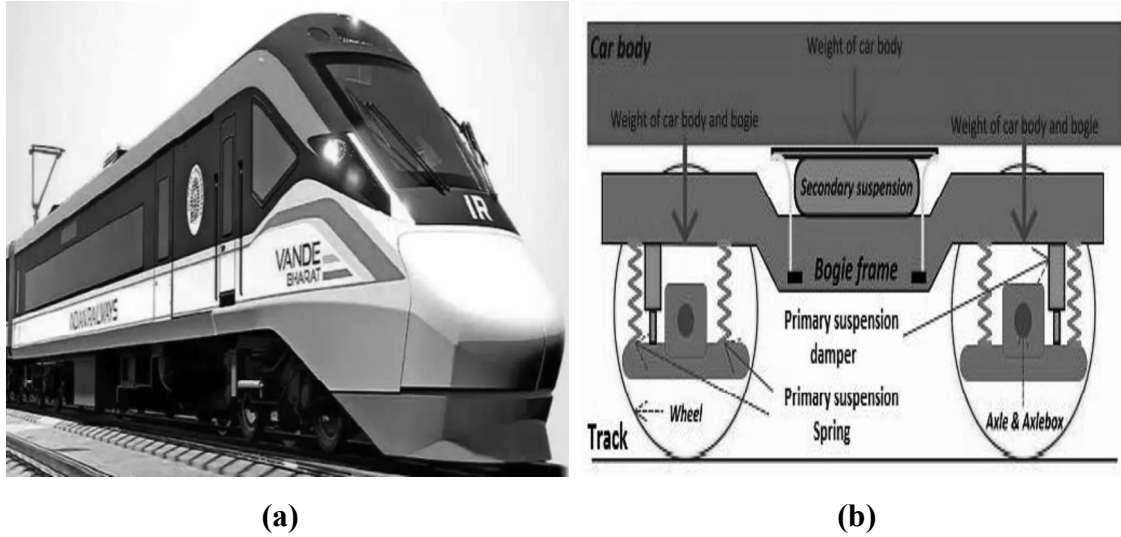


Figure 1.2 (a) Vande-Bharat express (b) sub-system of railway vehicle

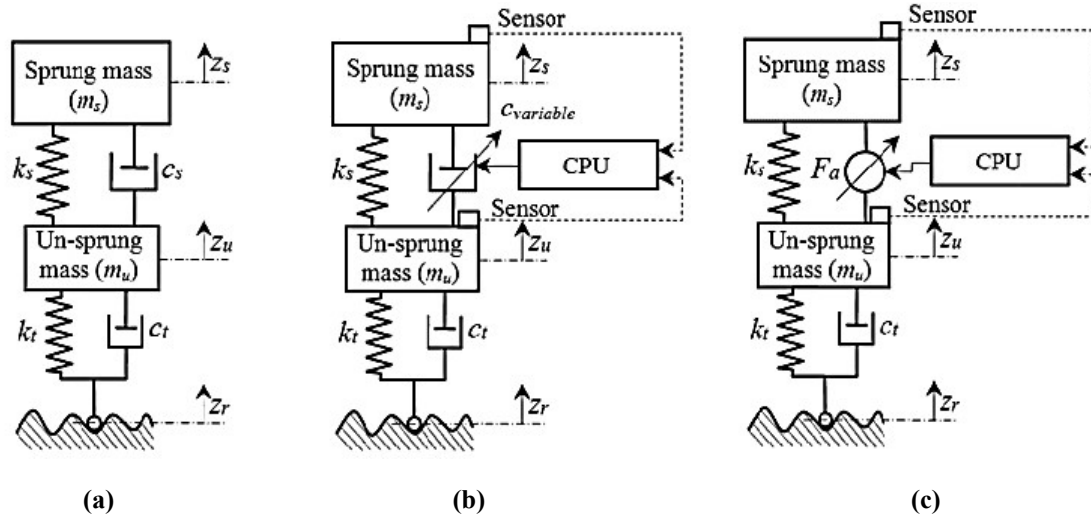


Figure 1.3 Types of suspension systems used in railway vehicles (a) passive (b) semi-active (c) Fully-active

$$Z_s = \text{Body's vertical displacement} \quad Z_u = \text{Bogie's vertical displacement}$$

$$K_s = \text{Secondary stiffness} \quad C_s = \text{Secondary damping}$$

$$K_t = \text{Primary stiffness} \quad C_t = \text{Primary damping}$$

$$Z_r = \text{Track disturbance} \quad F_a = \text{Active force}$$

A passive system consists of static springs and oil/pneumatic dampers. They do not need external power supplies for their operation and are comparatively simpler and less expensive. However, the performance of passive suspensions is limited since they can only store (like a spring) or dissipate (like a damper) energy. This limits the lower natural frequency to about 1 Hz with a corresponding static deflection of 250 mm (Goodall & Kortüm, 1983). This is a very fundamental limitation of passive elements. To address these drawbacks, self-levelling components, typically air springs and non-linear springs, have been used. Also, numerous papers on the optimization of passive suspension elements have been published (Abdessalem & Abdessalem, 2013; Guizani et al., 2015; J. et al. et al., 2012; Redfield; Sharp & Hassan, 1986; Shieh et al., 2005). Even with light loads and optimized elements, vehicles still experience the effects of rough tracks and fast speeds, making passive suspensions an inappropriate choice for improving ride comfort. (L. R. Miller, 1988).

The concept of semi-active suspension was first introduced by Karnopp et al. in 1988 for heavy cars and railway vehicles. The most common semi-active device used for vibration control is a variable orifice damper (Jezequel et al., 1992; Stribersky et al., 1998; J. et al., 1996). It consists of mechanical moving parts and valves that can improve the ride quality by up to 15 % in terms of root mean square acceleration. However, the time delay of the valve could degrade the performance of the suspension system. Another type of semi-active system is equipped with a variable gain damper filled with a rheological fluid whose viscosity changes when subjected to an electric or magnetic field. Two types of rheological fluids used in semi-active suspension are ER (electro-rheological) and MR (magneto-rheological), which are responsible for providing variable damping (Rabinow, 1948; Winslow, 1947). The pictorial representation of ER and MR damper are shown in Figure 1.4 (a) and (b), respectively. Compared with orifice-type dampers, these rheological dampers do not have any moving parts except pistons, which makes them more reliable. Various past research articles discuss the use of ER and MR fluid in semi-active suspension to reduce vibrations (Choi et al., 1998; Sims & Stanway, 2003; Wang & Liao, 2009b; Wei et al., 2016; X. et al., 1997; Zong et al., 2013). Among them, MR-based damper is more successful. It has a broader range of applications than ER damper because it generates higher power and a wide range of operating temperatures. However,



the complex control strategies of a semi-active suspension system make it problematic to effectively reduce the vibrations across the large frequency range of the excitations (Wang & Liao, 2009 b). Thus, by recognizing the limitations of both passive and semi-active systems, researchers have found an alternative way of vibration control in the form of active suspension (ElMadany & Samaha, 1992).

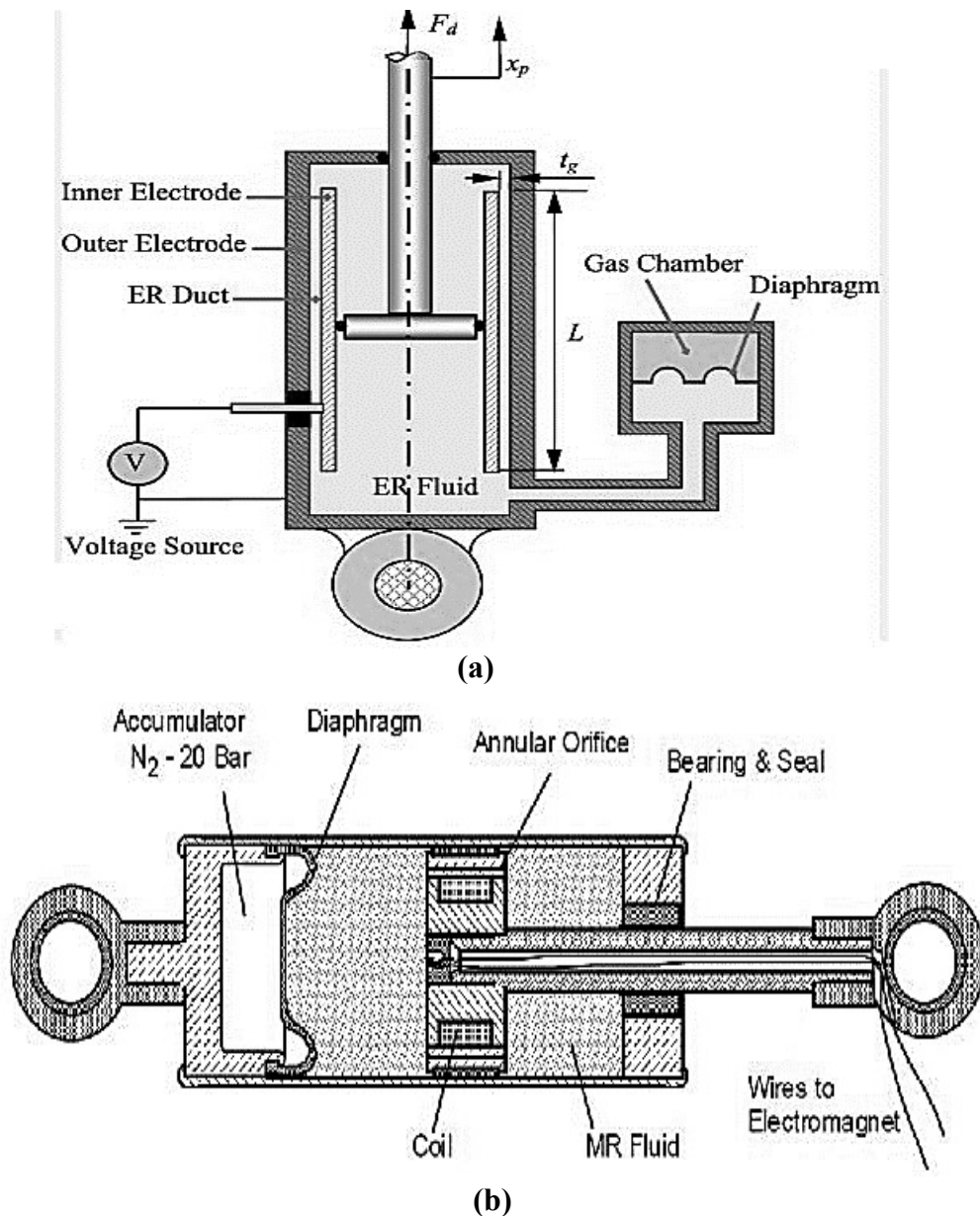


**Figure 1.4** Semi-active dampers (a) electro-rheological (b) magneto-rheological

An active suspension system combines the passive components with a controller-controlled unit that generates mechanical power. It is a complete mechatronic system that

incorporates an external power supply, actuator, sensors, amplifiers and an electronics processing unit. In this process, the measuring system will collect data about the vehicles' positions, velocities, and accelerations from various sensors and filters. A pre-planned control unit will examine this data to reach specified objectives. After that, an actuator system will generate the desired force to continually reduce the vehicle's vibrations over a wide range of frequencies to provide better ride comfort (Fu et al., 2020; Hrovat, 1990; Yoshimura et al., 1993).

The primary goal of the active suspension system is to reduce the vehicle body vibrations while maintaining better contact between the track and the wheelset. However, it can also be used for the following purposes:

- Provide good ride comfort
- Having adequate suspension clearance
- Following the low-frequency components of the track
- Isolate the high-frequency components of track irregularities

To achieve the objectives mentioned above, it is not enough to solely focus on designing the suspension system independently; instead, a thorough understanding of the complete railway systems, spanning from track inputs to output evaluation methods, is imperative. In other words, the performance assessment of the active suspension system is a chronological process that consists of four stages, as shown in Figure 1.5.

The initial stage focuses on formulating the problem by considering various inputs from track irregularities, rail profile, wheel-rail interface dynamics, and vehicle-track parameters. Once the problem is formulated with constant inputs (wheel-rail interface dynamics and vehicle-track parameters), the effect of different track irregularities on the vehicle dynamics and ride comfort are analyzed. For this, two types of track inputs, i.e., random and deterministic, are generally considered. The deterministic source of excitations is induced by specific vehicle and track factors, such as flat and out of the round wheel, rail dipped joint, rail dislocation, and rail corrugation (Jing & Wang, 2021; Zhai, 2020). The amplitude of such excitation sources is deterministic and falls under the regular class of irregularities. On the other hand, the excitation source whose amplitude

variation is not deterministic can fall under the random excitation source. The second stage involves constructing a mathematical model that captures the dynamic interactions between the railway vehicle and the track. Depending upon the complexity and nature of the system, the following techniques are utilized to construct the analytical model:

- First principle modelling (Newton-Euler's law, Conservation of energy and mass, Kirchhoff's law)
- System Identification (Statistical method, black box, transfer function model)
- Empirical modelling (Based on observation or experimental data, Curve fitting)
- Bond graph modelling (A graphical technique that represents the energy flow)
- Finite element analysis (Model physical structures by dividing them into small and simple elements)
- State-space modelling (Using ordinary differential equations and non-linear equations)

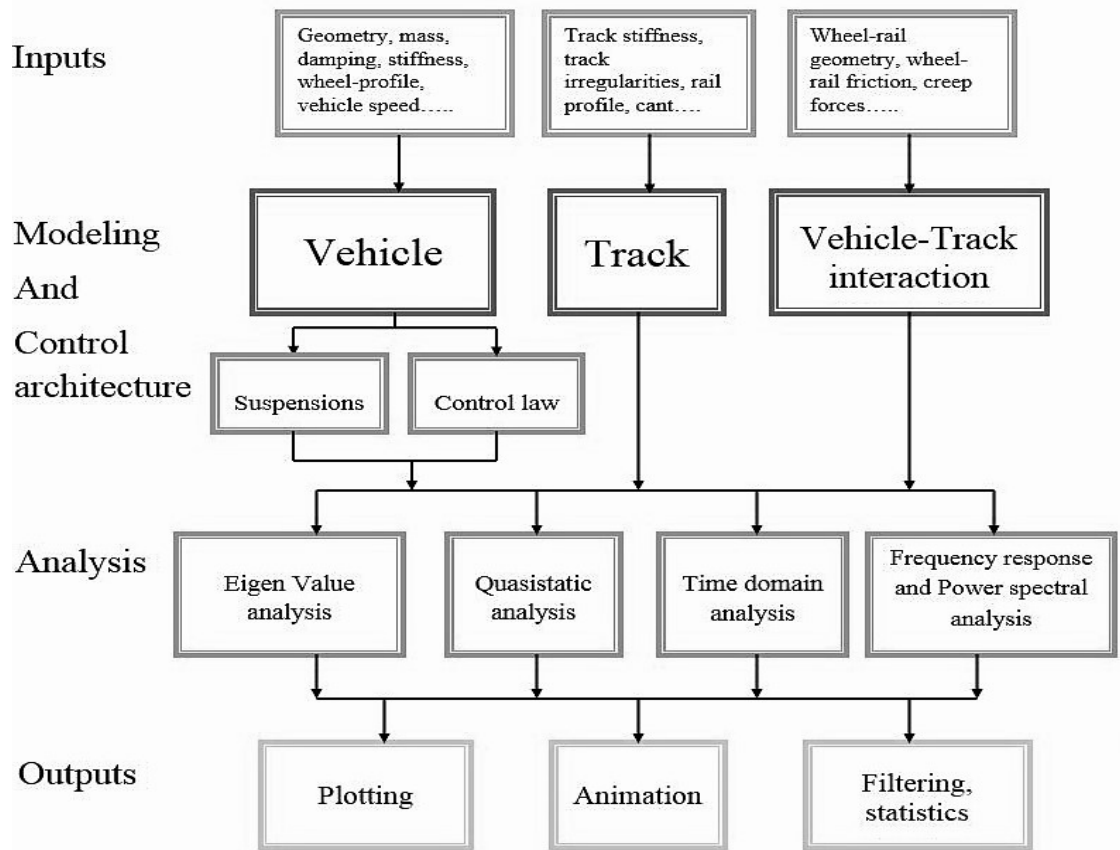


**Figure 1.5** Flow chart for the simulation process of the railway vehicle system

The mathematical modeling emerges as the universal language, weaving precision and insight across various fields varied as physics (S. Mitra et al., 2019), biology (Ashokkumar et al., 2023), and beyond. Formulating a mathematical model is a simple task when the system is small, linear, and uncoupled, but it has become a research topic when it comes to coupled multi-body systems. In the past, many mathematical models of varying complexity have been developed to study the dynamic effect of rail irregularities on vehicles' motions (Bhardawaj et al., 2020; C. et al. et al., 2021; Garivaltis et al., 1980; X. et al., 2002; Muñoz et al., 2019; Sedighi & Shirazi, 2012; Wang & Liao, 2009b). Also, many solutions have been employed to solve the complex nature of rail-wheel dynamics (Meymand et al., 2016; Rovira et al., 2011; Sharma & Kumar, 2016; Zhen et al., 2016). Most of them are focused on one point and small-scale modelling, and very few research studies are focused on considering the coupled motion. Whereas, in practice, the railway vehicle exhibits coupled motion while running on the railway track, and the rail-wheel contact has multi-point contacts. Hence, a full-scale dynamic model can be used to evaluate the complete performance of railway vehicles.

The second stage also incorporates sophisticated control algorithms and control elements designed to mitigate the track vibrations. At this step, the required amount of the controlling force is first predicted by the control algorithms and then given to the active suspension in terms of current and voltage to fulfil the desired objective. Various control strategies ranging from classical to modern approaches have been used mitigation purpose (Daniyan et al., 2019; Eski & Yildirim, 2009; Gomonwattanapanich et al., 2020; J. He et al., 2020; Metin & Guclu, 2014b, 2014a; Pang et al., 2017; Sezer & Atalay, 2011; Yin et al., 2022; Yoshimura et al., 1993; Q. Zhu, Ding, et al., 2018; Zong et al., 2013). However, due to the uncertainty and complexity of the system, these techniques have some issues in real-time implementations because most of them use classical tuning techniques such as Ziegler Nichols and Cohen-Coon in PID, Hit & Trial and Bryson rule in LQG, and small gain theorem in Robust control. These classical tuning techniques could not provide adequate solutions, especially to higher dimensional non-linear systems.

Recently, most general nature-inspired meta-heuristic approaches have been used over conventional methods to resolve the problems. They have a remarkable ability to deal with the ambiguity present in the railway environment. These Nature-Inspired Algorithms manage various activities to improve the performance of active suspension systems (U. Chauhan et al., 2019; Chhabra et al., 2019; Shukla et al., 2015). As optimization problems increase in complexity and dimension, the use of meta-heuristics algorithms is growing day by day. The key pros of meta-heuristic approaches are the following: (i) the Researcher may include adept information in the search procedure, and (ii) the method has the potential to work with numerous possible ways simultaneously instead of bumbling around the particular alternative. The evolutionary algorithms-based optimal controllers have been used for a variety of applications, including power generation (Ahmed, 2020; Robandi et al., 2001), motor speed control (Kaur & Ohri, 2022; Maghfiroh et al., 2022), aviation industries (Fessi & Bouallègue, 2019; Mobayen et al., 2011; Tsai et al., 2013; Vinodh Kumar et al., 2016), inverted pendulum (Howimanporn et al., 2017; Introduction, 2021), robotics (Bilgic et al., 2021), load frequency control (S. Jain et al., 2022; Sathans & Swarup, 2011), Biomedical and bio-informatics applications (H. Kumar et al., 2017; Patel et al., 2023; Wahab et al., 2011), image processing (Kang et al., 2021; S. Kumar et al., n.d.; Y. Yang et al., 2021) and many more. However, limited studies on metaheuristic-based controllers using an active suspension system in the context of vibration control have been published. Also, they have several shortcomings, including a lack of intelligence, being trapped in local minima, heavy computation requirements, high operational complexity, balancing issues, and a slow convergence rate (Bousmalis et al., 2008; Guo et al., 2022; Nyarko et al., 2014; Sonoda & Nakata, 2022). Therefore, a pressing need is still to develop a more advanced and effective search algorithm to attain smooth and optimal control force in a partially known or unknown environment.

The analysis stage is pivotal in evaluating the performance of the active vibration control system. It encompasses various methods, including eigenvalue analysis (Chamorro et al., 2014; El Beshbichi et al., 2020; Escalona et al., 2012; Srihari & Ramji, 2018; Zboinski & Dusza, 2017), time domain analysis (Kouroussis et al., 2014; Ronasi & Nielsen, 2013; Zhang et al., 2020; T. Zhu et al., 2022), and frequency domain analysis (Fourie et al.,

2019; Hurtado-Hurtado et al., 2022; S. Lei et al., 2023; Shim et al., 2021). Eigenvalue analysis helps in understanding the stability and dynamic characteristics of the system. Any system characterized by mass and stiffness has the propensity to undergo vibrations, particularly at specific frequencies and configurations known as modal frequencies and mode shapes. In cases where the motion equations exhibit linearity (or can be linearised for specific locations or amplitudes of motion), an eigenvalue analysis can be employed to identify the modes, their frequencies, and shapes. This analytical approach is called modal analysis (Gong et al., 2020; Gong et al., 2022; W. Sun et al., 2016). In time domain analysis, the most powerful way to simulate a vehicle's dynamic behavior is to fully solve the equations of motion at each of a sequence of very small time steps. The system's nonlinearities can be considered at each time step, and the equations are updated appropriately. For this kind of simulation, a variety of numerical approaches are available, such as Runge-Kutta, Newton-Raphson, Newmark, Wilson and finite-difference method; the Runge-Kutta procedures are one such technique that is frequently employed (Dai & Singh, 1997; Lu et al., 2022; J. et al., 2015). Each step must be short enough to prevent the solution from becoming unstable. Several algorithms employ a variable time step that is automatically modified to accommodate the simulation's current condition. This method is a powerful tool for analyzing vehicle stability in terms of hunting or critical speed. The frequency domain analysis explores the system's response to different frequencies. This method is beneficial when analyzing systems that exhibit time-varying or periodic characteristics, such as random signals or responses to periodic inputs. Some of the frequency domain approaches that are used for controller design are transfer function, Bode plot, Nyquist plot, loop shaping, Fourier transform, power spectral density, and noise filtering techniques (Z. et al., 2017; Frequency Domain Analysis of Systems 1997; Mršnik et al. 2013). The parameters derived from the frequency domain analysis provide a quantitative measure of the system's stability in terms of gain and phase margin. This third stage provides beneficial insights into how well the control system manages vibrations under different conditions.

The final stage focuses on presenting the simulation results. Different methods are employed for output representation, including pictorial and statistics-based approaches. Pictorial representation may involve graphical displays or animations illustrating the

dynamic response of the system. Statistics-based methods provide quantitative measures of the system's performance, offering insights into critical parameters such as ride quality or comfort of railway vehicles (Y. Kim et al., 2015). This stage aims to communicate the effectiveness of the active vibration control system clearly and comprehensively. The four most common/conventional methods used to evaluate human comfort and ride quality in railway systems are the ISO 2631 standard (C. Liu et al., 2020), the UIC 513 (Lauriks et al., 2003), the Mean Comfort index (J. Sun et al., 2021), EN 12299 (Y. Jiang et al., 2019; Standard, 2009), and Sperling's method (Dumitriu & Stănică, 2021). All these methods operate on the frequency-weighted acceleration data, which requires extensive measuring instruments and proper installation at appropriate locations. These requirements render these methods costly and time-consuming. To remove these problems, alternative ride comfort indices have been established that correlate human ride comfort with vibration level based on parameters of railway tracks and rolling stocks (Body & Graph, 2018; Y. S. Kim et al., 2008; Z. Yang et al., 2013). Among these methods, no unified global standard is present. Therefore, in this work, the Ride factor  $W_z$  method adopted by Research Design and Standard Organization (RDSO) has been preferred for the ride comfort evaluation.

By systematically progressing through these four stages, the simulation ensures a thorough understanding of the vibration control system's behavior and performance in real-world railway conditions. Other experts in the same field have already done much of this groundwork. The goal is to build on this work by looking at other paths that have yet to be looked into. A lot of other experts' work is summed up in Chapter 2, literature review. However, the primary focus of the proposed research in this dissertation is mainly on developing intelligent control strategies for vibration control of railway vehicles based on the classical approach, evolutionary approach, swarm intelligence, and their hybridization.

## 1.2 Motivations

Vibration control has emerged as a prominent subject of applied research, receiving significant attention from researchers and scientists in recent years. The quest for achieving the best possible performance, ensuring safety, and enhancing passenger

comfort has strongly emphasized the development of suspension systems. Therefore, the following problems are chosen to be solved in the proposed research work:

**1. Safety Enhancement:**

- Reducing Passenger Discomfort: Vibration control helps minimize vibrations experienced by passengers, improving the overall comfort and safety of the travel experience.
- Preventing Structural Fatigue: Excessive vibrations can lead to wear and tear on the vehicle's structure. A vibration control system can mitigate these effects, contributing to the railway vehicle's long-term structural integrity and safety.

**2. Operational Efficiency:**

- Reducing Wear and Tear: Vibration control systems can decrease the wear and tear on critical components, such as wheels, rails, and suspension systems. This, in turn, extends the maintenance intervals and improves the efficiency of the railway operation.
- Enhancing Track and Wheel Life: By minimizing vibrations, the control system contributes to the longevity of the railway track and the vehicle's wheels, resulting in cost savings over time.

**3. Energy Efficiency:**

- Optimizing Energy Consumption: Vibration control can help optimize the energy consumption of the railway vehicle. By minimizing unnecessary vibrations, the system ensures that the energy is efficiently utilized for propulsion rather than dissipating as vibrations.
- Regenerative Braking Optimization: Some advanced control systems can optimize regenerative braking, recovering and storing energy during braking phases.

**4. Compliance with Standards:**

- Meeting Regulatory Requirements: Railway vehicles are subject to strict regulatory standards regarding passenger safety and comfort.
- Implementing vibration control systems helps ensure compliance with these standards, preventing regulatory issues and potential liabilities.



**5. Passenger Comfort and Satisfaction:**

- **Enhancing Travel Experience:** Improving the ride quality by controlling vibrations enhances passenger comfort. This is particularly crucial for attracting and retaining passengers, contributing to overall customer satisfaction.
- **Competitive Advantage:** Providing a smoother and more comfortable ride can give a railway operator a competitive edge in the transportation market.

**6. Research and Development:**

- **Advancing Technological Innovation:** Constructing mathematical models and implementing vibration control systems contribute to technological advancements in the field of rail transportation. It promotes ongoing research and development, fostering innovation in railway vehicle design and control systems.

**7. Environmental Impact:**

- **Reducing Noise Pollution:** Vibration control systems can also reduce noise generated by railway vehicles, positively impacting the environment and the communities through which the rail lines pass.

**1.3 Research Gaps**

Based on the above discussions and cited literature, it is found that the development of a complete control strategy for vibration control of a railway vehicle is very complex because many factors affect the dynamics of railway vehicles under various conditions. Although much work has been done to study and control the dynamics of railway vehicles under various circumstances, the following research gaps are still found:

- Most of the study has been done by considering the decoupled motions of the vehicle body, Whereas, in real-time, the vertical and lateral motion of railway vehicles are strongly coupled with roll, pitch, and yaw motions. Hence, it provides a further direction to investigate the dynamics of railway vehicles with coupled behavior.
- In the case of contact forces between rail and wheel, a lot of work has been done by taking the rigid bodies. Meanwhile, in real-time, the wheel and rail structure is not rigid. Their configurations get changed at various conditions. Hence, an

advanced algorithm may be used with flexible contacts to determine the contact forces.

- The dynamic response of railway vehicles has been evaluated under similar types of deterministic and random track irregularities. However, different kinds of abnormalities can be considered.
- In most studies, independent controllers control the individual motion of railway vehicles, which is very costly. However, a cost-effective, decentralized controller can control individual motions.
- Also, the tuning methods used in previous studies are based on either classical approaches or old optimization algorithms. The simulated results with these methods will not provide the desired results for a complex system. Hence, it further gives the new idea to employ the new soft-computing-based solution techniques to solve such complex models and provide the required results.
- Classical and fuzzy-based controllers are used in most of the study. However, an intelligent algorithm-based control law can be integrated with these controllers to get a fast and desired response.
- Previous literature indicates that the robust and accurate control of the railway system is complex because of the presence of uncertainties, disturbances, and noise. Hence, it provides another dimension to investigate the robustness of the controller by using several techniques, including LQG and  $H_\infty$  design.
- Finally, the experimental validation has yet to be presented in most studies. Hence, it provides an opportunity to validate the simulated results with experimental results.

## 1.4 Research Objectives

In light of the presented facts and research gaps, the present work proposes to develop an active suspension system control system that mitigates the vibration of high-speed railway vehicles. Based on the above discussion, the research objectives are proposed:

- To develop a 38-degree-of-freedom (38-DOF) mathematical model of railway vehicles integrated with the wheel-rail contact model. The system is proposed to

cope with the vertical, lateral, roll, yaw, and pitch motions of the car body, bogies, and wheel sets.

- To Study the critical speed and dynamic response of full vehicle model under different kinds of random and periodic track irregularities.
- Design an optimal controller to provide better ride comfort and handling characteristics.
  - Development of a decentralized controller tuned with new optimization algorithms.
  - Development of a centralized controller integrated with state estimators.
- Design of empirical model-based actuator system.
- Design an intelligent controller integrated with the neuro-fuzzy controller to get the desired response and validate the results with the experimental data.
- Design and analysis of a robust controller with structured and unstructured uncertainties and compare the results with other controllers.

### **1.5 Research Significance**

The present work addresses the various issues raised in the above discussions, and it may be sketched as follows:

- The proposed active suspension system can significantly enhance passengers' ride comfort. It can actively adjust the suspensions in response to varying track conditions and provide a pleasant ride experience.
- Active suspension systems can reduce the risk of derailment by maintaining better contact between the wheels and the track. This is crucial for ensuring the safety of passengers and cargo.
- Active suspension systems can be designed to optimize energy efficiency by actively managing the energy absorbed and released during the suspension movements. This can contribute to overall energy savings, especially in electrically powered trains.
- The proposed control algorithms can help design a cost-effective vibration control system. Also, it can provide long-term stability as it can handle all types of uncertainties.

## **1.6 Thesis Outline**

Under the above discussion's umbrella, the thesis's prime objectives have been outlined in seven segments and discussed briefly (excluding this chapter) under this section.

### **Chapter 1:**

This introductory chapter provides a brief overview of the dissertation and emphasizes the inspiration behind the proposed research. The research objectives, gaps, significant contributions of the work, and dissertation outline are also explained in detail. In addition, the research outputs are presented as research publications in the final section.

### **Chapter 2:**

This chapter discusses the previously reported literature on dynamic modelling and control schemes used for comfort enhancement. The history and evolution of different mathematical models of railway vehicles with wheel-rail contact, solution approaches, actuators and control schemes adopted for vibration control applications are covered in this chapter. The merits and demerits of selected techniques in the proposed research are also defined.

### **Chapter 3:**

This chapter aims to describe the analytical model of railway vehicles used for dynamic performance analysis. A 38-DOF dynamic model of a railway vehicle integrated with wheel-rail contact forces and rail irregularities has been discussed. Then, using a two-dimensional (2-D) state space model, the critical speed and dynamic responses of the vehicle body under various track irregularities are also discussed. Further, for validation purposes, the simulated results of ride comfort analysis are compared with the experimental data of Research Design and Standard Organization (RDSO), Lucknow, India.

### **Chapter 4:**

This chapter describes the optimal control action adopted for the vibration control of railway vehicles under periodic and random track disturbances. In this chapter, a

decentralized Fraction Order Proportional Integral Derivative (FOPID) controller integrated with a hybrid PSO-GWO optimization algorithm is developed to suppress vehicle vibration. Comparative simulation results with conventional algorithms are also described in this chapter.

### **Chapter 5:**

An intelligent algorithm-based centralized controller is developed in this chapter to overcome the limitation of a decentralized control scheme. Here, a novel optimization-based linear quadratic Gaussian (LQG) controller integrated with adaptive neuro fuzzy interface system (ANFIS)- based actuation has been explored. Afterwards, the ride comfort evaluation of railway vehicles using Sperling's method is also presented in this chapter.

### **Chapter 6:**

In this chapter, a full-scale robust controller is developed to remove the robustness issue of the LQG controller. A comprehensive analysis of a robust control system has been discussed, considering structured uncertainties in vehicle mass and unstructured uncertainties in actuator dynamics. The simulated results of the proposed control scheme are compared with previously reported passive, semi-active and active suspension systems.

### **Chapter 7:**

This chapter gives concluding remarks about the significant findings of this work and suggests some suitable discussion for future research.

## **1.7 Thesis Outcomes**

### **Published/Accepted in international journals**

1. Nitish and A. K. Singh, "A Novel Metaheuristic Algorithm based FOPID Approach for Decentralized Control of Vibration of a Railway Vehicle," in *Mechanics Based Design of Structures and Machines; An International Journal*. <https://doi.org/15397734.2023.2297243> (Taylor & Francis) (SCIE).

2. Nitish and A. K. Singh, "Dynamic Modeling and Ride Comfort Evaluation of Railway Vehicle under Random Track Irregularities: A Case Study of a Linke-Hofmann-Busch Coach," in *Journal of Engineering Research*. <https://doi.org/10.1016/j.jer.2023.08.017>. (Elsevier) (SCIE).
3. Nitish and A. K. Singh, "A FO-PID based Decentralized Control System for vibration control of railway Vehicle using Hybrid Optimization," in *International Journal of Heavy Vehicle System*. <https://doi.org/10.1504/IJHVS.2023.10059063> (Inderscience) (SCIE).
4. Nitish and A. K. Singh, "Metaheuristic tuned Decentralized PID Controller based Active Suspension System for Railway Vehicle" in the *Journal of Expert System*. (Wiley) (SCIE).
5. Nitish and A. K. Singh, "Design of Robust Active Suspension System for Performance Improvement and Vibration Control of Railway Vehicles with  $H_\infty$  and  $\mu$ -synthesis" in *Proceeding of the Institution of Mechanical Engineering, Part C: Journal of Mechanical Engineering Science*. (SAGE) (SCIE).
6. Nitish and A. K. Singh, "Vibrations Control of Railway Vehicles using Decentralized PID controller with Flow Direction Optimization Algorithm," in *Journal of Mechanical Engineering and Sciences* SSN: 2289-4659 e-ISSN: 2231-8380 VOLUME 17, ISSUE 3, 2023, 9637–9655. <https://doi.org/10.15282/jmes.17.3.2023.9.0763> (JMES) (ESCI).
7. Nitish and A. K. Singh, "Active Suspension for the Vibration Control. of Railway Vehicle using Pole Placement Technique" in *Materials Today's Proceedings*. 2023, Vol. 80, Part 1, Pages 278-284. <https://doi.org/10.116/j.matpr.2023.01.188>. (Elsevier) (Scopus).

#### **Book Chapters/ Conferences Papers:**

1. Nitish and A. K. Singh, "The technological trends of control and modeling of railway vehicles: A review" (CIMS\_ 430) in *International Conference on Industrial and Manufacturing Systems* (CIMS-2020) at NIT Jalandhar.
2. Nitish and A. K. Singh, "Condition Monitoring and Fault Diagnosis Techniques of Electric Machines," 2019 3<sup>rd</sup> International Conference on *Recent Developments in Control, Automation & Power Engineering (RDCAPE)*, NOIDA, India, 2019, pp. 594-599, doi: [10.1109/RDCAPE47089.2019.8979045](https://doi.org/10.1109/RDCAPE47089.2019.8979045).

## CHAPTER 2

# LITERATURE REVIEW

---

*This chapter aims to present the formal definitions and a brief road map between the past and present reported literature. The historical background and the basic building blocks used for vibration control of railway vehicles have been described. The comprehensive analysis of various mathematical railway vehicle models, wheel-rail contact models, actuator technology and control algorithms has been reported in this chapter.*

### 2.1 Background

The historical background of a railway system comprises an extensive and distinguished past. It has a multi-dimensional evolution reflects the dynamic interaction of technological advancements, economic imperatives, and sociological changes. It is hard to exaggerate the significance of railway networks in terms of their impact on the environment of transportation and connection around the globe. The development of railways emerged as an essential aspect of the Industrial Revolution. From the early days of steam locomotives to the cutting-edge present technologies, the railway industry has undergone transformative changes. For example, the beginning of the 20th century witnessed the electrification of rail lines, offering cleaner and more efficient alternatives to steam power. The second half of the 20th century was focused on high-speed technology to cut travel times. In the 21st century, as innovation in materials science and digital technology gains popularity, there is a growing emphasis on utilizing lightweight and intelligent vehicles (Laiton-Bonadiez et al., 2022). This transformative technology completely changes the dynamics of travel, introducing trains that are not only faster but also represent a profound shift in the sustainability and overall quality (ride) of rail transit. This safe, secure and comfortable ride of railway vehicles is not a result of the single research field but a collective effort of the following areas, as demonstrated in Figure 2.1 (N. Jain & Mathur, 2017).

- (1) Railway track infrastructure and design of railway Vehicles.

- (2) Systems for controlling and monitoring with advanced signaling systems.
- (3) Security measures and security protocols.
- (4) Suspension system to provide better ride comfort for passengers.
- (5) Preparation for Emergencies.

Among the above areas, this study primarily aims to improve the ride comfort of a full-scale railway car, which requires a highly advanced and reliable suspension system.

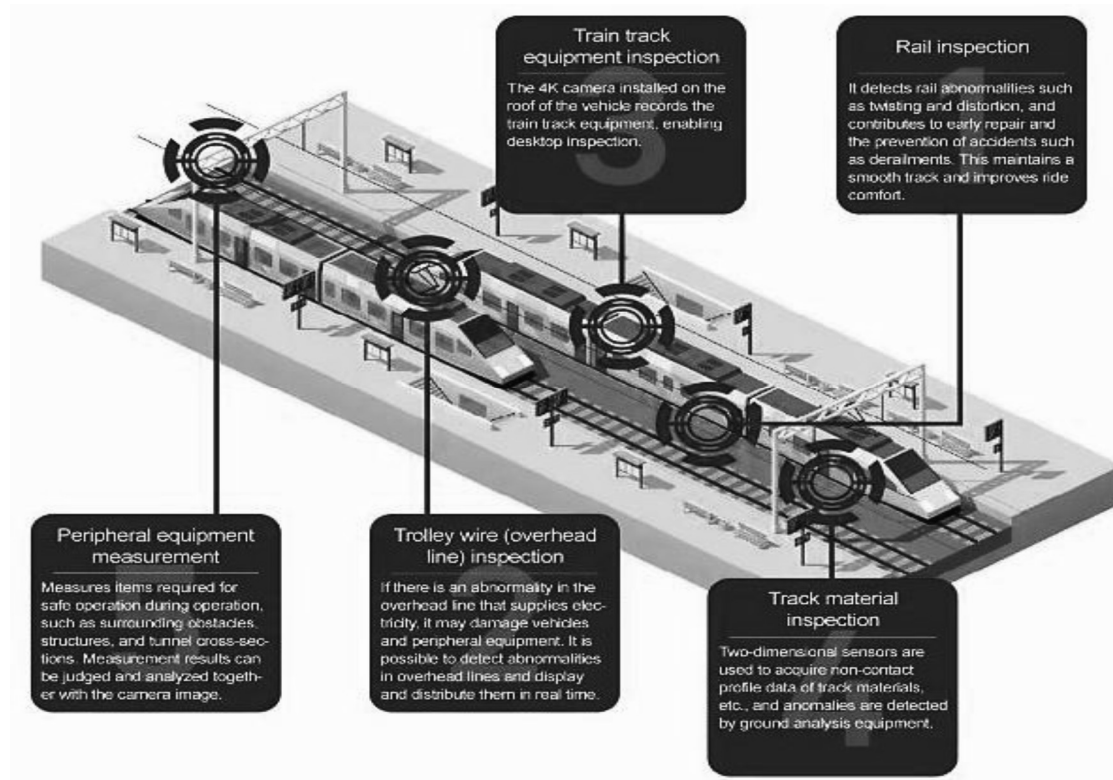


**Figure 2.1** Various inspection areas of railway vehicle systems

## 2.2 Basic building blocks of vibration control of railway vehicle

The primary goal of the suspension system is to reduce the vehicle body vibrations while maintaining better contact between the track and the wheelset. This objective is achieved with the help of a sophisticated control scheme that generates the required suppression force. The general control architecture used to control the vehicle's vibration is shown in Figure 2.2. From the figure, it is seen that the four key components/blocks that actively participate in the suppression process are as follows:



- (1) A comprehensive analytical model that covers every possible dynamics of railway vehicles, wheel-rail contact forces and track irregularities.
- (2) A proficient control algorithm that helps provide the precise desired controlling force.
- (3) An efficient actuation system that can track the desired control force with minimum error.
- (4) Economical and minimum number of sensors that provide accurate and precise information in a minimum amount of time.

By integrating these blocks cohesively, a vibration control system can achieve the desired response by actively adjusting the characteristics of the railway vehicle in real time. In the context of vibration control of railway vehicles, many research articles about these blocks have been published. Some of them are presented below:

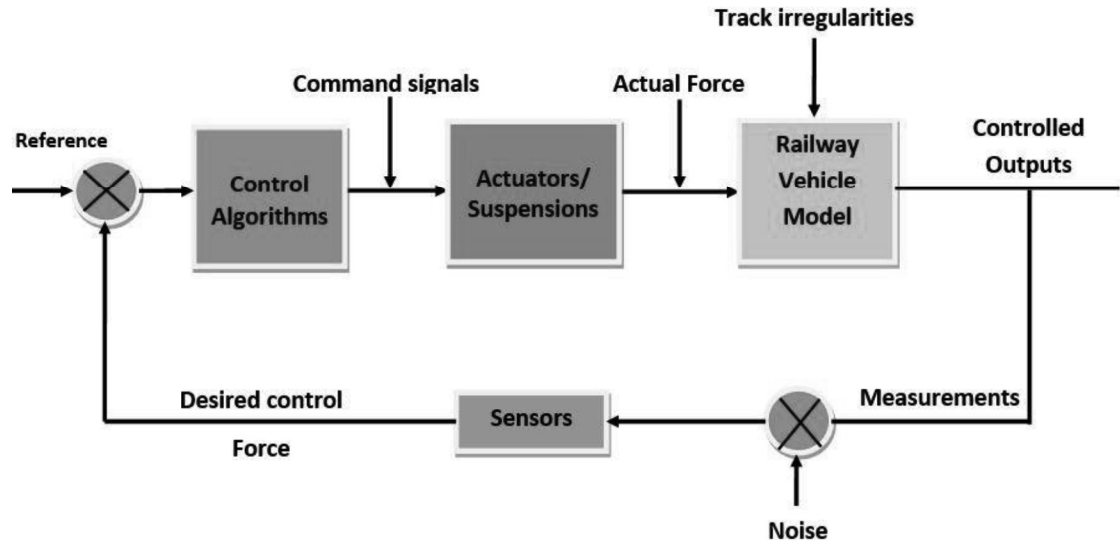


**Figure 2.2** The basic architecture for vibration control of railway vehicle

### 2.2.1 Mathematical modelling of railway vehicle and wheel-rail contact forces

The mathematical modelling of railway vehicles is a critical aspect of understanding and optimizing trains' dynamic behavior, performance, and safety. In the process of constructing, analyzing, and enhancing railway systems, these models serve as essential tools for engineers, researchers, and policymakers. This section focuses on the historical development of mathematical representations of the numerous forces, motions, and interactions between a railway car and the track.

### 2.2.1.1 Wheel-rail contact models

The contact between the wheel and rail plays a crucial role in railway vehicle dynamics. This is the main point where all forces from the track are transferred to the vehicle body. The nature of these forces is primarily affected by the wear, adhesion and creep characteristics, which ultimately depend on the area of contact and contact stresses at the wheel-rail interfaces, as shown in Figure 2.3. When a wheel rolls on the rail, relative slip can occur at its contact surface. The slip generates the creep forces in the longitudinal and lateral directions (Iwnicki, 2006), as shown in Figure 2.4. To evaluate these forces, the first step is to determine the geometry of contact, the contact pressure and the tangential forces. This determination is generally separated into two procedures:

1. Determining the normal forces
2. Determining the tangential forces

Hertz's contact theory for the normal forces and Kalker's linear theory (Kalker 1973) for the tangential forces provide a base for finding the wheel-rail contact forces. In 1880, Hertz first described the contact area and pressure distribution as an elliptical shape. He explained that when two elastic bodies with semi-infinite spaces are pressed together, a semi-ellipsoid-type contact pressure profile is developed between them. In 1926, a 2-D Carter theory of rolling contact showed the relationship between the circumferential and translational velocity of the wheel over the rail. Here, only longitudinal creepage is evaluated at a single point. In 1957, this theory was enhanced by Kalker (Kalker 1991), who considered the lateral creepage factor with longitudinal creepage and identified an approximate solution to the problem. Then, in 1958, the first 3-D theory of rolling contact was proposed by Johnson (Piotrowski & Kik, 2008), where both lateral and longitudinal creep forces were evaluated with the exact solutions. This theory did not become popular and was soon rejected, but it gives valuable information about the creep force law (Srivastava et al., 2013, 2014), which helps further development. Since then, extensive research has been performed to identify the creep forces with exact solutions. These include the Vermeulen theory, the strip theory, and the kalker theory. Among these, the Kalker linear theory has gained popularity because of its ability to determine both creep and spin creepage in short intervals. Shen et al. solved these formulations by inserting the accurate creepage coefficients instead of approximated values with little deviation. To

find these coefficients, computer programs such as CONTACT, ANALYN and FASTSIM were used (B. Liu & Bruni, 2022; Sh. Sichani et al., 2016; Sichani, 2016; Y. Sun & Ling, 2022; Tao et al., 2016).

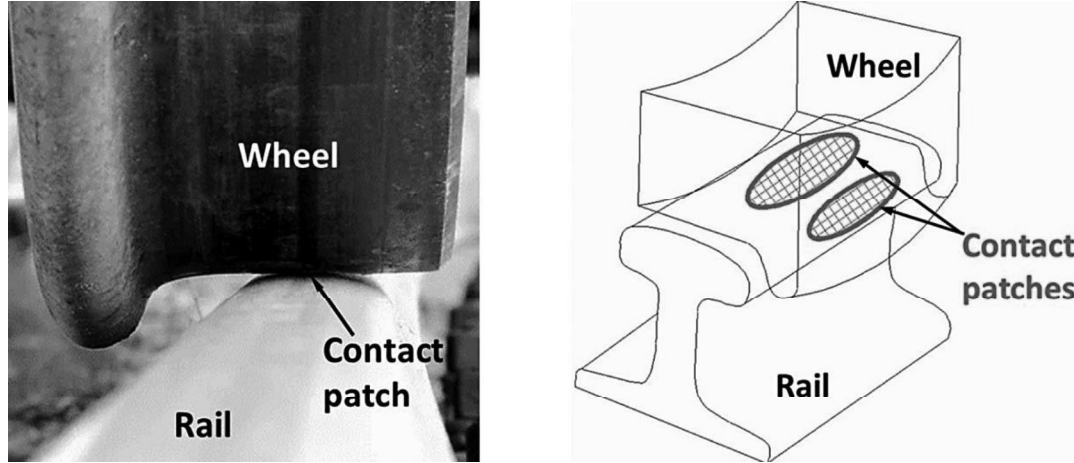


Figure 2.3 Normal wheel-rail contact

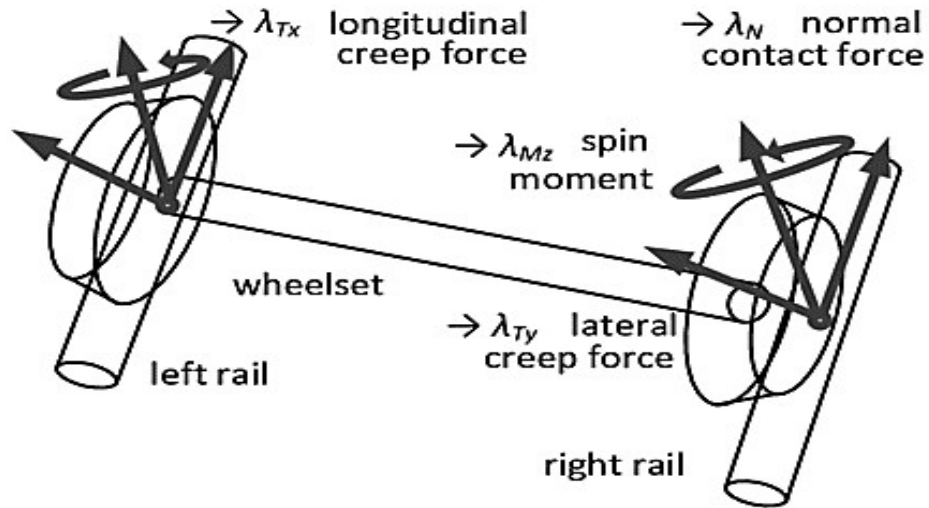


Figure 2.4 Tangential forces at the wheel-rail interface

Later, the wheel-rail contact problem was solved using the elastic approach (Shabana et al., 2004), where the wheel is considered an elastic material. Here, a 6-DOF track model is developed to evaluate the normal forces in terms of stiffness and damping. Then, the two-point contact problem is solved using the constraint method, where the hybrid approach is used with the wheel as it has 5-DOF motion. Piotrowski and Chollet (Taylor,

Piotrowski, et al., n.d.) review multi-point contact theories. Vollebregt et al. (Vollebregt, 2014) assess the accuracy of simplified contact models statistically and generally calculate the micro slip velocity and surface traction reliably. Vinayak Ranjan et al. uses three-dimensional finite element analysis for the rolling contact (Srivastava et al., 2015, 2017). Falomi et al. (Auciello et al., 2009) summarize the wheel–rail contact to multi-point, which helps to study the vehicles' multi-body dynamics. Zaazaa and Schwab (Zaazaa & Schwab, 2016) focus on Kalker's theories. Sugiyama and Suda discuss the methods for detection of wheel–rail contact points to avoid the wheel climbing and aids in curve negotiation (Sugiyama & Suda, 2009). At present, with the help of modern computer programs, it is possible to find these frictional coefficients at multiple points at lower computational costs (B. Liu et al., 2023; Meymand et al., 2016b; Ren et al., 2011; Sakalo et al., 2016; Spiriyagin et al., 2022; Z. Yang et al., 2016).

### 2.2.1.2 Modeling of Railway Vehicles

A railway vehicle is a complex system comprising numerous interconnected components linked through mechanical linkages. The system's inherent complexity and non-linear nature make it challenging to study the complete dynamics of a railway vehicle comprehensively, particularly when it is running on the track. Therefore, to study the complete dynamics and construct an error-free system, every vehicle component should be observed every second (Bosso et al., 2019; P. Li et al., 2007; Ngigi et al., 2012). For that, the trajectories of every component spanning from wheel-rail contact to inter-vehicle dynamics should be known mathematically. The essential components constituting a standard railway vehicle are as follows:

- (1) Vehicle body
- (2) Two bogies, including bolster and side frames
- (3) Four-wheel set including axle and bearing arrangement
- (4) Four secondary suspensions lying between the bogie and vehicle body
- (5) Eight primary suspensions connect the axle and wheelset
- (6) Couplers connect the two adjacent rail vehicles

Every individual component possesses its own set of benefits. For example, the vehicle body is used to carry people and goods, while the bolster and side frames on the bogies

give the car body mechanical support and help transfer load to the ground. Secondary suspensions aid in isolating the body from the bogie in the presence of high-frequency components, thereby providing passengers with a comfortable ride. In contrast, the primary suspensions linked between the wheel and axle mitigate the impact of track irregularities and provide stability to the vehicle against a variety of disturbances (R. M. Goodall & Mei, 2006; Harun et al., 2014). All these components are considered rigid bodies with six degrees of freedom: vertical, lateral, longitudinal, roll, pitch, and yaw motion. Although it is desirable to monitor every component equally to make a sound control system practically, it is impossible because of their interconnected dynamics and fiscal difficulties. So, there are some trade-offs between them. Many attempts have been devoted to improving the performance of railway vehicles, and various mathematical models have been studied. Based on the degree of freedom, three types of lumped parameter models are generally defined:

- (1) Quarter car
- (2) Half-car
- (3) Full-car

The pictorial representation of the quarter-car, half-car and full-car railway vehicles is shown in Figure 2.5 (a), (b) & (c), respectively. The quarter-car model is the simplest railway vehicle model, consisting of a maximum of 9-DOF steady-state motion. This model is generally used to study the vertical, lateral and longitudinal dynamics (translational) of the railway vehicle, as shown in Figure 2.5 (a). This model requires minimal mathematical equations but with a loss of originality. A half-car model, on the other hand, provides a maximum of 24-DOF motion. This model is significant for studying the 21-DOF translational motion (body, bogies, and wheelsets) and 3-DOF angular motion (pitching of body and bogies), as shown in Figure 2.5 (b). This model is also essential for studying the coupled behavior between the heave and pitch motions. However, a full-scale vehicle model is not only coupled in the vertical direction but also possesses coupling in the lateral and longitudinal directions. For that, a full-scale analytical model of the vehicle is required. A complete railway vehicle model consists of 42-DOF, out of which 21-DOF are responsible for translational and the remaining 21 degrees of freedom are concerned with the angular motion of the body, bogies and

wheelsets, as shown in Figure 2.5 (c). The implementation of these models entirely depends on the objectives of the applications.

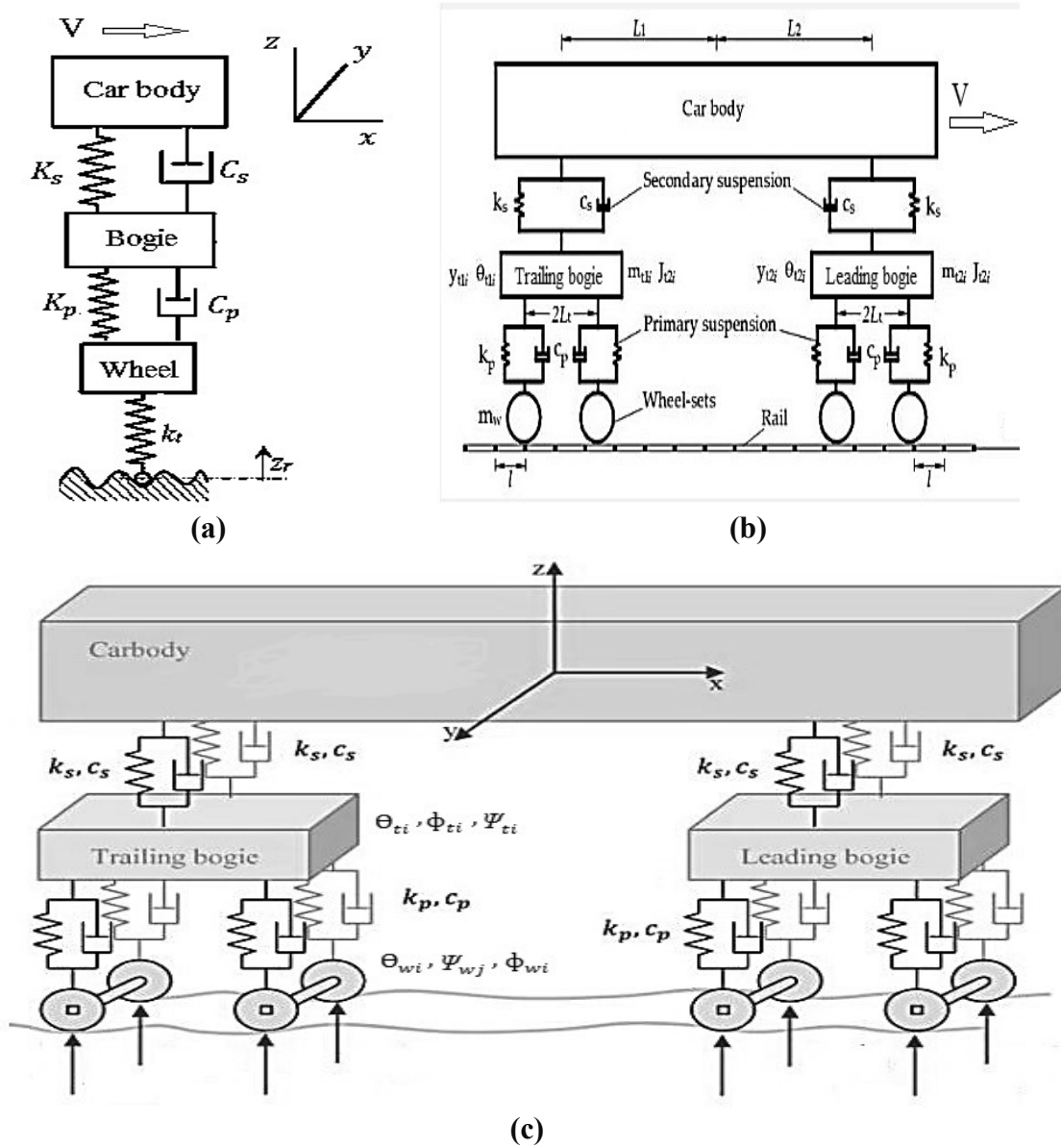


**Figure 2.5** Lumped parameter model of a railway vehicle (a) Quarter-car (b) Half-car (c) Full-car

$K_s$  = Secondary stiffness

$K_p$  = Primary stiffness

$z_r$  = Track disturbance

$l_1, l_2$  = Distance from vehicle's centre of gravity

$\phi_c, \phi_{ti}, \phi_{wi}$  = Pitch displacement of the car body bogie and wheel

$C_s$  = Secondary damping

$C_p$  = Primary damping

$V$  = Vehicle velocity

$\theta_c, \theta_{ti}, \theta_{wi}$  = Roll displacement of the body, bogie and wheel

$\psi_c, \psi_{ti}, \psi_{wj}$  =

Yaw displacement of the car body bogie and wheel

In the past, many mathematical models of varying complexity have been developed to study the dynamic effect of rail irregularities on vehicles' motions (Bhardawaj et al., 2020; C. J. Chen et al., 2021; Garivaltis et al., 1980; X. Lei & Noda, 2002; Muñoz et al., 2019; J. Sun et al., 2019; D. H. Wang & Liao, 2009a). Also, many solutions have been employed to solve the complex mathematics of vehicle dynamics that evaluate the impact of track and vehicle parameter variations. For example, the dynamic model for the vertical interaction between railway vehicles and the track was introduced by Wanming Zhai et al. (Zhai & Sun, 2008), where the 10-DOF model of a vehicle running with constant velocity was taken. The track is modelled as an infinite Euler on a discrete-continuous elastic foundation consisting of ballast and sleepers. The effect of vehicle track system parameters, such as sleeper spacing and track stiffness, on vertical dynamics has been studied. The low-frequency 11-DOF model of vehicle/track interaction was introduced by Robert D. Frohling (Taylor et al., 2010) to predict track deterioration due to dynamic wheel loading. Sun et al. introduced a similar model of vertical and lateral dynamics of wagon tracks (Ren et al., 2005). A three-dimensional 35-DOF model of a vehicle track system is introduced by Wanming Zhai et al. (Taylor et al., 2007). Chudzikiewicz (Chudzikiewicz, 2000) developed a 27 DOF model, which includes the wheel-rail contact model and interconnection of sub-parts to study the dynamics of the railway.

Guclu and Metin (2009) developed the half-light rail transport vehicle with 22 degrees of freedom to study the effect of irregularities on passengers and car bodies. A 17-DOF model of a full railway vehicle integrated with the semi-active controlled MR fluid dampers is proposed by D.H Wang et al. (D. H. Wang & Liao, 2009b) to study the lateral, yaw, and roll motions of the car body, bogies and wheelsets. The evaluation of the model is done with the help of MATLAB Simulink. A five-rigid body system with the 8-DOF model is proposed by Yuan Yao et al. (Yao et al., 2018) to study the lateral dynamics of bogie and the effect of bogie hunting under high speed is investigated. A 23-DOF model is proposed by Han Wu et al. (H. Wu et al., 2019) to study the hunting stability under aerodynamic load due to crosswind on a curved track. The model is coupled with a wheel track interface, and the effect of track irregularities is also taken into account. The summary of various mathematical models, such as the wheel-rail contact phenomenon of linear and non-linear contact forces, used in the previous study is rendered in Table 2.2.

The literature shows that most studies use lateral dynamics to investigate vehicle hunting instability and operating speed. However, some papers only investigate the vehicle's performance in a vertical direction. Very few studies focused on the coupled behavior of railway systems. Therefore, the first aim of this thesis is to develop a full-scale dynamic model of a railway vehicle integrated with wheel-rail contact forces and rail irregularities so that every dynamic of the vehicle sub-system is monitored.

### **2.2.2 Types of suspensions and actuation system**

A suspension system is an essential component of vibration control architecture, playing a vital role in maintaining a smooth and controlled ride experience. It isolates the vehicle from road or rail imperfections, absorbing shocks and vibrations to improve comfort, stability, and overall efficiency. The suspension system ensures that the tyres or wheels have the most contact with the surface so that the vehicle remains stable during manoeuvres. Throughout the evolution of railway technologies, suspension systems have undergone continuous advancements, integrating novel approaches to address the ever-changing demands of various terrains. According to previous literature, three types of suspension systems, i.e., passive, semi-active, and fully active (Karkoub & Zribi, 2006), are generally present in railway vehicles, which were already discussed in Chapter 1. Among them, the active suspension system is considered more beneficial. However, the performance of the active suspension system is purely dependent upon the actuation system. The following four types of actuators are generally used in active suspension:

1. Electro-mechanical actuators
2. Electro-hydraulic actuators
3. Electro-pneumatic actuators
4. Electro-magnetic actuators

Electro-mechanical actuators, as described by Friar in 1996, consist of an electric motor combined with a mechanism that converts rotating motion into linear motion (Watson, 2014). There are several types of electric motors, but a brushless DC motor attracts attention because of its exceptional reliability and suitable qualities. The conversion typically takes the shape of a screw thread, which can be either a 'recirculating ball-screw', 'roller-nut', or basic 'screw-jack' design. A typical electro-mechanical actuator is shown



in Figure 2.6. The speed with which the actuator moves is controlled by the voltages applied from electrical connections.

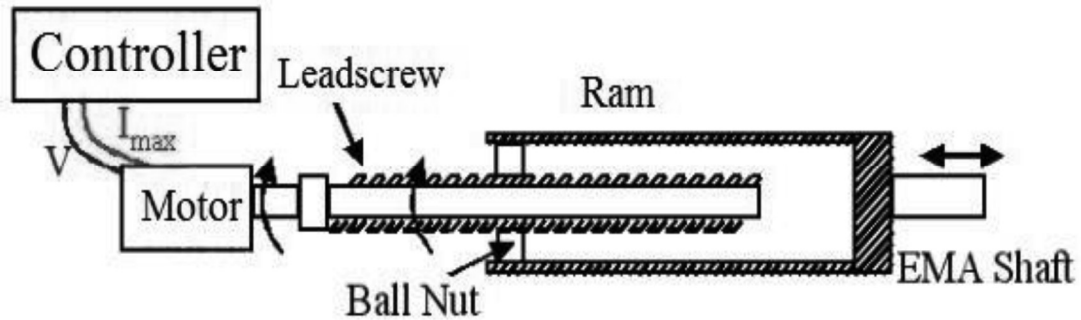


Figure 2.6 Electro-mechanical actuator

An electro-hydraulic actuation system utilizes a combination of electrical and mechanical (hydraulic) means to generate the required force, as shown in Figure 2.7. Here, the primary stage of the actuation system contains an electrical motor that provides the torque according to the current value, and a hydraulic cylinder connected to the throttle spool-valve serves as the secondary stage (Akers et al., 2006). The position of the spool valve is controlled with motor torque, and accordingly, the controlled oil flows into the cylinder, which ultimately generates the force. The mathematical description of the electro-hydraulic actuator will be presented in Chapter 4.

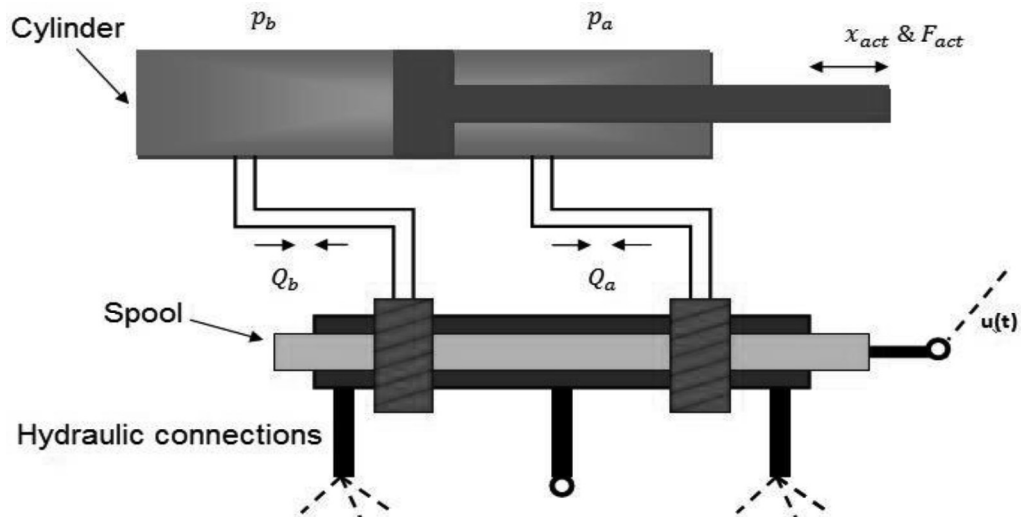
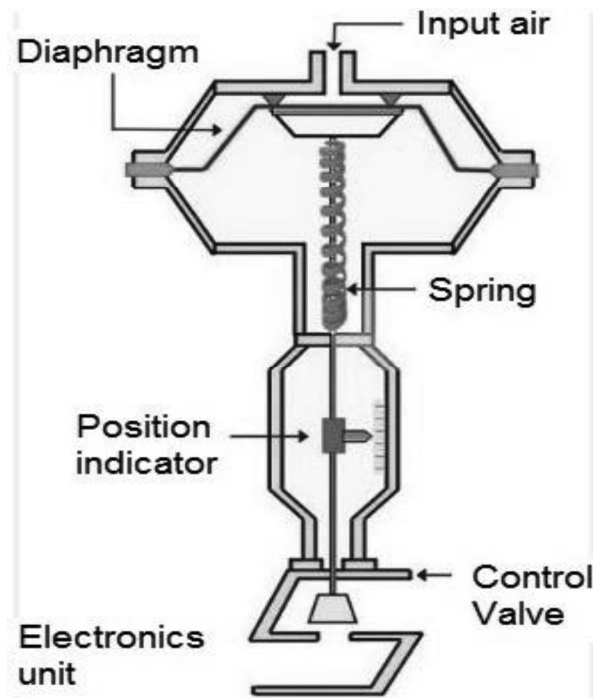


Figure 2.7 Electro-hydraulic actuator

Electro-pneumatic actuators convert electrical signals into mechanical motion by controlling compressed air flow to drive a pneumatic cylinder (Bartyś & Hryniewicki, 2019). The pictorial representation of the electro-pneumatic actuator is given in Figure 2.8. The working principle of the electro-pneumatic actuator is similar to that of an electro-hydraulic actuator, except that in electro-pneumatic, the air moves in and out of the air cylinder. The pressure of the compressed air is essential in determining the force and velocity of the actuator's movement. The actuator receives an electrical signal from a control system, which typically comes as a voltage or current. Then, these electrical signals are processed by the actuator's electronics to determine the desired position or movement of the piston. This type of actuator is widely used in industrial automation due to its reliability, speed, and precision in controlling various processes.



**Figure 2.8** Electro-pneumatic actuator

The electro-magnetic actuator is comprised of two pairs of electromagnets. One pair is mounted between the car body and bogies, and the second is placed between the bogie and wheelset. The basic diagram of the electro-magnetic actuator is shown in Figure 2.9. The working principle of electro-magnetic actuators involves the interaction between magnetic fields and electric currents (W. Wei et al., 2020). When an electric current flows through the coil, it generates a magnetic field around it. The strength of the magnetic field

is proportional to the current passing through the coil. The generated magnetic field can attract or repel the magnet, depending on the configuration. This interaction causes a force that results in mechanical movement (Debnath and Biswas, 2021). Electro-magnetic actuators have applications in many systems, including solenoids, relays, electric motors, and other electro-mechanical devices.

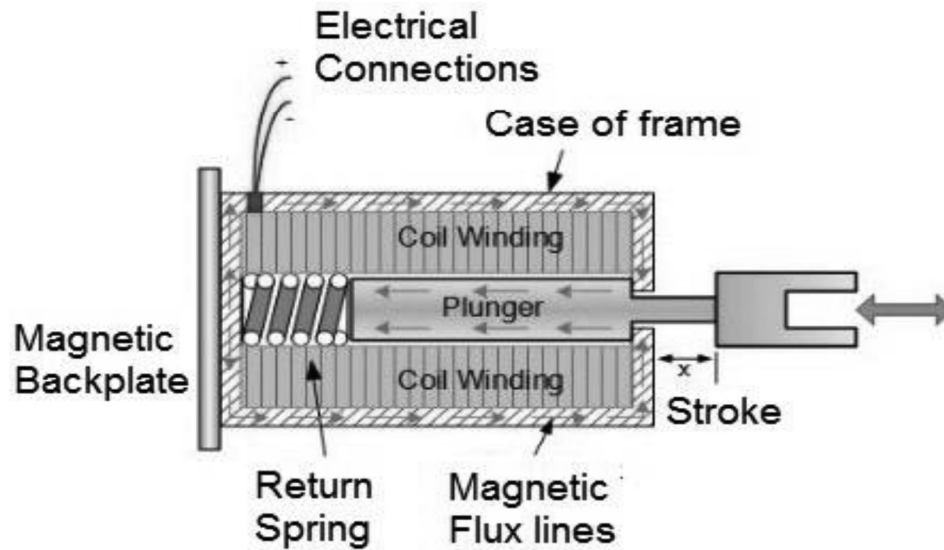


Figure 2.9 Electro-magnetic actuator

The actuator selection is based on the particular demands of the application, considering criteria such as accuracy, force generation, speed of reaction, and environmental circumstances. Every actuator possesses unique benefits and drawbacks, and choosing the most appropriate requires a comprehensive assessment of the system's requirements and limitations. For this reason, a comparison table between the aforementioned actuation techniques has been given in Table 2.1. From the table, it is concluded that the electro-hydraulic actuator is best suited for railway vehicle applications among other actuation systems because of its excellent force/size ratio, reasonable force bandwidth, and good reliability.

### 2.2.3 Control strategies and implementations

The vibration control architecture plays a crucial role in the railway system for ensuring passenger comfort and train safety. This architecture utilizes several passive and active control approaches to mitigate the vibrations caused by uneven tracks and wheel

imperfections. Previously, the input-output relationship of the control system solely depended upon the geometric arrangement of the passive system where the optimum value of mass, spring and damper defines the control elements (He et al., 2023; J. Z. Jiang et al., 2015; Mitra, Patil, and Banerjee 2015; Satyanarayana et al. 2021)

**Table 2.1** A comparison of different actuators

Properties	Actuator technology			
	Electro-mechanical	Electro-hydraulic	Electro-pneumatic	Electro-magnetic
Force-bandwidth	Moderate	Moderate	Low	Very high
Force-to-size ratio	Average	Excellent	High	Poor
Reliability	Good	Good	Good	Excellent
Stroke	High	Very high	High	Low
Power availability	High	Low	High	High
Efficiency	Average	Medium	High	High
Cost	Average	Low	Low	High
Maintainability	Good	Average	Moderate	Average

Now, in the case of active vibration control, the input-output relationship depends upon the configuration of the sensor, actuator and control strategies. In this case, the control system's performance is highly dependent upon selecting an appropriate control strategy. Specifically, when we talk about vibration control of railway vehicles, two types of controllers, the system controller and the force tracking controller, are generally required (D. H. Wang & Liao, 2009b). The system controller determines the desired control force according to the response, and the force-tracking controller modulates the current or voltage to track that desired force. Various control strategies ranging from classical to modern approaches that were used to predict the desired force have been given in Figure 2.10. These include classical control, optimal control, model predictive control, adaptive control, robust and sliding mode control, neural-network-based control and fuzzy logic control. A summary of their contributions in the context of vibration control of railway vehicles is presented in Table 2.2.

While all the aforementioned control techniques have achieved some degree of success in mitigating vehicle vibrations, the three specific control laws—classical control,

optimal control, and robust control—have demonstrated exceptional performance in this domain. As a result, these controllers form the basis of this study.

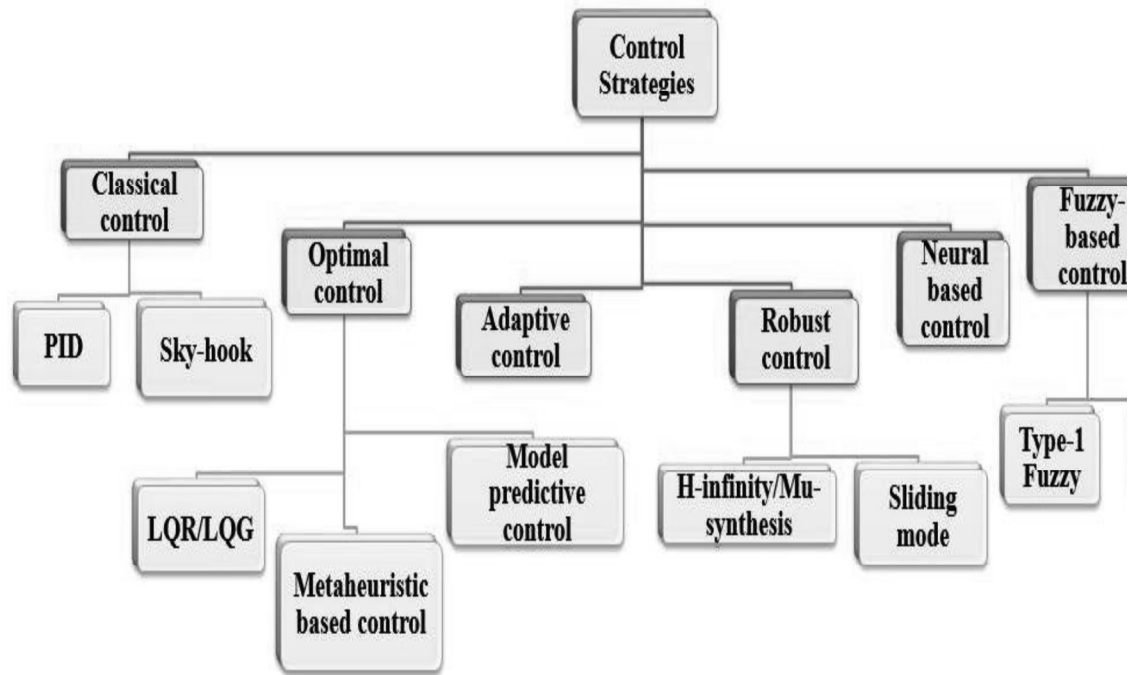


**Figure 2.10** Various control strategies used for vibration control of railway vehicle

### 2.2.3.1 Classical control

Earlier, classical controllers, such as sky-hook and PID, were the most common controllers used for the vibration control of railway vehicles. Railway vehicle suspensions, as widely recognized, must meet two distinct requirements: good ride quality and strong running stability. In passive suspensions, achieving a comfortable ride requires a soft connection between the weight of the vehicle body and the wheels while maintaining rigid support to improve stability. This conflicting problem can be solved by using an imagined sky-hook damper. However, this type of damper has a damping force proportional to the sprung mass's velocity and can only be used in a passive system.

On the other hand, PID is more prevalent in the modern control domains because of its simple tuning operation. As the name suggests, the PID controller consists of three parameters,  $K_P$ ,  $K_I$  and  $K_D$ , termed proportional, integral and derivative constants. The values of these constants generally depend upon the present, past and future values of error. The fundamental equation that explains the operation of PID can be expressed as:

$$U(t) = K_P e(t) + K_I \int e(t) + K_D \frac{de(t)}{dt} \quad (2.1)$$

Applying Laplace transform to Eq. (2.1), the control action of the PID controller is expressed in terms of the transfer function as:

$$C(s) = \frac{U(s)}{E(s)} = K_P + \frac{K_I}{s} + K_D s \quad (2.2)$$

where

- $C(s)$  is the controller transfer function,
- $E(s)$  is the error
- $U(s)$  is the output
- $K_P$ ,  $K_I$  and  $K_D$  are the controller's gains.

When combined, these parameters will provide significant advantages in many applications. For example, proportional control can produce a fast response, integral control can eliminate steady-state errors, and derivative control can increase the system's stability by reducing the overshoot and settling time. The traditional tuning methods, such as Ziegler-Nichols (Åström & Hägglund, 2004) and Cohen-Coon (36. Pdf), which were previously thought to be the best, are now being supplemented by heuristic and metaheuristic optimization techniques because traditional methods may fail to provide the desired performance in terms of overshoot, settling time, and steady-state error. Also, these methods could not provide a fully protected space in terms of data, which helps achieve the minimum cost function value. Thus, the intellectual methods based on metaheuristic algorithms are promising approaches to enhance search accuracy. The main objective of these intellectual methods is to minimize the cost function depending on the performance of algorithms. There are several types of evolutionary algorithms: genetic algorithm (Eiben, 1997), particle swarm optimization (Slowik, 2011), ant colony optimization (Mirjalili, 2019), grey wolf optimization (Mirjalili et al., 2014), firefly algorithm (Tilahun & Ong, 2012), cuckoo search algorithm (X. S. Yang & Deb, 2009), flower pollination algorithm (Al-Betar et al., 2019), are generally used as intelligent optimizers to solve any dynamic problems.

For instance, El-Deen et al. (El-Deen et al., 2015) and Mohammed et al. (Mohammed et al., 2014) used a GA-based algorithm to tune the PID for speed control of the DC motor

and synchronization of generators, respectively. The successful implementation of PSO, ACO, and GA for automatic voltage regulator systems has been reported in (39. Pdf) and (D. H. Kim & Park, 2005), respectively. Adubi and Misra (Adubi & Misra, 2014) use ACO in various applications, and a comparative study is presented. The implementation of PSO-based PID for locating the camera position in the unmanned aerial vehicle (UAV) and for control of an inverted pendulum has been successfully reported by Rajesh et al. in (Rajesh & Ananda, 2015) and Joseph et al. in (Joseph, S, B and Dada, 2018). Mahdiah Alamdar et al. (Alamdar Ravari & Yaghoobi, 2019) proposed a chaotic firefly algorithm to tune the parameters of FOPID for a continuous stirred tank reactor. The output shows better results than integer order PID regarding overshoot, settling time, and steady-state error. The cuckoo search algorithm has been used to optimize the PID parameters for various applications such as maximum power point tracking (MPPT) (Mosaad et al., 2019), speed control of induction motors (Peram et al., 2018), and LED driver circuits as buck booster converters (Sikander et al., 2018). Apart from these, Li et al. proposed GWO for condenser pressure control using a PI controller (S. X. Li & Wang, 2015). Yadav et al. used this algorithm to tune the parameters of PID used for the magnetic levitation system (Yadav et al., 2016). Ehab et al. (Nayak et al., 2020) used FPA to tune the parameters of PID for micro-robotic systems, and Nayak et al. used this algorithm to control the load frequency of a thermal power station (Ghith & Tolba, 2022). According to the literature, it is observed that PID controllers tuned with meta-heuristic optimization have been employed for various applications, including chemical processes, motor speed control, sun tracking systems, aviation industries, inverted pendulums, robotics, voltage regulation systems, and many more. However, just a few studies have been published in the context of vibration control employing an active suspension system.

### 2.2.3.2 Optimal control law

The optimal control is the oldest and broadest field used for the multi-input-multi-output (MIMO) control schemes. The main goal of the optimal control law is to find the minimum value of control signal ( $u$ ) that forces the system,  $\dot{X} = g(x(t), u(t), t)$ , to follow an optimum trajectory with the minimization of the following cost function:

$$J = \int_{t_0}^{t_f} [h(x(t), u(t), t)] \quad (2.3)$$

This problem of minimization can be solved using different approaches such as variational calculus, the principle of pontryagin, the dynamic programming and the quadratic solution method (Chachuat, 2007; F. Lin et al., 2010; Livesey, 1986; S. Singh, 2021). The variational calculus and pontryagin principle are based on Euler-Lagrange equations and can be employed in non-linear and time-varying systems. Here, a non-quadratic and time-varying performance index is formed, which is challenging to solve in real time. On the other hand, the Hamilton-Jacobi equation forms the basis of quadratic solution methods and can be successfully applied to linear time-invariant systems. This method produces an optimal control law, which is a linear function of state variables and can be solved linearly with the Matrix Riccati equation. The formulation of optimal control law requires three basic steps:

1. A mathematical description of the process with an accurate state-space model.
2. The specifications of the performance index.
3. The statement of boundary conditions with proper knowledge of physical constraints.

In the context of vibration control of railway vehicles, two types of optimal controllers, linear quadratic regulator (LQR) and linear quadratic Gaussian (LQG), are primarily used. The pictorial representation of these controllers is shown in Figure 2.11. The LQR is a full-state feedback controller that works on the principle of full rank. This implies that the all the system's state must be controllable and observable. This controller provides remarkable performance that guarantees gain and phase margins. However, two significant problems that the LQR encountered when applying to the vehicle suspensions are: (1) all the states are not physically available for feedback, and (2) zero steady-state error is not possible in deflection-type problems.

To overcome these limitations, a full-state estimator combined with an integral controller is required. The Kalman-bucy filter best estimates state variables and introduces an integral compensator (Davis & Thompson, 1988; Elmadany, 1990, 1991) in the state-



space model giving the zero steady-state error. The general equations of the Kalman estimator are as follows:

$$\begin{cases} \hat{\dot{X}} = A\hat{X} + Bu + (y - \hat{y}) K_f \\ \hat{Y} = C\hat{X} + Du \end{cases} \quad (2.4)$$

where  $A, B, C$  and  $D$  are system, input, output and transfer matrices, respectively. The coefficient,  $K_f$ , is Kalman filter gain. The value of  $K_f$  is evaluated so that Eigen values of system should remain highly negative and stable.

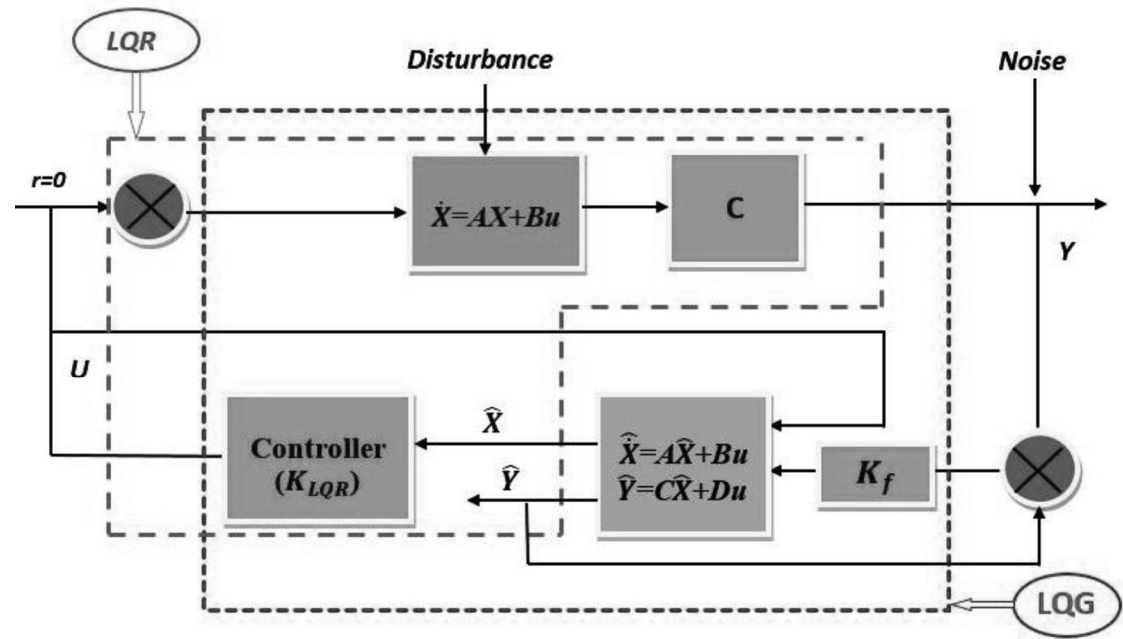


Figure 2.11 General structure of LQR and LQG control law

The idea of LQR/LQG was first applied to the quarter car model for analyzing the ride comfort and track holding (A. G. Thompson, 2007; Arabia, 2001; HaĆ, 1992; Likaj et al., 2017; Nagarkar & Vikhe Patil, 2012; Rawool & Mohan, 2022; Satapathy et al., 2014; Wilson et al., 1986; X. Yu et al., 2021). This implementation leads to the basic understanding of suspension design, and then this control is further applied to the higher dimensional models (Ben, Hasbullah, and Faris 2014; Elmadany and Qarmoush 2011; Esmailzadeh and Taghirad 1998; Fu and Bruni 2022a; Gommonwattanapanich et al. 2020; Graa et al. 2018; Karkoub and Zribi 2006; Sugahara et al. 2008; Taghirad and Esmailzadeh 1998; D. H. Wang and Liao 2009a; Yi-Xuan et al. 2018; Zhu, Ding, and

Yang 2018). As expected, the LQR/LQG control has been considered one of the most commonly used control structures for suspension control because of its simple design and relatively low online processing needs. Also, the state space formulation required for the functioning of optimal controllers may be quickly established by experts in vehicle dynamics.

Although LQ controllers are considered for preview-augmented suspension control, they aren't reliable because the performance of the optimal feedback controller depends on the optimum weighting matrices ( $Q$ ,  $R$ , and  $S$ ) of the quadratic cost function (Tyler & Tuteur, 1966). Most often, the traditional tuning methods such as hit and trial, and Bryson's rule were used to get the optimum values of weighting matrices (Esmailzadeh and Taghirad 1998; Fu and Bruni 2022b; Gomonwattanapanich et al. 2020; Graa et al. 2018; Sugahara et al. 2008; Taghirad and Esmailzadeh 1998; D. H. Wang and Liao 2009b; Yi-Xuan et al. 2018; Yu et al. 2021). Unfortunately, these methods could not provide the desired performance, even after spending ample time. Therefore, to reinforce these techniques, the neural network and evolutionary-based optimization algorithms play an essential role [37,38]. In these techniques, the values of weighting matrices are selected in the minimum time according to the designer's preferences.

The evolutionary algorithms based optimal controllers have been used for a variety of applications, including power generation (Ahmed, 2020; Robandi et al., 2001), motor speed control (Kaur & Ohri, 2022; Maghfiroh et al., 2022), aviation industries (Fessi & Bouallègue, 2019; Mobayen et al., 2011; Tsai et al., 2013; Vinodh Kumar et al., 2016), inverted pendulum (Howimanporn et al., 2017; Introduction, 2021), robotics (Bilgic et al., 2021), and many more. However, limited studies on metaheuristic-based-LQG have been published using an active suspension system in the context of vibration control. A few of them are: Nagarkar et al. (Nagarkar & VikhePatil, 2016) proposed genetic algorithms (GA) based linear quadratic regulator for the quarter car suspension system. The RMS values of sprung acceleration and controller force were optimized for better ride comfort. Similarly, Kun Wu et al. (K. Wu et al., 2021) used a genetic K-mean clustering LQG algorithm for quarter car suspension. Bauman et al. (Bauman et al., 1998) and Hui Pang et al. (Pang et al., 2017) used a GA-based LQG controller to optimize the

performance of a half-car vehicle model. The effect of particle swarm optimization (PSO) based LQG controller on the lateral and yaw displacement of the railway vehicle was evaluated by Arfah et al. (Nor, Selamat, and Alimin, 2011). The outcomes of the proposed scheme were compared with the hit-and-trial method. Mahmood Ali et al. (Ali et al., 2014) discussed the use of PSO-tuned LQG for active suspension systems. Here, the performance of the proposed algorithm was tested on a quarter-car vehicle model, and the results were simulated by adding a hydraulic actuator. Rashmi et al. (Ranjan et al., 2018) presented the adaptive predator-prey optimization for tuning the LQR, applied for vibration control, and the results were validated experimentally on a laboratory scale. From the above literature, it can be inferred that the effectiveness of metaheuristic-based LQG controllers has been examined on the quarter or half-car model. Also, most of the work has been done using traditional optimization techniques. However, a new optimization algorithm based on LQG with a full-scale model of the vehicle may be considered to suppress the track vibrations.

Moreover, the force tracking controller is another crucial part of the active suspension system, which determines the command current according to the desired force. In the past, some force feedback methods were used to build this part (Dyke et al., 1996; S. Singh & Kumar, 2022; D. H. Wang & Liao, 2009a). However, these methods require some extra force sensors that will increase the cost of the system. Therefore, some inverse-model-based methods must be required to accomplish the tasks economically. Previously, in semi-active suspensions, both parametric (Kwok et al., 2006; Spencer et al., 1997; Stanway et al., 1987) and non-parametric models (C.-C. Chang & Zhou, 2002; X. Lin & Chen, 2016; Schurter & Roschke, 2000; Tsang et al., 2006) were developed to describe the inverse behavior. The non-parametric models, such as neural networks and adaptive neuro-fuzzy-interface systems, are most accurate because of their strong non-linearity disposal ability. In the case of an active suspension system, the same approach may be adopted to predict the command current accurately.

### **2.2.2.3 Robust control**

The robustness of closed-loop systems is another critical aspect of the controller design. In the classical and optimal control architecture, we considered the vehicle system linear

and time-invariant. However, in practice, the vehicle's total mass varies due to changes in passenger and cargo loads. Also, the characteristics of the actuator may alter due to age and non-linearity (H. Li, Liu, Hilton, et al., 2013). Consequently, actual plants are considered time-variant systems. When such alterations occur in the system's parameters, the controller performance specified in the design phase tends to deteriorate (1998; Du, Lam, and Sze, 2003; Kashani and Kiriczi, 1992; Xu et al., 2021). Therefore, a robust control must be synthesized to maintain a constant performance of automotive suspensions. This technique has the primary advantage of keeping the controller robust even when the system response is significantly affected by unmodeled dynamics, non-linear behavior, parameter change, and vulnerability to disturbances (Chevrie et al., 2015; Fadiga et al., 2013; Farges et al., 2013; M. Kumar & Hote, 2022; S. Singh et al., 2023). This control law can also apply to heavily couple multivariable systems and circumstances in which the desired closed-loop modal characteristics are not clearly defined as part of the design requirements. The standard configuration of robust control law is shown in Figure 2.12. This approach is based on the minimization of  $H_2$  or  $H_\infty$  norms of transfer function taken from exogenous input ( $w$ ) to the desired outputs ( $Z$ ). Mathematically, it can be represented as:

$$\|T_{wz}(jw)\|_\infty = \sup \bar{\sigma}(T_{wz}(jw)) < \delta \quad (2.5)$$

where  $\delta$  is the predefined upper limit, and  $T_{wz}$  is the lower linear fractional transformation (LLFT) matrix.

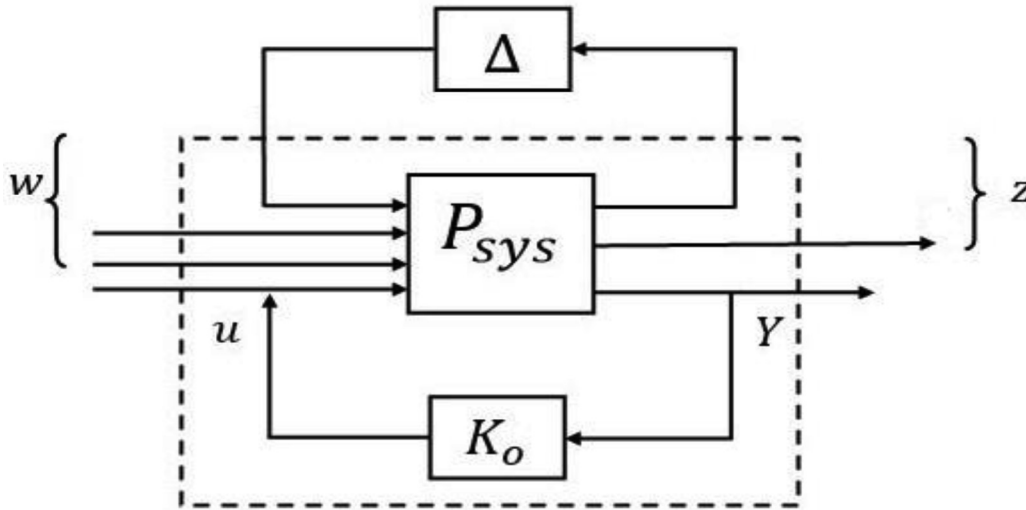


Figure 2.12 Standard configuration of robust control law

$P_{sys}$ = System transfer function matrix	$\Delta$ = Uncertainties block
$K_0$ = Controller gain matrix	$u$ = Control inputs
$W$ = Exogenous inputs	$Z$ = Controlled outputs

By introducing appropriate structured and unstructured uncertainties in the process, a continuous linear time-invariant system can be described by the following model:

$$\begin{cases} \dot{X}(t) = A X(t) + B_1 w(t) + B_2 u(t) \\ Z(t) = C_1 X(t) + D_{11} w(t) + D_{12} u(t) \\ Y(t) = C_2 X(t) + D_{21} w(t) + D_{22} u(t) \end{cases} \quad (2.6)$$

where  $Z(t)$  and  $Y(t)$  are the measured and the controlled outputs. The primary goal of robust control is determining the value of  $K_0$  so that the effect of disturbance on the controlled output is minimal. To achieve this, two types of robust control laws, i.e.,  $H_\infty$  and  $\mu$ -synthesis, are mostly adopted. In the past, many research papers have been published discussing the use of robust control in active/semi-active suspension systems. For example, M. Yamashita et al. (Automotive & Suspension, 1990) and L. Ray (2016) first introduced a robust control system for the active suspension system. Here, a  $H_\infty$  control scheme for a simple quarter-car model has been implemented. H. Chen et al. (Chentit, 2003) and H. Gao et al. (Gao et al., 2006) proposed a robust controller for a quarter-car model to deal with parametric uncertainties. Here, the linear matrix inequality (LMI) technique has been employed to solve the optimization problem. A robust control-based active suspension system for vibration mitigation has been proposed by Y. Yin et al. (Yin et al., 2022). In the design of the  $\mu$ -synthesis control scheme, the structural uncertainties with time delay in the actuator have been considered. The results are compared with *the*  $H_\infty$  controller. D. Sammier et al. (Sammier et al., 2000) proposed the  $H_\infty$  controller for a half-car model in which the vertical and roll motion of the car body is controlled with a mixed sensitivity approach. G. Wang et al. (G. Wang et al., 2016), H. Li et al. (H. Li, Liu, Hand, et al., 2013) and K. Afshar et al. (Afshar & Javadi, 2019) proposed the state feedback robust controller for the half-car model. Here, the robustness of the controllers is evaluated by considering the parametric uncertainties and input

delays. M. Yamashita et al. (Yamashita, 1994), A. Orvnäs et al. (Orvnäs et al., 2011), J. Park et al. (Park & Kim, 1999), and P. Gaspar et al. (Gaspar et al., 2010) extend the idea of robust control for the full-scale model. Here, the three controlling algorithms,  $H_\infty$ ,  $\mu$ -synthesis, and mixed-  $\mu$ -synthesis, are successfully implemented to enhance ride comfort. The closed-loop robustness of the proposed controllers is evaluated in the frequency domain. Apart from this, the concept of a robust controller is also applied to the flexible models (H. Cao et al., 2022; Fu & Bruni, 2022b; Kamada et al., 1997; Kamada & Karaki, 2023; Zheng et al., 2020a). From the literature, it is evident that the majority of the research has been carried out with the quarter-car or half-car models. Even in the full-car models, the controllers are designed with the decoupled approach. Moreover, most of the studies are primarily focused on the single uncertainties. However, a complete model consisting of structured and unstructured uncertainties can be developed, and a full-scale robust control scheme can be adopted to suppress the track vibrations effectively.

Apart from the above literature, a complete summary of various mathematical models of railway vehicles, wheel-rail contact models, actuators technology, and control laws used to control the vibration of railway vehicles is also presented in Table 2.2.

**Table 2.2** Summary of various mathematical modelling and control algorithms

Authors	Title	Model's type/ DOF	Control Technique	Proposed Work
(Q. Wang et al., 2023)	Parameter optimization of multi-suspended equipment to suppress car body vibration of high-speed railway vehicles: a comparative study	21-DOF	Improved niche Genetic algorithm (INGA)	A rigid-flexible coupling model with three suspended equipment is developed. A comprehensive analysis of the multi-objective parameter optimization theoretical optimization has been conducted.
(C. Zhang et al., 2023)	A combine review for vibration control strategies for high speed train and railway	2-DOF with passengers model	Sky-hook, ground-hook, LQG	A comprehensive study of direct and indirect methods applied for vibration control of railway vehicles are presented. The

	infrastructure: Challenges and solutions			available solutions for reducing undesired vibrations that effect the critical velocity and ride comfort are discussed.
(Shen et al., 2023)	Vibration suppression using a mechatronics PDD- ISD combine vehicle suspension system	Quarter-car model	Fractional- order sliding mode controller	In order to solve the issue of vehicle vibration suppression at low and high frequencies, the performance of a new combination suspension system using power-driven dampers and inerter- spring dampers is examined for a quarter- car model. The controller is a sliding mode controller with fractional-order derivatives.
(Fu et al., 2023)	Modelling, hardware-in-the-loop tests and numerical simulation of magneto-rheological semi-active primary suspensions in a railway vehicle	Quarter-car model	Sky-hook, LQG	This paper presents a semi-active primary suspension system designed to enhance the ride comfort of railway vehicles. The magneto-rheological dampers prototype undergoes testing, and three control strategies for semi-active primary suspensions are offered. Sky-hook, LQG, and Mix-1- Sensor.
(Kamada & Karaki, 2023)	Active vertical vibration suppression of high- speed railway vehicles by controlling internal	Full-car model	$\mu$ -synthesis	A vertical vibration reduction controller was designed using $\mu$ - synthesis. A comparison was made between the nominal performance and robust performance of a 1/6 scale train model

	pressure of the air spring using $\mu$ -synthesis control			using $H_{\infty}$ control theory. The advantage of $\mu$ -synthesis control lies in its ability to provide robust performance.
(Tiwari et al., 2023)	Ride comfort analysis of high-speed rail vehicle using laminated rubber isolator based secondary suspension	13-DOF	A laminated rubber based spring	The static stiffness spring is optimized in both inflated and deflated positions. The spring gives satisfactory results in terms of ride comfort enhancement at a speed of 16-200 Km/h.
(S. Singh & Kumar, 2022)	Modelling and Analysis of a Passenger Train for Enhancing the Ride Performance Using MR-Based Semi-active Suspension	17-DOF	Sky-hook and continuous state control algorithm	A rail vehicle model with seventeen degrees of freedom, incorporating Magneto-rheological (MR) dampers, is developed. The performance of the MR damper is assessed using a modified Bouc-Wen model. In this case, two separate controllers are utilized to manage the complete suspension system: one for rejecting disturbances and another for accurately tracking the damper force.



(H. Cao et al., 2022)	Active Vibration Control of Railway Vehicle Car Body by Secondary Suspension Actuators and Piezoelectric Actuators	Half-car flexible	$H_2$ and $H_\infty$	The study focused on the active reduction of vibrations in the automobile bodies of high-speed electric multiple units. The optimal placements of the piezoelectric actuators and sensors were determined using $H_2$ and $H_\infty$ norms. The vehicle's vibration acceleration decreased by 10% and 18% at speeds of 200 Km/h and 350 Km/h, respectively.
(Fu & Bruni, 2022a)	An examination of alternative schemes for active and semi-active control of vertical car-body vibration to improve ride comfort	9-DOF	LQG and H1 model-based control	A simplified representation of car-body bending modes is utilised to construct a two-dimensional 9-DOF vehicle model. Four mechatronic suspensions, which incorporate both active and semi-active technology in both secondary and primary suspensions, are being compared to demonstrate their respective advantages. The control strategies based on LQG and H1 models have been established.
(Joseph et al., 2022)	Metaheuristic algorithms for PID controller parameters tuning: A review, approaches and open problems	Numerous mathematical model	Classical and Metaheuristic based PID	Several classical and metaheuristic-based optimization algorithms used to tune the PID controller used in various applications has been presented.

(Zeng et al., 2022)	Lateral-vertical coupled active suspension on railway vehicle and optimal control methods	14-DOF	LQG and optimal sky-hook	The lateral and vertical coupled dynamics of secondary suspension system is studied with 14 DOF non-linear model. The theoretical study proves that optimal sky-hook method is more successful as compare to LQG control method.
(Yan et al., 2022)	Vibration control of superconducting electro-dynamic suspension train with electro-magnetic and sky-hook damping methods	14-DOF	ON-OFF Sky-hook damping	The vertical and pitch vibrations of EDS train are suppressed with active primary suspension system. The electro-magnetic damping of $5\text{kN}\cdot\text{s/m}$ to $10\text{kN}\cdot\text{s/m}$ . is successfully achieved.
(S. Liu et al., 2022)	Strongly perturbed sliding mode adaptive control of vehicle active suspension system considering actuator non-linearity	Non-linear Half car model	Sliding mode adaptive control	The vertical and pitch motions of railway vehicle are successfully controlled by active suspension system. The uncertainty in vehicle parameters with non-linearity in actuator dynamics has been added to check the robustness of control algorithm.
(Theunissen et al., 2021)	Preview-based techniques for vehicle suspension control: a state-of-the-art review	Quarter and half-car	LQR, $H_2$ and $H_\infty$ and MPC	A comprehensive review of preview based control strategies used in active suspensions has been presented.
(Gong et al., 2021)	Research on mechanism and control methods of car body chattering	23-DOF	Multi-objective synchronization Optimization (MOSO)	To study the car body chattering, wheel and rail profile test, modal parameters test and root locus analysis is carried out. The car body acceleration at 10 Hz is decreased by 40

	of an electric multiple-unit train			% using proposed optimization technique.
(Dumitriu & Stănică, 2021)	Study on the Evaluation Methods of the Vertical Ride Comfort of Railway Vehicle—Mean Comfort Method and Sperling's Method	Vertical and lateral comfort	—	This research examines the ride comfort of railway vehicles in terms of vertical vibrations. The evaluation is conducted using two methods: the mean comfort technique and Sperling's method. The perception of comfort is measured using comfort indices, specifically the ride comfort index $N_{mvz}$ and ride comfort $W_z$ index.
(J. Sun et al., 2021)	An investigation into evaluation methods for ride comfort of railway vehicles in the case of car body hunting instability	Field test	Sperling method, Mean Comfort standard method and Continuous Comfort method	Three methods of ride comfort analysis have been reviewed. The simulated results are compared with experimental results of hunting instability.
(Dahunsi et al., 2020)	Proportional +integral + derivative control of non-linear full-car electrohydraulic suspensions using global and evolutionary optimization techniques	Non-linear full-car	Metaheuristic based PID	An active vehicle suspension system using multi-loop proportional integral derivative controllers tuned with global and evolutionary optimization is proposed. Non-linear full-car electrohydraulic active vehicle suspension is used. Controlled random search, differential evolution, particle swarm optimization, modified particle swarm optimization, and modified controlled

				random search are Global and evolutionary optimization approaches.
(Jin et al., 2020)	Development and evaluation of a versatile semi-active suspension system for high-speed railway vehicles	Proto type of variable stiffness variable damping suspension (VSVD) model	Sky- hook and short term Fourier Transform (STFT)	A versatile semi-active (VSVD) suspension for the mitigation of lateral vibration is developed. A comparison between the passive-off, passive-on, pure VS, pure VD and proposed model is conducted.
(Alfi et al., 2019)	Active secondary yaw control to improve curving behavior of a railway vehicle	Lateral wheel-set model	LQR and LQG.	Investigated an active secondary suspension control method using secondary yaw control to improve the curving behavior. To achieve desired state feedback controller is designed using LQR and LQG. The effectiveness of the proposed actuation concept is investigated in a multi-body simulator.
(Y. Jiang et al., 2019)	A comparison study of ride comfort indices between Sperling's method and EN 12299	Continuous Comfort index, Mean Comfort index, and Sperling index.	—	Ride comfort evaluation methods such as ISO 2631, EN 12,299 and Sperling's method, for assessing passenger comfort on trains are presented. The dynamic response of a V/Line passenger train in Australia is evaluated and utilized to evaluate the Continuous Comfort index, Mean Comfort index, and Sperling index.

(Dumitriu & Fologea, 2019)	Numerical analysis on the correlation between bogie dynamic response and vertical track Irregularities	Half-car model	(Pearson correlation) Covariance method	Presented a frequency response analysis of correlation between the bogie dynamic response and vertical track irregularities. The result shows that correlation function between the bogie dynamics and displacement are highly dependent upon velocity, frequency and suspension damping.
(Zheng et al., 2020b)	Combined active suspension and structural damping for suppression of flexible bodied railway vehicle vibration	Flexible and rigid half-car model	$H_2$ , $H_\infty$ and Sky hook damping	A decentralized active control scheme for suppressing the vertical vibration is presented in which sky hook damping is used for active suspension control. The model/parametric uncertainties are also added in both flexible and rigid mode to guaranteed the robustness of system.
(Muñoz et al., 2019)	Multi-body model of railway vehicle with weakly coupled vertical and lateral dynamics	3-D coupled dynamic model between vehicle and track irregularities	Numerical procedure	Presented a numerical model which calculate the lateral and vertical dynamics in the presence of track irregularities on straight track. While on a curved path, the simulation is done without irregularities.
(Zhu et al., 2018)	A Low-Cost Lateral Active Suspension System of the High-Speed Train for Ride Quality Based on the	A 17 DOF	IM -based resonant, LQR and H-infinity	An internal model based resonant control system is presented to control the lateral vibrations. A 17 DOF model including suspension deflection, actuator saturation and irregularities (random and periodic) is

	Resonant Control Method			considered. To suppress the vibration three principles (IM - based resonant, LQR and H-infinity) are presented.
(Molatefi et al., 2017)	Stability and safety analysis of an active steering bogie according to EN 14363 standard	Five wagons with single wheel-set bogie	Phase lead-lag compensator/ SIMPACK software	Proposed a dynamic model which study the effect of change in angle of attack and conicity of wheelset on lateral dynamics. This system uses a simple phase lead-lag compensator controller for active steering to improve the derailment coefficient and ride characteristics.
(Verma et al., 2017)	Optimization of Fractional Order PID Controller Using Grey Wolf Optimizer	Second-order plus time-delay	GWO tuned PID	This study proposes a novel evolutionary technique for optimising the parameters of a fractional order controller in order to regulate two types of systems: systems with time-delay and higher order systems. The grey wolf optimizer, an evolutionary approach, is employed for the optimization of both integer and fractional order controllers.
(X. Wei et al., 2016)	A semi-active control suspension system for railway vehicles with magneto-rheological fluid dampers	17-DOF	Simple feedback control method	Proposed a system which is composed of four magneto-rheological fluid damper in the primary suspension to improve the ride comfort and curving performance. A 17 DOF model is used to study the lateral dynamic behavior of vehicle.

(Leblebici & Türkay, 2016)	Track Modelling and Control of a Railway Vehicle	14-DOF	LQG	Active suspensions are designed with the help of LQG controller to resist the vibration level that comes due to random track input. 14 DOF lumped parameter model is used in which 10 DOF represent the half rail model and one degree of freedom each under four wheels represent the track model.
(Bailey & Hedrick, 2015)	Railway vehicle energy dissipation due to lateral vehicle/track interaction	23-DOF	Kalker's DUVOROL algorithm	This paper reviews the use of active suspension to improve the ride quality of a railway vehicle in lateral and vertical direction along with stability analysis in lateral direction. The various actuation technological ongoing work across world at that time are also discussed.
(Zhou et al., 2014)	Robust system state estimation for active suspension control in high-speed tilting trains	12- DOF tilting model	H-infinity	Proposed an active control for train tilting integrated with active lateral suspension system. The extended H-infinity state estimator filter is used to estimate the vehicle body lateral acceleration and cant deficiency. To check the robustness of system various model uncertainties are also added.
(Metin & Guclu, 2014a)	Rail Vehicle Vibrations Control Using Parameters	5-DOF	GA based PID controller	An adaptive PID controller is designed to control the vertical vibration of a quarter car rail. A 5 DOF

	Adaptive PID Controller			model is used. GA is used for select the new parameters of PID controller. The simulation is done on different rail speed and varying load conditions to check the robustness of proposed system.
(Zong et al., 2013)	Semi-active $H_{\infty}$ control of high-speed railway vehicle suspension with magneto-rheological dampers	17-DOF	$H_{\infty}$ and ANFIS	A semi-active suspension system to improve the lateral dynamics of railway vehicle is proposed. The suggested semi-active controller consists of a ANFIS inverse MR damper model for the damper control and a $H_{\infty}$ controller for the system controller.
(Sezer & Atalay, 2011)	Dynamic modeling and fuzzy logic control of vibrations of a railway vehicle for different track irregularities	54-DOF	Fuzzy logic controller	The simulations of vibration analysis with fuzzy logic controller are obtained in time and frequency domains with 54 DOF mathematical model and the results are compared with passive controlled status.
(Jalili & Salehi, 2011)	Wheel/rail contact model for rail vehicle dynamics	A new wheel-rail contact model	Virtual penetration theory	A new method to find the contact angle and contact forces is proposed which allows to calculate the contact forces by taking flexible, non-elliptical and multiple contact patches. This is the advancement of STRIPE method in which contact points at penetrated surface are joined as such they make isosceles triangle as their projection.



(Metin & Guclu, 2011)	A Comparison of Control Algorithms for a Half Rail Vehicle Model under Track Irregularity Effect	Half-car model	PID and Fuzzy controller	Bounce and pitch motion (vertical motion) of railway vehicle body with passenger seat is investigated. The suspensions are actively controlled by the PID and Fuzzy controller. Then performance of both controllers is compared with each other for same track irregularities.
(Pacchioni et al., 2010)	Active suspension for a two-axle railway vehicle	Half car model	sky hook damping and LQG optimal control	Proposed a system to improve the ride comfort of a two-axle light weighted train. Two active configurations are considered: sky hook damping and LQG optimal control. The transfer function model of actuation element is also considered with suspension element to review the performance of whole system.
(D. H. Wang & Liao, 2009a)	Semi-active suspension systems for railway vehicles using magnetorheological dampers. Part I: System integration and modelling	17-DOF	LQG	Acceleration level of car body, truck (bogie) frame and wheelset are evaluated. The simulated results are compared with passive control strategies (ON and OFF mode) used for suspension in railway vehicle.
(Eski & Yildirim, 2009)	Vibration control of vehicle active suspension system using a new robust	7-DOF	Robust recurrent	Proposed a neural network based robust controller for vehicle active suspension to suppress the vibration. A full 7 DOF model is

	neural network control system,		Neural-Network	used along with relative displacement of sprung mass with respect to all four unsprung masses. The PID controller is used to compare the developed RNN control system.
(D. H. Wang & Liao, 2009b)	Semi-active suspension systems for railway vehicles using magneto-rheological dampers. Part II: simulation and analysis	17-DOF	Kalman filter with LQG control law	This part of paper proposed the 17 DOF mathematical model to investigate the lateral, yaw and roll motion of rail body, bogie and wheelset using MR damper. The state variables of model are predicted with the help of Kalman filter corporate with LQG control law.
(Piotrowski & Chollet, 2007)	Wheel – rail contact models for vehicle system dynamics including multi-point contact	Multi-point contact model	Computer program CONTACT	Presented a multi-point interaction model to find the contact forces. The various non-elliptical contact patches geometry is approximated by ellipse and resulted creep forces are calculated. Another way is to represent the contact surfaces geometry as penetrated one and creep forces are calculated by the use of approximation method and program CONTACT. The results are compared with the results that come from FEM.
(R. Goodall, 2007)	Active railway suspensions: Implementation	Review on multi-models	Various control strategies	This paper gives a comprehensive survey of active suspension technology evolved for last thirty years. This

	status and technological trends			gives a brief idea about the scope, degree and technology used so far in railway history. This survey mainly focusses on establishment of active steering and active primary suspension
(Steenbergen, 2006)	Modelling of wheels and rail discontinuities in dynamic wheel–rail contact analysis	Two- or multi-point contact model	Numerical solution method based on time and frequency domain.	The behavior of contact forces is studied by applying step or dip type of irregularities over the track. The transient double or multi-point contact is considered. Forces developed at wheel rail interface are not only due to geometrical impact load but also due to short length irregularities.
(Shabana et al., 2004)	Development of elastic force model for wheel/rail contact problems	An elastic based wheel-rail contact model	Differential equations; Lagrange formulation	A new formulation based on elastic approach for wheel rail contact is presented. Four surface parameters are used to describe the wheel rail surface and multiple contact points are taken. Train arc length travelled by wheelset is calculated by adding first order differential equation to multi body equation separately. Numerical results obtained by this method are compared with constraint approach.
(Tronic et al., 2000)	Mechatronic solutions for high-speed railway vehicles	Various active steering models	$H_2$ optimal control and robust $H_\infty$	Different control schemes are presented for active steering of railway vehicle. The main purpose of study is to improve the

				curving behavior and ride comfort of three wheelset vehicle system. The lateral acceleration is studied with active control strategy such as IRW, DSW and compared with passive control strategies.
(Eickhoff et al., 1995)	A Review of Modelling Methods for Railway Vehicle Suspension Components	All railway vehicle suspension to control algorithms defined above.	—	This paper gives the comprehensive idea for studying the dynamic behavior of railway vehicle in real situation. Since real systems are non-linear in nature it, is necessary to include that non linearity in the mathematical model. This paper also provides the complication that comes by adding the non-linearity in the simulation process and how accuracy affected.
(Zhai & Sun, 1994)	A Detailed Model for Investigating Vertical Interaction between Railway Vehicle and Track	10-DOF	Hertzian non-linear elastic contact theory	A model is developed to study the vibrational characteristics and dynamic vertical interaction between vehicle and track coupling system in the domain of high speed. It concluded that wheel rail forces are directly proportional to velocity and also affected by the un-sprung mass.
(Hrovat, 1993)	Applications of optimal control to advanced automotive suspension design	Quarter, half and full-car model	LQG	The optimal control technique for study the ride and handling capabilities of vehicles by considering quarter, half and full car model is presented.
(Jawahar et al., 1990)	Mathematical modelling for lateral dynamic simulation of a railway vehicle with conventional	7-DOF	ADAMS method	Present a non-linear mathematical model of railway vehicle and track model to find the lateral dynamics by evaluating the contact

	and unconventional wheelset			forces. The factors which affect the hunting behavior along with vibration of rail are calculated. The time domain analysis shows that unconventional system has lower level of vibration as compare to conventional wheelset.
(Kaiker 1991; Willumeit and Kalker 1979)	Wheel-Rail Contact Theory Survey of Wheel-Rail Rolling Contact Theory	Hertzian model to 3-dimensional model	Various computer program such as CONTACT, FASTSIM etc.	This paper surveyed the rolling contact theories that are established to solve the common problem of contact forces. It surveyed the evolution of force-creepage law starting from Carter 2-D theory to kalker complete theory which involve kalker simplified theory and others contribution also. Numerical solutions with the help of computer programs such as CONTACT or FASTSIM are also discussed.

## 2.3 Conclusions

This chapter covers various facets of active suspension systems: 'Modeling of vehicle and rail-wheel contact', 'real actuators', and control architecture. A wide range of research on active vibration control of railway vehicles has been documented. Over 1000+ relevant articles have been published in this field within the past three decades. Nevertheless, a significant portion of the controller development has primarily been examined on small-scale models, and only a small number of them have been put into practice. Although the theoretical studies have shown promising results, there needs to be more documentation on the full-scale model of high-performance controllers in real systems. This lack of reporting may raise concerns about the reliability of the techniques.

Inspired by the aforementioned literature, the present work is focused on intelligent control strategies aimed at improving the ride comfort of railway vehicles through the application of hybrid techniques that combine classical methods with metaheuristic approaches.

## DYNAMIC MODELING OF RAILWAY VEHICLE

---

*Mathematical modeling is a navigator that leads us to an in-depth understanding of the behavior, complexities, and practical applications of dynamic systems. This chapter introduces a mathematical model of the railway vehicle that has 38 degrees of freedom. The model includes the wheel-rail contact forces and the rail irregularity model. The critical and operating speed of LHB coach under different track irregularities are evaluated using the 2-dimensional state space model. Then, the proposed model is validated with the experimental data on human ride comfort.*

### 3.1 Introduction

The ride comfort of passengers is an important parameter for evaluating the performance of railway vehicles. As discussed in the literature, many standards/models, such as quarter car, half car, and full car, have been proposed to evaluate the human comfort of railway vehicles. Most of the analytical models have predominantly focused on the uncoupled behavior of the railway vehicle. But, in the real world, a strong coupling exists between the six motions of a railway vehicle. Therefore, in this work, first, a 38-DOF coupled dynamic model of railway vehicles integrated with the wheel-rail contact forces and rail irregularities is developed. All the equations of motion are developed in the body frame of reference. For this purpose, a general coordinate system of the vehicle body with respect to an inertial frame of reference is selected. Then, the developed model is solved using the two-dimensional state-space continuous approach, and the performance is analyzed in three parts. In the first part, the model determines the vehicle's stability region, specifically focusing on critical speed. This analysis helps to identify the speed range within which the vehicle remains stable. The second part uses the model to evaluate the acceleration response of the vehicle's motions under three types of random track irregularities (vertical profile, lateral alignment, and cross-level) (Q. Zhu, Li, et al., 2018), and the 3-D graphical representation of the response PSDs has been given. The root mean square values of the vehicle's vertical, lateral, pitch, roll, and yaw acceleration at different train speeds are analyzed numerically. Finally, in the third part, the ride comfort index of

railway vehicle is evaluated using Sperling's method, and the simulated results are validated with experimental results reported by the Research Design and Standard Organization (RDSO), Lucknow (India). In this work, the system outputs are represented in the frequency range, aligning with the sensitivity range of human organs.

### 3.2 General Co-ordinate system

Multibody dynamics are expressed by rigid and flexible bodies on the basis of their elastic deformation. Consider vehicle body, bogies and wheels as rigid bodies' co-ordinates system are defined, in which OXYZ defines the global inertial frame of reference and  $o'x'y'z'$  are the fixed body coordinates at center of mass shown in Figure 3.1.

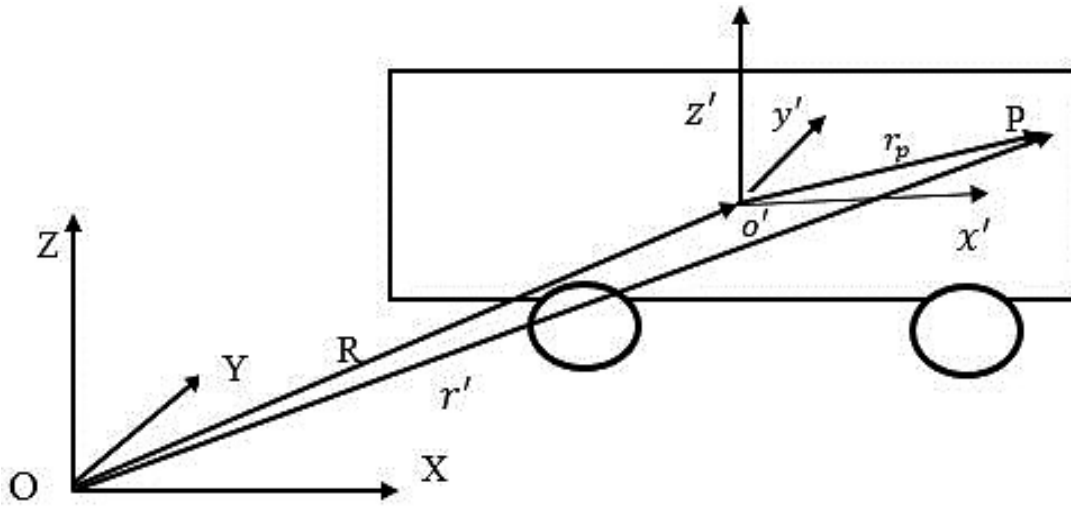


Figure 3.1 General co-ordinate system of railway system

Consider an arbitrary point P on one rigid body, then absolute position vector  $r_p$  can be expressed as:

$$r' = R + r_p \quad (3.1)$$

$$r' = R + T_i \vec{r}_p \quad (3.2)$$

where  $T_i$  is the rotational matrix with respect to global co-ordinate system described as:

About Z-axis:

$$\begin{bmatrix} \cos\alpha & -\sin\alpha & 0 \\ \sin\alpha & \cos\alpha & 0 \\ 0 & 0 & 1 \end{bmatrix} \quad (3.3)$$

About Y-axis:

$$\begin{bmatrix} \cos\alpha & 0 & \sin\alpha \\ 0 & 1 & 0 \\ -\sin\alpha & 0 & \cos\alpha \end{bmatrix} \quad (3.4)$$

About X-axis:

$$\begin{bmatrix} 1 & 0 & 0 \\ 0 & \cos\alpha & -\sin\alpha \\ 0 & \sin\alpha & \cos\alpha \end{bmatrix} \quad (3.5)$$



### 3.3 Wheel-rail contact model

For calculating the forces at contact point same global co-ordinate system is considered. The only difference is that a local coordinate system  $O'X'Y'Z$  is added in the system in which position  $X'=X-Vt$ , where  $V$  is the velocity of vehicle. Contact forces between wheel and rail can be calculated by using Hertzian spring stiffness model in which normal contact forces are developed due to deformation (Spring et al., 2011) of surfaces at contact and tangential creep forces are calculated using Kalker linear theory by considering the bodies as elastic in nature. These creep forces arise because of relative velocities difference at wheel and rail contact patch. The calculation of normal and tangential stresses assumes that the pressure distribution at the contact patch is parabolic, as described in Eqn. (3.6), and pressure profile is shown in Figure 3.2 (a). Hertzian spring coefficients are derived by using Simpson 1/3<sup>rd</sup> rule whose values are given in Appendix 1 and pressure profile along half space is shown in Figure 3.2 (b).

$$p(x, y) = p_o \sqrt{1 - \frac{x^2}{a^2} - \frac{y^2}{b^2}} \quad (3.6)$$

Where  $p_o$  is maximum load on the wheelset.

The creep forces are determined by imagining a train going on a straight track without any curves (Srivastava et al., 2019). The three creep factors—lateral, longitudinal, and spin moment (along the z-axis)—are expressed as follows in the Kalker linear theory:

$$F_{cx} = -f_{11} \xi_x \quad (3.7)$$

$$F_{cy} = -f_{22} \xi_y - f_{23} \xi_{sp} \quad (3.8)$$

$$M_{cz} = -f_{23} \xi_y - f_{33} \xi_{sp} \quad (3.9)$$

where,

$$\xi_x = 2 \left( \frac{a \dot{\varphi}_{wJ}}{V} \right) \quad (3.10)$$

$$\xi_y = \frac{y_{wJ}}{V} + \varphi_{wj} \quad (3.11)$$

$$\xi_{sp} = \frac{\dot{\varphi}_{wJ}}{V} \quad (3.12)$$

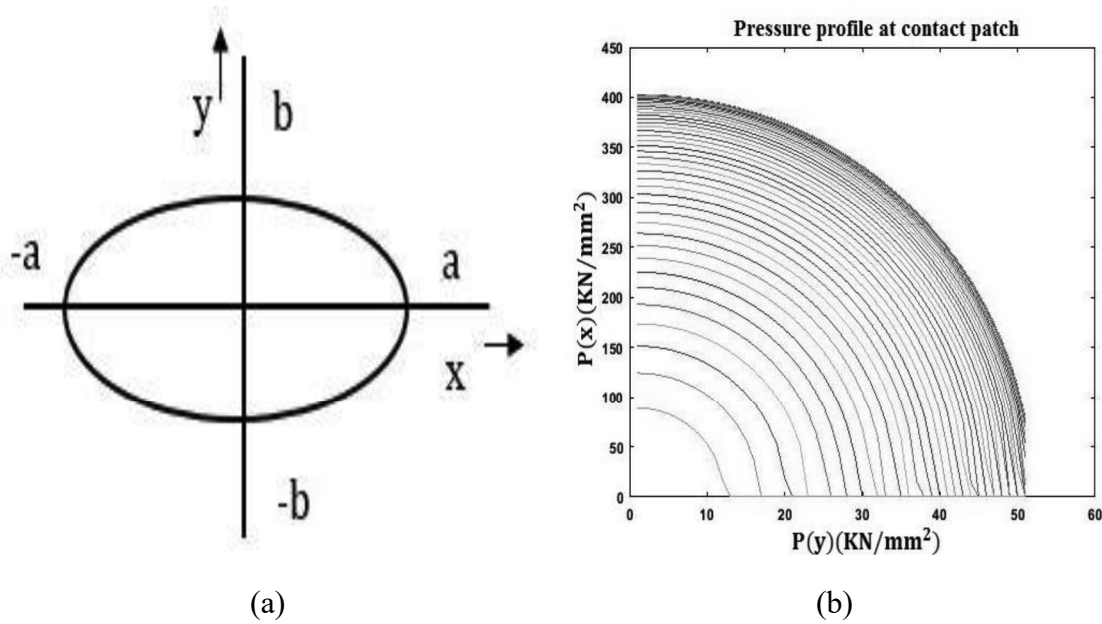


Figure 3.2 (a) Pressure distribution and (b) Pressure profile at contact patch

### 3.4 Analytical model of railway vehicle system

The railway vehicle used in this study is similar to LHB coaches used in the Shatabdi Express (Mech, 2018) chair train, which has one car body, two FIAT bogies (Handbook & Bogie, 2012), and four pairs of wheelsets. The spring system connecting the wheelsets with bogies is a primary suspension system. In contrast, the system that connects the bogies with the car body is the secondary suspensions system. This part focuses on dynamic modelling, namely the analysis of the six-degrees-of-freedom (6-DOFs) behaviors of the car body and bogie, along with the five-degrees-of-freedom (5-DOF) motions of the wheelsets. It gives a total of 38-degrees-of-freedom (DOFs) lumped parameter model as shown in Figure 3.3. The proposed mathematical model also collaborates with the wheel-rail creep forces and tracks irregularities as given in the Eqns. (3.14)-(3.30). For the wheel-rail contact forces, the non-Hertzian contact model proposed by Piotrowski et al. has been utilized (Piotrowski & Kik, 2008), in which the creep forces are determined with the help of FASTSIM algorithm. The physical parameters used in this study have been collected from Rail Coach Factory Kapurthala (Rail Coach Factory Kapurthala Official Website 2021), Jalandhar. The dynamic model of the vehicle is developed by using the Newton-Euler equations (Bongardt & Kirchner, 2017) of force-moment balance given as:

$$\sum F_i = \frac{dP_i}{dt} ; \sum M_i = \frac{dL_i}{dt} \quad (3.13)$$

Where  $\sum F_i$  is the sum of all forces and  $\frac{dP_i}{dt}$  is the change in linear momentum

$\sum M_i$  is the sum of all moments and  $\frac{dL_i}{dt}$  is the change in angular momentum

Assumptions:

- (1) All bodies are rigid.
- (2) The parameters of vehicle and track do not change with time.
- (3) The linear range of spring stiffness is used with viscous damping.
- (4) Rolling, pitching, and yawing angles are small such that,  
 $\sin(\beta_i) = \beta_i$  and  $\cos(\beta_i) = 1$ , where  $\beta_i = \theta, \phi, \varphi$
- (5) The vehicle is moving with constant velocity in +ve  $X_c$ - direction.
- (6) There is no wheel lift, and wheels are always in contact with rails.

### 3.4.1 38-DOF dynamic model of railway vehicle

The definitions of various symbols used in the dynamic modeling of the vehicle have been given in the list of symbols.

#### 3.4.1.1 Vehicle body differential equations

$$M_c \ddot{X}_c + 2K_{2x}[2(X_c + h_3\varphi_c) - X_{t1} - X_{t2}] = 0 \quad (3.14)$$

$$M_c \ddot{Z}_c + 2K_{2z}[(Z_c - Z_{t1}) + (Z_c - Z_{t2})] + 2C_{2z}[(\dot{Z}_c - \dot{Z}_{t1} + \dot{Z}_c - \dot{Z}_{t2})] = [F_{z1} + F_{z2} + F_{z3} + F_{z4}] \quad (3.15)$$

$$M_c \ddot{Y}_c + 2K_{2y}[2(y_c + h_3\theta_c) - y_{t1} - y_{t2} - h_2\theta_{t1} - h_2\theta_{t2}] + 2C_{2y}[2(\dot{y}_c + h_3\dot{\theta}_c) - \dot{y}_{t1} - \dot{y}_{t2} - h_2\dot{\theta}_{t1} - h_2\dot{\theta}_{t2}] = [F_{y1} + F_{y2}] \quad (3.16)$$

$$I_{zc} \ddot{\Psi}_c + 2L_b K_{2y}(2L_b \Psi_c - y_{t1} + y_{t2} - h_2\theta_{t1} + h_2\theta_{t2}) + 2L_b C_{2z}(2L_b \dot{\Psi}_c - \dot{y}_{t1} + \dot{y}_{t2} - h_2\dot{\theta}_{t1} + h_2\dot{\theta}_{t2}) + 2d_s K_{2x}(2\Psi_c - X_{t1} - X_{t2}) = L_b [F_{y1} - F_{y2}] \quad (3.17)$$

$$I_{xc} \ddot{\theta}_c + 2b_2^2 K_{2z}(2\theta_c - \theta_{t1} - \theta_{t2}) + 2b_2^2 c_{2z}(2\dot{\theta}_c - \dot{\theta}_{t1} - \dot{\theta}_{t2}) + 2h_3 K_{2y}\{2(y_c + h_3\theta_3) - y_{t1} - y_{t2} + h_2\theta_{t1} + h_2\theta_{t2}\} + 2h_3 c_{2y}(2(\dot{y}_c + h_3\dot{\theta}_3) - \dot{y}_{t1} - \dot{y}_{t2} + h_2\dot{\theta}_{t1} + h_2\dot{\theta}_{t2}) = [h_3(F_{y1} + F_{y2}) + b_2((F_{z1} + F_{z3}) - (F_{z2} + F_{z4}))] \quad (3.18)$$

$$I_{yc} \ddot{\phi}_c + 2L_2 K_{2z}(2L_b \phi_c + Z_{t1} - Z_{t2}) + 2L_b C_{2z}(2L_b \dot{\phi}_c + \dot{Z}_{t1} - \dot{Z}_{t2}) = [L_b(F_{z1} + F_{z2}) - (F_{z1} + F_{z2})] \quad (3.19)$$

## 3.4.1.2 Bogies differential equations (i=1, 2)

$$M_{t1}\ddot{X}_{ti} + 2c_{1x} \left[ \left( 2\dot{X}_{ti} - (\dot{X}_{w(2i-1)} + \dot{X}_{w(2i)}) \right) \right] + 2k_{1x} \left[ \left( 2X_{ti} - (X_{w(2i-1)} + X_{w(2i)}) \right) \right] + 2k_{2x}[X_{ti}X_c] = 0 \quad (3.20)$$

$$M_t\ddot{Z}_{ti} + 2c_{1z} \left[ \left( 2\dot{Z}_{ti} - (\dot{Z}_{w(2i-1)} + \dot{Z}_{w(2i)}) \right) \right] + 2c_{1z}[(\dot{Z}_{ti} - \dot{Z}_c) - (-1)^i L_b \dot{\phi}_c] + 2k_{1z} \left[ \left( 2Z_{ti} - (Z_{w(2i-1)} + Z_{w(2i)}) \right) \right] + 2k_{2z}[(Z_{ti} - Z_c) - (-1)^i L_b \phi_c] = -(F_{z(2i-1)} + F_{z(2i)}) \quad (3.21)$$

$$M_t\ddot{y}_{ti} + 2c_{1y} \left[ 2\dot{y}_{ti} - (\dot{y}_{w(2i-1)} + \dot{y}_{w(2i)}) + 2h_1\dot{\theta}_{ti} \right] + 2c_{2y}[(\dot{y}_{ti} - \dot{y}_{w(2i-1)}) - (h_3\dot{\theta}_c + h_2\dot{\theta}_{ti}) - (-1)^i L_b \dot{\psi}_c] + 2k_{1y} \left[ 2y_{ti} - (y_{w(2i-1)} + y_{w(2i)}) + 2h_1\theta_{ti} \right] + 2k_{2y}[(y_{ti} - y_c) - (h_3\theta_c + h_2\theta_{ti}) - (-1)^i L_b \psi_c] = -F_{yi} \quad (3.22)$$

$$J_{zt}\ddot{\psi}_{ti} + 2d^2_p c_{1x} \left[ 2\dot{\psi}_{ti} - (\dot{\psi}_{w(2i-1)} + \dot{\psi}_{w(2i)}) \right] + 2L_d c_{1y} \left[ 2L_d \dot{\psi}_{ti} - (\dot{Y}_{w(2i-1)} - \dot{Y}_{w(2i)}) \right] + 2d^2_p k_{1x} \left[ 2\psi_{ti} - (\psi_{w(2i-1)} + \psi_{w(2i)}) \right] + 2d^2_s k_{2x}[\psi_{ti} - \psi_c] + 2L_d k_{1y} \left[ 2L_d \phi_{ti} - (Y_{w(2i-1)} - Y_{w(2i)}) \right] = 0 \quad (3.23)$$

$$J_{xt}\ddot{\theta}_{ti} + 2h_1 c_{1y} \left[ 2h_1 \dot{\theta}_{ti} + \left( 2\dot{y}_{ti} - (\dot{y}_{w(2i-1)} + \dot{y}_{w(2i)}) \right) \right] + 2h_2 c_{2y} \left[ h_3 \dot{\theta}_c + h_2 \dot{\theta}_{ti} + (\dot{y}_{ti} + \dot{y}_c) - (-1)^i L_b \dot{\psi}_c \right] + 2b^2_1 c_{1z} \left[ 2\dot{\theta}_{ti} - (\dot{\theta}_{w(2i-1)} + \dot{\theta}_{w(2i)}) \right] + 2b^2_2 c_{2z} \left[ \dot{\theta}_{ti} - \dot{\theta}_c \right] + 2h_1 k_{1y} \left[ 2h_1 \theta_{ti} + \left( 2Y_{ti} - (Y_{w(2i-1)} + Y_{w(2i)}) \right) \right] + 2h_2 k_{2y} \left[ h_3 \theta_c + h_2 \theta_{ti} + (Y_{ti} + Y_c) - (-1)^i L_b \psi_c \right] + 2b^2_1 k_{1z} \left[ 2\theta_{ti} - (\theta_{w(2i-1)} + \theta_{w(2i)}) \right] + 2b^2_2 k_{2z} [\theta_{ti} - \theta_c] = -F_{yi} h_3 \quad (3.24)$$

$$J_{yt}\ddot{\phi}_{ti} + 2L_d c_{1z} \left[ 2L_d \dot{\phi}_{ti} + (\dot{Z}_{w(2i-1)} - \dot{Z}_{w(2i)}) \right] + 2L_d k_{1z} \left[ 2L_d \phi_{ti} + (Z_{w(2i-1)} - Z_{w(2i)}) \right] = 0 \quad (3.25)$$

## 3.4.1.3 Wheelsets differential equations (i=1, 2, while j=1; i=3, 4, while j=2)

$$M_{w1}\ddot{X}_{wi} + 2c_{1x}[\dot{X}_{wi} - \dot{X}_{tj}] + 2k_{1x}[X_{wi} - X_{tj}] - 2f_{11}\left(\frac{a\dot{\phi}_{wi}}{v}\right) = 0 \quad (3.26)$$

$$M_w\ddot{Z}_{wi} + 2c_{1z}[(\dot{Z}_{wi} - \dot{Z}_{tj}) - (-1)^i L_d \dot{\phi}_{tj}] + 2k_{1z}[(Z_{wi} - Z_{tj}) - (-1)^i L_d \phi_{tj}] + k_{hz}[2Z_{wi} - Z_{vi}] = 0 \quad (3.27)$$

$$M_w\ddot{y}_{wi} + 2k_{1y}[(Y_{wi} - Y_{tj}) - h_1\theta_{tj} + (-1)^i L_d \psi_{tj}] + 2c_{1y}[(\dot{Y}_{wi} - \dot{Y}_{tj}) - h_1\dot{\theta}_{tj} + (-1)^i L_d \dot{\psi}_{tj}] + k_{gy}[Y_{wi} - Y_{ai} - R_1\theta_{cli}] + 2f_{22} \left[ \frac{1}{v} \left( 1 + \frac{\sigma R_1}{a} \right) \dot{Y}_{wi} - \frac{\sigma R_1}{v a} \dot{Y}_{ai} - \frac{\sigma R_1^2}{v a} \dot{\theta}_{cli} - \psi_{wi} \right] = 0 \quad (3.28)$$

$$J_{zw} \ddot{\Psi}_{wi} + 2d_p^2 k_{1x} [\Psi_{wi} - \Psi_{tj}] + 2d_p^2 c_{1x} [\dot{\Psi}_{wi} - \dot{\Psi}_{tj}] + 2f_{11} \left[ \frac{\lambda_e a}{R_1} (Y_{wi} - Y_{ai} - R_1 \theta_{cli}) + \frac{a^2}{v} \dot{\Psi}_{wi} \right] + k_{gy} \Psi_{wi} = 0 \quad (3.29)$$

$$J_{xw1} \ddot{\Theta}_{wi} + 2b_1^2 c_{1z} [\dot{\Theta}_{wi} - \dot{\Theta}_{tj}] + 2b_1^2 k_{1z} [\Theta_{wi} - \Theta_{tj}] + ak_{hz} [2a\theta_{wi} + (Z_{v(i)} - Z_{v(i+1)})] + R_1 k_{hy} [R_1 \theta_{wi} + (Y_{wi} - Y_{ai})] = 0 \quad (3.30)$$

The values of parameters used in Eqns. (3.14) - (3.30) are given in Appendix 1, which are the same as that in (S. D. Singh et al., 2017), and (D. H. Wang & Liao, 2009b).

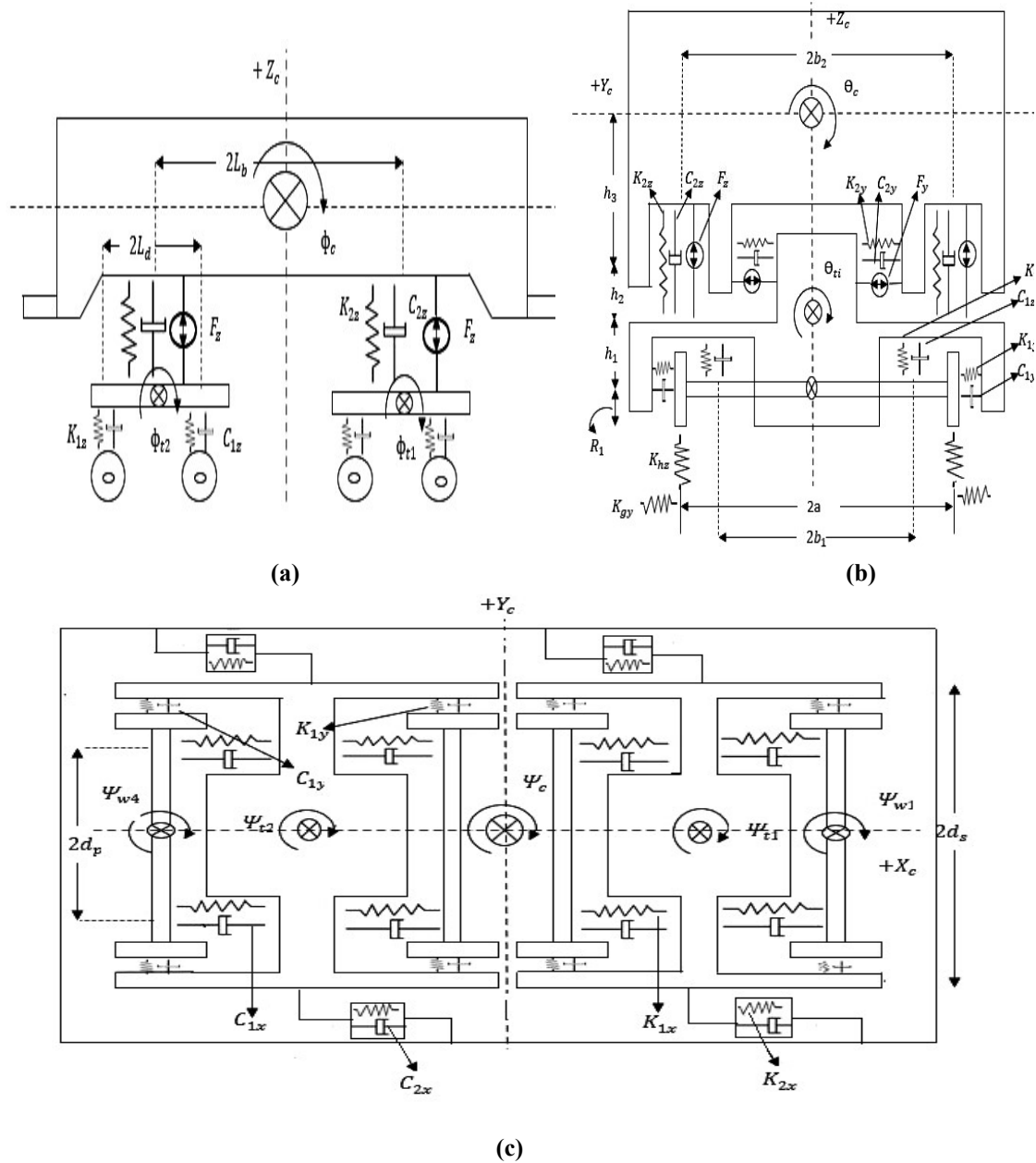


Figure 3.3 38-DOF analytical model of a railway vehicle (a) end view (b) front view (c) top view

### 3.4.2 State-space formulation

In this section, the state-space model is formulated by defining the state vector as  $x(t) = [q(t) \dot{q}(t)]^T$ , control vector as  $u(t)$ , and the disturbance vector as  $W_p(t) = [W_1(t), \dot{W}_1(t)]^T$ .

where  $q(t)$  and  $W_1(t)$  vectors are defines as:

$$q = \quad (3.31)$$

$$[Z_c, Y_c, \psi_c, \Theta_c, \varphi_c, Z_{t1}, Y_{t1}, \psi_{t1}, \Theta_{t1}, \varphi_{t1}, Z_{t2}, Y_{t2}, \psi_{t2}, \Theta_{t2}, \varphi_{t2}, Z_{w1}, Y_{w1}, \psi_{w1}, Z_{w2}, \psi_{w2}, Z'_{w3} Y_{w3}, \psi_{w3}, Z_{w4}, Y_{w4}, \psi_{w4}]^T$$

$$W_1(t) = [Z_{v1}, Z_{v2}, Z_{v3}, Z_{v4}, Y_{a1}, Y_{a2}, Y_{a3}, Y_{a4}, \theta_{cl1}, \theta_{cl2}, \theta_{cl3}, \theta_{cl4}]^T \quad (3.32)$$

$$u(t) = [F_{z1}, F_{z2}, F_{z3}, F_{z4}, F_{y1}, F_{y2}]^T, \quad (3.33)$$

Then, the governing Eqns. (3.14) - (3.30) can be written in the following matrix form:

$$[M] \ddot{q}(t) + [C] \dot{q}(t) + [K] q(t) = [F_{W_p}] W_p(t) + [F_u] u(t) \quad ; u(t)=0 \quad (3.34)$$

where  $[M]$  ( $\mathcal{R}^{n \times n}$ ),  $[K]$  ( $\mathcal{R}^{n \times n}$ ) are the constant mass and stiffness coefficient matrix.  $C(\mathcal{R}^{n \times n})$  is the variable damping coefficient matrix which can be segregated as  $[C]$  ( $\mathcal{R}^{n \times n}$ ) =  $\{[C_1] + [C_2]\}$ , where  $C_1$  is the viscous damping matrix, taken as structural damping proportional to the stiffness matrix (S. D. Singh et al., 2017) and  $C_2$  is the constant coefficient matrix that contains the constant creep forces.  $F_{W_p}(\mathcal{R}^{n \times p})$  is the disturbances coefficient matrix, acting as an input to the railway vehicle. At different speeds of vehicle, the values of  $M$ ,  $C$ ,  $K$ , and  $F_{W_p}$  matrices can be determined from the two dimensional steady space model as given in Eqns. (3.35) & (3.36).

Now, the state and output equations of the railway vehicle using two-dimensional state-space model (Duan & Xiang, 2017) are defined as:

$$\begin{bmatrix} \frac{\partial x^S(i,j)}{\partial i} \\ \frac{\partial x^E(i,j)}{\partial j} \end{bmatrix} = [A] \begin{bmatrix} x^S(i,j) \\ x^E(i,j) \end{bmatrix} + [B] [W_p(i,j)] \quad (3.35)$$

$$[y(i,j)] = [C] \begin{bmatrix} x^S(i,j) \\ x^E(i,j) \end{bmatrix} + [D] [W_p(i,j)], \quad (i,j) > 0 \quad (3.36)$$

where,  $x^S(i, j)$  is a  $2n \times 1$  state vector toward South and,  $x^E(i, j)$  is a  $1 \times j$  state vector toward East, respectively.  $W_p(i, j)$  and,  $y(i, j)$  are the disturbances and output vectors, where  $n, i, j$  &  $p$  denotes the DOFs, time, velocity points and no. of perturbations, respectively. According to Eqn. (3.34), the coefficient matrices of Eqns. (3.35), and (3.36) are determined as:  $[A]^{2n \times 2n \times j} = \begin{bmatrix} \text{zero} & I \\ -M^{-1}K & -M^{-1}C \end{bmatrix}$ ,  $[B]^{2n \times p \times j} = \begin{bmatrix} \text{zero} \\ -M^{-1}F_{w_p} \end{bmatrix}$ ,  $[C]^{n \times 2n \times j} = [-M^{-1}K \quad -M^{-1}C]$  and,  $[D]^{n \times p \times j} = [M^{-1}F_{w_p}]$ .

### 3.5 Modeling of railway track irregularities

The leading cause of vibrations in the railway's vehicle body is due to the irregularities on railway tracks and wheel structure. These irregularities act as input excitation to the railway vehicle. There are three types of track irregularity, such as vertical profile( $Z_r$ ), lateral alignment( $Y_a$ ), and cross-level( $\theta_{cl}$ ) are defined in the literature (Goodwin, 1987), which excite the vehicle's body in both vertical and lateral directions. These irregularities can be periodic as well as random in nature.

#### 3.5.1 Periodic track irregularities

The track irregularities can be broken down into harmonic components with the help of a Fourier transformation, in which the wavelengths possess special significance. At a particular speed and direction, the car body's bounce, pitch, roll, lateral and yaw motion is excited by some wavelengths, as shown in Figure 3.4. These wavelengths can be described as "critical wavelengths" for the speed (Lewis & Olofsson, 2006). According to this, the sinusoidal or periodic input function used for bounce and lateral motions is defined as

$$Z_{v1}(t), Y_{a1}(t) = A_o \sin\left(2\pi \frac{V}{\lambda_1} t\right) \quad (3.37)$$

where  $V$  is the velocity of the vehicle.  $A_o$  is the amplitude, and  $\lambda_1$  is the spatial wavelength for bounce and lateral motion, respectively, as shown in Figure 3.4 (a) & (c).

Similarly, the input function used for bounce and yaw motion is defined as:

$$Z_{v1}(t), Y_{a1}(t) = A_o \sin\left(2\pi \frac{V}{\lambda_2} t\right) \quad (3.38)$$

where  $\lambda_2$  represents the spatial wavelength for bounce and yaw motion, respectively, as shown in Figure 3.4 (b) & (d).

And the input function used for roll motion is defined as:

$$\theta_{cl1}(t) = A_o \sin(2\pi \frac{V}{\lambda_1} t) \quad (3.39)$$

where,  $\lambda_1$  is the spatial wavelength for roll motion as shown in Figure 3.4 (e).

If  $Z_{v1}$ ,  $Y_{a1}$ , and  $\theta_{cl1}$  are the excitations applied on the front wheelsets of railway vehicle, then  $Z_{v1} \sim Z_{v4}$ ,  $Y_{a1} \sim Y_{a4}$ , and  $\theta_{cl1} \sim \theta_{cl4}$  are related by the following relation:

$$\begin{cases} Z_{v2} = Z_{v1}(t - \tau_1), Z_{v3} = Z_{v1}(t - \tau_2), Z_{v4} = Z_{v1}(t - \tau_3) \\ Y_{a2} = Y_{a1}(t - \tau_1), Y_{a3} = Y_{a1}(t - \tau_2), Y_{a4} = Y_{a1}(t - \tau_3) \\ \theta_{cl2} = \theta_{cl1}(t - \tau_1), \theta_{cl3} = \theta_{cl1}(t - \tau_2), \theta_{cl4} = \theta_{cl1}(t - \tau_3) \end{cases} \quad (3.40)$$

where  $\tau_1 = \frac{2L_d}{V}$ ,  $\tau_2 = \frac{2L_b}{V}$ ,  $\tau_3 = \frac{2(L_d + L_b)}{V}$  are the time delays between the front and consecutive wheelsets.

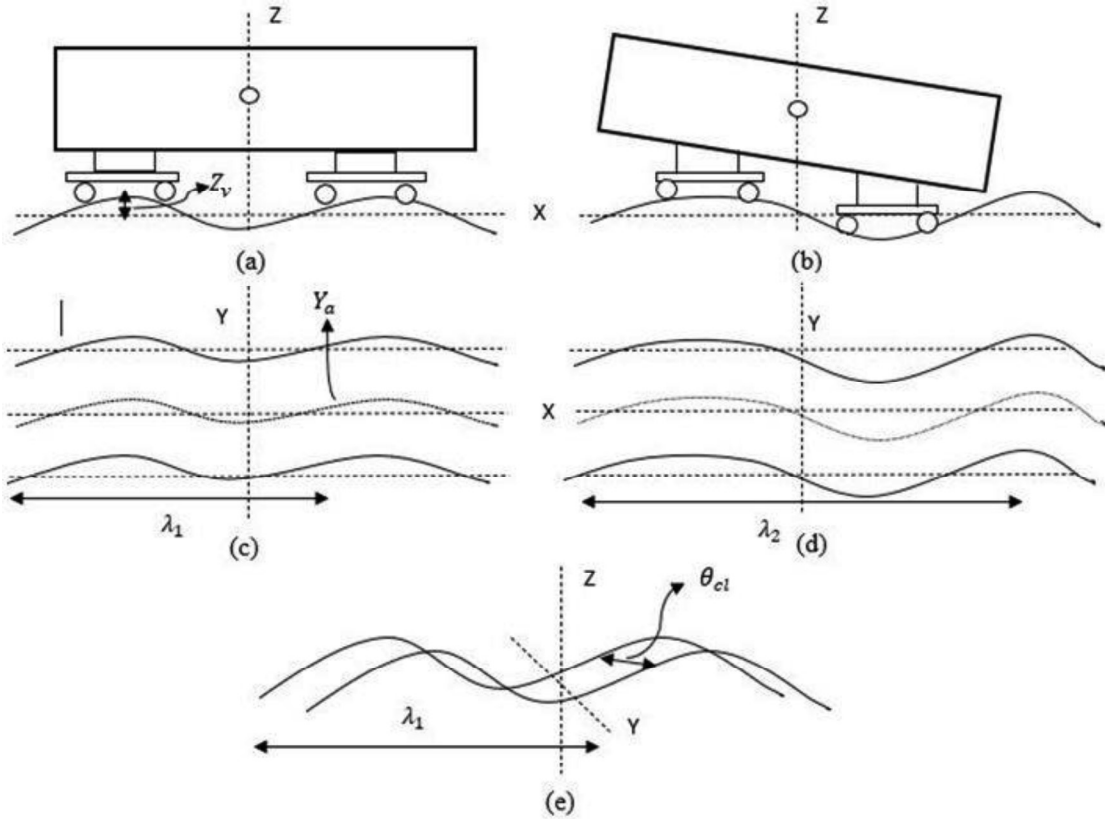


**Figure 3.4** Track irregularities (a) vertical profile (b) Lateral alignment (c) Cross-level



### 3.5.2 Random track irregularities

The real track irregularities are the superposition of harmonic waves of different amplitude, phase, and wavelength. Describing the random track irregularities is always convenient in the form of PSD (power spectral density), which are calculated by taking the Fourier Transform of the autocorrelation function (W. Zhai, 2020). In this study, the vertical and lateral responses of the vehicle's body to random track input from different classes are examined. The single-sided density function for the vertical profile, lateral alignment, and cross-level are defined in Eqns. (3.41) - (3.43). These PSDs are generally determined from the extensive collection of measured data of tracks recorded by the German Railway (Iwnicki, 2006) are given in the form of the spatial domain as:

$$S_v(\Omega) = \frac{A_v \cdot \Omega_c^2}{(\Omega^2 + \Omega_r^2)(\Omega^2 + \Omega_c^2)} \frac{m^2}{(\frac{rad}{m})} \quad (3.41)$$

$$S_a(\Omega) = \frac{A_a \cdot \Omega_c^2}{(\Omega^2 + \Omega_r^2)(\Omega^2 + \Omega_c^2)} \frac{m^2}{(\frac{rad}{m})} \quad (3.42)$$

$$S_{cl}(\Omega) = \frac{A_v \cdot \Omega_c^2 \cdot \Omega^2}{l_r^2(\Omega^2 + \Omega_r^2)(\Omega^2 + \Omega_c^2)(\Omega^2 + \Omega_s^2)} \frac{1}{(\frac{rad}{m})} \quad (3.43)$$

where  $\Omega$  is the spatial frequency of the track measured in rad/m, while  $\Omega_r$ ,  $\Omega_c$  and  $\Omega_s$  denote the cut off frequencies in rad/m. Additionally,  $A_v$ ,  $A_a$ , and  $A_g$  are the roughness constant measured in  $m^2 \cdot \frac{rad}{m}$ , and  $l_r$  represents half the distance between the two-rolling cycles of wheelset (m) (D. H. Wang & Liao, 2009a).

Now, for a railway vehicle moving at a velocity  $V$ , the excitation or input function is converted from spatial domain to time domain by using the following dispersion relation as;

$$\omega = V \Omega, \quad \Omega = \frac{2\pi}{\lambda(s)} \quad (3.44)$$

where  $\omega$  is the angular frequency,  $\lambda(s)$  is the spatial wavelength of rail

Since in both spectrums, i.e., in  $S(\omega)$  and  $S(\Omega)$  the energy contents should be the same. Therefore, let,

$$S(\omega) = \frac{S(\Omega)}{V} \quad (3.45)$$

Now, the irregularity functions are obtained by putting the Eqns. (3.44), and (3.45) into Eqs. (3.41) - (3.43), and the obtained single-sided PSDs functions can be rewritten as:

$$S_v(\omega) = \frac{A_v \cdot \Omega_c^2 \cdot V^3}{((\omega)^2 + (V \cdot \Omega_r)^2)((\omega)^2 + (V \cdot \Omega_c)^2)} \frac{m^2}{\left(\frac{rad}{sec}\right)} \quad (3.46)$$

$$S_a(\omega) = \frac{A_a \cdot \Omega_c^2 \cdot V^3}{((\omega)^2 + (V \cdot \Omega_r)^2)((\omega)^2 + (V \cdot \Omega_c)^2)} \frac{m^2}{\left(\frac{rad}{sec}\right)} \quad (3.47)$$

$$S_{cl}(\omega) = \frac{A_v \cdot \Omega_c^2 \cdot V^3 \cdot (\omega)^2}{l_r^2((\omega)^2 + (V \cdot \Omega_r)^2)((\omega)^2 + (V \cdot \Omega_c)^2)((\omega)^2 + (V \cdot \Omega_s)^2)} \frac{m^2}{\left(\frac{rad}{sec}\right)} \quad (3.48)$$

where  $\omega$  is the angular frequency of the track measured in rad/sec and  $\Omega_r$ ,  $\Omega_c$  and  $\Omega_s$  are the cut-off frequencies taken in rad/m;  $A_v$ ,  $A_a$  and  $A_g$  are roughness constant taken in  $m^2 \cdot \frac{rad}{m}$ ;  $V$  is the velocity of the vehicle;  $l_r$  is the half the distance between the two-rolling circle of the wheelset (m). The values of these constant factors and cut-off frequencies for different classes of track (W. Zhai, 2020) are given in Appendix 1. The pictorial representations of track PSDs in frequency and time domain are given in Figure 3.5. The required frequency ranges of PSDs are obtained by varying the track wavelength from 1.24-125 m.

### 3.6 System response to track irregularities and vehicle velocity

Now, for system output, the Eq. (3.34) can be simplified as follows:

$$\ddot{x}(t) + 2\zeta\omega_n\dot{x}(t) + \omega_n^2x(t) = \vec{A}W_p(t) \quad (3.49)$$

where  $x(t)$  denotes states,  $W_p(t)$  are the disturbances,  $\zeta$  are the damping ratios and  $\omega_n$  are natural frequencies of respective DOFs. Suppose  $H(\omega)$  is the complex frequency response function for state ' $x$ ' when a sinusoidal input of a specific frequency is applied to it, and  $F_p(\omega)$  be the frequency response function of that input. In this case, the frequency domain output and input of the system are related by the following equation:

$$y(\omega) = H(\omega) \times F_p(\omega) \quad (3.50)$$

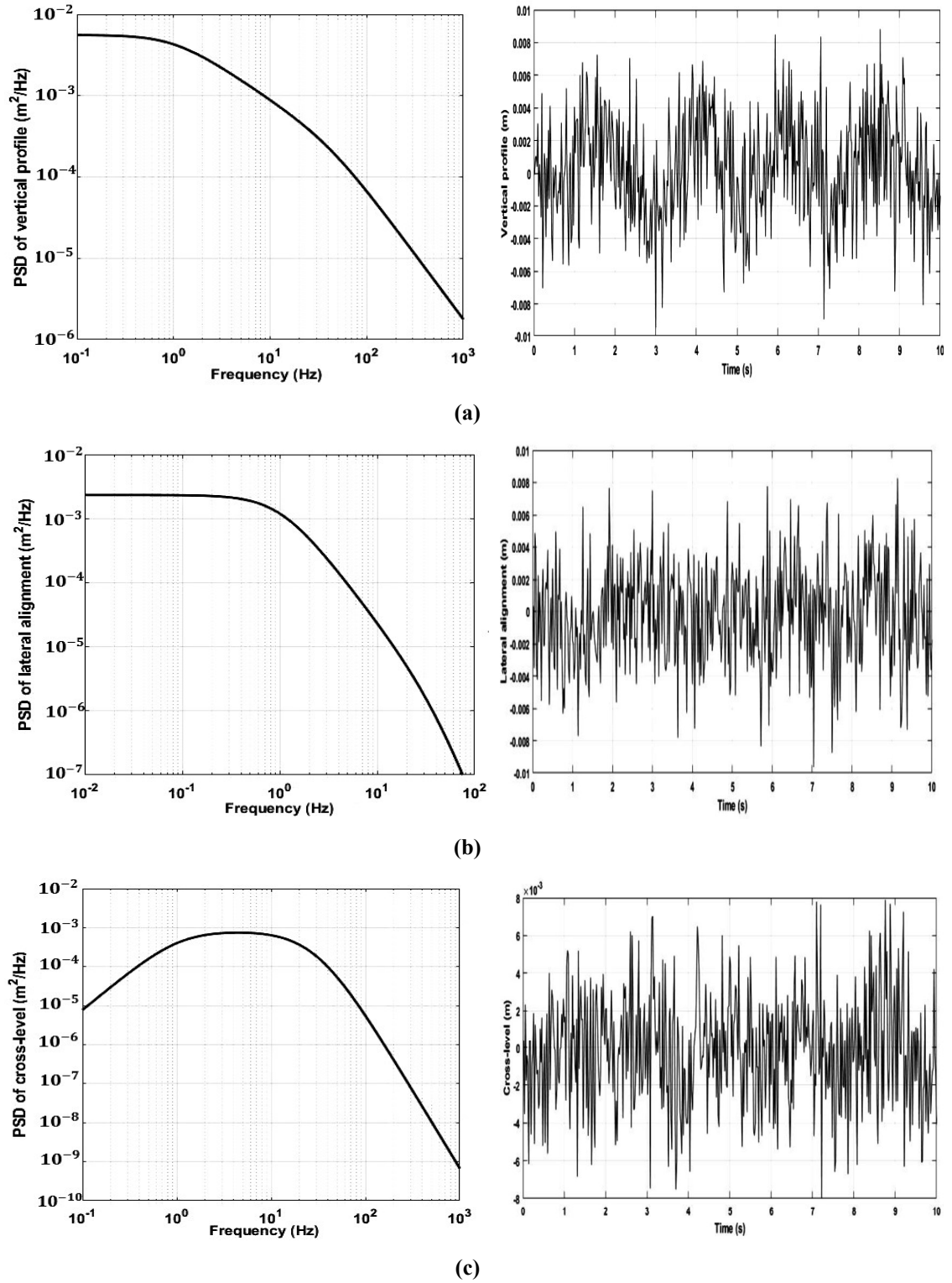


Figure 3.5 PSDs and time series of track irregularities (a) vertical profile (b) lateral alignment (c) cross-level

For the complex frequency response, three PSDs of random track irregularities i.e., vertical irregularities( $Z_v$ ), lateral irregularities( $Y_a$ ), and cross-level ( $\Theta_{cl}$ ) are considered as disturbance to the system. Now,

Let  $n_p = [Z_{v1}, Y_{a1}, \Theta_{cl1}, \dot{Y}_{a1}, \dot{\Theta}_{cl1}]^T \triangleq [Z_{vp}, Y_{ap}, \Theta_{clp}, \dot{Y}_{ap}, \dot{\Theta}_{clp}]^T$  and,

$$\hat{G}_{W1}(s) = [1, e^{-j\omega\tau_1}, e^{-j\omega\tau_2}, e^{-j\omega\tau_3}]^T$$

$$\text{Then, } N_p(s) = G_{Wp}(s) \times W_p(s) \quad (3.51)$$

$$\text{where } G_{Wp}(s) = [\hat{G}_{W1}(s), \hat{G}_{W1}(s), \hat{G}_{W1}(s), \hat{G}_{W1}(s), \hat{G}_{W1}(s)]$$

Accordingly, the delayed versions of rail disturbances are expressed in their spectral term as:

$$\begin{aligned} S_{v1}(\omega) &= S_v(\omega); S_{v2}(\omega) = S_v(\omega)e^{-j\omega\tau_1}; S_{v3}(\omega) = S_v(\omega)e^{-j\omega\tau_2}; \\ S_{v4}(\omega) &= S_v(\omega)e^{-j\omega\tau_3} \end{aligned} \quad (3.52)$$

$$\begin{aligned} S_{a1}(\omega) &= S_a(\omega); S_{a2}(\omega) = S_a(\omega)e^{-j\omega\tau_1}; S_{a3}(\omega) = S_a(\omega)e^{-j\omega\tau_2}; \\ S_{a4}(\omega) &= S_a(\omega)e^{-j\omega\tau_3} \end{aligned} \quad (3.53)$$

$$\begin{aligned} S_{cl1}(\omega) &= S_{cl}(\omega); S_{cl2}(\omega) = S_{cl}(\omega)e^{-j\omega\tau_1}; S_{cl3}(\omega) = S_{cl}(\omega)e^{-j\omega\tau_2}; \\ S_{cl4}(\omega) &= S_{cl}(\omega)e^{-j\omega\tau_3} \end{aligned} \quad (3.54)$$

where  $\tau_1 = \frac{2L_d}{V}$ ,  $\tau_2 = \frac{2L_b}{V}$ ,  $\tau_3 = \frac{2(L_d+L_b)}{V}$  and  $V$  is the velocity of the vehicle, while  $L_b, L_d$  are given in Appendix 1.

In the case of random excitations, the spectral densities provide a convenient way to analyze the system's behavior across different frequencies. Therefore, the relation between the output mean square  $S_y(\omega)$  and the input mean square spectral density  $S_{fp}(\omega)$  can be written as:

$$S_y(\omega) = |H_{i,j}(\omega)|^2 \times S_{fp}(\omega) \quad (3.55)$$

where

$$H_{i,j}(\omega) = \frac{1}{1 - \left(\frac{\omega}{\omega_n}\right)^2 + j 2\zeta_n \left(\frac{\omega}{\omega_n}\right)} \quad (3.56)$$

where  $\left(\frac{\omega}{\omega_n}\right)$  is the normalized frequency and  $\zeta$  is the damping ratio.

Then finally, the root mean square acceleration response is calculated as:

$$a_0 = \sqrt{\frac{1}{\pi} \int_{\omega_1}^{\omega_2} \omega^4 \cdot S_y(\omega) d\omega} \quad (3.57)$$

### 3.7 Results and discussions

In this section, the critical velocity of the railway vehicle is evaluated under periodic track irregularities, and then, the dynamic response of railway vehicle in terms of accelerations, and ride comfort is examined under random track irregularities.

#### 3.7.1 Calculation of critical velocity of the train

Since the vehicle's dynamic equations of motion involved the velocity term. So, with the help of governing equations of motion, we can estimate the critical speed of the vehicle at a given value of damping. To do this, we first equate the right side of Eqn. (3.34) equal to zero. Then, using the matrix  $[A]$ , the poles or eigenvalues of the dynamic system are calculated with the help of MATLAB®. These eigenvalues are expressed as:

$$\lambda_{2J-1}, \lambda_{2J} = \alpha_J \pm i\beta_J \quad (3.58)$$

where  $J$  varies from 1 to  $n$  and  $n$  is the no. of the degree of freedom and  $\alpha_J$  and  $\beta_J$  are the real and imaginary parts of poles of the system's dynamics.

Similarly, the poles of the 38-DOFs system are evaluated by varying the vehicle speed. As the train speed increases, the system's poles start moving and eventually cross the zero line, as shown in Figure 3.6. The speed at which the poles cross the zero line and become positive is the critical speed of the train. In this study, the critical point occurs at a speed of 62 m/s. Figure 3.6 (a), illustrates the variation of poles for all degree of freedom, demonstrating that the poles for most DOFs remain negative. However, only the poles associated with wheelsets move towards the positive side, rendering the system unstable, as depicted in Figure 3.6 (b).

Based on the above observation of the critical speed, the RMS value of the vehicle body's acceleration under high class-track irregularities are evaluated. In which body acceleration will be further used to calculate and compare the ride comfort of passengers in both vertical and lateral directions.

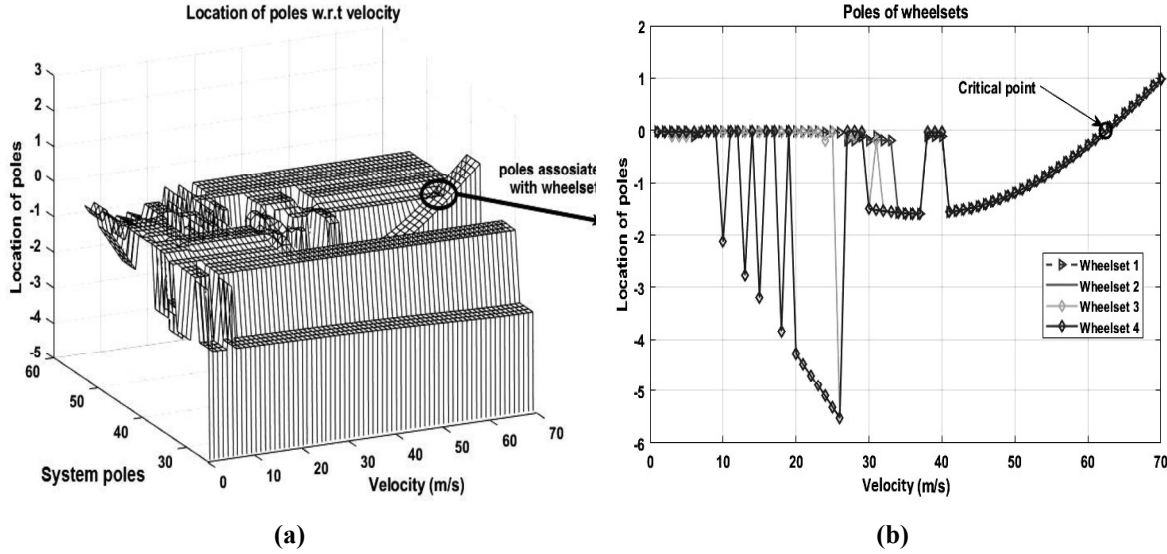


**Figure 3.6** Movement of locations of poles with respect to velocity (a) all poles of the 38-DOFs system  
(b) poles of the wheelsets

### 3.7.2 Car body accelerations

In this section, the acceleration responses of the vehicle body are evaluated under three types of random track irregularities. Using Eqns. (3.35), (3.36) & (3.51), the output frequency responses of vertical, lateral, roll, pitch, and yaw motion are represented in the form of power spectral densities (PSDs). The 3-D PSDs of acceleration responses are plotted against two variables: vehicle velocity and the frequency range sensitive to human organs. Moreover, the RMS values of the outputs are calculated using Eqn. (3.57). The high-class track irregularities from the German Railway dataset have been considered for the simulation.

The frequencies at which the PSDs of generalized accelerations exhibit their most prominent peaks are referred to as resonant peaks for the respective motion under consideration. At different speeds, the PSDs of vertical and pitch acceleration of the car body under vertical track imperfections are shown in Figure 3.7. From Figure 3.7; it is observed that the vertical and pitch motion of the car body are highly sensitive in the lower frequency range and has two dominant peaks at approximately 10 *rad/sec* and 20 *rad/sec*. It is also seen that with increasing vehicle speed, the output responses do not show significant variation along the frequency axis, except at two resonant points. In contrast, the magnitude of acceleration response increases linearly along the velocity axis.

Also, the RMS values of the acceleration response of the vertical and pitch motion under high-class track disturbances are given in Table 3.1.

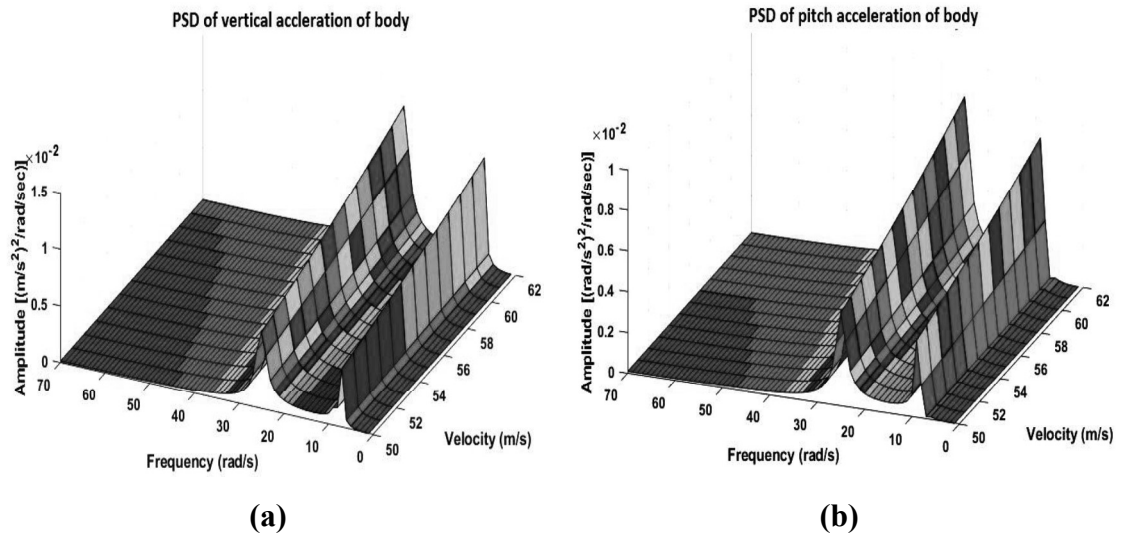


**Figure 3.7** PSDs of vehicle body acceleration under vertical irregularities (a) vertical acceleration (b) pitch acceleration

The PSDs of the car body's lateral, roll, and yaw acceleration under lateral track irregularities are shown in Figure 3.8. From Figure 3.8 (a) & (b), it is seen that the lateral and roll acceleration of the car body has three dominant peaks. Among these peaks, two demonstrate dominance in the low-frequency range ( $6 \text{ rad/sec}$ ,  $8 \text{ rad/sec}$ ), while one is prominent in the middle-frequency range ( $42 \text{ rad/sec}$ ). Notably, the magnitude of the third peak becomes more pronounced as the vehicle's velocity approaches the critical point. Simultaneously, the magnitudes of the other two peaks increase linearly. Despite these changes in magnitudes, the overall response along the frequency axes remains unchanged. On the other hand, the yaw acceleration has two resonant peaks around  $8 \text{ rad/sec}$  and  $42 \text{ rad/sec}$ , as depicted in Figure 3.8 (c). The growing behaviors of these two peaks are similar to that of vertical and roll motion. However, in terms of magnitudes, a significant difference is observed in the vehicle's yaw motion, which exhibits higher sensitivity to the track's lateral irregularities. These differences in amplitude can also be conformed from the RMS values provided in Tables 3.1.

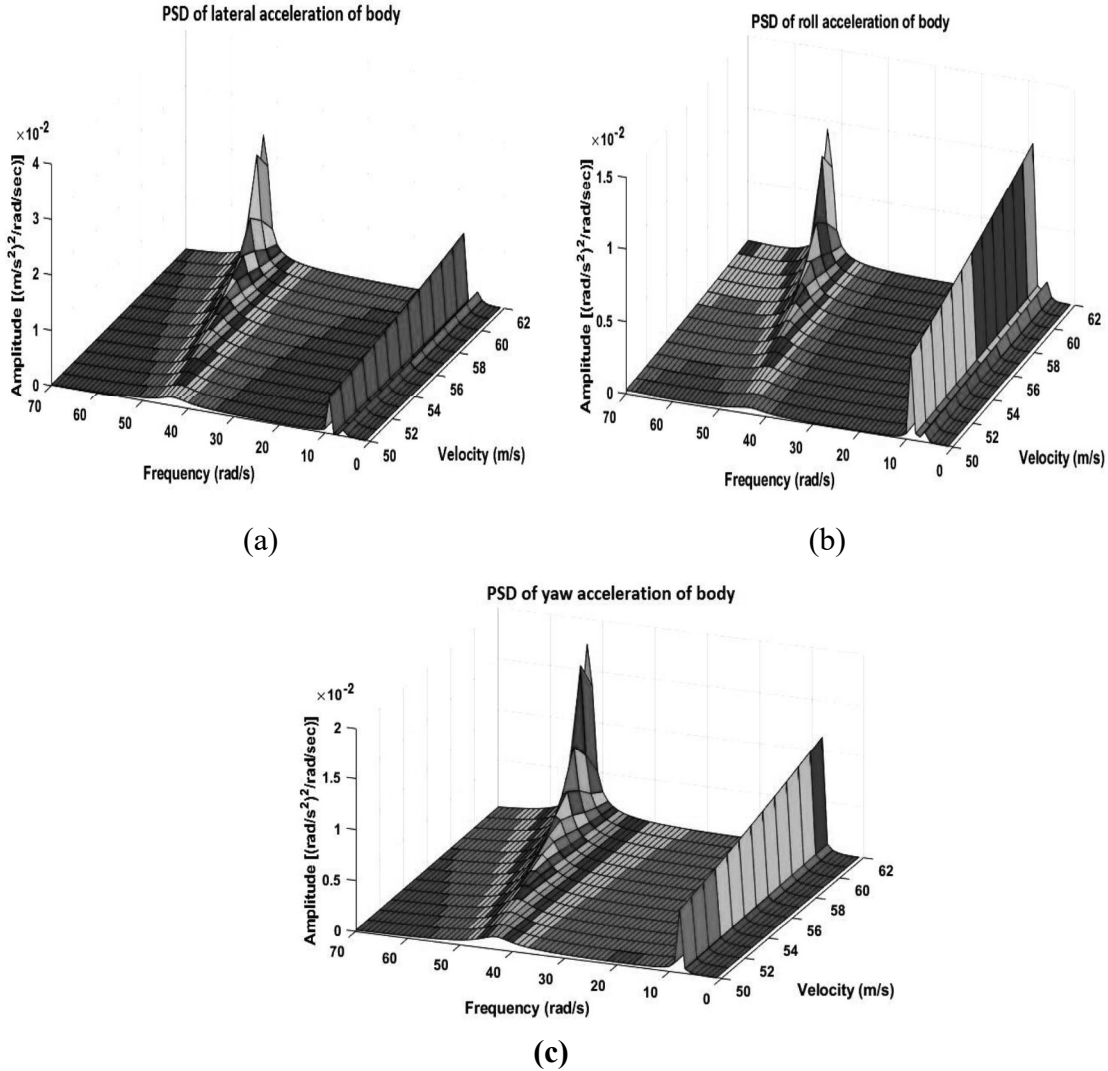


**Figure 3.8** PSDs of vehicle body acceleration under lateral irregularities (a) lateral acceleration (b) roll acceleration (c) yaw acceleration

The PSDs of the car body's lateral, roll, and yaw motions under high-class cross-level track irregularities are presented in Figure 3.9. On observing, Figures 3.9 (a) & (b), it is observed that the lateral and roll acceleration of the car body exhibit three dominant peaks (around 6 *rad/sec*, 8 *rad/sec*, and 40 *rad/sec*), with the first peak being flatter than the other two resonant peaks. This behavior is similar to what is observed in the case of lateral irregularities. However, under the cross-level irregularities, the magnitude of lateral acceleration is greater than that of lateral acceleration evaluated under the same amplitude of lateral alignment. In the case of vehicle roll and yaw motions, from Figures 3.9 (b) & (c), it is seen that the resonant peak under cross-level irregularities shows the same



behavior as we have seen in the case of lateral irregularities. The primary and significant difference between cross-level and lateral irregularities is that the RMS level of acceleration has comparatively large values under cross-level conditions. In the case of yaw motion, this difference is minimal but still higher than lateral irregularities. The RMS values of lateral, roll and yaw motions under cross-level track irregularities are given in Table 3.1.

**Table 3.1** RMS value of vehicle body acceleration under high class disturbances

	Vertical Profile		Lateral Alignment			Cross-Level		
Speed (m/s)	Vertical (m/s <sup>2</sup> )	Pitch (rad/s <sup>2</sup> )	Lateral (m/s <sup>2</sup> )	Roll (rad/s <sup>2</sup> )	Yaw (rad/s <sup>2</sup> )	Lateral (m/s <sup>2</sup> )	Roll (rad/s <sup>2</sup> )	Yaw (rad/s <sup>2</sup> )
50	0.0416	0.0106	0.0379	0.0251	0.0105	0.0451	0.0299	0.0125
51	0.0428	0.0109	0.0395	0.0263	0.0110	0.0471	0.0313	0.0131
51	0.0441	0.0112	0.0413	0.0275	0.0115	0.0491	0.0327	0.0136
53	0.0453	0.0115	0.0431	0.0287	0.0120	0.0512	0.0341	0.0142
54	0.0466	0.0118	0.0450	0.0300	0.0125	0.0534	0.0357	0.0148
55	0.0478	0.0121	0.0469	0.0314	0.0130	0.0558	0.0373	0.0155
56	0.0491	0.0125	0.0491	0.0329	0.0136	0.0583	0.0391	0.0162
57	0.0504	0.0128	0.0513	0.0344	0.0142	0.0610	0.0409	0.0169
58	0.0517	0.0131	0.0538	0.0362	0.0149	0.0639	0.0430	0.0177
59	0.0529	0.0134	0.0566	0.0381	0.0156	0.0672	0.0453	0.0186
60	0.0542	0.0138	0.0598	0.0404	0.0165	0.0710	0.0479	0.0196
61	0.0556	0.0141	0.0642	0.0433	0.0177	0.0762	0.0514	0.0218
62	0.0569	0.0144	0.0676	0.0458	0.0186	0.0802	0.0544	0.0221

Furthermore, time-varying profiles of car body accelerations in response to three different categories of random track deficiencies are illustrated in Figures (3.10) – (3.12). Here for the simulation purpose, two different vehicle velocities (180 km/h and 200 km/h) have been considered. From Figures 3.10 (a) & (b), it is seen that the amplitude of vertical and pitch acceleration of the vehicle body is greater at the speed of 200 km/h. Similarly, the vehicle body's lateral, roll, and yaw accelerations show dominance at a speed of 200 km/h compared to 180 km/h, as depicted in Figures (3.11) & (3.12). However, it is also noted

that the vehicle running at the cross-level type of irregularities will encounter higher acceleration values when compared to those resulting from lateral irregularities.

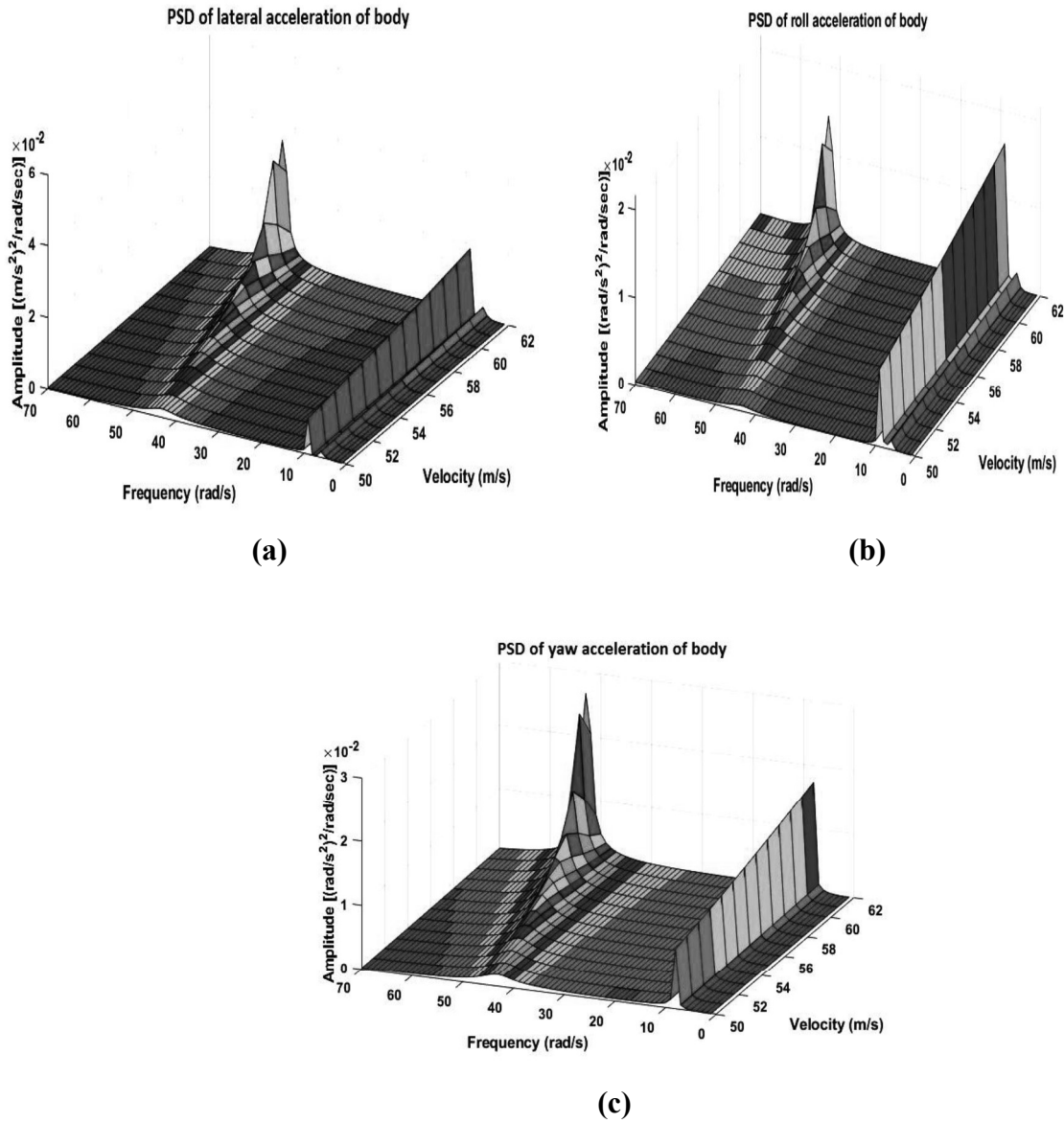


**Figure 3.9** PSDs of vehicle body acceleration under cross-level irregularities (a) lateral acceleration (b) roll acceleration (c) yaw acceleration

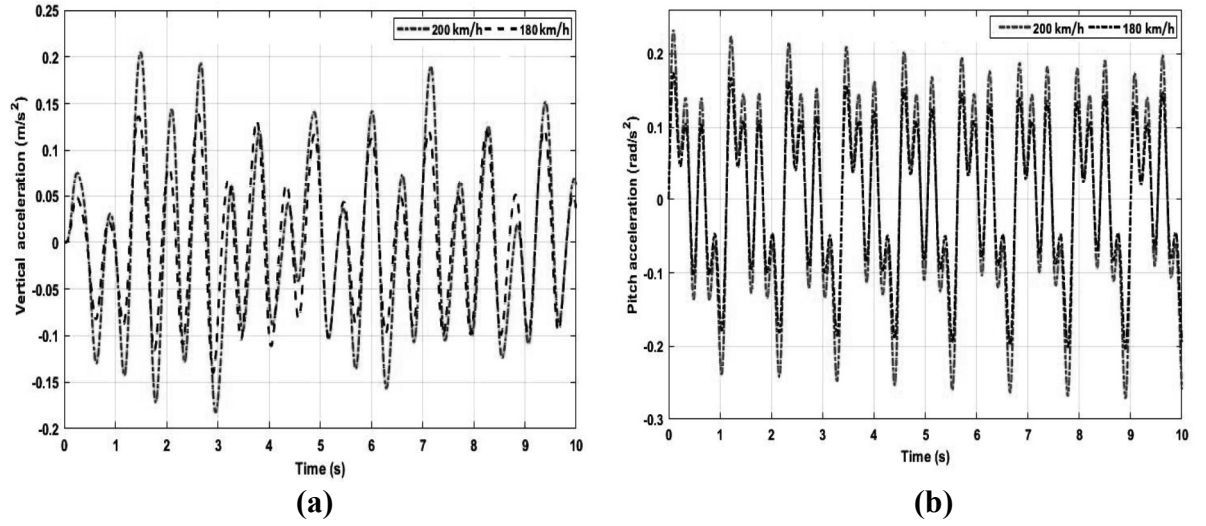


**Figure 3.10** Time histories of vehicle body acceleration under vertical irregularities (a) vertical acceleration (b) pitch acceleration

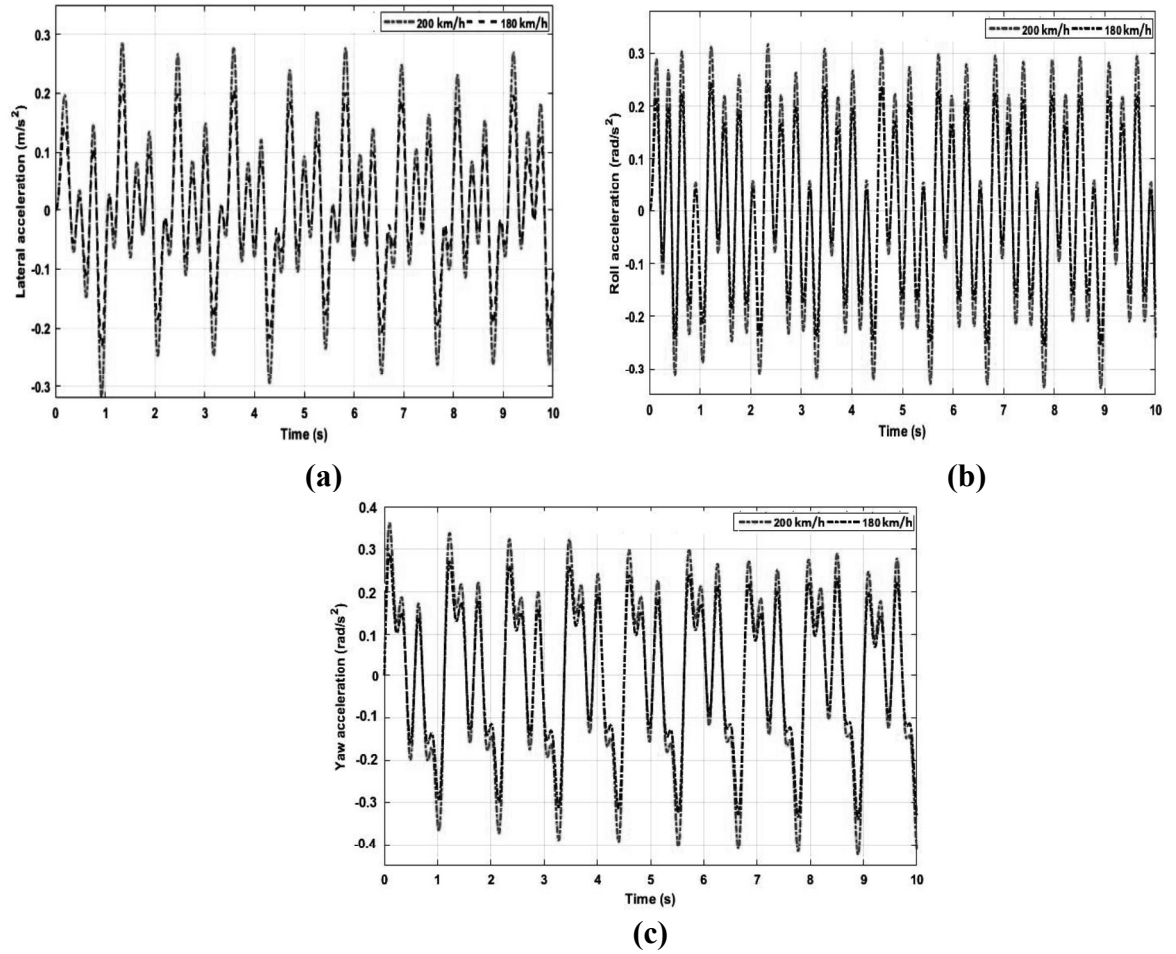


**Figure 3.11** Time histories of vehicle body acceleration under lateral irregularities (a) lateral acceleration (b) roll acceleration (c) yaw acceleration

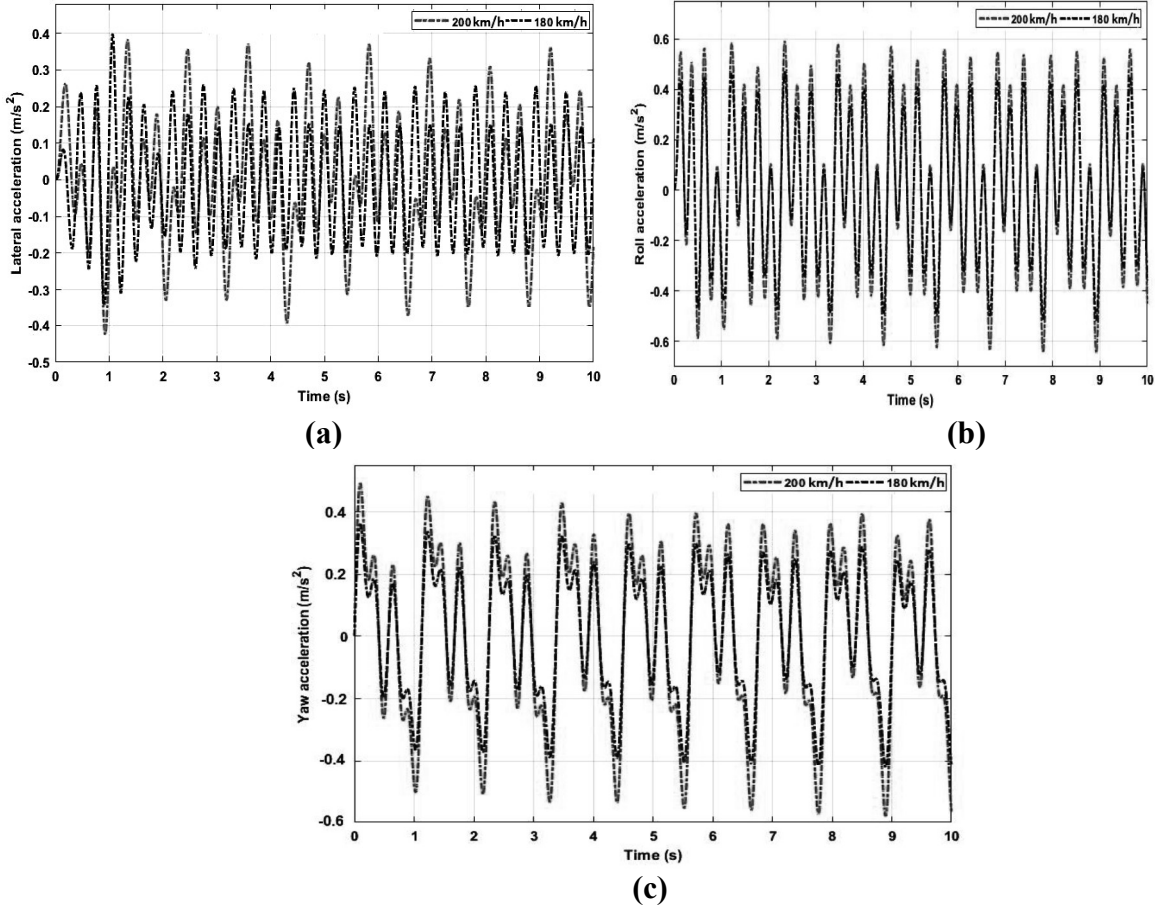


Figure 3.12 Time histories of vehicle body acceleration under cross-level irregularities (a) lateral acceleration (b) roll acceleration (c) yaw acceleration

### 3.8 Evaluation of ride comfort using Sperling's method

To evaluate the ride comfort of passengers, the  $W_z$  ride factor introduced by Sperling (Alehashem et al., 2021) is used. In this method, the vehicle's ride comfort is to be assessed according to the effect of mechanical vibration on the occupants. The evaluation scale used for determining ride comfort is given in Appendix 1. Given that the acceleration spectrum is a continuous function of frequency,  $W_z$  should also be a continuous function of frequency. The following equations can be used to find the comfort index  $W_z$  in the frequency domain:

$$W_z = \sqrt{10 \int_{0.5}^{30} a_0^3 B_s^3 d\omega} \quad (3.59)$$

$$W_z = \sqrt{10 \int_{0.5}^{30} a_0^3 B_w^3 d\omega} \quad (3.60)$$

where  $a_0$  is the acceleration amplitude, and  $B_w$  and  $B_s$  are the frequency weighting functions given as:

For vertical motion

$$B_s(f) = 0.588 \sqrt{\frac{1.911 (2\pi f)^2 + (0.25 (2\pi f)^2)^2}{(1 - 0.277(2\pi f)^2)^2 + (1.563 (2\pi f) - 0.0368 (2\pi f)^3)^2}} \quad (3.61)$$

For lateral motion

$$B_w(f) = 0.737 \sqrt{\frac{1.911 (2\pi f)^2 + (0.25 (2\pi f)^2)^2}{(1 - 0.277 (2\pi f)^2)^2 + (1.563 (2\pi f) - 0.0368 (2\pi f)^3)^2}} \quad (3.62)$$

The ride comfort index for the vertical motion of the body is calculated by multiplying and integrating the PSDs of the vertical acceleration with the vertical weighing function ( $B_s$ ) within the frequency range of 0.5-30 Hz. The graphical representation of ride comfort for vertical motion under a vertical profile is shown in Figure 3.13 (a). From Figure 3.13(a), it is seen that human exposure to mechanical vibration increases with the vehicle's velocity. The ride comfort index surpasses the safe limit as the vehicle's velocity exceeds 58 m/s speed.

Similarly, the ride comfort index of lateral motion is calculated by multiplying and integrating the PSDs of lateral acceleration output with lateral weighing function ( $B_w$ ) within the frequency range of 0.5-30 Hz. The ride comfort indices for the body's lateral motion under the high class of lateral and cross-level track irregularities are shown in Figures 3.13 (b) & (c), respectively. On observing Figure 3.13 (b), it is found that in the case of high-class track disturbances, there is a sharp increase in the level of lateral vibration as the velocity of the vehicle starts increasing beyond 58 m/s (208 km/h) and becomes worst in terms of human comfort at speed overcome 62m/s (223 km/h).

From Figure 3.13 (c), it is seen that the ride comfort index of the body's lateral motion under cross-level track disturbance shows more slope than lateral track disturbances. The value of ride comfort crosses the safe limit as the vehicle's velocity reaches 55 m/s speed

in case of high-class disturbance. Thus, based on the above findings, it can be concluded that the cross-level track irregularities affect the passenger's comfort more than vertical and lateral irregularities of the same class.

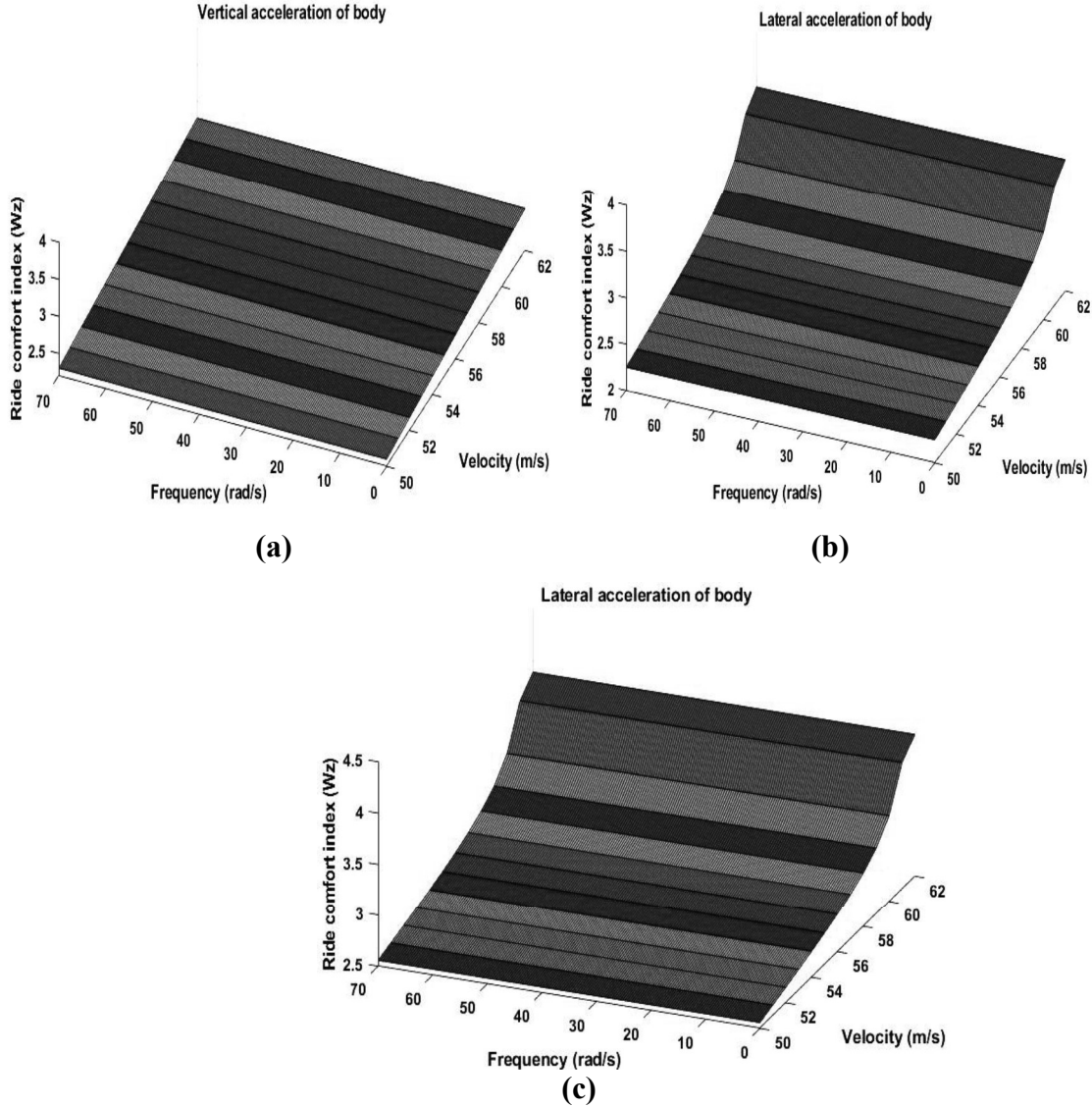


**Figure 3.13** Ride comfort index ( $W_z$ ) of (a) vertical motion under vertical profile, (b) lateral motion under lateral alignment, (c) lateral motion under cross-level

### 3.9 Experimental verification of the proposed model

The results of the proposed analytical model of LHB-FIAT coach with passive suspension are validated using the oscillations test experiment results. In particulars, RDSO conducted the test trials on a prototype LHB chair car (as shown in Figure 3.14 (a) to evaluate the ride comfort in a test speed range of 33.33–55.55 m/s (120–200 km/h). In

the measurement, strain gauge-based accelerometers ( $\pm 2 g$  range) and optical displacement sensors (max. range  $\pm 100$  mm) are connected by a cable to the data acquisition system in the equipment cabin, as shown in Figures 3.14 (b) & (c), respectively. During oscillation test trials, these sensors record acceleration and displacement signals on the wheelsets axle-box, the car body's floor, and the test coach's bogie frame (RDSO Test Trials 2013). The data acquisition sampling rate is 200 sample/sec/channel within the 0-10 Hz frequency band.

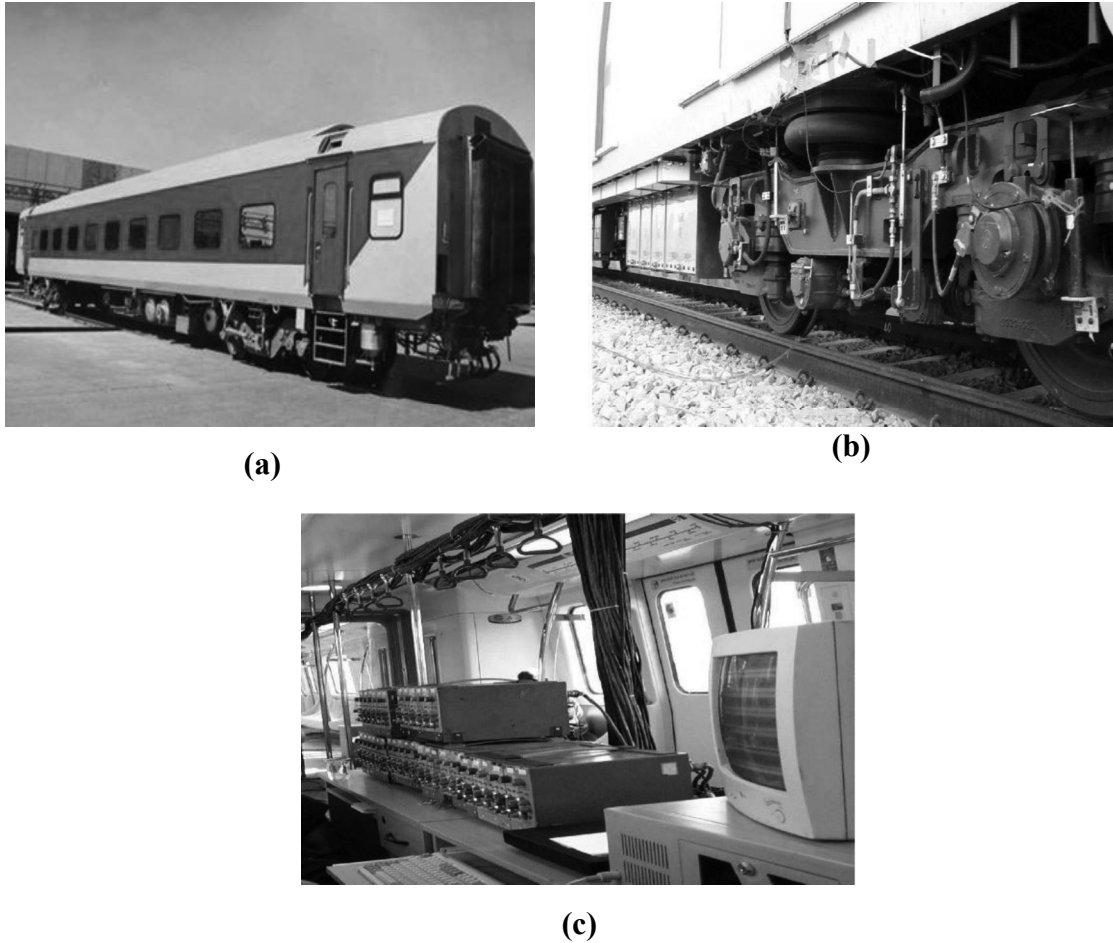


**Figure 3.14** Field test photo of (a) prototype LHB chair coach (b) sensor installation (c) data acquisition chamber

RDSO/Sperling's criteria were used to evaluate the ride index of coaches equipped with coil springs in the secondary suspensions. The comparison between the experimental and simulated results of ride comfort ( $w_z$ ) in both vertical and lateral directions have been shown in Figures 3.15 (a), (b) & (c), respectively. The simulation has been performed at 180 km/h and 200 km/h of speed. From Figure 3.15, it can be noted that the values

obtained using the suggested model exhibit a more significant level of agreement with the experimental data. The error ranges for vertical motion are found to be between 2.36% to 8.81%. Similarly, for lateral motion, the error ranges from 5.84% to 8.30% under lateral alignment and 8.68% to 18.65% under cross-level irregularities. The above findings signify the model's effectiveness in assessing ride comfort or quality under different track conditions and vehicle speeds.

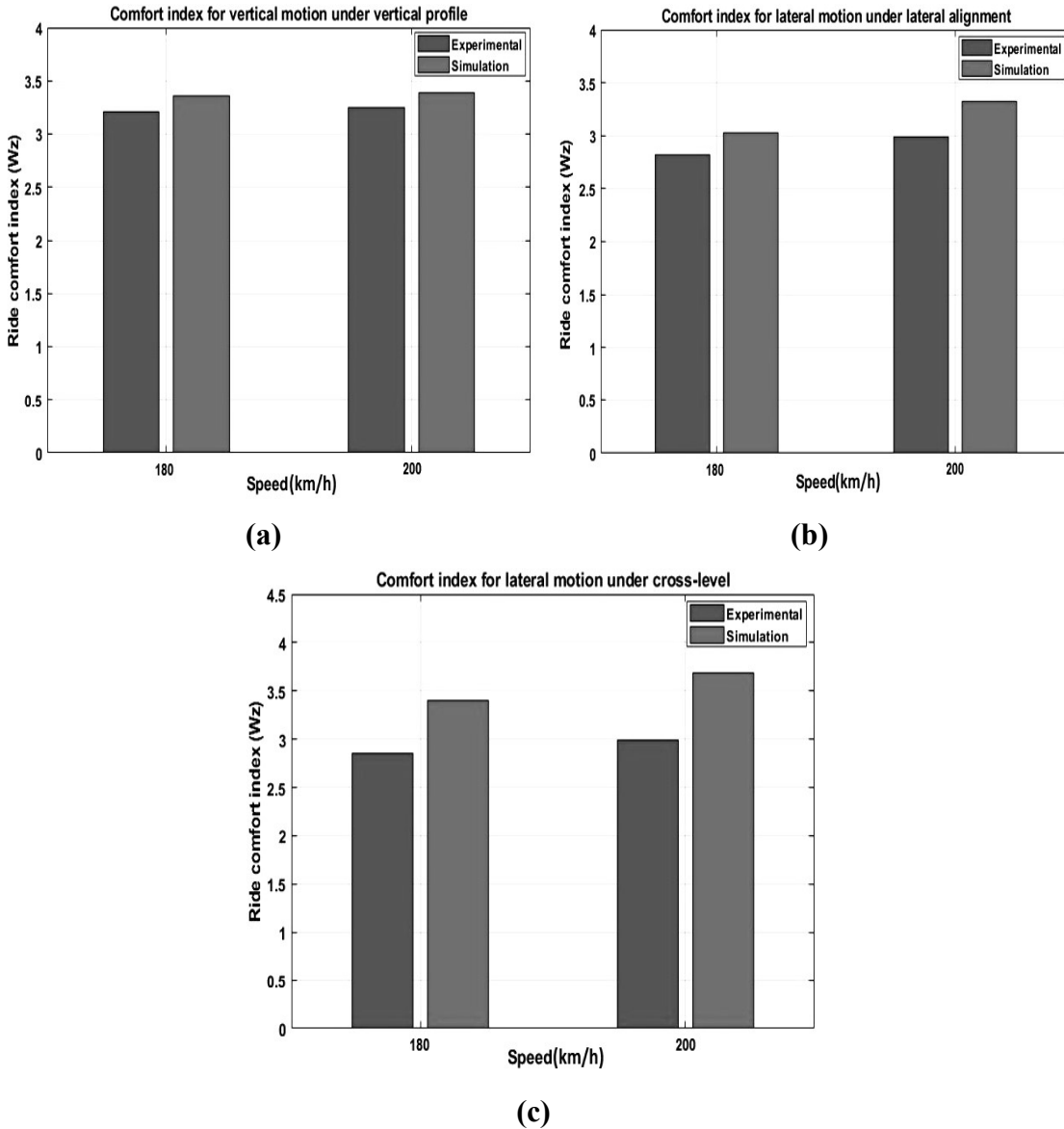


**Figure 3.15** Comparison of experimental and simulation ride comfort index (a) vertical ride index (b) lateral ride index under lateral alignment (c) lateral ride index under cross-level



### 3.10 Conclusions

This chapter presents a 38-DOFs dynamic model of the Linke-Hofmann-Busch (LHB) coach integrated with wheel-rail creep forces and track irregularities. The effect of various track irregularities and vehicle speed on the ride comfort of railway vehicle has been evaluated. The analysis is performed with the help of a 2-D state-space continuous model under three types of random track irregularities (vertical profile, lateral alignment, and cross-level). The efficiency of the proposed model has been demonstrated in three parts: In the first part, the critical velocity of the vehicle is calculated using the classical method of poles-zeros theory. Then in the second part, the 3-D acceleration power spectral densities (PSDs) of the vehicle body under random track disturbances are calculated. The root mean square (RMS) values of the vehicle's vertical, lateral, pitch roll, and yaw motion have also been calculated. Finally, in the third part, the ride comfort index of railway vehicle is evaluated using Sperling's method, and the simulated results are compared with the experimental results.

As per the simulation, the following outcomes are obtained:

- Different track irregularities have different impacts on the dynamic performance of high-speed vehicles.
- The vertical and pitch acceleration of the body shows a linear relationship with velocity. In contrast, lateral, roll, and yaw accelerations behave differently (discontinuously) as the velocity approaches the critical point.
- The vehicle's lateral, roll, and yaw motions are more sensitive to cross-level irregularities than lateral and vertical irregularities, which means these motions require extra attention during cross-level type rail irregularities.
- At specific constant values of vehicle and rail parameters, the operating and critical speeds of the vehicle are found to be different while running on the same track.
- According to Sperling's criteria, the simulated result suggests an average operating speed of up to 208 km/h, satisfying the human comfort level. In contrast, the critical speed is 223.2 km/h, nearly identical to that reported by the Indian railway board for LHB coaches.

- The simulated results of the proposed model demonstrate a remarkable alignment with the experimental data, exhibiting a small error ranging from 2.36–8.81% for vertical motion, 5.84–8.30% for lateral motion under lateral alignment, and 8.68–18.65 % under cross-level rail irregularities.

Although the 38-DOF model successfully evaluates the vehicle body's vertical, lateral, pitch, roll and yaw acceleration under various track irregularities. However, the longitudinal acceleration of the car body, bogies or even wheelset cannot be affected by these irregularities significantly, as shown in Figure 3.16. Under the high class of cross-level track disturbance, the range of acceleration level is about  $10^{-18}$  to  $10^{-21}$  m/s<sup>2</sup>, which is a minimum value to affect the human ride comfort. Therefore, a **27-DOF** model will be utilized for analytical and control purposes in further study.

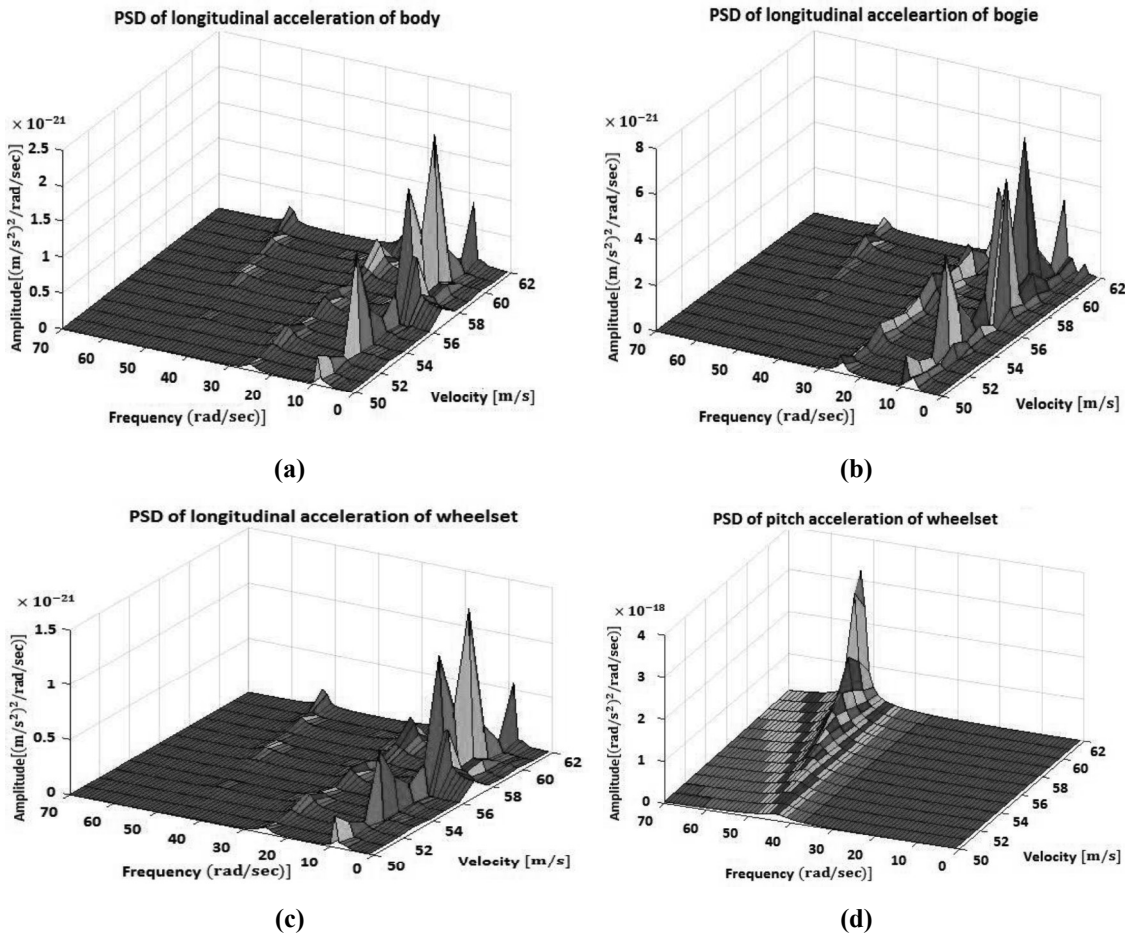


**Figure 3.16** PSDs of longitudinal acceleration of (a) vehicle body (b) bogie (c) wheelset and pitch acceleration of (d) wheelset under cross-level irregularities

## SYNTHESIS OF DECENTRALIZED CONTROLLER

---

*The pursuit of a smoother, more comfortable train journey leads us into the area of controller design for vibration control in railway vehicles. This chapter delves into the complexity of designing intelligent controllers that handle the complexities of rail dynamics and assure an efficient and vibration-free ride. To achieve this, a decentralized control approach with five metaheuristic-tuned FOPID controllers has been presented. A novel hybrid PSO-GWO optimization algorithm is proposed to tune the parameters. The performance of the proposed controller is evaluated under both periodic and random track disturbances.*

### 4.1 Introduction

Optimizing the dynamic performance of railway vehicles is crucial for ensuring passenger comfort and system stability. In this chapter, we explore advanced vibration control techniques, explicitly employing a Multi-Input Multi-Output (MIMO) control strategy to enhance the ride quality of railway vehicles. For a MIMO system, two types of control structures, i.e., centralized and decentralized, are reported in the literature (Luo et al., 2011). In a centralized control structure, all the data collected from an individual sensor is fed back to the central controller to take necessary actions. However, this technique creates the problem of a large amount of data transmission at one time and makes the system complex. This problem of large data transmission can be overcome using a decentralized or multi-loop control strategy (Saxena & Hote, 2016), which has a single loop structure for every control element and also offers a simple control structure (Lengare et al. 2012; Lei et al. 2011). As a result, in this chapter, a multi-loop or decentralized control structure is developed to suppress the vibrations of the railway vehicle, as illustrated in Figure 4.1. The developed control structure constitutes five optimally tuned FOPID controllers that operate diagonally and work independently to control the vertical, lateral, pitch, roll, and yaw motion of the vehicle body. Based on the error and command signal, the above five body motions are controlled by implementing six hydraulic actuators. The four actuators are vertically mounted on the right and left

side of the front and rear bogies, which accelerate to control the bounce, pitch, and roll motions. The two actuators are mounted horizontally above the front and rear bogies, which control the lateral and yaw motion of the vehicle body, as demonstrated in Eqn. 4.1.

$$\left\{ \begin{array}{l} \text{Front right actuator} = \text{Bounce}(u_1) + \text{Pitch}(u_2) + \text{roll}(u_3) \\ \text{Front left actuator} = \text{Bounce}(u_1) + \text{Pitch}(u_2) - \text{roll}(u_3) \\ \text{Rear right actuator} = \text{Bounce}(u_1) - \text{Pitch}(u_2) + \text{roll}(u_3) \\ \text{Rear left actuator} = \text{Bounce}(u_1) - \text{Pitch}(u_2) - \text{roll}(u_3) \\ \text{Above front bogie actuator} = \text{Lateral}(u_4) + \text{yaw}(u_5) \\ \text{Above rear bogie actuator} = \text{Lateral}(u_4) - \text{yaw}(u_5) \end{array} \right. \quad (4.1)$$

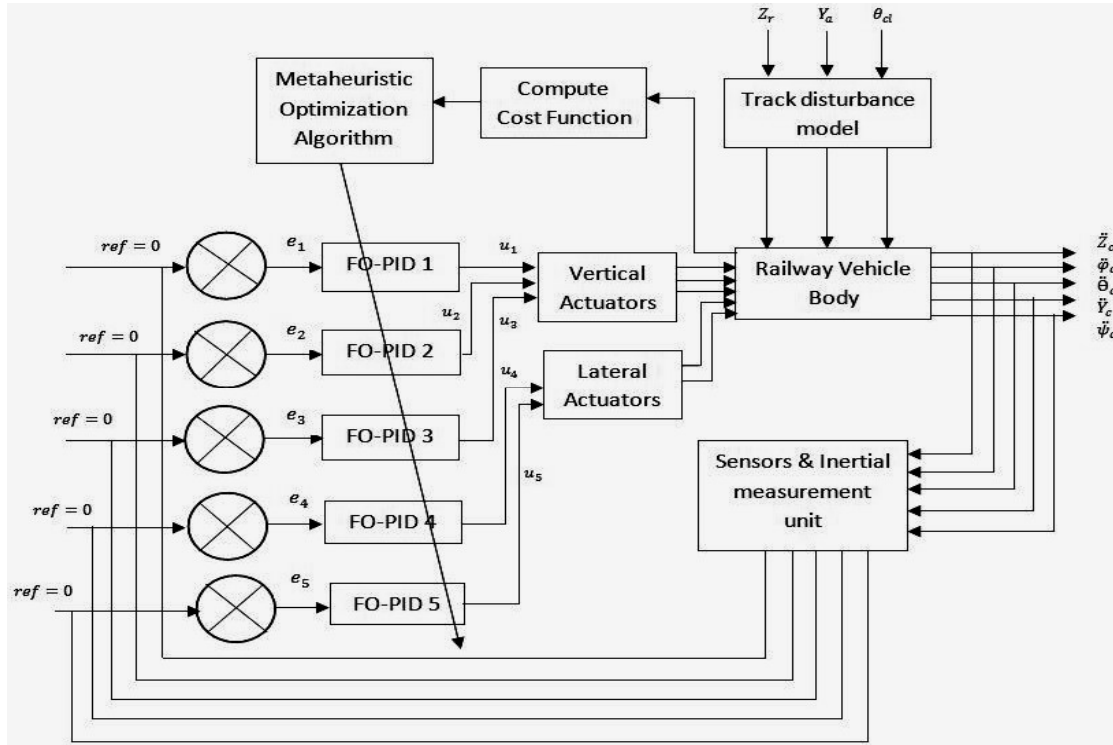


**Figure 4.1** Decentralized control structure for railway vehicle

Oustaloup et al. first put up the idea of FOPID controllers in 1991. It is a more sophisticated form of traditional PID since it has five tuning parameters ( $K_p, K_i, K_d, \lambda$  and  $\mu$ ) instead of three, which allows for more design flexibility. The performance of the PID controller may also degrade, if the order of the system increases (Arora et al., 2019; A.

Kumar & Suhag, 2017; Mohan et al., 2019). This limitations of PID controller can be overcome by using fractional order PID (FOPID) combining with heuristic or meta-heuristic optimization algorithms as the real-world applications are well represented in terms of higher fractional order (Stephen Bassi Joseph et al., 2022).

Duarte Valerio et al. (Valério & da Costa, 2006) proposed two sets of tuning for FOPID using the same method as that of Z-N, and the results were successfully observed on first-order plus time delay processes. A comparative study of tuning FOPID in the time and frequency domain has been given by Saptarshi Das et al. (Das et al., 2011). The results demonstrate the superiority of the frequency domain technique over the time domain in terms of noise rejection and robustness. Jun-Yi-Cao et al. (J. Y. Cao et al., 2005) presented a GA-based FOPID controller for providing good dynamic response and stability in various systems. The successful implementation of FOPID using PSO, ACO, and GA for automatic voltage regulator systems (AVRS) has been reported in (Babu et al., 2016) and (D. H. Kim & Park, 2005), respectively. Gad et al. (Sherif Gad et al., 2015; 2017) employed GA to optimize the parameters of FOPID and PID used for semi-active suspensions, in which semi-active suspension with a human body model was used to investigate the influence of vertical vibration. Verma et al. (Verma et al., 2017) use GWO optimization to tune the parameters of FOPID, and the simulation has been performed for higher order and time-delay process. The effect of adding fractions to control the DC servo motor velocity has been analyzed by Ramiro S. Barbosa et al. (Barbosa et al., 2010), in which the ZN tuning method was used to tune the parameters of the fractional order controller. The implementation of PSO-based FOPID for a second-order system has been successfully reported by Mohammad Reza et al. (Dastranj et al., 2012). A comparison of PSO and ABC-based FOPID has been performed for second order system with time delay (Bingul & Karahan, 2018), and the robustness of the controller has been checked by using different cost functions such as mean square error (MSE), mean time square error (MTSE). Mahdiah Alamdar et al. (Alamdar Ravari & Yaghoobi, 2019) proposed a chaotic firefly algorithm to tune the parameters of FOPID for a continuous stirred tank reactor (CSTR). The output shows better results than integer order PID in terms of overshoot, settling time, and steady-state error. Shivam Jain et al. (S. Jain & Hote, 2020)

proposed a new technique for tuning FOPID using modified ZN rules and a big bang crunch optimization algorithm, and results are verified on different applications.

According to the literature, FOPID controllers with meta-heuristic optimization have been employed for various applications, including electrical (S. Singh et al., 2022), physiological processes (H. Singh et al., 2021), robotics (Delavari et al., 2013; Mohan et al., 2019), sun tracking systems, vibration control, voltage regulation systems, and many more. However, just a few studies on FOPID have been published in the context of active vibration control of railway vehicle. As per the contribution of this chapter, a decentralized FOPID controller integrated with the metaheuristic optimization techniques for active suspension is proposed, which is expected to provide the optimum results that satisfy the need for better ride comfort of railway vehicles. In order to accomplish this, a comprehensive state-space representation of a full-scale railway vehicle with 27 degrees of freedom is developed. The governing equations of motion represent the translational and rotational motions of the car body, bogies, and wheelsets. Then, a decentralized control structure with five independent FOPID controllers is adopted to suppress the vibration of the car body's vertical, lateral, roll, pitch, and yaw motion. A novel hybrid optimization technique hybrid PSO-GWO has been utilized to calculate the optimal active force for the suspension system. To justify the performance of the proposed work, the FOPID is also tuned using the ZN, PSO, and GWO and the results are critically analyzed in the time and frequency domains. A comparison between the proposed metaheuristic algorithm and passive system is carried out on the basis of root mean square values of acceleration. The results of the simulations and studies demonstrate the performance of the suggested controller with the highest possible potential gains that are based on the quadratic cost function.

## 4.2 State-space formulation

In this section, the control force vector,  $u(t)$ , exempted in the previous mathematical model, is now incorporated for the control analysis.

Now, let,

$$q = [Z_c, Y_c, \psi_c, \Theta_c, \varphi_c, Z_{t1}, Y_{t1}, \psi_{t1}, \Theta_{t1}, \varphi_{t1}, Z_{t2}, Y_{t2}, \psi_{t2}, \Theta_{t2}, \varphi_{t2}, Z_{w1}, Y_{w1}, \psi_{w1}, Z_{w2}, Y_{w2}, \psi_{w2}, Z'_{w3}, Y_{w3}, \psi_{w3}, Z_{w4}, Y_{w4}, \psi_{w4}]^T, u = [F_{z1}, F_{z2}, F_{z3}, F_{z4}, F_{y1}, F_{y2}]^T, \text{ and } w = [Z_{v1}, Y_{a1}, \theta_{cl1}, \dot{Z}_{v1}, \dot{Y}_{a1}, \dot{\theta}_{cl1},$$

$Z_{v2}, Y_{a2}, \theta_{cl2}, \dot{Z}_{v2}, \dot{Y}_{a2}, \dot{\theta}_{cl2}, Z_{v3}, Y_{a3}, \theta_{cl3}, \dot{Z}_{v3}, \dot{Y}_{a3}, \dot{\theta}_{cl3}, Z_{v4}, Y_{a4}, \theta_{cl4}, \dot{Z}_{v4}, \dot{Y}_{a4}, \dot{\theta}_{cl4}]^T$  be define the displacement (linear and angular), control, and disturbance vectors, respectively.

Then, the equations of motion, represented by the Eqns. (3.14)-(3.30) can be written in the following matrix form:

$$[M]\ddot{q} + [C]\dot{q} + [K]q = [F_u]u + [F_w]w \quad (4.2)$$

where  $[M]$  ( $\mathcal{R}^{27 \times 27}$ ),  $[C]$  ( $\mathcal{R}^{27 \times 27}$ ), and  $[K]$  ( $\mathcal{R}^{27 \times 27}$ ) are the mass, damping, and stiffness matrices of the vehicle system;  $[F_u]$  ( $\mathcal{R}^{27 \times 6}$ ),  $[F_w]$  ( $\mathcal{R}^{27 \times 24}$ ) are the position matrices of control inputs and track disturbances acting on the railway vehicle body and wheels of wheelsets, respectively.

Now by defining the state vector as  $x = [q^T \dot{q}^T]^T$ , the state and output equations of the railway vehicle system in the form of state-space are given as

$$\begin{cases} \dot{x} = [A]x + [B_1]u + [B_2]w \\ y = [C]x + [D_1]u + [D_2]w \end{cases} \quad (4.3)$$

where  $[A] = \begin{bmatrix} 0 & I \\ -M^{-1}K & -M^{-1}C \end{bmatrix} \in \mathcal{R}^{54 \times 54}$ ,  $[B_1] = \begin{bmatrix} 0 \\ M^{-1}F_u \end{bmatrix} \in \mathcal{R}^{54 \times 6}$ ,  $[B_2] = \begin{bmatrix} 0 \\ M^{-1}F_w \end{bmatrix} \in \mathcal{R}^{54 \times 24}$ ,  $[C] = [-M^{-1}K \quad -M^{-1}C] \in \mathcal{R}^{27 \times 54}$ ,  $[D_1] = [M^{-1}F_u] \in \mathcal{R}^{27 \times 6}$ , and  $[D_2] = [M^{-1}F_w] \in \mathcal{R}^{27 \times 24}$  are the coefficient matrices, which can be derived from Eqn. (4.2).

### 4.3 Controller and optimization algorithms

This section presents the description of proposed FOPID controller and the different algorithms used to tune the controller parameters.

#### 4.3.1 FOPID controller

Over the last decade, the applications of fractional calculus have shown a significant impact in the field of Engineering and Mathematics. Leibniz and L'Hospital, in 1695, first coined the idea of fractional calculus. Since then, fractional calculus has been an ongoing research area. Its applications in control engineering have attracted many researchers because fractional order differential equations better characterize real-world physical systems. Recent research studies show that fractional order controllers perform better than integer order controllers in terms of system performance and robustness. Fractional

calculus is the main foundation of FOPID. Here, the differentiation and integration operations are collaboratively used in fractional order (Nisar et al., 2016). The continuous form of integral-differential is defined as

$$\alpha \mathcal{D}_t^s = \begin{cases} \frac{dS}{dt} & R(s) > 0 \\ 1 & R(s) = 0 \\ \int_{\infty}^t d\tau^{-s} & R(s) < 0 \end{cases} \quad (4.4)$$

where  $s$  is the order of operation,  $\alpha$  and  $t$  are the confines of operation. Fractional calculus empowers the derivative and integral to be in non-integer order.

In the fractional order PID the integral-differential equation which defines the control action of the controller can be expressed as:

$$U(t) = K_P e(t) + K_I D^{-\lambda} e(t) + K_D D^{\mu} e(t) \quad (4.5)$$

Applying Laplace transform to Eq. (18), the control action of the FOPID controller is expressed in terms of the transfer function as:

$$C(s) = \frac{U(s)}{E(s)} = K_P + K_I s^{-\lambda} + K_D s^{\mu}, \quad (\lambda, \mu > 0) \quad (4.6)$$

where

- $C(s)$  represents the transfer function of controller
- $E(s)$  defines the error
- $U(s)$  is the output
- $K_P$ ,  $K_I$  and,  $K_D$  are proportional, integral, and derivative gains of the controller
- $\lambda$  defines the degree of integration
- $\mu$  is the degree of differentiation.

The fractional order PID is an expanded version of the integer PID. It is obtained by applying fractional-ordering to the integral and derivative action. In other words, the FOPID combines fraction operators with controller gains. From the Eqns. (4.6), it can be seen that FOPID has two more parameters (such as  $\lambda$  and  $\mu$ ) as compared to conventional PID, which provides additional flexibility in designing the control system. The controller architecture of the proposed system utilizes the FOMCON toolbox, employing Oustaloup's analytical approximation technique as stated in (Baranowski et al., 2015;



Lanusse et al., 2015). Many tuning methods are available for these five parameters, generally named rule-based, numerical, and analytical methods. Here, the following methods are used for tuning the optimum parameters of FOPID.

#### **4.4. Optimization Algorithms**

##### **4.4.1 Ziegler-Nichols (Z-N) Method**

To tune the FOPID parameters, firstly, the modified form of the Z-N method proposed by Duarte Valerio et al. has been implemented, which comes under rule-based methods. The tuning rules of FO-PID are similar to that of conventional PID. Here, the step response of the plant assumes to have an S-shaped curve and depending upon the value of  $L$  and  $T$ , two sets of tuning are established, as shown in (Valério & da Costa, 2006). The parameters obtained from these rules can be used as a good initial guess for the metaheuristic optimization algorithms discussed below.

##### **4.4.2 Particle swarm optimization (PSO) algorithm**

The PSO algorithm uses the nature-inspired mechanism of bird flocking or fish schooling with a targeted position in searching for potential food. Kennedy et al. (Slowik, 2011) proposed this algorithm in 1995, which uses the actions of swarm intelligence in which each particle focuses on finding the potential solution according to the given objective function. Each particle reaches its best position according to its own experience and awareness of the neighboring particle they are going through. Due to its diverse nature, such as by changing its parameters and population size, PSO can be easily used in conjunction with other heuristic algorithms. It uses in various kinds of applications such as medical, financial, structural studies, communications and control applications (W. Der Chang & Chen, 2014; Eshtay et al., 2018; Ganguly et al., 2010; Hajihassani et al., 2018; Shie et al., 2012). In the control system the use of PSO is mainly to solve the single or multi-objective function, which helps to get the desired transient and steady-state responses. The present investigation employed this algorithm to solve a single objective multivariable optimization problem using for proposed vibration control structure. The pseudo-codes of this algorithm for the present investigated problem are illustrated in Appendix 2.

#### 4.4.3. Grey wolf optimization (GWO) algorithm

GWO is a new optimization technique developed by Mirjalili et al. in 2014 (Mirjalili, and Lewis 2014). The motivation for developing the GWO algorithm is inspired by the intellectual hunting tactics followed by grey wolves. Generally, grey wolves have well-defined groups of 10-12 wolves called packs, and the duty of each wolf in a group is defined in a particular way. It has four levels of hierarchy named alpha ( $\alpha$ ), beta ( $\beta$ ), delta ( $\delta$ ), and omega ( $\omega$ ) that guide the hunting process. The top level of this hierarchy, called alpha ( $\alpha$ ), has a leader who dominates in making decisions. The other two levels, beta and delta, are the sub-ordinates that help the alpha to make the best possible solutions. The applications of GWO show tremendous results in the field of machine learning (Al-Tashi et al., 2019; Emary et al., 2016), medical or bioinformatics (Sharma et al. 2019; 2020), image processing (L. Li et al., 2017), and wireless sensor network (Rajakumar et al., 2017). However, in recent years there has been an explosion in the publication that explores the use of GWO in control engineering applications (M. K. Debnath, 2016; Sule et al., 2020). In this work, we use this algorithm to tune the five parameters of the FOPID controller that helps to achieve the desired output response. The pseudo-code of this algorithm used for the proposed control scheme is illustrated in Appendix 2.

#### 4.4.4 Hybrid PSO-GWO algorithm

The metaheuristic algorithms work on the principle of randomization, which employs a particular mix of local and global searches. Heuristics and metaheuristic are not defined in a way that can be checked or used as a standard. However, these techniques show significant results by providing the optimum solution for integer order systems within a reasonable time. But when it comes to the non-integer world, it may get trapped into local minimum points and can take ample time to provide the optimum solution. Therefore to address these problems, a novel hybrid PSO-GWO optimization algorithm is proposed, in which the three parameters (i.e.  $K_p$ ,  $K_I$  and  $K_D$ ) of the FOPID controller are tuned with the help of PSO, and the other two parameters ( $\lambda$  and  $\mu$ ) are tuned with GWO. The proposed hybrid algorithm has been worked in two stages, with each stage being performed to accomplish the same cost function without getting into the trapping

problem. The functional flow diagram of hybrid PSO-GWO has been illustrated in Figure 4.2.

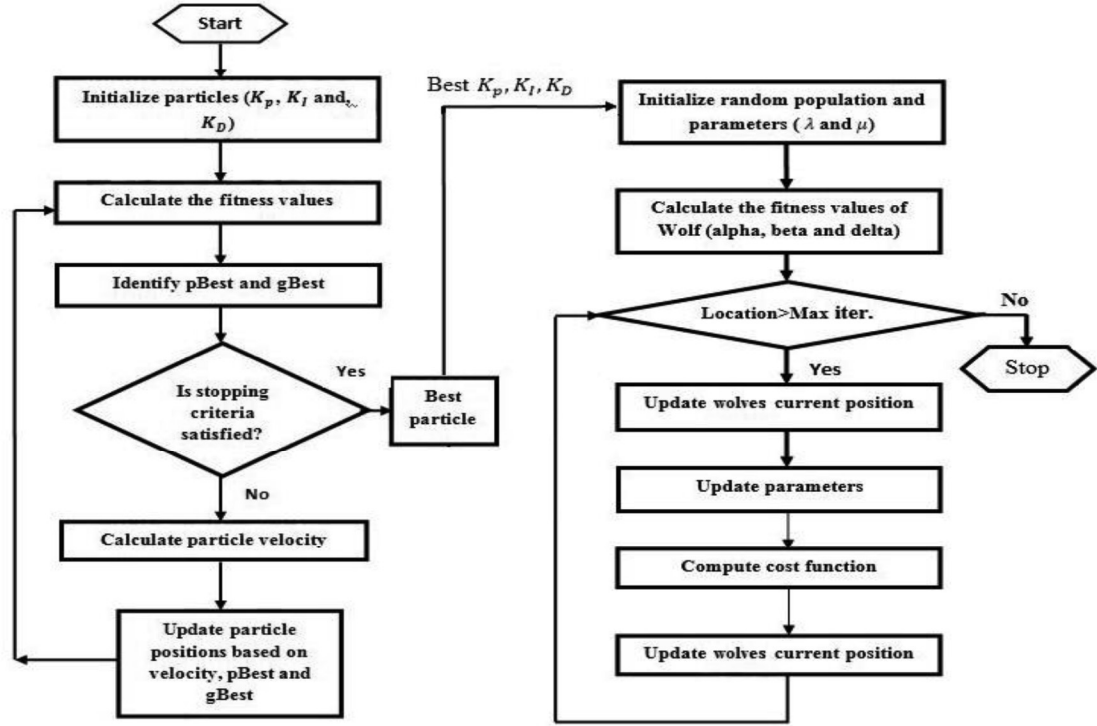


Figure 4.2 Work flow diagram of hybrid PSO-GWO

#### 4.5 System response based on a decentralized control structure

In order to achieve better ride comfort, the acceleration response of the vehicle body in translational as well as rotational motion should be minimized. Thus, from Eqn. (4.2), the controlled output vector  $y = y_1$ , defined as:

$$y_1 = [\ddot{Z}_c, \ddot{Y}_c, \ddot{\psi}_c, \ddot{\Theta}_c, \ddot{\phi}_c] \quad (4.7)$$

If  $Z_{v1}$ ,  $Y_{a1}$ , and  $\theta_{cl1}$  are the excitations applied on the front wheelsets of railway vehicle, then  $Z_{v1} \sim Z_{v4}$ ,  $Y_{a1} \sim Y_{a4}$ , and  $\theta_{cl1} \sim \theta_{cl4}$  are related by the following relation:

$$\begin{cases} Z_{v2} = Z_{v1}(t - \tau_1), Z_{v3} = Z_{v1}(t - \tau_2), Z_{v4} = Z_{v1}(t - \tau_3) \\ Y_{a2} = Y_{a1}(t - \tau_1), Y_{a3} = Y_{a1}(t - \tau_2), Y_{a4} = Y_{a1}(t - \tau_3) \\ \theta_{cl2} = \theta_{cl1}(t - \tau_1), \theta_{cl3} = \theta_{cl1}(t - \tau_2), \theta_{cl4} = \theta_{cl1}(t - \tau_3) \end{cases} \quad (4.8)$$

where  $\tau_1 = \frac{2L_d}{V}$ ,  $\tau_2 = \frac{2L_b}{V}$ ,  $\tau_3 = \frac{2(L_d + L_b)}{V}$  are the time delays between the front and consecutive wheelsets.

Let,  $n = [Z_{v1}, Y_{a1}, \theta_{cl1}, \dot{Z}_{v1}, \dot{Y}_{a1}, \dot{\theta}_{cl1}]^T \cong [Z_{v1}, Y_{a1}, \theta_{cl1}, \dot{Z}_{v1}, \dot{Y}_{a1}, \dot{\theta}_{cl1}, Z_{v2}, Y_{a2}, \theta_{cl2}, \dot{Z}_{v2}, \dot{Y}_{a2}, \dot{\theta}_{cl2}, Z_{v3}, Y_{a3}, \theta_{cl3}, \dot{Z}_{v3}, \dot{Y}_{a3}, \dot{\theta}_{cl3}, Z_{v4}, Y_{a4}, \theta_{cl4}, \dot{Z}_{v4}, \dot{Y}_{a4}, \dot{\theta}_{cl4}]^T$  and  $\hat{G}_{wn}(s) = [1, e^{-\tau_1 s}, e^{-\tau_2 s}, e^{-\tau_3 s}]^T$ , Then we have

$$N(s) = G_{wn} W(s) \quad (4.9)$$

where  $G_{wp} = \text{diag} \{ \hat{G}_{wn}(s), \hat{G}_{wn}(s), \hat{G}_{wn}(s), \hat{G}_{wn}(s) \}$

Thus, from Eqns. (4.2), (4.7), and (4.9), the two transfer function matrix, i.e., between the inputs and outputs of the system, can be evaluated as

$$P(s) = \frac{Y_1(s)}{W(s)} = \begin{bmatrix} p_{11}(s) & \cdots & p_{1n}(s) \\ \vdots & \ddots & \vdots \\ p_{n1}(s) & \cdots & p_{nn}(s) \end{bmatrix}; \quad G(s) = \frac{Y_1(s)}{U(s)} = \begin{bmatrix} g_{11}(s) & \cdots & g_{1n}(s) \\ \vdots & \ddots & \vdots \\ g_{n1}(s) & \cdots & g_{nn}(s) \end{bmatrix} \quad (4.10)$$

where,  $[P(s)]^{n \times n}$  represents the disturbance transfer function matrix and  $[G(s)]^{n \times n}$  is a system transfer function matrix.

Now, for a  $n \times n$  control system, the transfer function matrix for the decentralized controller can be represented as:

$$C(s) = \frac{U(s)}{E(s)} = \begin{bmatrix} c_{11}(s) & 0 & \cdots & 0 \\ 0 & c_{22}(s) & \cdots & 0 \\ \vdots & \vdots & \ddots & \vdots \\ 0 & 0 & \cdots & c_{nn}(s) \end{bmatrix} \quad (4.11)$$

The single-loop structure of the regulatory feedback system with actuator transfer function  $A(s)$  is shown in Figure 4.3. The closed-loop transfer function between the disturbance and output is

$$T(s) = \frac{Y(s)}{W(s)} = [1 + P(s) C(s) H(s)]^{-1} p(s) \quad (4.12)$$

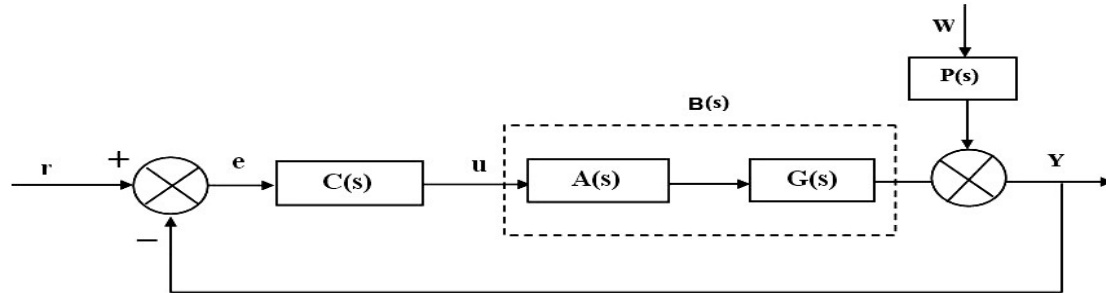


Figure 4.3 Single loop structure of regulatory feedback system

Likewise, the overall transfer function matrix of the decentralized control system shown in Fig. 2 can be written as:

$$H(s) = \text{diag}[(1 + p_{11}(s)c_{11}(s)b_{11}(s)]^{-1}p_{11}(s); (1 + p_{22}(s)c_{22}(s)b_{22}(s)]^{-1}p_{22}(s); \dots; (1 + p_{nn}(s)c_{nn}(s)b_{nn}(s)]^{-1}p_{nn}(s)] \quad (4.13)$$

Now, if  $H_n(\omega)$  is considered as frequency response function due to harmonically varying input of unit amplitude having frequency response function  $W_n(\omega)$  for  $n^{\text{th}}$  input with all other input kept at zero. Then output and input of the system in the frequency domain are related by the relation as:

$$Y_n(\omega) = H_{nn}(\omega) \times W_n(\omega) \quad (4.14)$$

And such equation in the time domain can be represented as:

$$Y_n(t) = \int_0^t H_{nn}(t - \tau) W_n(\tau) d\tau \quad (4.15)$$

In the case of random input, the input is generally considered in terms of PSD's. Then, the output mean square spectral density  $S_y(\omega)$  is related to input mean square spectral density  $S_n(\omega)$  as:

$$S_y(\omega) = |H_{nn}(\omega)|^2 \times S_n(\omega) \quad (4.16)$$

where,

$$H_{nn}(\omega) = \frac{1}{1 - \left(\frac{\omega}{\omega_n}\right)^2 + j 2\zeta_n \left(\frac{\omega}{\omega_n}\right)} \quad (4.17)$$

where  $\left(\frac{\omega}{\omega_n}\right)$  is the normalized frequency and  $\zeta$  is the damping ratio.

Then finally, the root mean square acceleration response is calculated as:

$$a_0 = \sqrt{\frac{1}{\pi} \int_{\omega_1}^{\omega_2} \omega^4 \cdot S_y(\omega) d\omega} \quad (4.18)$$

## 4.6 Results and Discussions

This section consists of three parts that thoroughly evaluates the performance of FOPID based active suspension control system used for vibration mitigation of railway vehicles. In the first part, the controller parameters are tuned with metaheuristic optimization algorithms and, in the second part the effectiveness of the tuned controller have been investigated in the time and frequency domain under periodic and random track disturbances, respectively. Then in the third part, the ride comfort of railway vehicle using Sperling criteria has been calculated.

### 4.6.1 Tuning of decentralized controller

In this paper, the five motions (vertical, lateral, pitch, roll, and yaw) of railway vehicle have been controlled by using the decentralized control structure which comprises of five independent FOPID controllers, as discussed in section 4.1. The performance of these controllers depends on how well the controller parameters are tuned to control the maximum ranges of vehicle motion. The maximum responses of vehicle body are generally occurs at the particular wavelengths ( $L$ ) of the track irregularities. For that purpose, the following function  $0.01 \sin\left(2\pi \frac{V}{L_i} t\right)$  has been used to tune the controller parameters. Where,  $L_i$  defines the spatial wavelengths for respective motion and,  $V$  is the velocity of vehicle. Also, a comparison was conducted between the proposed FOPID control with the Z-N, PSO, GWO, and hybrid PSO-GWO tuning strategies. The improvement of proposed control schemes over the passive system was evaluated based on the following linear quadratic regulator cost function

$$J = \frac{1}{2} \int_0^{t_f} w_1 \cdot \ddot{q}_{max}^2 + w_2 \cdot u_{max}^2 \quad (4.19)$$

where  $\ddot{q}$  and  $u$  represents the maximum accelerations and control efforts of controlling states, respectively. According to the cost function, the vertical, lateral, pitch, roll, and yaw motion of the vehicle body can be regulated by changing the values of the coefficients  $w_1$ , and  $w_2$ . The appropriate choices of the coefficients for translational and angular motion have been provided in Table 4.1. The various parameters of railway vehicle, and track used in this study have been given in Appendix 1. The simulation has

been done in MATLAB/SIMULINK environment using the FOMCON toolbox with a maximum step size of  $1e-3$ .

**Table 4.1** Different Values of coefficients used in the cost function

<i>Motions</i>	$w_1$	$w_2$
Vertical	0.50	3000
Lateral	0.50	3000
Pitch	0.50	3000
Roll	0.50	3000
Yaw	0.50	3000

The performance of an optimization-based FOPID controller depends on the values of controller parameters that are tuned within the constraints of the required objective function. Thus, by taking the classical approach (Z-N) as training optimum parameters, this method can provide an excellent initial guess for controller parameters and be a benchmark in designing the FOPID with the other metaheuristic techniques. The parameters required for implementing the proposed optimization techniques have been given in Pseudo code (Appendix 2). Each algorithm has been run ten times by setting the same number of iterations, particles, and other parameters of PSO, GWO and hybrid PSO-GWO. Then, the best convergence graphs to find the optimum values of the FOPID controller have been given in Figure 4.3. As discuss above in section 4.2.3, the proposed algorithm is a two stage algorithm, in which the best optimum FOPID parameters is calculated in two stages. The first stage provides the value of  $K_p$ ,  $K_i$ ,  $K_d$  and second stage is used to evaluate the other two parameters  $\lambda$  and  $\mu$ . The values of these parameters and their corresponding cost function ( $O_f$ ) values for vertical, lateral, pitch, roll, and yaw motion, results from classical and metaheuristic tuning have been provided in Table 4.2. According to Figure 4.4, it is observed that the convergence rate of PSO and GWO is slower than that of hybrid PSO-GWO, and also they have the problem of being trapped in local minima, as demonstrated in Figures 4.4 (c), (d) and (e). Therefore, one cannot rely on PSO and GWO for the optimum solution. On the other hand, the hybrid PSO-GWO shows faster convergence rate with better performance for the minimization of the cost function ( $O_f$ ) as given in Table 4.2. Moreover, it does not have the problem of

getting trapped into local minimum points, which shows the efficacy of the proposed algorithm over PSO and GWO.

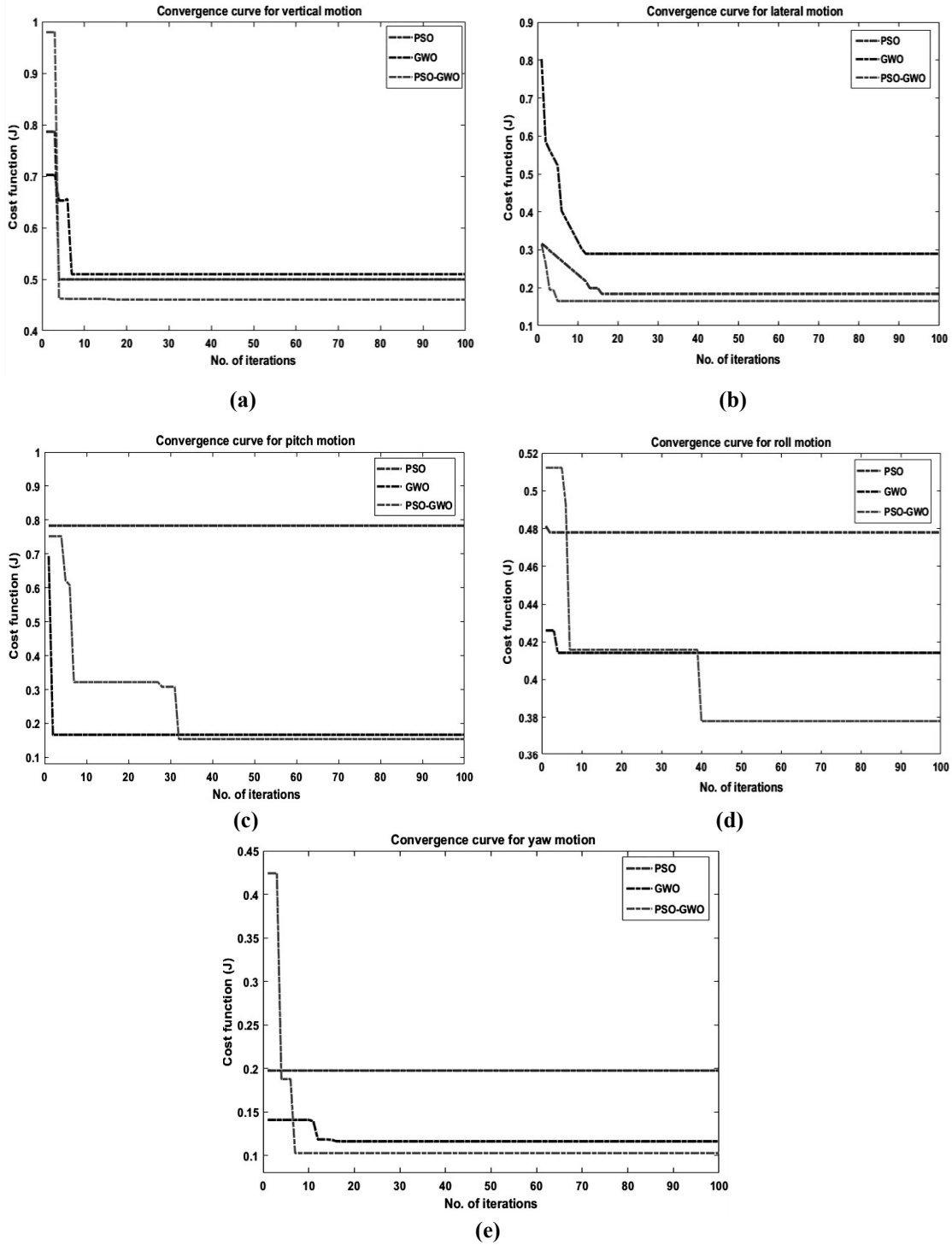


**Figure 4.4** Convergence curves for (a) vertical, (b) lateral, (c) pitch, (d) roll, and (e) yaw motions



**Table 4.2** FOPID parameters and cost function values resulted from different tuning algorithms

<i>(a) For vertical motion</i>						
<i>index</i>	$K_P$	$K_D$	$K_I$	$\lambda$	$\mu$	$O_f$
<i>Open loop</i>	-	-	-	-	-	-
<i>Z – N</i>	3.732e+04	6.086e+03	3.015e+04	0.022	0.041	-
<i>PSO</i>	1.842e+05	4.322e+04	4.803e+04	0.953	0.422	0.510
<i>GWO</i>	1.820e+04	2.251e+04	1.492e+04	0.648	1.431	0.507
<b><i>PSO – GWO</i></b>	<b>2.642e+05</b>	<b>5.804e+04</b>	<b>3.642e+04</b>	<b>0.696</b>	<b>0.440</b>	<b>0.485</b>
<i>(b) For lateral motion</i>						
<i>index</i>	$K_P$	$K_D$	$K_I$	$\lambda$	$\mu$	$O_f$
<i>Open loop</i>	-	-	-	-	-	-
<i>Z – N</i>	4.694e+03	5.783e+03	2.404e+04	0.058	0.082	-
<i>PSO</i>	3.648e+04	2.955e+04	3.0675e+04	0.065	1.208	0.198
<i>GWO</i>	2.880e+04	3.274e+04	3.008e+04	0.440	0.783	0.305
<b><i>PSO – GWO</i></b>	<b>4.841e+04</b>	<b>5.475e+04</b>	<b>2.748e+03</b>	<b>0.274</b>	<b>0.405</b>	<b>0.182</b>
<i>(c) For pitch motion</i>						
<i>index</i>	$K_P$	$K_D$	$K_I$	$\lambda$	$\mu$	$O_f$
<i>Open loop</i>	-	-	-	-	-	-
<i>Z – N</i>	4.655e+04	3.573e+04	2.672e+04	0.071	0.072	-
<i>PSO</i>	2.645e+05	4.328e+04	1.994e+04	0.642	0.694	0.791
<i>GWO</i>	5.601e+05	6.118e+04	3.332e+04	0.642	0.408	0.182
<b><i>PSO – GWO</i></b>	<b>4.607e+05</b>	<b>5.221e+04</b>	<b>3.842e+04</b>	<b>0.672</b>	<b>0.844</b>	<b>0.170</b>
<i>(d) For roll motion</i>						
<i>index</i>	$K_P$	$K_D$	$K_I$	$\lambda$	$\mu$	$O_f$
<i>Open loop</i>	-	-	-	-	-	-
<i>Z – N</i>	2.668e+04	3.853e+04	2.053e+04	0.069	0.073	-
<i>PSO</i>	2.700e+05	4.284e+04	5.588e+04	0.132	0.274	0.480
<i>GWO</i>	5.601e+04	4.729e+04	2.052e+04	0.183	0.205	0.439
<b><i>PSO – GWO</i></b>	<b>4.482e+05</b>	<b>6.022e+04</b>	<b>3.502e+04</b>	<b>0.481</b>	<b>0.595</b>	<b>0.378</b>

(e) For yaw motion

<i>index</i>	$K_P$	$K_D$	$K_I$	$\lambda$	$\mu$	$O_f$
<i>Open loop</i>	-	-	-	-	-	-
<i>Z – N</i>	2.268e+04	3.853e+04	3.252e+04	0.080	0.038	-
<i>PSO</i>	2.004e+03	5.883e+04	5.588e+05	0.067	1.320	0.203
<i>GWO</i>	3.082e+03	2.580e+05	3.084e+03	0.572	0.205	0.136
<b><i>PSO – GWO</i></b>	<b>2.266e+05</b>	<b>3.954e+05</b>	<b>5.820e+03</b>	<b>0.382</b>	<b>0.788</b>	<b>0.118</b>

#### 4.6.2 Simulation under periodic track irregularities

The mathematical expressions of periodic track irregularities are already discussed in chapter 3. In this section, their first harmonic periodic functions are used as input to check the performance of an optimally tuned FOPID controller. Let the parameters  $A_z$ ,  $A_y$ ,  $\lambda_1$ ,  $\lambda_2$ , and  $V$  in Eqns. (3.37) - (3.39) be 0.01m, 0.01m, 18m, 9m and  $50 \text{ ms}^{-1}$ , respectively, which implies that the fundamental frequency ( $\omega = \frac{2\pi V}{\lambda}$ ) for vertical, lateral, and roll motion equals  $17.45 \text{ rads}^{-1}$ , and for pitch and yaw motion, equal  $8.72 \text{ rads}^{-1}$ .

##### 4.6.2.1 Time domain responses of acceleration of the body

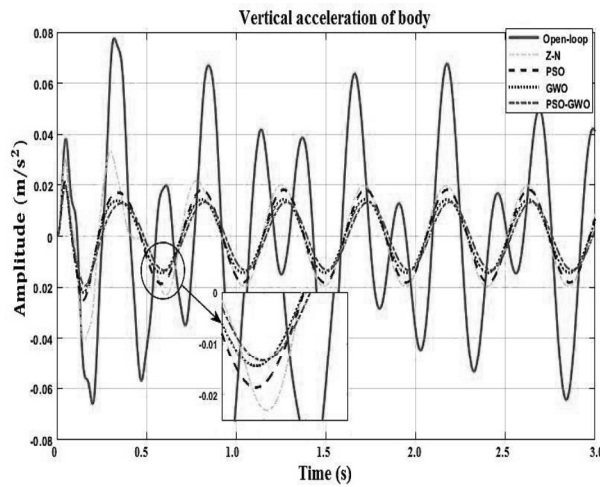
The time histories of open-loop output responses and the FOPID-tuned closed-loop responses for the accelerations of the vehicle body in all five modes (vertical, lateral, pitch, roll, and yaw) have been illustrated in Figure 4.5. Also, the root mean square (RMS) values, and the percentage improvement of RMS value of vertical, lateral, pitch, roll and yaw acceleration over passive system (open loop) are given in Tables 4.3. The percentage improvement of RMS values using different tuning algorithms over the passive system has been calculated by using the following equation:

$$\% \text{ improvement of RMS} = \frac{p_s - c_s}{p_s} \times 100 \quad (4.20)$$

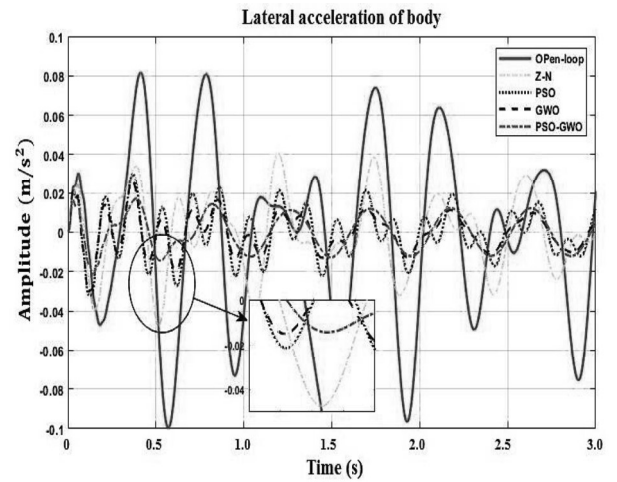
where  $p_s$  and  $c_s$  are the RMS values of the passive system and different FOPID tuned control systems, respectively.

In the case of vertical motion, from Figure 4.5 (a) and Table 4.3 (a), it is evident that the FOPID controller tuned with the ZN method can reduce the vertical vibrations only up to

74.32% as compared to the passive system. However, when the controller is tuned with PSO, GWO, and hybrid PSO-GWO algorithms, this % improvement has increased to 75.65%, 82.05%, and 84.60%, respectively. As for lateral motion, from Figure 4.5 (b) and Table 4.3 (b), it is observed that the hybrid PSO-GWO technique provides better results over ZN and PSO when compared to the passive system as it can lower the lateral acceleration up to 77.81%, which is greater than the percentages achieved by ZN (50.08%) and PSO (75.02%). However, compared to GWO, the percentage improvement of RMS values with a hybrid algorithm is almost similar (approx. 77%). From the Figure 4.5 (c) and Table 4.3 (c), regarding the pitch motion, it can be seen that when compared to the passive system, the ZN, PSO, GWO, and hybrid algorithm reduces the pitch acceleration by up to 49.98%, 70.42%, 58.52%, and 71.42%, respectively. In the case of pitch acceleration, the vibration attenuation capability of the suspension control system using hybrid and PSO algorithms are almost identical. From Figure 4.5 (d) and (e), it is worth observing that when compared to a passive control system, the percentage accelerations (RMS) of roll and yaw motion achieved with FOPID controllers employing the proposed hybrid algorithm are reduced by 75.29% and, 63.74%, respectively, which are comparatively more than other tuning methods as shown in Tables 4.3 (d) and (e), respectively.



(a)



(b)

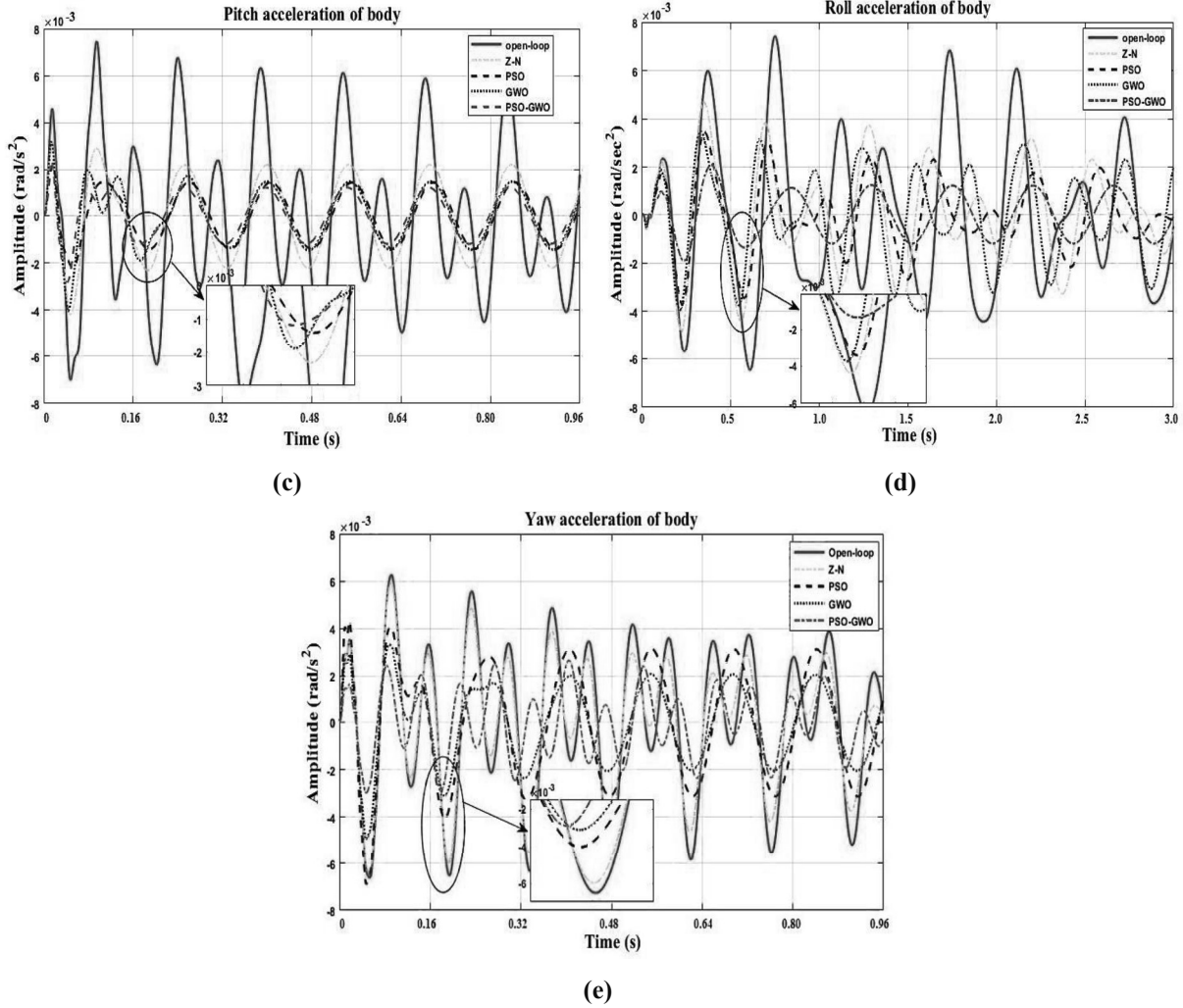


**Figure 4.5** Time histories of vehicle body acceleration under periodic track disturbances (a) vertical acceleration ( $\ddot{Z}_c$ ) (b) lateral acceleration ( $\ddot{Y}_c$ ) (c) pitch acceleration ( $\ddot{\psi}_c$ ) (d) roll acceleration ( $\ddot{\theta}_c$ ), (e) yaw acceleration ( $\ddot{\phi}_c$ )

Now, by using the FOPID controller (4.14), the control force  $u$  could be calculated, which is regarded as the desired force. For the different modes of railway vehicle, the desired force could be achieved with a hydraulic/pneumatic actuator or motor (P. Wang et al., 2015). Based on Eqn. (4.3), the time histories of the active force generated by the optimally tuned suspension system to suppress the vibrations of the car body in five modes are shown in Figure 4.6. Observing Figure 4.6, it can be seen that the FOPID with hybrid algorithm provides a balanced and optimum actuation force for all modes of vehicle, which satisfies all the parameters of the cost function. Moreover, the FOPID controller satisfies the constraints of maximum force ( $w_2$ ) in all five modes (given in Table 4.1) because all the values of the corresponding cost function are less than unity.

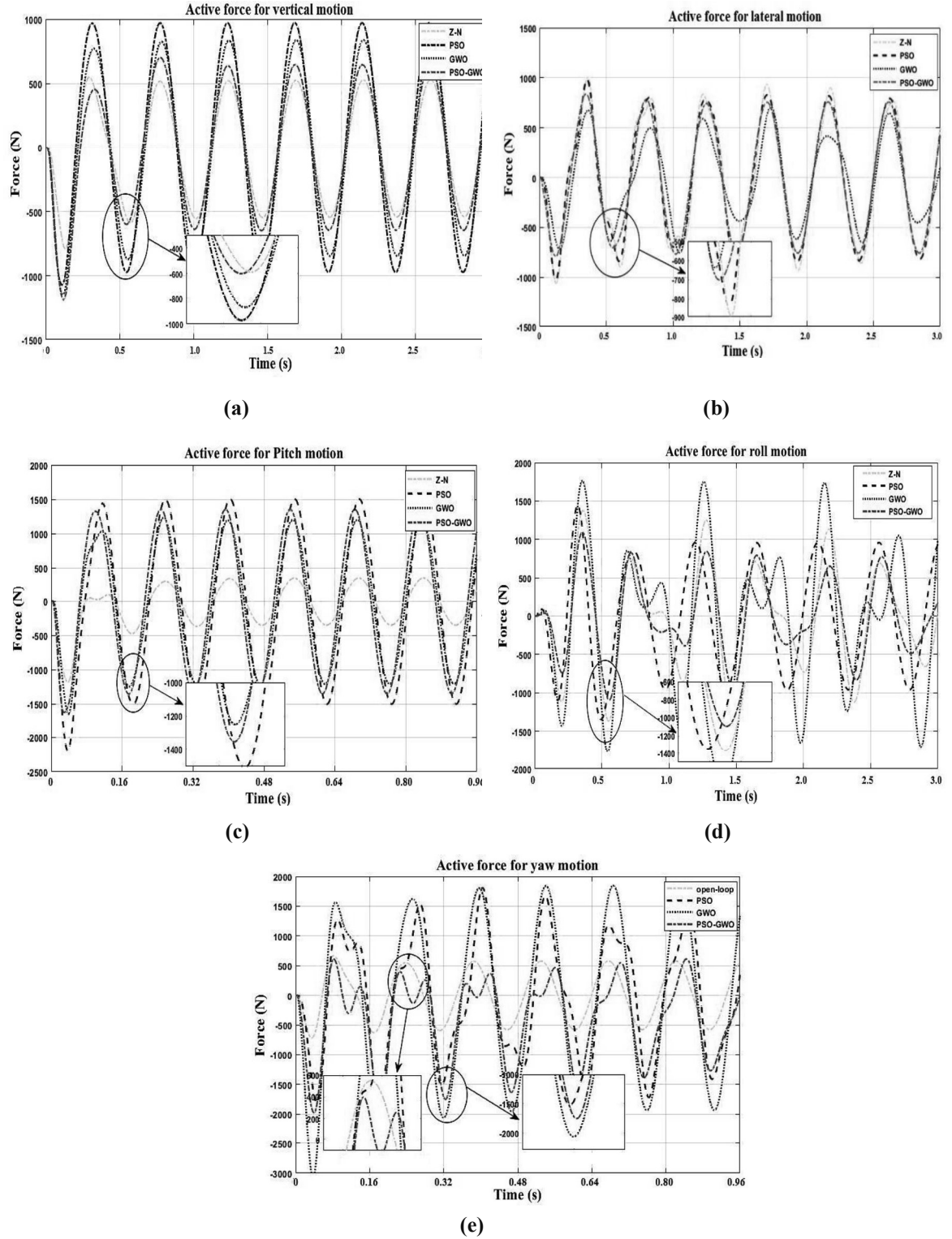


**Figure 4.6** Time histories of active force for different motions of railway vehicle (a) vertical motion ( $u_1$ ) (b) lateral motion( $u_2$ ) (c) pitch motion ( $u_3$ ) (d) roll motion( $u_4$ )and (e) yaw motion ( $u_5$ )

**Table 4.3** RMS values and % improvements of vehicle body accelerations under periodic track disturbances*(a) For vertical acceleration*

<i>index</i>	Open-loop	Z-N	PSO	GWO	<b>PSO-GWO</b>
RMS Values	5.512e-02	1.415e-02	1.342e-02	9.891e-03	<b>8.484e-03</b>
% improvement	-	74.32 %	75.65 %	82.05 %	<b>84.60 %</b>

*(b) For lateral acceleration*

<i>index</i>	Open-loop	Z-N	PSO	GWO	<b>PSO-GWO</b>
RMS Values	5.662e-02	2.826e-02	1.414e-02	1.271e-02	<b>1.256e-02</b>
% improvement	-	50.08 %	75.02 %	77.55 %	<b>77.81 %</b>

*(c) For pitch acceleration*

<i>index</i>	Open-loop	Z-N	PSO	GWO	<b>PSO-GWO</b>
RMS Values	5.264e-03	2.633e-03	1.557e-03	2.184e-03	<b>1.504e-03</b>
% improvement	-	49.98 %	70.42 %	58.52 %	<b>71.42 %</b>

*(d) For roll acceleration*

<i>index</i>	Open-loop	Z-N	PSO	GWO	<b>PSO-GWO</b>
RMS Values	5.445e-03	3.386e-03	2.623e-03	2.848e-03	<b>1.345e-03</b>
% improvement	-	37.81 %	51.82 %	47.64 %	<b>75.29 %</b>

*(e) For yaw acceleration*

<i>index</i>	Open-loop	Z-N	PSO	GWO	<b>PSO-GWO</b>
RMS Values	4.380e-03	4.103e-03	2.944e-03	1.862e-03	<b>1.588e-03</b>
% improvement	-	6.3 %	32.78 %	57.48 %	<b>63.74 %</b>

### 4.6.3 Simulation under random track irregularities

In this part, the performance of an optimally tuned FOPID controller is evaluated under random track disturbances. To obtain the results in both time and frequency domain, the PSD functions defined in Eqns. (3.46)-(3.48) of chapter 3 have been utilized.

#### 4.6.3.1 Frequency domain Responses of acceleration of the body

The power spectral densities (PSDs) of the vehicle body's vertical, lateral, pitch, roll, and yaw accelerations calculated from the open loop and closed loop control systems have been represented in Figure 4.7. The frequencies at which the PSDs of generalized accelerations show its largest peaks are denoted as resonant frequencies for the respective motion. The calculated natural frequencies of car body accelerations have been provided in Table 4.4. Also, the root mean square (RMS) values, and the percentage improvement of RMS value for different motions are given in Table 4.5. The percentage improvement of RMS values using different tuning algorithms over the passive system has been calculated by using Eqn. (4.20).

**Table 4.4** Resonance frequencies of car body

Car body motion	Resonant frequency (Hz)
Bounce	1.884
Lateral	0.502
Pitch	1.652
Roll	0.433
Yaw	0.856

In the case of vertical motion, from Figure 4.7 (a), it is found that the two resonant peaks of vertical acceleration are effectively reduced by the FOPID controller tuned with metaheuristic algorithms. However, among metaheuristic algorithms, hybrid PSO-GWO performs better in attenuating the vertical vibration at the range [1-10] Hz. Also, the % improvement (RMS) of vertical acceleration with a hybrid algorithm over the passive system is found to be 34.83%, which is comparatively higher than that of other metaheuristic algorithms, as rendered in Table 4.5(a). When it comes to lateral motion, if we take a look at Figure 4.7 (b), we can see that the active suspension system has good vibration attenuation ability for the first and second resonant peaks with all tuning algorithms. However, for the third resonant peak in the range of [1-5] Hz, the ZN and PSO algorithms perform worse compared to the GWO and hybrid algorithms. However, among GWO and hybrid algorithms, the performance of the hybrid algorithm retains the good attenuation ability as it can reduce the lateral vibration up to 29.27%, which is more

than that of GWO and other tuning techniques shown in Table 4.5 (b). It can be seen from Figure 4.7 (c) that the resonant peak of pitch acceleration at the range [0-1.5] Hz is successfully reduced with a suspension system controlled by an optimally-tuned FOPID controller, where the proposed hybrid mode algorithm dominates the other tuning methods.

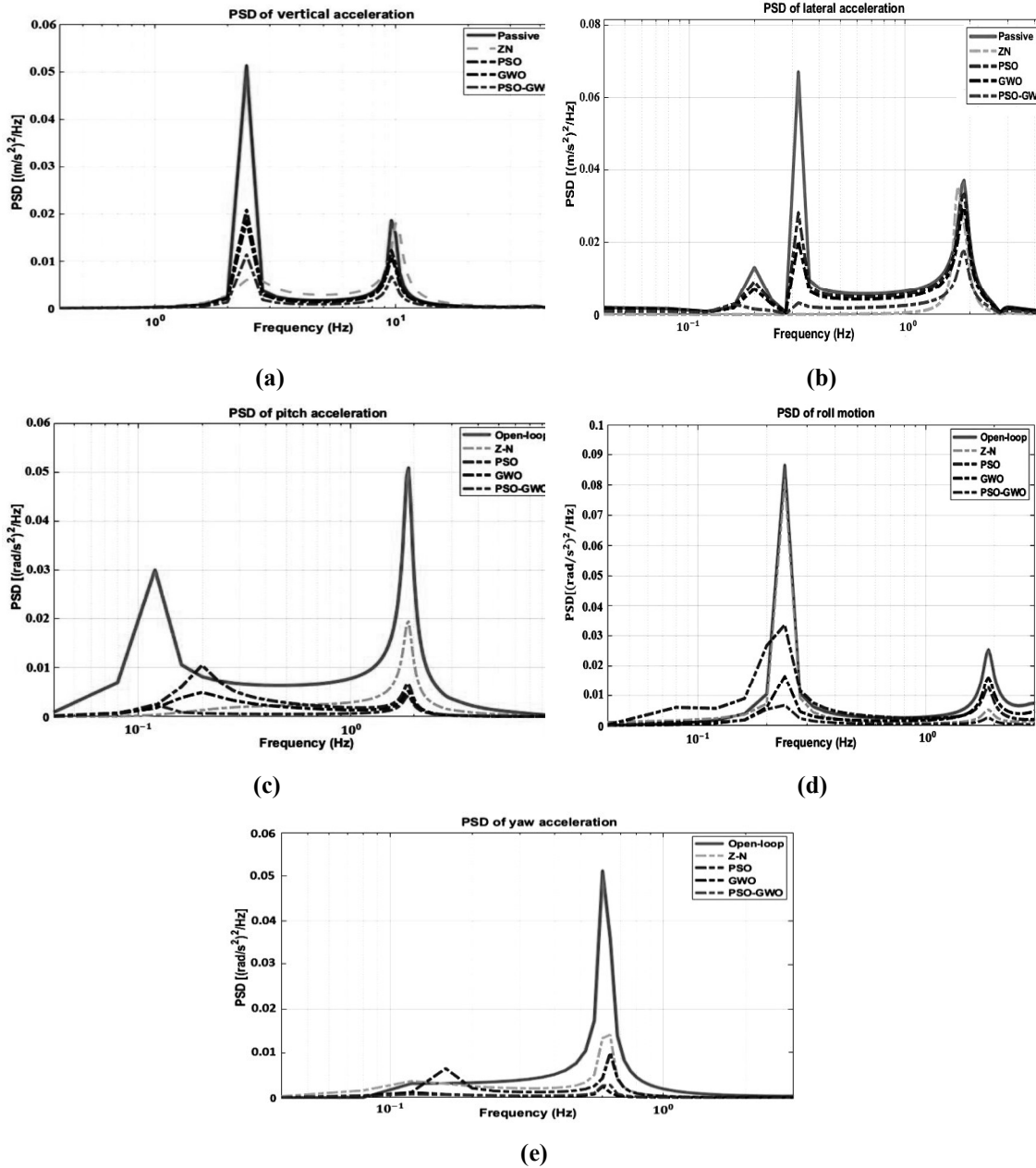


**Figure 4.7** Power spectral densities of vehicle body acceleration under random track inputs (a) vertical acceleration ( $\ddot{Z}_c$ ) (b) lateral acceleration ( $\ddot{Y}_c$ ) (c) pitch acceleration ( $\ddot{\psi}_c$ ) (d) roll acceleration ( $\ddot{\theta}_c$ ), and (e) yaw acceleration ( $\ddot{\phi}_c$ )



**Table 4.5** RMS values and % improvement of vehicle body acceleration under random track disturbances

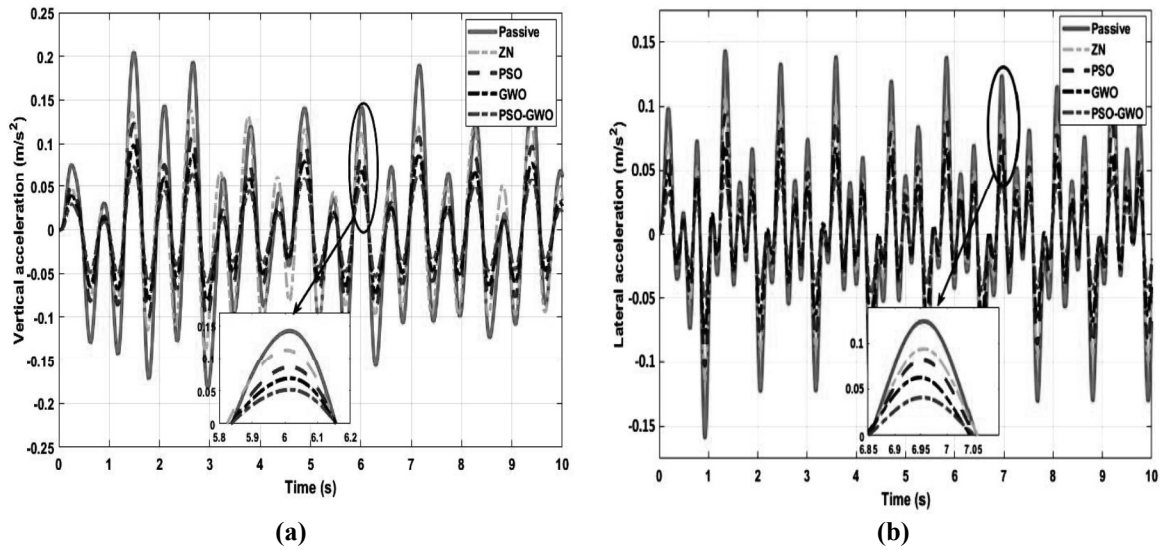
<i>(a) For vertical acceleration</i>					
<i>index</i>	Open-loop	Z-N	PSO	GWO	<b>PSO-GWO</b>
RMS Values ( $m/s^2$ )	3.828e-02	3.304e-02	2.866e-02	2.706e-02	<b>2.505e-02</b>
% improvement	-	13.78 %	25.32 %	29.54 %	<b>34.83 %</b>
<i>(b) For lateral acceleration</i>					
<i>index</i>	Open-loop	Z-N	PSO	GWO	<b>PSO-GWO</b>
RMS Values ( $m/s^2$ )	5.253e-02	4.664e-02	4.233e-02	4.009e-02	<b>3.715e-02</b>
% improvement	-	11.21 %	19.41 %	23.08 %	<b>29.27 %</b>
<i>(c) For pitch acceleration</i>					
<i>index</i>	Open-loop	Z-N	PSO	GWO	<b>PSO-GWO</b>
RMS Values ( $rad/s^2$ )	5.603e-02	4.295e-02	4.128e-02	3.908e-02	<b>3.408e-02</b>
% improvement	-	23.34 %	26.32 %	30.25 %	<b>39.17 %</b>
<i>(d) For roll acceleration</i>					
<i>index</i>	Open-loop	Z-N	PSO	GWO	<b>PSO-GWO</b>
RMS Values ( $rad/s^2$ )	6.285e-02	5.790e-02	5.468e-02	5.106e-02	<b>4.714e-02</b>
% improvement	-	7.87 %	12.99 %	18.75 %	<b>24.99 %</b>
<i>(e) For yaw acceleration</i>					
<i>index</i>	Open-loop	Z-N	PSO	GWO	<b>PSO-GWO</b>
RMS Values ( $rad/s^2$ )	4.174e-02	3.592e-02	3.276e-02	3.019e-02	<b>2.778e-02</b>
% improvement	-	13.94 %	21.52 %	27.67 %	<b>33.45 %</b>

The dominance of the FOPID controller with a hybrid algorithm over passive, ZN, PSO, and GWO is also verified in Table 4.5 (c), where the suspension system tuned with the hybrid method can reduce the vibration level up to 39.17%, which is higher than that of other tuning methods. Regarding roll acceleration, as shown in Figure 4.7 (d), it can be noticed that the active suspension system, when tuned with three metaheuristic algorithms, exhibits better attenuation capabilities for the first and second resonant peaks compared to the passive suspension system and ZN tuning algorithm. According to Table 4.5 (d), the hybrid algorithm has a lower RMS value of roll acceleration compared to other tuning methods. The decrease percentage of RMS values is approximately 24.99%, which is the highest among all the tuning algorithms. Moreover, in the case of yaw

motion, from Figure 4.7 (e) and Table 4.5 (e), it is also seen that an active suspension system controlled with an optimal tuned FOPID controller can reduce the yaw acceleration of the vehicle body by a large extent as compared to the passive system. However, among all tuning methods, hybrid PSO-GWO achieves a 33.45% reduction in RMS values of yaw acceleration. In contrast, the percentage reduction is only 13.94%, 21.52%, and 27.67%, as in the case of ZN, PSO, and GWO.

#### 4.6.3.2 Time responses of acceleration of the body

The time histories of open-loop output responses and the FOPID-tuned closed-loop responses for the accelerations of the vehicle body in all five modes (vertical, lateral, pitch, roll, and yaw) have been illustrated in Figure 4.8. From Figure 4.8, it is seen that the FOPID controller tuned with the ZN and metaheuristic algorithms are able to reduce the body acceleration when compared to the passive system. However, when the controller is tuned with hybrid PSO-GWO algorithms, this % improvement has increased and also it satisfies the constraints of cost function. Therefore, we can conclude that the suspension control system using hybrid PSO-GWO has a greater ability to reduce vibrations compared to passive systems and other metaheuristic algorithms.



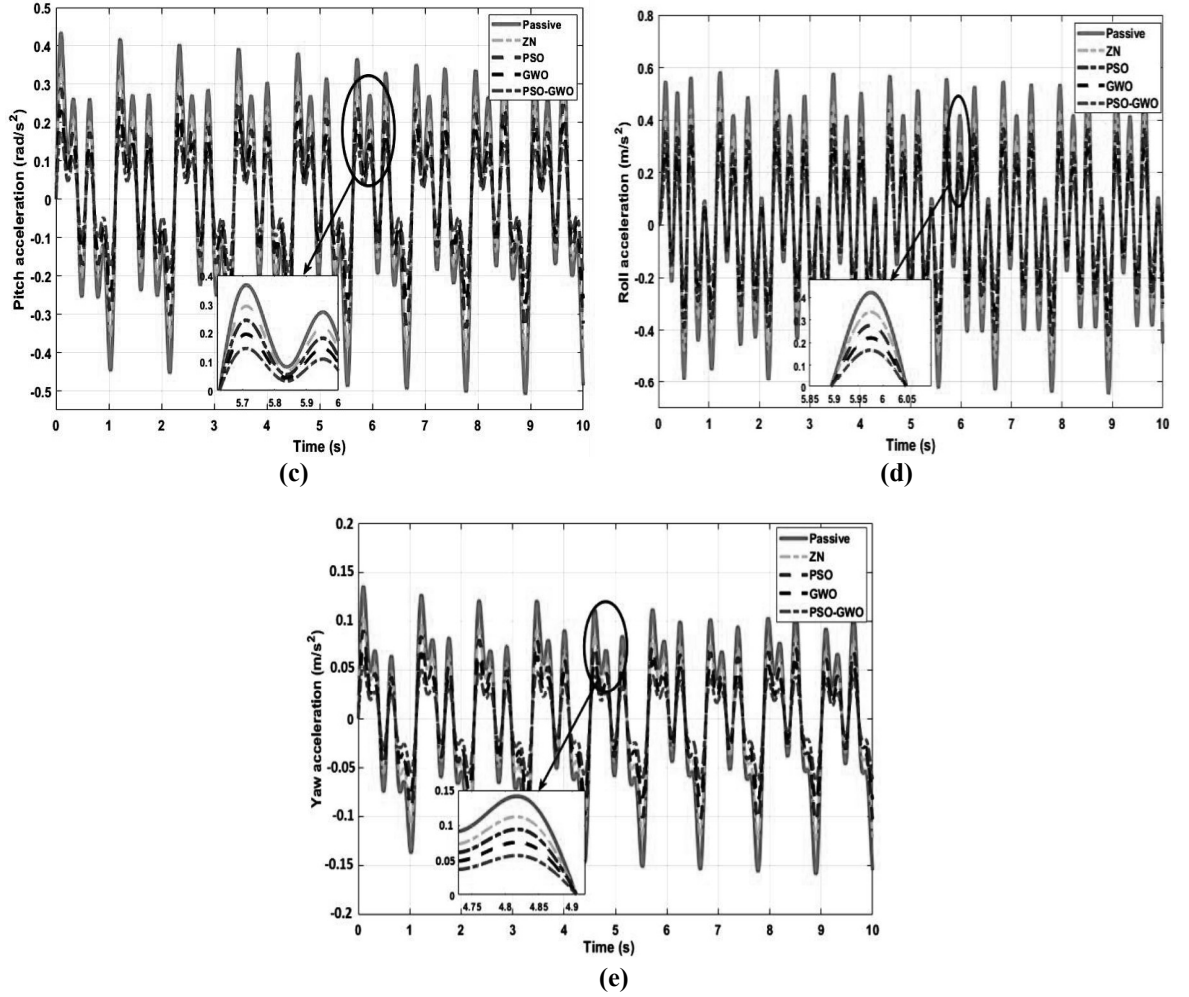


**Figure 4.8** Time histories of vehicle body acceleration under periodic track disturbances (a) vertical acceleration ( $\ddot{Z}_c$ ) (b) lateral acceleration ( $\ddot{Y}_c$ ) (c) pitch acceleration ( $\ddot{\psi}_c$ ) (d) roll acceleration ( $\ddot{\theta}_c$ ), and (e) yaw acceleration( $\ddot{\phi}_c$ )

#### 4.7 Conclusions

This chapter introduces a novel active suspension system that regulates an optimally tuned FOPID controller. The model consists of 27 degrees-of-freedom. A decentralized control structure having five independent FODIP controllers was adopted to suppress the vibration of the different motions of the car body. To calculate the optimal active force, a novel hybrid metaheuristic algorithm named hybrid PSO-GWO was proposed, and the simulated results were compared with a passive system as well as classical (ZN) and two metaheuristic tuning algorithms (PSO, GWO). The outcomes of the car body's vertical, lateral, pitch, roll, and yaw acceleration under periodic and random track irregularities were analyzed in both time and frequency domains. According to simulation and analysis, the following outcomes are encased:

- The proposed hybrid algorithm (PSO-GWO) tuned FOPID controller provides the best trade-off between maximum acceleration and control efforts expressed in terms of quadratic cost function compared to PSO and GWO. Apart from this it is also seen that the PSO and GWO have a trapping issue at the local minimum points with the slower convergence rate as compared to proposed hybrid algorithm.
- Under periodic track disturbances, it was also noted that the suspension system controlled with a hybrid-tuned FOPID controller has comparatively better attenuation towards the vehicle vibration in terms of the percentage improvement in RMS values. It provides approximately 84.60%, 77.81%, 71.42%, 75.29 %, and 63.74% improvement of RMS values as in the case of the vehicle's vertical, lateral, pitch, roll, and yaw motions, respectively.
- Under random track disturbances, it is evident that the FOPID controller using hybrid algorithm provides better suppression results of resonant peaks at the extensive range of frequency. The percentage reduction in RMS values for the vertical, lateral, pitch, roll, and yaw motion were 34.83%, 29.27%, 39.17%, 24.99%, and 33.45%, respectively, as compared to the classical and other metaheuristic (PSO and GWO) techniques.

From the above discussions, it may be concluded that the active suspension system with PSO-GWO tuned FOPID controller shows its effectiveness in attaining good vibration attenuation ability under periodic and random excitations. However, it can also be seen that the attenuation ability of the proposed controller is significantly higher in the case of periodic track irregularities compared to the random track. The reason behind this is the configuration of a decentralized controller, which calculates the control force based on the periodic wavelengths of the track. In practical scenarios, a train is more likely to encounter random track irregularities than periodic ones. Consequently, this point suggests that a centralized control strategy is required, which would independently determine the required damping force to manage such chaotic circumstances successfully. Also, the dynamics of the actuator will be added in further study, which make the control system more practicable and real.

## SYNTHESIS OF CENTRALIZED CONTROLLER

---

*In the quest for precision and efficiency in railway dynamics, the spotlight turns to centralized controller design. This section addresses the fundamental ideas and revolutionary effects of a centralized approach, in which a single intelligence performs the symphony of control, guaranteeing a harmonious and optimal riding experience for railway cars. A modified LQG controller with ANFIS-based actuation is presented in this chapter. The efficiency of the proposed control scheme is evaluated under random track disturbance, and the results are validated with the human comfort data of RDSO.*

### 5.1 Introduction

As per previously reported literature on control algorithms, the optimal control law is the most preferred field of vibration control in railway vehicles. This control technique is based on the centralized control architecture in which a single controller is responsible for every control action. The schematic of the proposed active suspension control system used to control the vibrations of railway vehicle is shown in Figure 5.1. From Figure 5.1, it can be seen that the proposed scheme constitutes two types of controllers: the system controller and the force tracking controller. These two controllers can work in two steps alternately. Based on the measured output, the system controller generates the desired controlling force in the first step. Then, in the second step, with the help of the force-tracking controller, the command current is generated that compels the actuators to track the required controlling force. In this study, the part of the system controller is realized by the metaheuristic-based linear quadratic Gaussian control law. On the other hand, the ANFIS inverse model is used as a force-tracking controller. The five body motions are controlled by implementing the six electro-hydraulic actuators. Among them, the four actuators are vertically mounted on the right and left sides of the front and rear bogies, which control the bounce, pitch, and roll motions, and the remaining two actuators are mounted horizontally above the front and rear bogies, controlling the lateral and yaw motion of the vehicle body as demonstrated in the previous chapter.

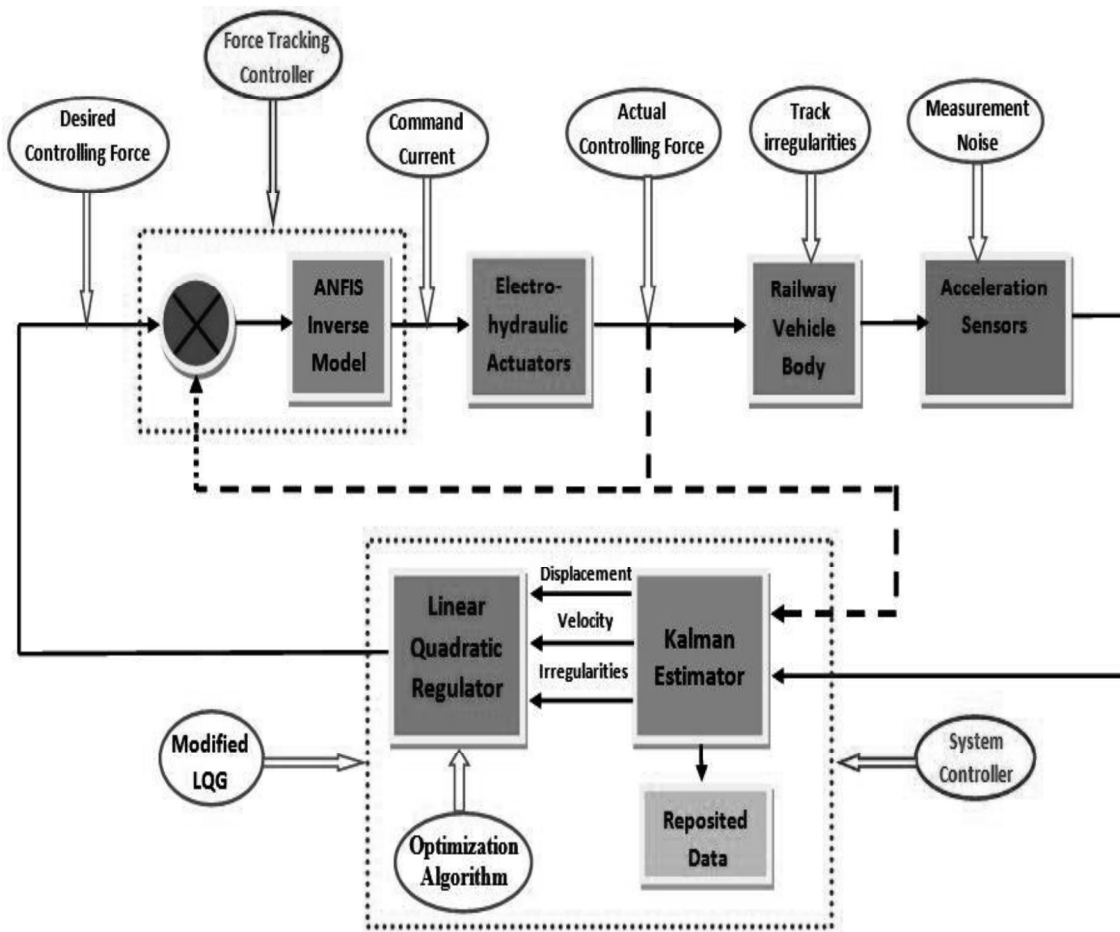


**Figure 5.1** Schematic of centralized vibration control system for railway vehicle

As per contribution of this chapter, following points are worthy to note:

- A twenty-seven-degree-of-freedom dynamic model of a full-car railway vehicle incorporated with rail irregularities and wheel-track contact forces is developed.
- An ANFIS inverse model using a hybrid algorithm is trained to mimic the forward dynamic behavior of an electro-hydraulic (E-H) actuator.
- A linear quadratic Gaussian controller tuned with a novel evolutionary algorithm (EO-LQG) is adopted to generate the active control forces, in which state variables are estimated with the Kalman filter.
- The performance of the proposed strategy is assessed by integrating the LQG controller with the ANFIS inverse model. The evaluation is conducted using random track abnormalities, and the results are thoroughly studied in both the time and frequency domains.

- The proposed control scheme, passive system, and classical tuning methods are compared using root mean square (RMS) acceleration data.
- Additionally, the assessment of the comfort of railway vehicles is conducted utilizing Sperling's methodologies. Comparing the simulation findings with previously reported semi-active and active suspension systems, it is evident that the proposed controller has the potential to enhance the ride comfort of railway trains.

## 5.2 A 27-DOF dynamic model of a railway vehicle

The analytical model of vehicle-track system integrated with active suspension system is developed in this section. The definitions of various symbols related to the vehicle body, bogies, and wheel-set motion used in dynamic modeling have already been given in list of symbols. The governing equation of motion of railway vehicle dynamics is presented as follows:

### 5.2.1 Vehicle body dynamics

$$M_c \ddot{Z}_c + 2K_{2z}[(Z_c - Z_{t1}) + (Z_c - Z_{t2})] + 2C_{2z}(\dot{Z}_c - \dot{Z}_{t1} + \dot{Z}_c - \dot{Z}_{t2}) = [F_{z1} + F_{z2} + F_{z3} + F_{z4}] \quad (5.1)$$

$$M_c \ddot{Y}_c + 2K_{2y}[2(y_c + h_3\theta_c) - y_{t1} - y_{t2} - h_2\theta_{t1} - h_2\theta_{t2}] + 2C_{2y}[2(\dot{y}_c + h_3\dot{\theta}_c) - \dot{y}_{t1} - \dot{y}_{t2} - h_2\dot{\theta}_{t1} - h_2\dot{\theta}_{t2}] = [F_{y1} + F_{y2}] \quad (5.2)$$

$$I_{zc} \ddot{\Psi}_c + 2L_b K_{2y}(2L_b \Psi_c - y_{t1} + y_{t2} - h_2\theta_{t1} + h_2\theta_{t2}) + 2L_b C_{2z}(2L_b \dot{\Psi}_c - \dot{y}_{t1} + \dot{y}_{t2} - h_2\dot{\theta}_{t1} + h_2\dot{\theta}_{t2}) + 2d_s^2 K_{2x}(2\Psi_c - X_{t1} - X_{t2}) + 2d_s^2 C_{2x}(2\dot{\Psi}_c - \dot{X}_{t1} - \dot{X}_{t2}) = L_b[F_{y1} - F_{y2}] \quad (5.3)$$

$$I_{xc} \ddot{\theta}_c + 2b_2^2 K_{2z}(2\theta_c - \theta_{t1} - \theta_{t2}) + 2b_2^2 c_{2z}(2\dot{\theta}_c - \dot{\theta}_{t1} - \dot{\theta}_{t2}) + 2h_3 K_{2y}[2(y_c + h_3\theta_3) - y_{t1} - y_{t2} + h_2\theta_{t1} + h_2\theta_{t2}) + 2h_3 c_{2y}(2(\dot{y}_c + h_3\dot{\theta}_3) - \dot{y}_{t1} - \dot{y}_{t2} + h_2\dot{\theta}_{t1} + h_2\dot{\theta}_{t2})] = [h_3(F_{y1} + F_{y2}) + b_2((F_{z1} + F_{z3}) - (F_{z2} + F_{z4}))] \quad (5.4)$$

$$I_{yc} \ddot{\phi}_c + 2L_2 K_{2z}(2L_b \phi_c + Z_{t1} - Z_{t2}) + 2L_b C_{2z}(2L_b \dot{\phi}_c + \dot{Z}_{t1} - \dot{Z}_{t2}) = [L_b(F_{z1} + F_{z2}) - (F_{z1} + F_{z2})] \quad (5.5)$$

### 5.2.2. Bogie dynamics ( $i=1, 2$ )

$$M_t \ddot{Z}_{ti} + 2k_{1z}[(2Z_{ti} - (Z_{w(2i-1)} + Z_{w(2i)}))] + 2k_{2z}[(Z_{ti} - Z_c) - (-1)^i L_b \phi_c] + 2c_{1z}[(2\dot{Z}_{ti} - (\dot{Z}_{w(2i-1)} + \dot{Z}_{w(2i)}))] + 2c_{1z}[(\dot{Z}_{ti} - \dot{Z}_c) - (-1)^i L_b \dot{\phi}_c] = -(F_{z(2i-1)} + F_{z(2i)}) \quad (5.6)$$

$$M_t \ddot{y}_{ti} + 2k_{1y}[2y_{ti} - (y_{w(2i-1)} + y_{w(2i)}) + 2h_1\theta_{ti}] + 2k_{2y}[(y_{ti} - y_c) - (h_3\theta_c + h_2\theta_{ti}) - (-1)^i L_b \psi_c] + 2c_{1y}[2\dot{y}_{ti} - (\dot{y}_{w(2i-1)} + \dot{y}_{w(2i)}) + 2h_1\dot{\theta}_{ti}] + 2c_{2y}[(\dot{y}_{ti} - \dot{y}_{w(2i-1)}) - (h_3\dot{\theta}_c + h_2\dot{\theta}_{ti}) - (-1)^i L_b \dot{\psi}_c] = -F_{yi} \quad (5.7)$$

$$J_{zt} \ddot{\psi}_{ti} + 2d_p^2 k_{1x}[2\psi_{ti} - (\psi_{w(2i-1)} + \psi_{w(2i)})] + 2d_p^2 c_{1x}[2\dot{\psi}_{ti} - (\dot{\psi}_{w(2i-1)} + \dot{\psi}_{w(2i)})] + 2d_s^2 k_{2x}[\psi_{ti} - \psi_c] + 2d_s^2 c_{2x}[\dot{\psi}_{ti} - \dot{\psi}_c] + 2L_d k_{1y}[2L_d \phi_{ti} - (Y_{w(2i-1)} - Y_{w(2i)})] + 2L_d c_{1y}[2L_d \dot{\psi}_{ti} - (\dot{Y}_{w(2i-1)} - \dot{Y}_{w(2i)})] = 0 \quad (5.8)$$

$$J_{xt} \ddot{\theta}_{ti} + 2h_1 k_{1y}[2h_1\theta_{ti} + (2Y_{ti} - (Y_{w(2i-1)} + Y_{w(2i)}))] + 2h_2 k_{2y}[h_3\theta_c + h_2\theta_{ti} + (Y_{ti} + Y_c) - (-1)^i L_b \psi_c] + 2b^2 k_{1z}[2\theta_{ti} - (\theta_{w(2i-1)} + \theta_{w(2i)})] + 2b^2 k_{2z}[\theta_{ti} - \theta_c] + 2h_1 c_{1y}[2h_1\dot{\theta}_{ti} + (2\dot{y}_{ti} - (\dot{y}_{w(2i-1)} + \dot{y}_{w(2i)}))] + 2h_2 c_{2y}[h_3\dot{\theta}_c + h_2\dot{\theta}_{ti} + (\dot{y}_{ti} + \dot{y}_c) - (-1)^i L_b \dot{\psi}_c] + 2b^2 c_{1z}[2\dot{\theta}_{ti} - (\dot{\theta}_{w(2i-1)} + \dot{\theta}_{w(2i)})] + 2b^2 c_{2z}[\dot{\theta}_{ti} - \dot{\theta}_c] = -F_{yi} h_3 \quad (5.9)$$

$$J_{yt} \ddot{\phi}_{ti} + 2L_d c_{1z}[2L_d \dot{\phi}_{ti} + (\dot{Z}_{w(2i-1)} - \dot{Z}_{w(2i)})] + 2L_d k_{1z}[2L_d \phi_{ti} + (Z_{w(2i-1)} - Z_{w(2i)})] = 0 \quad (5.10)$$

### 5.2.3. Wheel-set dynamics ( $i=1, 2$ , while $j=1$ ; $i=3, 4$ , while $j=2$ )

$$M_w \ddot{Z}_{wi} + 2k_{1z}[(Z_{wi} - Z_{tj}) - (-1)^i L_d \phi_{tj}] + 2c_{1z}[(\dot{Z}_{wi} - \dot{Z}_{tj}) - (-1)^i L_d \dot{\phi}_{tj}] + k_{hz}[2Z_{wi} - Z_{vi}] = 0 \quad (5.11)$$

$$M_w \ddot{Y}_{wi} + 2k_{1y}[(Y_{wi} - Y_{tj}) - h_1\theta_{tj} + (-1)^i L_d \psi_{tj}] + 2c_{1y}[(\dot{Y}_{wi} - \dot{Y}_{tj}) - h_1\dot{\theta}_{tj} + (-1)^i L_d \dot{\psi}_{tj}] + k_{gy}[Y_{wi} - Y_{ai} - R_1\theta_{cli}] + 2f_{22}\left[\frac{1}{V}\left(1 + \frac{\sigma R_1}{a}\right)\dot{Y}_{wi} - \frac{\sigma R_1}{V a}\dot{Y}_{ai} - \frac{\sigma R_1^2}{V a}\dot{\theta}_{cli} - \psi_{wi}\right] = 0 \quad (5.12)$$

$$J_{zw} \ddot{\psi}_{wi} + 2d_p^2 k_{1x}[\psi_{wi} - \psi_{tj}] + 2d_p^2 c_{1x}[(\dot{\psi}_{wi} - \dot{\psi}_{tj})] + 2f_{11}\left[\frac{\lambda_e a}{R_1}(Y_{wi} - Y_{ai} - R_1\theta_{cli}) + \frac{a^2}{V}\dot{\psi}_{wi}\right] + k_{gy}\psi_{wi} = 0 \quad (5.13)$$

## 5.3 State-space formulation

In this section the complete state-space formulation of vehicle-track system is presented.

Let,

$$q = [Z_c, Y_c, \psi_c, \theta_c, \varphi_c, Z_{t1}, Y_{t1}, \psi_{t1}, \theta_{t1}, \varphi_{t1}, Z_{t2}, Y_{t2}, \psi_{t2}, \theta_{t2}, \varphi_{t2}, Z_{w1}, Y_{w1}, \psi_{w1}, Z_{w2}, Y_{w2}, \psi_{w2}, Z_{w3}, Y_{w3}, \psi_{w3}, Z_{w4}, Y_{w4}, \psi_{w4}]^T, u = [F_{z1}, F_{z2}, F_{z3}, F_{z4}, F_{y1}, F_{y2}]^T, \text{ and } w = [Z_{v1}, Y_{a1}, \theta_{cl1}, Z_{v2}, Y_{a2}, \theta_{cl2}, Z_{v3}, Y_{a3}, \theta_{cl3}, Z_{v4}, Y_{a4}, \theta_{cl4}, \dot{Z}_{v1}, \dot{Y}_{a1}, \dot{\theta}_{cl1}, \dot{Z}_{v2}, \dot{Y}_{a2}, \dot{\theta}_{cl2}, \dot{Z}_{v3}, \dot{Y}_{a3}, \dot{\theta}_{cl3}, \dot{Z}_{v4}, \dot{Y}_{a4}, \dot{\theta}_{cl4}]^T \text{ are}$$

the displacements, control, and disturbance vectors, respectively.

Then the Eqns. (5.1)-(5.13) can be represented in the following matrix form:

$$[M]\ddot{q} + [C]\dot{q} + [K]q = [F_u]u + [F_w]w \quad (5.14)$$



where  $[M]$  ( $\mathcal{R}^{27 \times 27}$ ),  $[C]$  ( $\mathcal{R}^{27 \times 27}$ ), and  $[K]$  ( $\mathcal{R}^{27 \times 27}$ ) are the mass, damping, and stiffness matrices of the railway vehicle;  $[F_u]$  ( $\mathcal{R}^{27 \times 6}$ ),  $[F_w]$  ( $\mathcal{R}^{27 \times 24}$ ) are the position matrices of control inputs and track disturbances acting on the railway vehicle body and wheels of wheelsets, respectively.

Now by defining the state vector  $x_r = [q^T \dot{q}^T]^T$  for railway vehicle system, the state and output equations are given as

$$\begin{cases} \dot{x}_r = [A_r]x_r + [B_r]u + [E_r]w \\ y_r = [C_r]x_r + [D_r]u + [H_r]w + N \end{cases} \quad (5.15)$$

where  $[A_r] = \begin{bmatrix} 0 & I \\ -M^{-1}K & -M^{-1}C \end{bmatrix} \in \mathcal{R}^{54 \times 54}$ ,  $[B_r] = \begin{bmatrix} 0 \\ M^{-1}F_u \end{bmatrix} \in \mathcal{R}^{54 \times 6}$ ,  $[E_r] = \begin{bmatrix} 0 \\ M^{-1}F_w \end{bmatrix} \in \mathcal{R}^{54 \times 24}$ ,  $[C_r] = [-M^{-1}K \quad -M^{-1}C] \in \mathcal{R}^{27 \times 54}$ ,  $[D_r] = [M^{-1}F_u] \in \mathcal{R}^{27 \times 6}$ , and  $[H_r] = [M^{-1}F_w] \in \mathcal{R}^{27 \times 24}$  are the coefficient matrices, which can be derived from Eq. (14). The vector  $N$  defines the sensors noise.

### 5.3.1 Track irregularities model

The abnormalities present on the tracks are the fundamental cause of vibrations in the railway vehicle. These irregularities can be periodic or random in nature. Here, three types of random track irregularities such as vertical profile ( $Z_{vi}$ ), lateral alignment ( $Y_{ai}$ ), and cross-level ( $\theta_{cli}$ ), are used as an input to the system, where  $i = 1, 2, 3, 4$ . A good approximation of the random irregularities can be realized by stationary random processes in the form of power spectral densities (PSDs) (Zhai 2020). These PSDs are calculated by taking the Fourier Transform of the autocorrelation function and can be expressed as:

$$S_v(\omega) = \frac{\sqrt{A_v} \cdot \Omega_c \cdot V^2}{(s + |V \cdot \Omega_r|)(s + |V \cdot \Omega_c|)} \quad (5.16)$$

$$S_a(\omega) = \frac{\sqrt{A_a} \cdot \Omega_c \cdot V^2}{(s + |V \cdot \Omega_r|)(s + |V \cdot \Omega_c|)} \quad (5.17)$$

$$S_{cl}(\omega) = \frac{\sqrt{A_v} \cdot \Omega_c \cdot V^2 \cdot s}{l_r(s + |V \cdot \Omega_r|)(s + |V \cdot \Omega_c|)(s + |V \cdot \Omega_s|)} \quad (5.18)$$

where  $\Omega_r$ ,  $\Omega_c$  and  $\Omega_s$  are the cut-off frequencies taken in rad/m;  $A_v$ ,  $A_a$  and  $A_g$  are roughness constant taken in  $m^2 \cdot \frac{rad}{m}$ ;  $V$  is the velocity of the vehicle;  $l_r$  is the half the distance between the two-rolling circle of the wheel-set (m). The values of these constants and cut-off frequencies are given in *Appendix 1*.

According to Eqns. (16)-(18), for a white noise input  $[\Gamma] = [\xi_v, \xi_v, \xi_v]^T$ , the following state space representation can be used to define the PSDs in the time domain

$$\begin{cases} \begin{bmatrix} \dot{x}_v \\ \dot{x}_a \\ \dot{x}_{cl} \end{bmatrix} = \begin{bmatrix} a_v & 0 & 0 \\ 0 & a_a & 0 \\ 0 & 0 & a_{cl} \end{bmatrix} \begin{bmatrix} x_v \\ x_a \\ x_{cl} \end{bmatrix} + \begin{bmatrix} b_v & 0 & 0 \\ 0 & b_a & 0 \\ 0 & 0 & b_{cl} \end{bmatrix} [\Gamma] \\ \begin{bmatrix} y_v \\ y_a \\ y_{cl} \end{bmatrix} = \begin{bmatrix} c_v & 0 & 0 \\ 0 & c_a & 0 \\ 0 & 0 & c_{cl} \end{bmatrix} \begin{bmatrix} x_v \\ x_a \\ x_{cl} \end{bmatrix} \end{cases} \quad (5.19)$$

where  $\dot{x}_v \in \mathcal{R}^{2 \times 1}$ ,  $\dot{x}_a \in \mathcal{R}^{2 \times 1}$ ,  $\dot{x}_{cl} \in \mathcal{R}^{3 \times 1}$  are the states, and  $y_v \in \mathcal{R}^{1 \times 1}$ ,  $y_a \in \mathcal{R}^{1 \times 1}$ ,  $y_{cl} \in \mathcal{R}^{1 \times 1}$  are the output vectors related to vertical, lateral and cross-level irregularities, respectively.

Similarly,  $a_v$ ,  $a_a$ ,  $a_{cl}$ ,  $b_v$ ,  $b_v$ ,  $b_v$ ,  $c_v$ ,  $c_v$ ,  $c_v$  are the coefficient matrices of shaping filter (D. H. Wang & Liao, 2009a).

If  $Z_{v1}$ ,  $Y_{a1}$ , and  $\theta_{cl1}$  are the excitations applied on the front wheelsets of railway vehicle, then  $Z_{v1} \sim Z_{v4}$ ,  $Y_{a1} \sim Y_{a4}$ , and  $\theta_{cl1} \sim \theta_{cl4}$  are related by the following relation

$$\begin{bmatrix} Z_{v1} \\ Y_{a1} \\ \theta_{cl1} \end{bmatrix} = \begin{bmatrix} y_v \\ y_a \\ y_{cl} \end{bmatrix} e^{-\tau_1 s}, \quad \begin{bmatrix} Z_{v2} \\ Y_{a2} \\ \theta_{cl2} \end{bmatrix} = \begin{bmatrix} Z_{v1} \\ Y_{a1} \\ \theta_{cl1} \end{bmatrix} e^{-\tau_2 s}, \quad \begin{bmatrix} Z_{v3} \\ Y_{a3} \\ \theta_{cl3} \end{bmatrix} = \begin{bmatrix} Z_{v1} \\ Y_{a1} \\ \theta_{cl1} \end{bmatrix} e^{-\tau_3 s}, \quad \begin{bmatrix} Z_{v4} \\ Y_{a4} \\ \theta_{cl4} \end{bmatrix} = \begin{bmatrix} Z_{v1} \\ Y_{a1} \\ \theta_{cl1} \end{bmatrix} e^{-\tau_4 s} \quad (5.20)$$

where  $\tau_1 = 0$ ,  $\tau_2 = \frac{2L_d}{V}$ ,  $\tau_3 = \frac{2L_b}{V}$ ,  $\tau_4 = \frac{2(L_d+L_b)}{V}$  are the time delay between the wheelsets and can be realized using fifth order Padé approximation (Hanta & Procházka, 2014).

$$e^{-\tau_i s} = \frac{30240 - 15120(\tau_i s) + 3360(\tau_i s)^2 - 420(\tau_i s)^3 + 30(\tau_i s)^4 - (\tau_i s)^5}{30240 + 15120(\tau_i s) + 3360(\tau_i s)^2 + 420(\tau_i s)^3 + 30(\tau_i s)^4 + (\tau_i s)^5} \quad (5.21)$$

Now, using Eqns. (5.19)-(5.21), the complete state space form of random rail input for all wheels can be represented as:

$$\begin{cases} \dot{x}_w = [A_w] x_w + [B_w] \Gamma \\ w = \begin{bmatrix} C_w \\ C_w A_w \end{bmatrix} x_w + \begin{bmatrix} 0 \\ C_w B_w \end{bmatrix} \Gamma \end{cases} \quad (5.22)$$

where  $w \in \mathcal{R}^{24 \times 1}$  is the disturbance vector defined in Eqn. (5.14). The coefficient matrices,  $A_w \in \mathcal{R}^{82 \times 82}$ ,  $B_w \in \mathcal{R}^{82 \times 3}$ , and  $C_w \in \mathcal{R}^{24 \times 82}$  can be determined from Eqns. (5.19)-(5.21).

### 5.3.2 State-space formulation for complete vehicle-track system

Let us consider a vector  $X = [x_r^T \ x_w^T]^T$ . Then, according to Eqns. (5.15) & (5.22), the following state space representation can be used to define the combined dynamics of the vehicle and track system.

$$\begin{cases} \dot{X} = [A]X + [B]u + [E]\Gamma \\ Y = [C]X + [D]u + [H]\Gamma + N \end{cases} \quad (5.23)$$

where  $[A] = \begin{bmatrix} A_r & E_r C_w A_w + E_r C_w \\ 0 & A_w \end{bmatrix} \in \mathcal{R}^{136 \times 136}$ ,  $[B] = \begin{bmatrix} B_r \\ 0 \end{bmatrix} \in \mathcal{R}^{136 \times 6}$ ,  $[E] = \begin{bmatrix} E_r C_w B_w \\ B_w \end{bmatrix} \in \mathcal{R}^{136 \times 3}$ ,  $[C] = \begin{bmatrix} C_r & H_r C_w A_w + H_r C_w \end{bmatrix} \in \mathcal{R}^{27 \times 136}$ ,  $[D] = [D_r] \in \mathcal{R}^{27 \times 6}$ , and  $[H] = \begin{bmatrix} H_r C_w B_w \end{bmatrix} \in \mathcal{R}^{27 \times 3}$  are the coefficient matrices of complete system.

The expected or mean values for the random white noise ( $\Gamma$ ) and measurement noise ( $N$ ) are:

$$E(\Gamma) = 0, \text{ and } E(N) = 0 \quad (5.24)$$

### 5.4 Dynamics of electro-hydraulic actuator

An essential component of any active suspension system is an actuator. It is a complete unit by which the external force is injected into the system, complementing the passive suspension system. The fundamental requirements of high frequency isolation and low frequency track undulation are achieved with suspension system that contains a superior

actuation system. There are three major type of actuation systems that are reported in the literature (Abdelkareem et al., 2018): Electro-hydraulic, Electro-pneumatic and Electro-magnetic. Among them, the electro-hydraulic actuator is best suited, because of its excellent force/size ratio, good force bandwidth and reliable operation.

Electro-hydraulic actuation system utilizes the combination of electrical and mechanical means to generate the required force as shown in Figure 5.2 (a). The primary stage of the actuation system contains an electrical motor that delivers torque based on the current value, and the secondary stage contains a hydraulic cylinder connected to a throttle spool valve. The position of spool valve is controlled with motor torque and accordingly the controlled oil flows into the cylinder which ultimately generates the force expressed as:

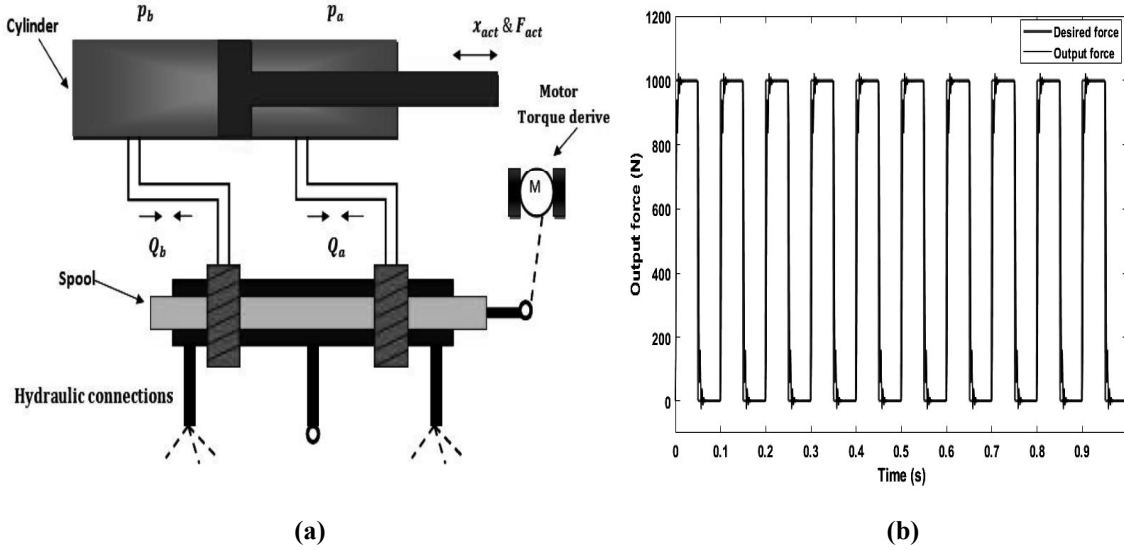


**Figure 5.2** Hydraulic actuator **(a)** basic architecture **(b)** dynamic behavior

For the modeling purpose, the two stages are segregated into electrical and mechanical sub-parts. In the mechanical part, the actuation force is generated on the either side of cylinder by compression or decompression. Eqns. (5.25) & (5.26) represents the oil flow which is the main cause of pressure.

$$Q_a = -\frac{V_a}{\beta} \frac{dp_a}{dt} + a_a \frac{dx_{act}}{dt} \quad (5.25)$$

$$Q_b = -\frac{V_b}{\beta} \frac{dp_b}{dt} + a_b \frac{dx_{act}}{dt} \quad (5.26)$$

where  $Q_a$  and  $Q_b$  represents the flow into two side of cylinder and accordingly  $p_a$  and  $p_b$  are the pressure on that side of cylinder.  $V_a$  is the oil volume,  $\beta$  is oil compressibility and  $x_{act}$  is the extension of actuator.

As we know that the flow described by Eqns. (5.25) & (26) are controlled by the position of spool valve, which follows a square root characteristics as

$$Q_b = k_v x_v \sqrt{p_s - p_b} \quad (5.27)$$

$$Q_a = k_v x_v \sqrt{p_a} \quad (5.28)$$

where  $p_s$  is the hydraulic supply pressure,  $x_v$  is the spool valve displacement and  $k_v$  is the flow coefficient.

Eqns. (5.27) & (5.28), can be represented in the linearised form as

$$Q_a = \frac{\partial Q_a}{\partial x_v} x_v + \frac{\partial Q_a}{\partial p_a} p_a \quad (5.29)$$

$$Q_b = \frac{\partial Q_b}{\partial x_v} x_v + \frac{\partial Q_b}{\partial p_b} p_b \quad (5.30)$$

By equating the cylinder oil flow Eqns. (5.25) & (5.26) with the spool valve oil flow Eqns. (5.27) & (5.28), it will provide the following equations

$$Q_a = \frac{V_a}{\beta} \frac{dp_a}{dt} + a_a \frac{dx_{act}}{dt} = \frac{\partial Q_a}{\partial x_v} x_v + \frac{\partial Q_a}{\partial p_a} p_a \quad (5.31)$$

$$Q_b = \frac{V_b}{\beta} \frac{dp_b}{dt} + a_b \frac{dx_{act}}{dt} = \frac{\partial Q_b}{\partial x_v} x_v + \frac{\partial Q_b}{\partial p_b} p_b \quad (5.32)$$

Here the Eqns. (5.31) & (5.32) represents the pressure of cylinder in terms of spool-valve and actuator extension.

Now the relation between the spool valve and motor torque may be described as

$$x_v = \frac{k_i \cdot i}{m_s s^2 + c_s s + k_s} \quad (5.33)$$

where  $x_v$  is the spool displacement for a input current,  $i$ . The motor develop a torque proportional to current, and this torque is converted into linear force which derives the spool-valve as shown in Fig. 3(a). According to Eqns. (5.31), (5.32) & (5.33), the following state-space model may be used to define the actuator performances:

$$\begin{bmatrix} \dot{x}_v \\ \ddot{x}_v \\ \dot{p}_a \\ \dot{p}_b \end{bmatrix} = \begin{bmatrix} 0 & 1 & 0 & 0 \\ \frac{-k_s}{m_s} & \frac{-c_s}{m_s} & 0 & 0 \\ -\frac{B}{v_a} \frac{\partial Q_a}{\partial p_a} & 0 & \frac{B}{v_a} \frac{\partial Q_a}{\partial p_a} & 0 \\ -\frac{B}{v_b} \frac{\partial Q_b}{\partial x_v} & 0 & 0 & -\frac{B}{v_b} \frac{\partial Q_b}{\partial p_b} \end{bmatrix} \begin{bmatrix} x_v \\ \dot{x}_v \\ p_a \\ p_b \end{bmatrix} + \begin{bmatrix} 0 \\ \frac{k_i}{m_s} \\ 0 \\ 0 \end{bmatrix} i + \begin{bmatrix} 0 \\ 0 \\ \frac{Ba_a}{v_a} \\ \frac{-Bb_a}{v_b} \end{bmatrix} \dot{x}_{act} \quad (5.34)$$

$$f_{act} = [0 \quad 0 \quad -a_a \quad a_b] \begin{bmatrix} x_v \\ \dot{x}_v \\ p_a \\ p_b \end{bmatrix} + [0] i + [-c_d] \dot{x}_{act} \quad (5.35)$$

The various parameters of electro-hydraulic actuator used in simulations have been given in (Williamson et al., 2009). The basic architecture and dynamic behavior of the hydraulic actuator is illustrated in Figures 3(a), and (b), respectively. Figure 3(b) shows the output force response to a square wave input of 1000 N at 10 Hz frequency. From the figure, it is clear that the performance of actuator may satisfy the need of application.

## 5.5 Inverse modeling of electro-hydraulic actuator

The inverse electro-hydraulic model constitutes the force tracking controller that is used to determine the command current based on the required force. In the present study, the adaptive neuro fuzzy-interface technique (ANFIS) is adopted to build the inverse E-H model.

### 5.5.1 Training of ANFIS model

To train the electro-hydraulic actuator, a five layer two-input two-rule ANFIS technique is employed (Zong et al., 2013). The architecture used for training of ANFIS model has been shown in Figure 5.3. In general, the accuracy of ANFIS model relies on the size of the input dataset (A. Singh & Sathans, 2017). As the number of input data set increases, its accuracy improves, but concurrently, the training time of model will also increase. Therefore, in order to maintain a balance between time consumption and accuracy, the inputs are selected as current damping force, previous damping force, current velocity, and previous velocity. The resulting output is the current command current. Then, based on hybrid algorithm, the ANFIS constructs the fuzzy interface system and the membership function are adjusted with given input/output datasets.

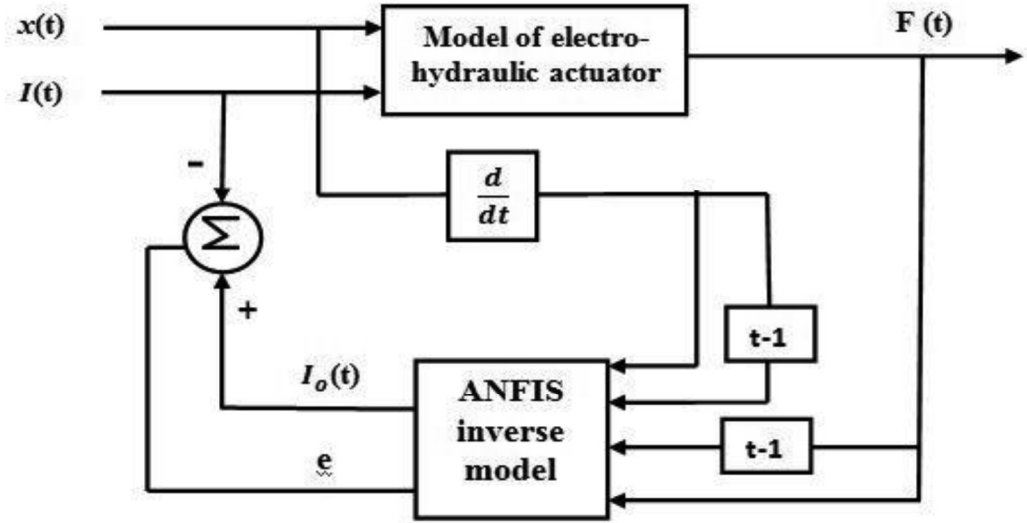


**Figure 5.3** ANFIS modeling for inverse dynamics of electro-hydraulic actuator

The input command current  $I(t)$ , and input velocity  $\dot{x}(t)$  are considered as white noise signal with amplitudes ranging from 0-2 A and  $\pm 30$  mm, respectively. The operational frequency range is 0-2 Hz for both the inputs. According to command current and displacement, the desired damping force is generated with electro-hydraulic model as discussed in section 5.4. The data is collected at a sampling rate of 1000 Hz for duration of 20 seconds, resulting in generation of 20000 data points. Out of which 10000 points are chosen for training purpose, and remaining 10000 points are used for test the system. The effectiveness of ANFIS inverse model in active suspension control system will be discussed in result section. However, the testing performance of inverse model is shown in Figure 5.4. Figure 5.4 (a) and (b) demonstrate a close alignment between the active force generated by the expected command current and the desired controlling force. Also, the predicted amount of force and command current remains in defined limits, indicates that inverse model can satisfy the need of proposed scheme.

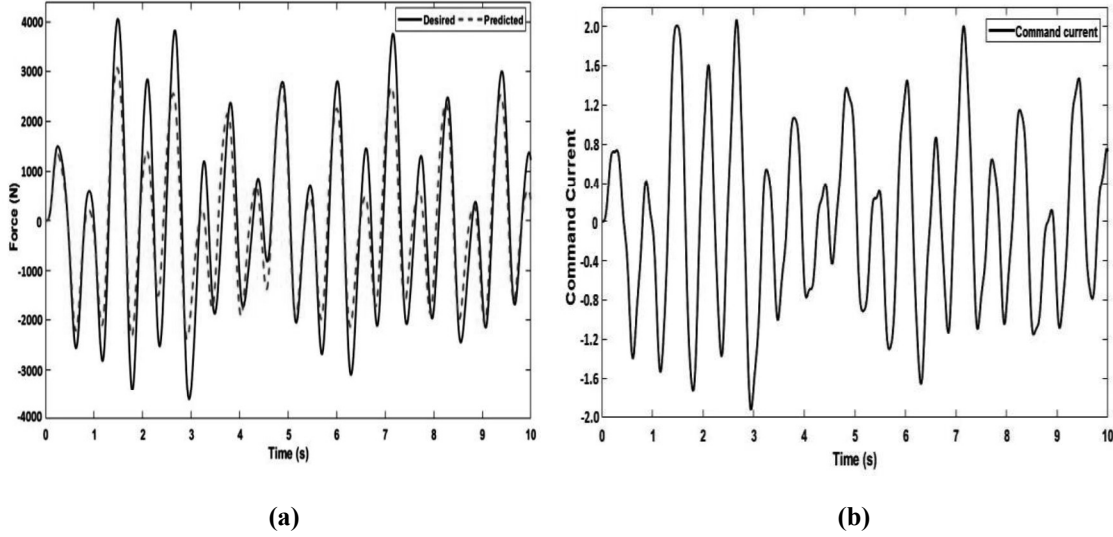


**Figure 5.4** Validation of ANFIS inverse model (a) force prediction (b) command current

### 5.6 System controller based on LQG control law

The LQG controller combines the linear quadratic regulator with the Kalman filter. The mathematical equations that describe the operation of LQG controller are given as (Q. Zhu, Li, et al., 2018)

$$\hat{\dot{X}} = [A]\hat{X} + [B]u + K_f(Y - CX - Du) \quad (5.36)$$

$$u = -K_c \hat{X} \quad (5.37)$$

where  $\hat{X}$  are the observed states of  $X$ , and  $K_f$  is the Kalman filter gain given by following equation:

$$K_f = R_n^{-1} C^T P + H^T Q_n H \quad (5.38)$$

where  $P$  is the solution of following algebraic Riccati Equation (ARE),  $A^T P + P A - P C^T R_n^{-1} C P + E Q_n E^T = 0$ , with the covariance matrices  $R_n$  and  $Q_n$  defined as  $E\{V V^T\} = R_n$ ,  $E\{\Gamma \Gamma^T\} = Q_n$ .

*Note: There is no correlation exist between  $\Gamma$  and  $V$  i.e.  $E\{\Gamma V^T\} = 0$ .*

In Eqn. (5.37),  $u$  is the control signal that is designed to minimize the following performance index



$$J = \lim_{T \rightarrow \infty} \frac{1}{T} \int_0^T [X^T Q X + u^T R u + 2X^T S u] \quad (5.39)$$

and,  $K_c$  is the controller gain matrix given by the following equation:

$$K_c = R^{-1} B^T M + R^{-1} M \quad (5.40)$$

where  $Q$  (semi-positive-definite),  $R$  (positive-definite), and  $S$  are the weighting matrices.  $P_c$  is determined by following Riccati equation  $A^T M + M A - (M B + S) R^{-1} (B^T M + S^T) + Q = 0$ .

### 5.7 Methods of finding the weighing matrices (Q, R and S)

The performance of LQG controller depends upon the weighting matrices  $Q$ ,  $R$  and  $S$ , which needs to be optimally tuned according to the cost function. Since, this study focuses on the improvement of ride comfort while minimizing the acceleration and control effort. Therefore, considering the assumption that the pair  $(A, B)$  is stabilizable and  $(A, C)$  is detectable (Aslam et al., 2023), the performance index (5.39) can be rewritten in the following form:

$$J = \lim_{T \rightarrow \infty} \frac{1}{T} \int_0^T \{ q_1 \ddot{z}_c^2 + q_2 \ddot{y}_c^2 + q_3 \ddot{\theta}_c^2 + q_4 \ddot{\phi}_c^2 + q_5 \ddot{\psi}_c^2 + r_1 u_1^2 + r_2 u_2^2 + r_3 u_3^2 + r_4 u_4^2 + r_5 u_5^2 \} \quad (5.41)$$

where  $\ddot{z}_c, \ddot{y}_c, \ddot{\theta}_c, \ddot{\phi}_c, \ddot{\psi}_c$  are the car body accelerations.  $u_i$  are the control forces which are calculated by multiplying the position vector with the control vector,  $u$ . (where  $i = 1, 2, 3, 4, 5$ ).

According to the Eqn. (5.39) and 41, the weighting matrices  $Q$ ,  $R$  and  $S$  can be determined as:

$$Q \in \mathcal{R}^{5 \times 5} = \begin{pmatrix} q_1 & \cdots & 0 \\ \vdots & \ddots & \vdots \\ 0 & \cdots & q_5 \end{pmatrix}, \quad R \in \mathcal{R}^{5 \times 5} = \begin{pmatrix} r_1 & \cdots & 0 \\ \vdots & \ddots & \vdots \\ 0 & \cdots & r_5 \end{pmatrix}, \quad S \in \mathcal{R}^{5 \times 5} = [0] \quad (5.42)$$

where  $q_1, q_2, q_3, q_4$ , and  $q_5$  are the weights of vertical, lateral, roll, pitch, and yaw acceleration, respectively. Similarly,  $r_1$  to  $r_5$  are the weights related to the control inputs. The combinations of these weights have a greater impact on the system's performance

(Chevrie et al., 2019; Soni & Sathans, 2018). Most often, these weights are evaluated by the hit & trial method and Bryson's rule, as demonstrated by Robandi et al. (Robandi et al., 2001). An experience-based iterative procedure is performed in the hit-and-trial method to get the desired response. On the other hand, Bryson's rule is also a normalization-based iterative process. In both methods, several steps are repeated until the cost function reaches to small value. Even performing a number of iterations, these methods failed to achieve satisfactory results. Hence, to rectify these problems, the metaheuristic-based optimization algorithms are introduced in the LQG controller design framework. In this paper, two types of metaheuristic algorithms, i.e. PSO and EO are utilized to compute the dynamic weights of LQG controller. The descriptions of these algorithms are given below:

### 5.7.1. Particle Swarm Optimization (PSO)

In particle swarm optimization, the principle of swarm intelligence (Slowik, 2011) is used to find the optimum values of controller gain matrix ( $K_c$ ), whereas no optimization has been used for the Kalman gain ( $K_f$ ). The diagonal elements ( $q_1 - q_5$ ,  $r_1 - r_5$ ) of weighting matrices  $Q$  and  $R$ , are considered as PSO particles and chosen as positive real number, initially. Then, for each particle the solution of  $P_c$  is solved from ARE, and the feedback gain  $K_c$  is calculated. Using feedback gain, the fitness of each particle is evaluated according to the following cost function:

$$J_1 = \sum_{i=1}^5 e_i^2 \quad (5.43)$$

where  $e_i$  (where  $i = 1 - 5$ ) is the weighted sum mean square error (MSE) of the output accelerations. If the current fitness value is less than the previous value, then the current values of  $Q$  and  $R$  are considered the best solution. Else, the values with the previous best solution are given preference. The particles with minimum MSE among all the particles are chosen as the global best (Pandey, 2017; Samuel et al., 2022). The present investigation employed this algorithm to solve a single objective optimization problem used for vibration control of railway vehicle. The parameters and pseudo-codes of this algorithm for the present investigated problem are illustrated in Appendix 2.

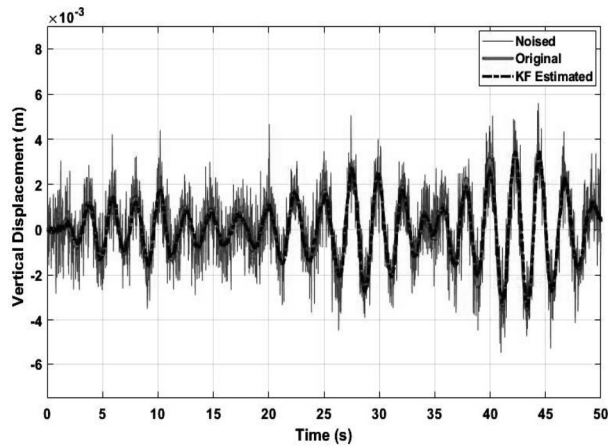
### 5.7.2. Equilibrium optimization (EO)

In equilibrium optimization algorithm, the concept of physics-based dynamic source and sink model are used to estimate the equilibrium states or best solutions (Faramarzi et al., 2020). In this method, the diagonal elements  $(q_1 - q_5, r_1 - r_5)$  of  $Q$  and  $R$ , with its concentration acts as a search agent equivalently to particles and positions in PSO. Then, based on formation of equilibrium pool in exploration state, the solutions of ARE and corresponding feedback gain  $K_c$ , is calculated. Using feedback gain, the concentration (positions) of each candidate is calculated using the cost function defined in Eqn. (5.43). After that, the attentiveness of each particle is updated according to generation rate and particle's memory saving procedures. These procedures help the equilibrium candidates to come closer and will aid the local search to find the equilibrium state or optimum solution. Hence, in this paper, we proposed this algorithm is used to tune the LQG parameters, which control the suspension system of railway vehicles. The values of parameters and pseudo-code of the proposed algorithm are given in Appendix 2.

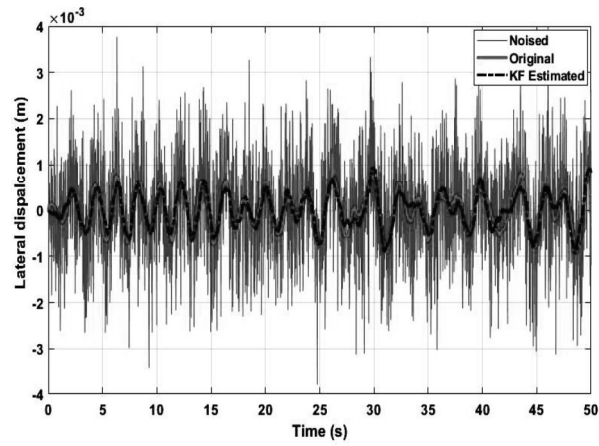
## 5.8 Results and Discussions

This section evaluates the performance of a modified LQG-based active suspension system used for vibration control of railway vehicles. The effectiveness of the controller tuned with equilibrium optimization (EO) is investigated in the time and frequency domains, and the results are compared to the passive system as well as conventional tuning technique, i.e., Bryson's rule and PSO. The various parameters of railway vehicles, tracks, and electro-hydraulic actuators, used in the simulation are given in Appendix 1 (Alexander, Vacca, and Cristofori 2017). The architecture of the proposed active vibration control system is already illustrated in Figure 5.1. From Figure 5.1, it can be seen that the complete process of vibration suppression consists of two units: force prediction and force tracking. It may also be noted that although the working procedures of both units differs from each other, the overall performance of entire system relies on the minimization of same cost function, defined in Eqn. (5.43). Therefore, to minimize the cost function, the simulation is run ten times by setting the same number of iterations, particles, and other parameters. In each iterations, the Kalman filter, the LQR and the ANFIS controller works together to achieve the desired performance.

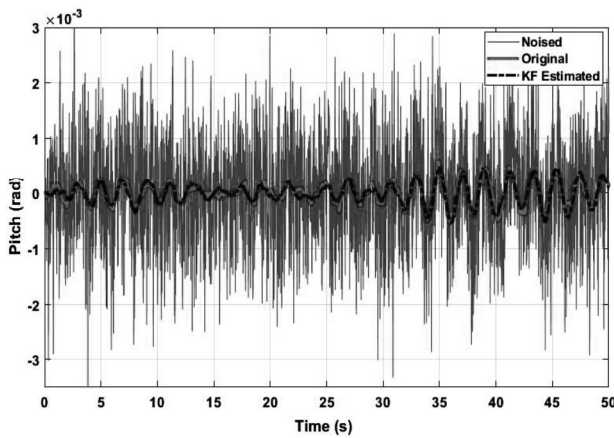
The outputs evaluated by the Kalman filter in the first step remain constant throughout the whole process and serves as an input to the LQR controller. The successful operation of the Kalman filter depends upon the values of Kalman gain ( $K_f$ ), which ultimately rely on covariance matrices ( $Q_n$  and  $R_n$ ) as discussed in Eqn. 5.42. In this study, the covariance matrix of disturbance source ( $Q_n$ ) is taken as  $diag[300, 300]$  that can imitate the track irregularities. The covariance matrix of sensor noise ( $R_n$ ) is determined as  $diag[0.0023, 0.0034, 0.0023, 0.0045, 0.0053 \dots \dots 0.0053]$  that can available from commercially used accelerometer. With these parameters, the outputs of Kalman filter is evaluated and demonstrated in Figure 5.5. From Figure 5.5, it is seen that the Kalman filter successfully filters the noise components and also provide appropriate outputs.



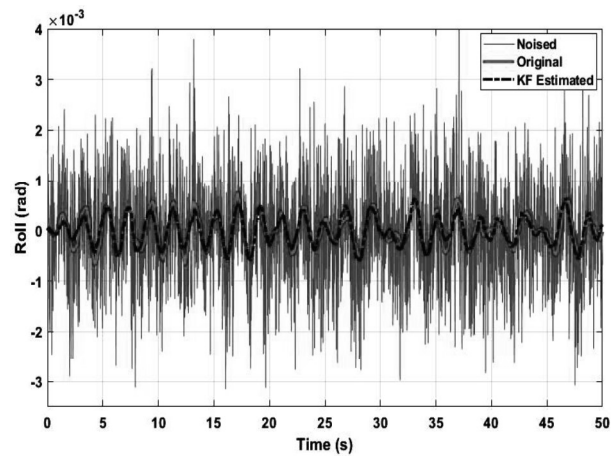
(a)



(b)



(c)



(d)

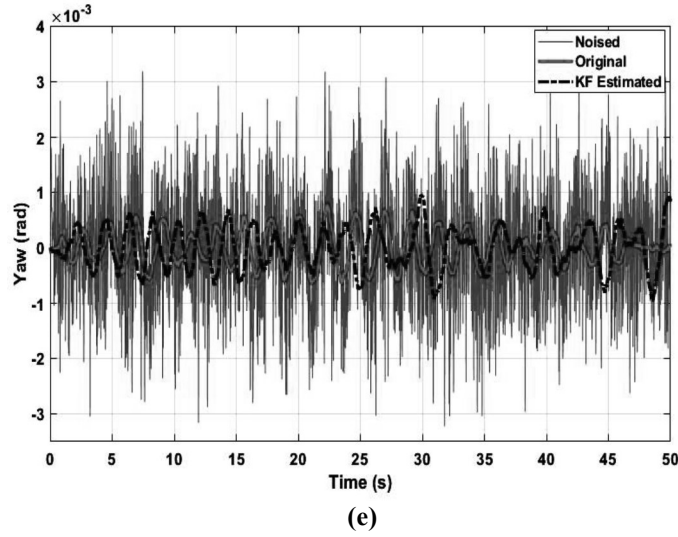


**Figure 5.5** Outputs of Kalman filter estimated different states (a) vertical (b) lateral (c) Pitch (d) roll (e) yaw

Based on these estimated outputs, the controller gain ( $K_c$ ) is tuned with Bryson's rule and two metaheuristic algorithms (PSO and EO) in order to minimize the acceleration level of vehicle body. The best convergence graph to find the optimum values of the LQG controller using these techniques have been given in Figure 5.6. According to Figure 5.6, it is observed that the convergence rate of equilibrium optimization is substantially faster than the PSO and Bryson's rule, which guarantee an optimum solution. Also, the best optimum values of  $Q$ ,  $R$ , and  $K_c$  results from classical and metaheuristic tuning have been provided in Table 5.1. The effect of these calculated values on the vehicle's body acceleration and human comfort are discussed in the next section.

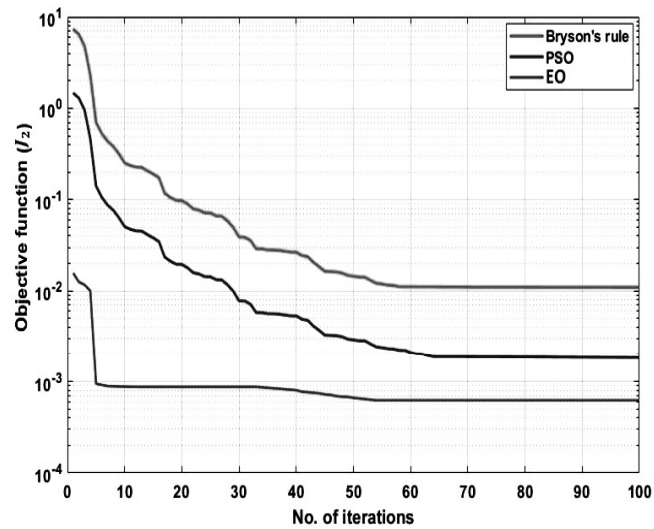


**Figure 5.6** Convergence curves of tuning methods

**Table 5.1** Values of Q, R and K<sub>c</sub> calculated different from tuning techniques

Bryson's rule	PSO	EO
$Q = \begin{bmatrix} 488.45 & 0 & 0 & 0 & 0 \\ 0 & 324.43 & 0 & 0 & 0 \\ 0 & 0 & 305.43 & 0 & 0 \\ 0 & 0 & 0 & 223.43 & 0 \\ 0 & 0 & 0 & 0 & 242.43 \end{bmatrix}$	$Q = \begin{bmatrix} 688.55 & 0 & 0 & 0 & 0 \\ 0 & 724.43 & 0 & 0 & 0 \\ 0 & 0 & 532.29 & 0 & 0 \\ 0 & 0 & 0 & 698.67 & 0 \\ 0 & 0 & 0 & 0 & 868.65 \end{bmatrix}$	$Q = \begin{bmatrix} 896.62 & 0 & 0 & 0 & 0 \\ 0 & 954.88 & 0 & 0 & 0 \\ 0 & 0 & 922.05 & 0 & 0 \\ 0 & 0 & 0 & 884.77 & 0 \\ 0 & 0 & 0 & 0 & 908.68 \end{bmatrix}$
$R = \begin{bmatrix} 0.0012 & 0 & 0 & 0 & 0 \\ 0 & 0.0014 & 0 & 0 & 0 \\ 0 & 0 & 0.0017 & 0 & 0 \\ 0 & 0 & 0 & 0.0020 & 0 \\ 0 & 0 & 0 & 0 & 0.0022 \end{bmatrix}$	$R = \begin{bmatrix} 0.0032 & 0 & 0 & 0 & 0 \\ 0 & 0.0046 & 0 & 0 & 0 \\ 0 & 0 & 0.0048 & 0 & 0 \\ 0 & 0 & 0 & 0.0042 & 0 \\ 0 & 0 & 0 & 0 & 0.0033 \end{bmatrix}$	$R = \begin{bmatrix} 0.027 & 0 & 0 & 0 & 0 \\ 0 & 0.063 & 0 & 0 & 0 \\ 0 & 0 & 0.083 & 0 & 0 \\ 0 & 0 & 0 & 0.075 & 0 \\ 0 & 0 & 0 & 0 & 0.068 \end{bmatrix}$
$K = \begin{bmatrix} 4884.5 & 4543.3 & 3659.4 & 4123.2 & 2234.5 \\ 3864.3 & 2224.5 & 3987.7 & 3465.1 & 2387.7 \\ 2378.3 & 3364.9 & 2325.4 & 3784.0 & 2934.4 \\ 3671.4 & 2998.4 & 3651.8 & 2273.7 & 2219.3 \\ 2997.6 & 2802.3 & 3382.4 & 4112.3 & 2022.2 \end{bmatrix}$	$K = \begin{bmatrix} 6004.3 & 5632.4 & 6439.3 & 5932.2 & 4652.8 \\ 6227.5 & 5212.4 & 4327.4 & 5507.5 & 5001.7 \\ 6943.2 & 6321.2 & 5223.7 & 4456.8 & 4459.4 \\ 5578.5 & 5586.4 & 3887.8 & 5013.3 & 5123.8 \\ 5883.7 & 6320.0 & 4012.4 & 4092.3 & 4887.8 \end{bmatrix}$	$K = \begin{bmatrix} 8765.4 & 8018.5 & 7882.5 & 7792.6 & 8845.4 \\ 8253.2 & 7885.2 & 8756.4 & 8398.4 & 8127.5 \\ 7975.3 & 8893.7 & 7659.8 & 7998.5 & 7784.5 \\ 7001.4 & 9012.4 & 9002.7 & 8003.2 & 8104.6 \\ 7195.5 & 8196.3 & 7654.4 & 7992.8 & 9265.8 \end{bmatrix}$

## 5.9 Simulation under random track irregularities

In this part, the performance of an optimally tuned LQG controller is evaluated under random track profile and the results are shown in both frequency and time domain.

### 5.9.1 Acceleration responses of the vehicle body

The performance of a metaheuristic tuned LQG controller has been demonstrated under the random track disturbances depicted in chapter 3 (section 3.5.2). Figure 5.7 shows the amplitude spectra and time series of the vehicle body's accelerations in yaw, pitch, roll, and vertical. Tables 5.2 also include the root mean square (RMS) values and the percentage improvement of RMS value for various motions. Also, the root mean square (RMS) values, and the percentage improvement of RMS value for different motions are given in Tables 5.2. The percentage improvement of RMS values using different tuning algorithms over the passive system has been calculated by using the following equation

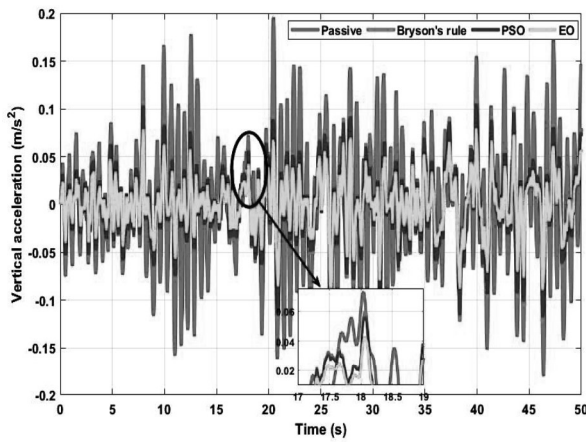
$$\% \text{ improvement} = \frac{\text{passive} - \text{active}}{\text{passive}} \times 100 \quad (5.44)$$

Observing Figure 5.7 (a), it is found that the vertical acceleration of the vehicle body is effectively reduced by the LQG controller tuned with metaheuristic algorithms. However, among them, EO-LQG performs better in attenuating the vertical vibrations at the range [1-10] Hz as depicted in Figure 5.7 (b). Also, the % improvement (RMS) of vertical acceleration with EO optimization over the passive system is found to be 35.62%, which is comparatively higher than that of other metaheuristic algorithms, as shown in Table 5.2 (a). In case of lateral motion, from Figure 9 (c) and (d), it can be seen that the vibration attenuation ability of the active suspension system using metaheuristic algorithm at [2-12] Hz is higher than that at [0-2] Hz frequency range. This situation arises because the resonant peaks of lateral motion mostly occur at this particular frequency range. Moreover, the RMS reduction of lateral acceleration using Bryson's method is found to be 5.68 %, while the percentage reduction with PSO and EO optimization algorithms are 19.43% and 24.97 %, respectively, as rendered in Table 5.2 (b). Therefore, we can say that the EO-LQG controller has more attenuation ability as compare to passive system and other tuned controller.

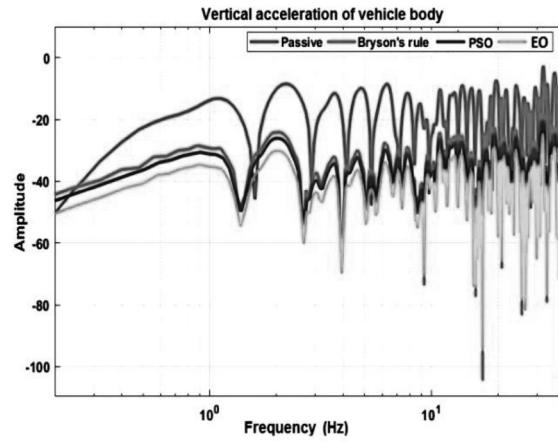
From Figure 5.7 (e) and (f), it can be seen that the amplitude spectrum of pitch acceleration in the range [0-2.5] Hz is successfully reduced with a suspension system controlled by an optimally-tuned LQG controller, where the proposed EO algorithm dominates the other tuning methods. The dominance of the LQG controller with EO algorithm over passive, Bryson, and PSO is also verified from Table 5.2 (c), where the suspension system tuned with the EO method can reduce the vibration level up to 38.77%. On the other hand, the % improvements of RMS values with Bryson and PSO over passive system are 13.53 %, and 30.55%, respectively. In terms of roll acceleration, we can see from Figure 5.7 (g) and (h) that the active suspension system, which is tuned using metaheuristic algorithms, has a better ability to reduce vibrations in the required frequency range of [0-2] Hz compared to the passive suspension system and conventional tuning algorithm. Table 5.2 (d) shows that the RMS value of roll acceleration with the EO algorithm is lower than that of other tuning methods; the percentage reduction of RMS values is about 27.98%, which is the highest among all the tuning algorithms. Furthermore, in the case of yaw motion, from Figure 5.7 (i, j) and Table 5.2 (e), it is also observed that an active suspension system controlled with an optimal tuned LQG

controller can reduce the yaw acceleration of the vehicle body by a large extent as compared to the passive system. However, among all tuning methods, EO algorithm achieves a 35.68% reduction in RMS values of yaw acceleration. In contrast, the percentage reduction is only 14.82%, and 29.72%, as in the case of Bryson and PSO tuning algorithms.

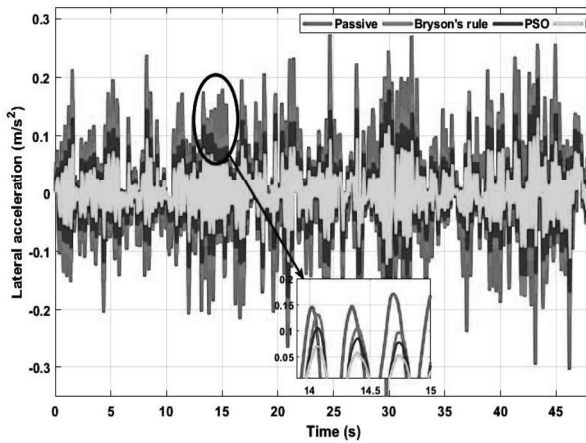
Therefore, we can say that the comfort enhancement capability of the active suspension system using EO- based LQG controller is better than that of passive and other metaheuristic algorithms.



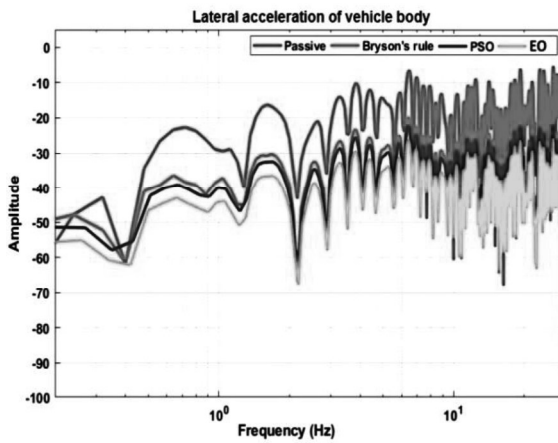
(a)



(b)

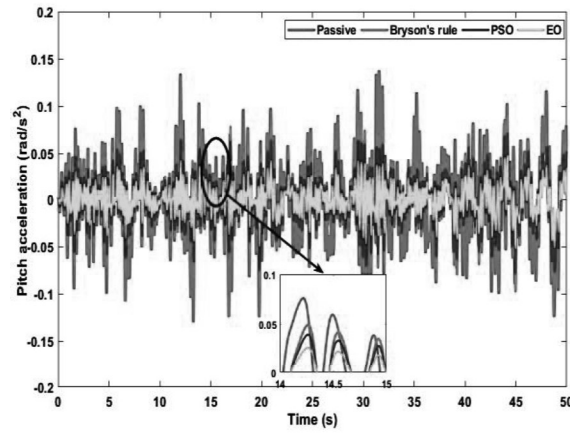


(c)

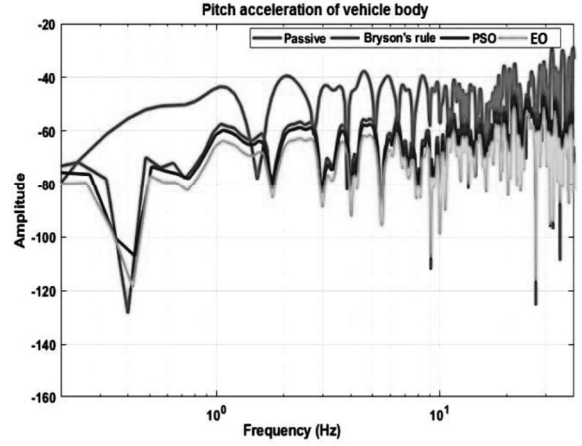


(d)

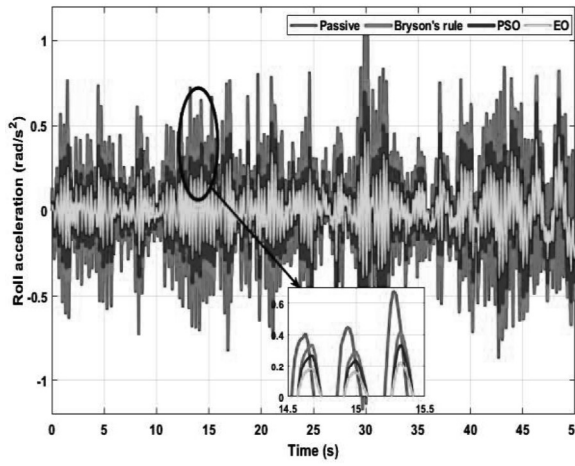




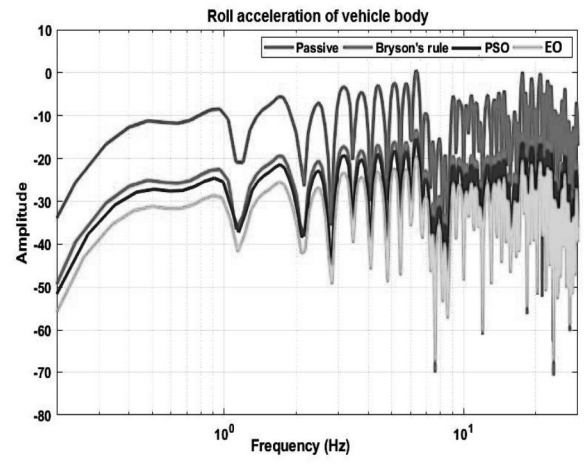
(e)



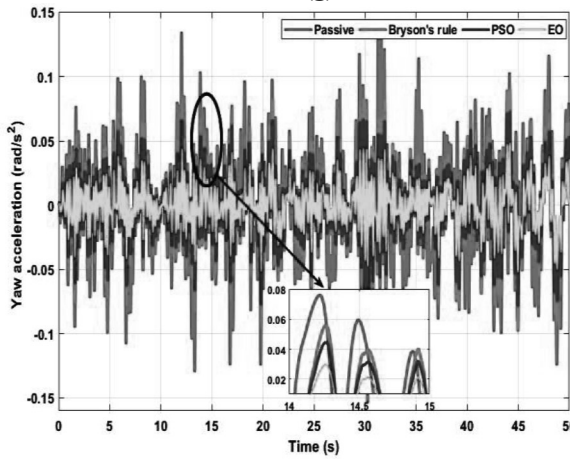
(f)



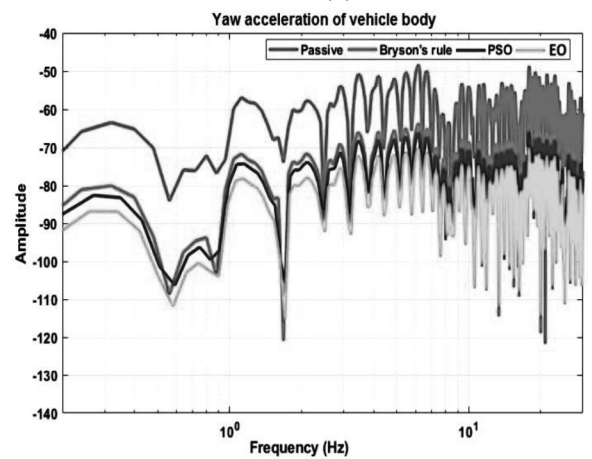
(g)



(h)



(i)



(j)

**Figure 5.7** Time series and amplitude spectrums of vehicle body acceleration under random track inputs (a, b) vertical acceleration ( $\ddot{Z}_c$ ) (c, d) lateral acceleration ( $\ddot{Y}_c$ ) (e, f) pitch acceleration ( $\ddot{\psi}_c$ ) (g, h) roll acceleration ( $\ddot{\theta}_c$ ), and (i, j) yaw acceleration ( $\ddot{\phi}_c$ )

**Table 5.2** RMS values and % improvement of vehicle body acceleration under random track disturbances

<i>(a) For vertical acceleration</i>				
<i>index</i>	Passive	Bryson's rule	PSO	EO
RMS Values ( $m/s^2$ )	3.864e-02	3.359e-02	2.690e-02	<b>2.488e-02</b>
% improvement	-	13.06 %	30.38 %	<b>35.62 %</b>
<i>(b) For lateral acceleration</i>				
<i>index</i>	Open-loop	Bryson's rule	PSO	EO
RMS Values ( $m/s^2$ )	6.235e-02	5.880e-02	5.023e-02	<b>4.678e-02</b>
% improvement	-	5.68 %	19.43 %	<b>24.97 %</b>
<i>(c) For pitch acceleration</i>				
<i>index</i>	Open-loop	Bryson's rule	PSO	EO
RMS Values ( $rad/s^2$ )	5.534e-02	4.785e-02	3.843e-02	<b>3.388e-02</b>
% improvement	-	13.53 %	30.55 %	<b>38.77 %</b>
<i>(d) For roll acceleration</i>				
<i>index</i>	Open-loop	Bryson's rule	PSO	EO
RMS Values ( $rad/s^2$ )	7.465e-02	6.862e-02	5.824e-02	<b>5.376e-02</b>
% improvement	-	8.07 %	21.98 %	<b>27.98 %</b>
<i>(e) For yaw acceleration</i>				
<i>index</i>	Open-loop	Bryson's rule	PSO	EO
RMS Values ( $rad/s^2$ )	4.642e-02	3.954e-02	3.262e-02	<b>2.985e-02</b>
% improvement	-	14.82 %	29.72 %	<b>35.68 %</b>

Moreover, the time histories of the active force generated by the optimally tuned suspension system to suppress the vibrations of the car body in five modes are also shown in Figure 5.1. Now, by using the system controller, the control force  $u$  could be calculated, which is regarded as the desired force. For the different modes of railway vehicle, the desired force has been achieved with the combination of ANFIS controller and hydraulic actuator as discussed in section 5.4. Observing Figure 5.8, it can be seen that the LQG controller with EO optimization provides a balanced and optimum actuation force for all

modes of vehicle, which satisfies all the parameters of the cost function. Moreover, the proposed LQG controller satisfies the constraints of maximum force and controlled currents in all five modes because all the values of the corresponding cost function are less than unity.

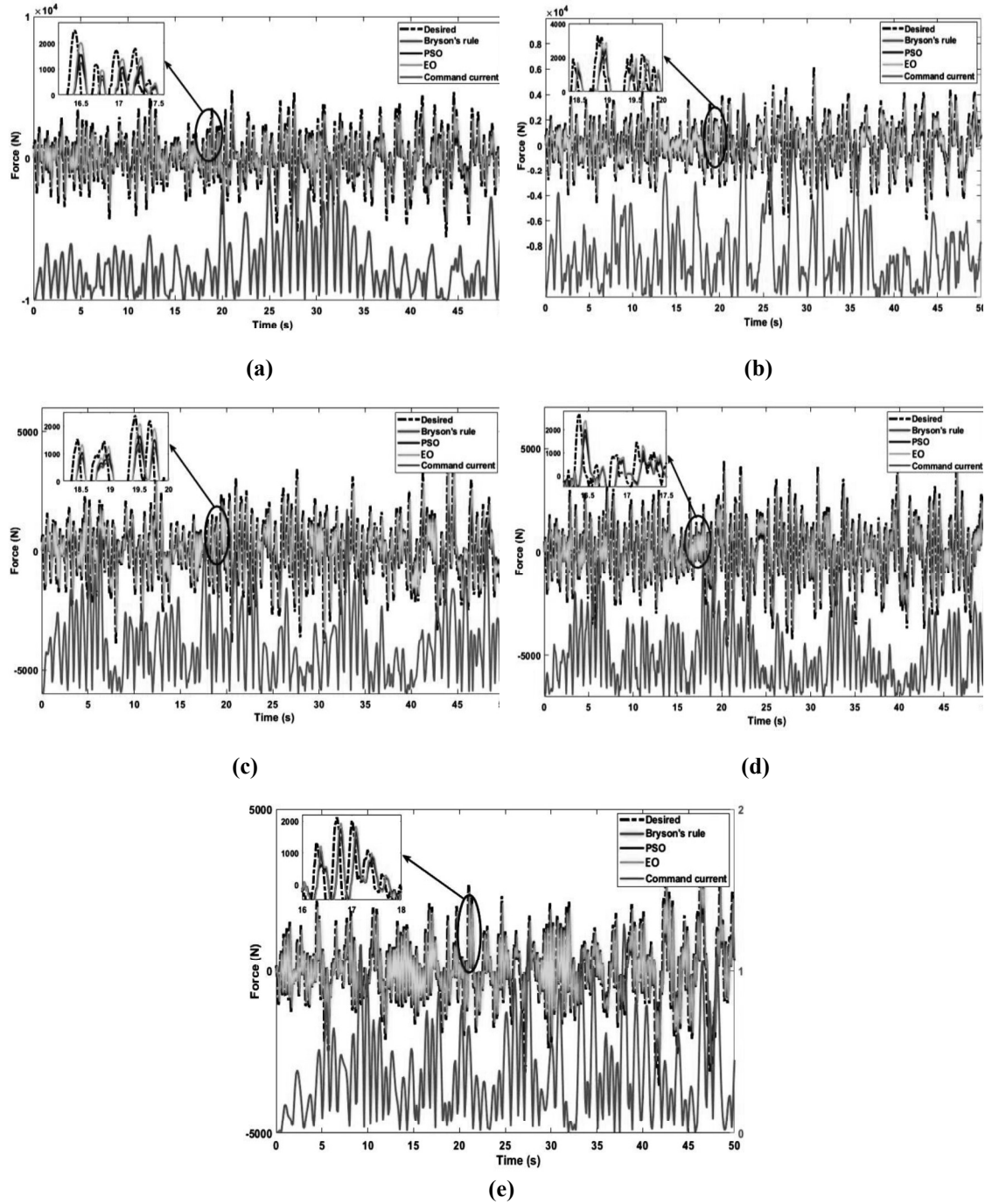


**Figure 5.8** Time histories of active force for different motions of railway vehicle (a) vertical motion ( $u_1$ ) (b) lateral motion ( $u_2$ ) (c) pitch motion ( $u_3$ ) (d) roll motion ( $u_4$ ) and (e) yaw motion ( $u_5$ )

### 5.10 Ride comfort analysis using Sperling's method

In this section, for the ride comfort evaluation, Ride factor  $W_z$ , method has been used. The evaluation scale used for determining the ride comfort has also been given in chapter 3. The ride comfort indices of this methods has been obtained by integration over the frequency interval of the human sensitivity range, i.e. 0-30 Hz. The graphical representations of ride comfort indices for passive and active control strategies (Bryson's rule, PSO, and EO) have been given in Figure 5.9. From Figure 5.9 (a), in case of vertical motion, it is observed that the ride index of passive suspension system with Sperling method is found to be 3.223, which may cause unpleasant ride. On the other hand, the ride indices for active control system using metaheuristic algorithms (PSO and EO) are found to be 2.598, and 2.203, that can significantly improves the ride quality of a railway vehicle. Observing Figure 5.9 (b), a similar kind of behavior is found in case of lateral motion, where the ride indices of railway vehicle using passive suspension are found to be 3.014. However, the ride indices reach to 2.695 and 2.408 when we use PSO, and EO tuned active suspension system.

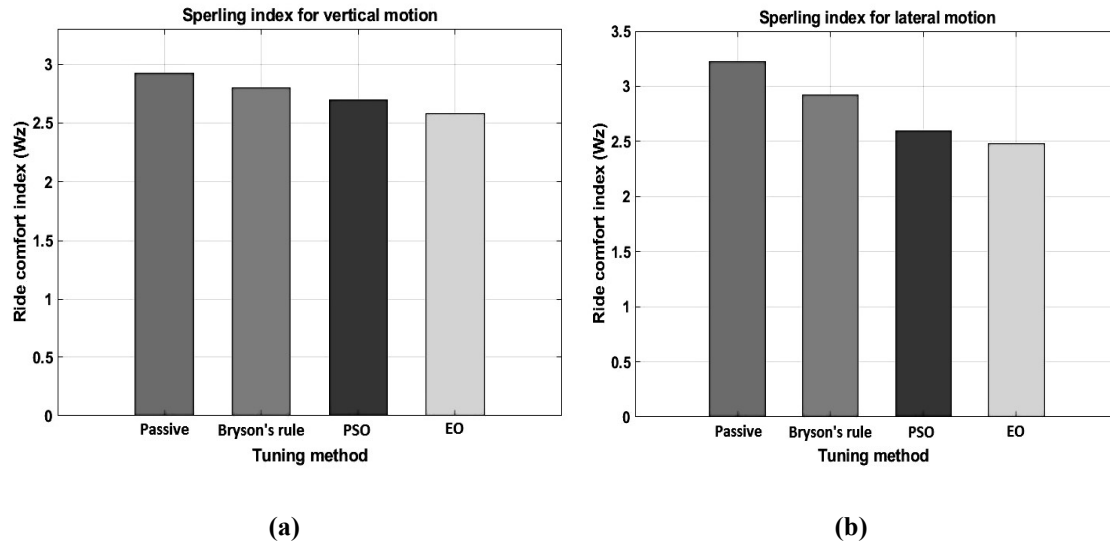


Figure 5.9 Ride comfort indices ( $W_z$ ) of (a) vertical motion (b) lateral motion

Based on the simulation results presented and discussed in the preceding sections, it is observed that the utilization of a metaheuristic-based LQG controller can significantly improves the acceleration level of the vehicle body as compared to the passive system.

## 7. Conclusions

This chapter explore an active suspension system controlled with an optimal tuned LQG controller to suppress the translational and angular vibrations of the car body. A 27-DOF dynamic model of a full-scale railway vehicle incorporated with wheel-rail contact forces and track irregularities is proposed. After constructing the 27-DOF dynamic model, two controller termed as system controller (LQG) and force tracking controller (ANFIS) with electro-hydraulic actuator is adopted to suppress the vibration of the five motions of the car body. To calculate the optimal active force for the suspension system, two metaheuristic algorithms named PSO and EO with one classical method i.e. Bryson's rule are used and the simulated results are compared with a passive system. The simulated results of the car body's vertical, lateral, pitch, roll, and yaw acceleration under random track irregularities are analyzed in both time and frequency domains. Furthermore the ride comfort of the railway vehicle is also evaluated using the Sperling's methods. According to simulation and analysis, the following outcomes are encased:

- The active suspension system controlled with metaheuristic based LQG controller provides the best trade-off between maximum acceleration and control efforts expressed in terms of quadratic cost function. It is also seen that the controller tuned with Bryson's rule and PSO have the slower convergence rate as compared to proposed equilibrium optimization algorithm.
- The output of ANFIS inverse model trained with hybrid algorithm is closely aligned with the forward dynamics of electro-hydraulic actuator, indicating the effectiveness of tracking the desired controlling force.
- In case of EO optimization, the percentage reduction in RMS values for the vertical, lateral, pitch, roll, and yaw acceleration were 35.62%, 24.98%, 38.77%, 27.98%, and 35.68%, respectively. On the other hand, the active suspension system tuned with Bryson's rule and PSO, shows lower reduction capability as compared to proposed EO optimization technique.
- Also, the ride comfort indices for vertical motion using EO algorithms are found to be 2.482, and for lateral motion, the indices were 2.528, respectively. These

values represent a superior level of comfort compared to that of passive and other tuning algorithms.

However, from the above discussion, it is evident that an active suspension system equipped with an EO-tuned LQG controller exhibits a tremendous capability to mitigate the track vibrations effectively. The proposed LQG controller has an inherent problem of robustness. To check the robustness of the proposed controller, the response of EO-LQG is evaluated considering the 10% variation in vehicle mass and the results are shown in the frequency domain. The bode plot of the proposed control strategy is shown in Figure 5.10, and the corresponding stability margins are given in Table 5.3. According to the investigated results, the range of stability margin with a proposed controller is very low, which signifies that if a controller is implemented in an uncertain environment, it might not deliver the desired results. These observations motivate a shift toward the robust control theory, which can provide a comfortable ride despite certain uncertainties.

**Table 5.3** Stability margin evaluated from EO-LQG control law

Gain margin:  $[0.8836 \ 1.1317]$

Phase margin:  $[-7.0730 \ 7.0730]$

Disk margin:  $[0.1236]$

Lower bound:  $[0.1236]$

Upper bound:  $[0.1239]$

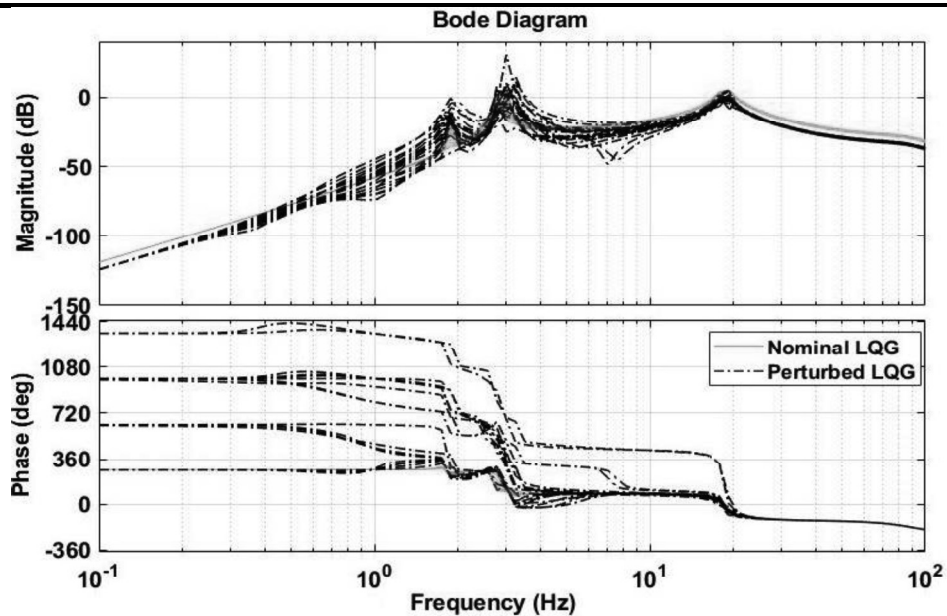


**Figure 5.10** Perturbed frequency response of LQG controller

## SYNTHESIS OF ROBUST CONTROLLER

---

*As the railway journey encounters the unpredictable terrain of external disturbances and uncertainties, the need for resilience and stability takes center stage. In this section, we delve into the realm of robust controller design—a sophisticated approach that fortifies railway systems against uncertainties, ensuring steadfast performance and reliability in the face of challenging conditions. For the purpose of control, two types of robust controllers i.e.,  $H_\infty$  and  $\mu$ -synthesis have been used to address both structured and unstructured uncertainties. After that, the evaluation of the ride comfort provided by the proposed active suspension system is conducted, and the simulated outcomes are compared to the experimental data.*

### 6.1 Introduction

Robust control theory is a fundamental paradigm in control systems engineering that aims to enhance the performance and stability of a system even when uncertainties and disturbances are present (Haq et al., 2020; Mohan et al., 2017; V. Sharma et al., 2017). Unlike traditional control methods that assume perfect knowledge of system dynamics, robust control theory acknowledges the inherent imperfections and variations that might arise in real-world systems (Dorato, 1987). As per previously reported literature, it is evident that the majority of the research has been carried out with the quarter-car or half-car models. Even in the full-car models, the controllers are designed with the decoupled approach. Moreover, most of the studies are primarily focused on the single uncertainties. However, a complete model consisting of structured and unstructured uncertainties can be developed, and a full-scale robust control scheme can be adopted to suppress the track vibrations effectively. Therefore, in this chapter, a robust active vibration control system for a full-scale railway vehicle is proposed. For the analytical purposes, a 27-DOF dynamic model of railway vehicles (discussed in previous chapter), consisting of structured and unstructured uncertainties has been considered (Y. Chauhan et al., 2021).

Two robust control techniques,  $H_\infty$  and  $\mu$ -synthesis, have been utilized to estimate the desired controlling force. The robust stability and robust performance of the proposed control strategies have been evaluated using the structured singular value theorem. Then, the effectiveness of the  $H_\infty$  and  $\mu$ -synthesis controllers is analyzed in time and frequency domains under the random track disturbances. Finally, using Sperling's method, the ride comfort of the railway vehicle is investigated, and the simulated results are validated with experimental data given by the Research Designs and Standards Organization, Lucknow, India. From the findings, it is believed that the proposed robust control techniques might be beneficial to mitigate the track vibration even in the presence of various uncertainties.

## 6.2 Analysis and synthesis of a robust controller

The schematic of the active suspension system used to control the vibrations of railway vehicles is shown in Figure. 6.1. Figure shows that the proposed control scheme constitutes a system controller integrated with electro-hydraulic (E-H) actuators. In this section, the part of the system controller is realized by combining the Kalman estimator and robust controller that generates the desired controlling force based on the measured and estimated output (Mathur & Sharma, 2017). Then, with the combination of six E-H actuators, the controlling force is applied to control the five motions of the vehicle body as demonstrated in Chapter 4 (section 4.1).

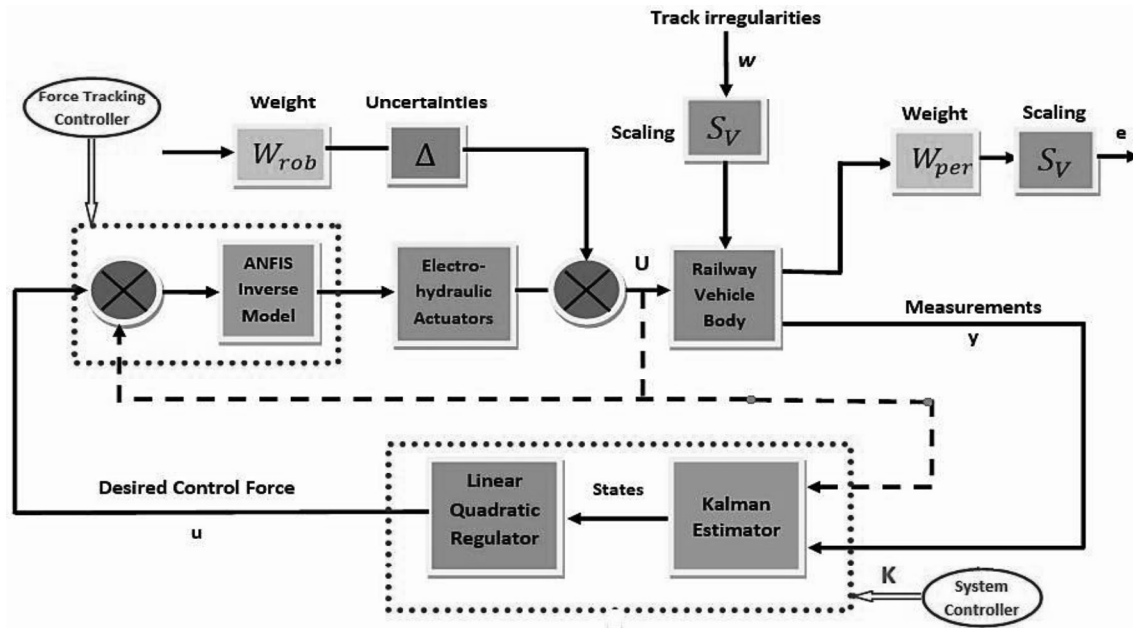


Figure 6.1 Schematic of robust vibration control system for railway vehicle



### 6.3 Mathematical formulation of Robust control strategy

Let,

$q$

$= [Y_c, Z_c, \varphi_c, \Theta_c, \psi_c, Y_{t1}, Z_{t1}, \varphi_{t1}, \Theta_{t1}, \psi_{t1}, Y_{t2}, Z_{t2}, \varphi_{t2}, \Theta_{t2}, \psi_{t2}, Y_{w1}, Z_{w1}, \psi_{w1}, Y_{w2}, Z_{w2}, \psi_{w2}, Y_{w3}, Z_{w3}, \psi_{w3}, Y_{w4}, Z_{w4}, \psi_{w4}]^T$ ,  $u = [F_{y1}, F_{y2}, F_{z1}, F_{z2}, F_{z3}, F_{z4}]^T$ , and  $w_1 = [Y_{a1}, Z_{v1}, \theta_{cl1}, Y_{a2}, Z_{v2}, \theta_{cl2}, Y_{a3}, Z_{v3}, \theta_{cl3}, Y_{a4}, Z_{v4}, \theta_{cl4}, \dot{Y}_{a1}, \dot{Z}_{v1}, \dot{\theta}_{cl1}, \dot{Y}_{a2}, \dot{Z}_{v2}, \dot{\theta}_{cl2}, \dot{Y}_{a3}, \dot{Z}_{v3}, \dot{\theta}_{cl3}, \dot{Y}_{a4}, \dot{Z}_{v4}, \dot{\theta}_{cl4}]^T$  are the displacements, control, and disturbance vectors, respectively. Then, the equation of motion derived in chapter 3, can be represented in the following matrix form:

$$[M]\ddot{q} + [C]\dot{q} + [K]q = [F_u]u + [F_w]w_1 \quad (6.1)$$

where  $[M]$  ( $\mathcal{R}^{27 \times 27}$ ),  $[C]$  ( $\mathcal{R}^{27 \times 27}$ ), and  $[K]$  ( $\mathcal{R}^{27 \times 27}$ ) are the nominal mass, damping, and stiffness matrices of the railway vehicle;  $[F_u]$  ( $\mathcal{R}^{27 \times 6}$ ),  $[F_w]$  ( $\mathcal{R}^{27 \times 24}$ ) are the position matrices of control inputs and track disturbances acting on the railway vehicle body and wheels of wheelsets, respectively.

If the uncertainties and perturbations are taken into account, the Eqn. (6.1) can be rewritten in the following form

$$\ddot{q} = \frac{1}{[M + \Delta M]} [(-C + \Delta C)]\dot{q} - (K + \Delta K)q + (F_u + \Delta F_u)u + (F_w + \Delta F_w)w \quad (6.2)$$

where  $M, C, K, F_u$ , and  $F_w$  are the nominal system parameter matrices;  $\Delta C, \Delta K, \Delta F_u$ , and  $\Delta F_w$  are the uncertain damping, uncertain stiffness, uncertain control, and uncertain disturbance matrices. These matrices can be constant or time-varying.

#### 6.3.1 Uncertain model of the railway vehicle system

Generally, two types of uncertainties, i.e., structured and unstructured, exist in any system (Grimble & Johnson, n.d.). Especially the structured one usually exists in the railway system. However, in this study, both types of uncertainties have been considered. Structured uncertainties are treated in body mass ( $M_c$ ) and moments of inertia ( $I_{zc}, I_{yc}, I_{xc}$ ), while unstructured uncertainties are considered in actuator dynamics. In this section, the dynamic model with unstructured uncertainties is described. The block diagram of the railway system with parametric uncertainties has been shown in Figure 6.2. Where  $\Delta_m$  is the perturbed block, and  $w_2$  and  $z_2$  are the input and outputs of the

perturbed block, respectively. The following parametric uncertainties have been considered in the mass and moment of inertia of the vehicle body.

$$M_i = M_i(1 + p_i \delta_i), I_j = I_j(1 + s_j \varepsilon_j); i = 1, 2 \text{ \& } j = 1, 2, 3. \quad (6.3)$$

where  $M_i$  and  $I_j$  are nominal values of the corresponding mass and moment of inertia, respectively.  $p_i$  and  $s_j$  are the maximum relative error with  $-1 \leq \delta_i, \varepsilon_j \leq 1$ .

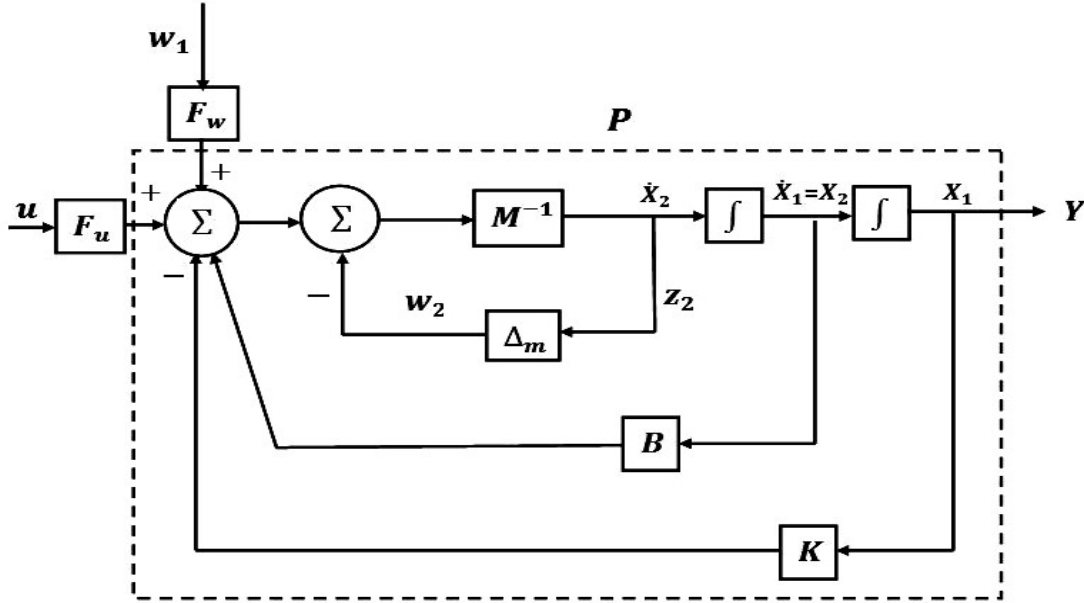


Figure 6.2. Block diagram of uncertain railway system

Now, define the state vector,  $X = [X_1 \ X_2]^T = [q^T \dot{q}^T]^T \in \mathcal{R}^{54 \times 1}$ , perturbed signal,  $w_2 \in \mathcal{R}^{5 \times 1}$  and sensor noise signals  $w_3 \in \mathcal{R}^{5 \times 1}$ . The state and output equations of the perturbed system are presented as follows.

$$\begin{cases} \begin{bmatrix} \dot{X}_1 \\ \dot{X}_2 \end{bmatrix} = \begin{bmatrix} 0_{17 \times 17} & I_{17 \times 17} \\ -M^{-1}K & -M^{-1}C \end{bmatrix} \begin{bmatrix} X_1 \\ X_2 \end{bmatrix} + \begin{bmatrix} 0_{17 \times 24} & 0_{17 \times 5} & 0 \\ M^{-1}F_w & -M^{-1} & 0 \\ 0_{17 \times 24} & 0_{17 \times 5} & 0 \end{bmatrix} \begin{bmatrix} w_1 \\ w_2 \\ w_3 \end{bmatrix} + \begin{bmatrix} 0_{17 \times 6} \\ M^{-1}F_u \end{bmatrix} u \\ \begin{bmatrix} Z_1 \\ Z_2 \end{bmatrix} = \begin{bmatrix} -M^{-1}K & -M^{-1}C \\ -M^{-1}K & -M^{-1}C \end{bmatrix} \begin{bmatrix} X_1 \\ X_2 \end{bmatrix} + \begin{bmatrix} 0 & -M^{-1} & 0 \\ 0 & -M^{-1} & 0 \end{bmatrix} \begin{bmatrix} w_1 \\ w_2 \\ w_3 \end{bmatrix} + \begin{bmatrix} M^{-1}F_u \\ M^{-1} \end{bmatrix} u \\ [Y] = [-M^{-1}K \quad -M^{-1}C] \begin{bmatrix} X_1 \\ X_2 \end{bmatrix} + [M^{-1}F_w \quad 0 \quad I] \begin{bmatrix} w_1 \\ w_2 \\ w_3 \end{bmatrix} + [M^{-1}F_u] u \end{cases} \quad (6.4)$$

where  $Z = [Z_1 \ Z_2]^T$  is the controlled output vector, and  $Y$  is the measured output vector. The open loop input/output relation of the uncertain railway vehicle is described as follows:

$$\begin{bmatrix} Z \\ Y \end{bmatrix} = [P] \begin{bmatrix} w \\ u \end{bmatrix} \quad (6.5)$$

where

$$P(s) = \begin{bmatrix} A & B_1 & B_2 \\ C_1 & D_{11} & D_{12} \\ C_2 & D_{21} & D_{22} \end{bmatrix} \quad (6.6)$$

### 6.3.2 Dynamics of the electro-hydraulic actuator with unstructured uncertainties

In this section, the actuator dynamics with unstructured uncertainties have been described. An actuator is an essential component of the active suspension system (Beltran-carbajal et al., n.d.). It is the mechanism by which the external force is injected into the system that complements the passive suspension system (Omar & Abdelghaffar, 2018). In this paper, an electro-hydraulic actuator is used to provide the desired force. The actuator's nominal transfer function, denoted as  $(\bar{P}_a)$ , is modeled as a second-order phase lag according to Eqn (6.7).

$$\bar{P}_a(s) = \frac{k_i}{m_a s^2 + c_c s + k_a} \quad (6.7)$$

The various parameters of electro-hydraulic actuators used in simulations have been given in (Taylor, Williamson, et al., n.d.). The nominal output force response to a square wave input of 1000 N at a 10 Hz frequency has already been given in chapter 5 (section 5.4).

Now, in order to account for unstructured uncertainties, the actuator model is approximated by input multiplicative uncertainties that give rise to the perturbed transfer function as:

$$P_a = \bar{P}_a(1 + W_{ai}\Delta_{ai}) \quad (6.8)$$

where  $\Delta_a \leq 1$  and  $W_a$  are the frequency-dependent uncertain blocks denoted as  $W_{rob}$ .

Now, by introducing the vector  $F = [f_1, f_2, f_3, f_4, f_5, f_6]^T$ , the equation of actuation force can be rewritten  $u = P_{act} F$ , where  $P_{act} = \text{diag}(P_{ai}); i = 1, 2, \dots, 6$ . Finally, modeled the railway vehicle and actuator with possible perturbation, the complete block diagram of the railway vehicle system is shown in Figure 6.3.

Following is a representation of an upper linear fractional transformation (ULFT) that can be utilized to represent the entire perturbed railway vehicle system:

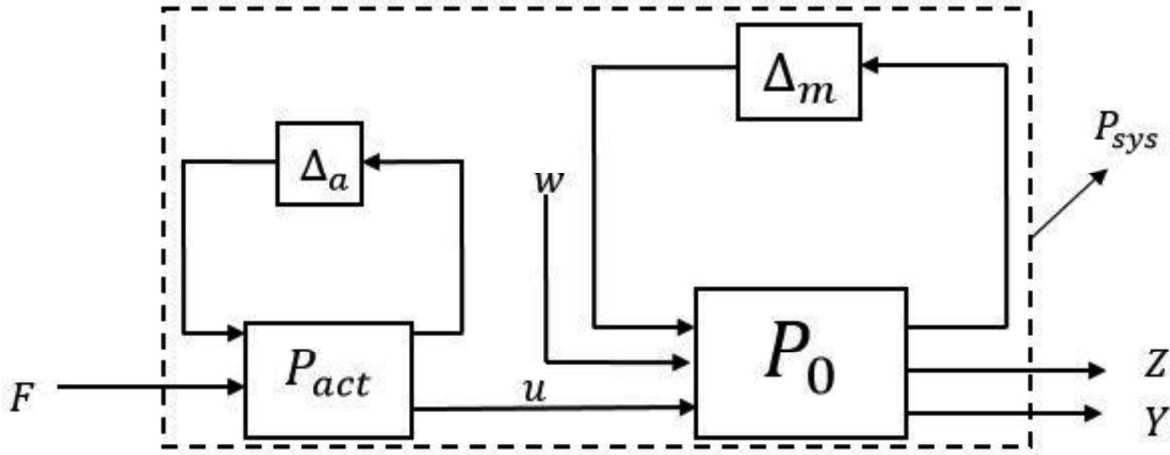


Figure 6.3 Uncertain model of the railway system

$$\begin{bmatrix} Z \\ Y \end{bmatrix} = F_u(P_{sys}, \Delta) \begin{bmatrix} w \\ F \end{bmatrix} \quad (6.9)$$

where  $P_{sys}$  is a complete transfer function matrix of the system, and  $\Delta$  represents the overall perturbation block.

#### 6.4 System controller based on robust control laws

When accounting for both structured and unstructured uncertainty, it is necessary to build the controller to have higher robustness.  $H_\infty$  and  $\mu$ -synthesis are the two robust techniques that proved more successful in providing robust stability and performance for the vehicle system (Kamada & Karaki, 2023; M. Yu et al., 2023). Thus, in this section, the  $H_\infty$  and  $\mu$ -controllers are emphasizing to establish the system controller that mitigates the vehicle vibrations in the wide range of uncertainties.

In order to achieve better ride comfort, the acceleration response of the vehicle body ( $\ddot{X}_b$ ) in all five modes should be minimized. Also, at the same time, the control effort ( $F$ ) of the actuators should be limited. For this reason, the controlled output vector before weighting is chosen as  $\tilde{Z}_s = [Z_1 \ Z_2 \ Z_3]^T$ , which constitutes parametric uncertainties ( $Z_1 = \mathcal{R}^{5 \times 1}$ ), the acceleration of vehicle body ( $Z_3 = \ddot{X}_b = \mathcal{R}^{5 \times 1}$ ), and control effort ( $Z_3 = F \in \mathcal{R}^{6 \times 1}$ ). On the other hand, the measured signal vector used to provide feedback to the controller is  $Y_b = \ddot{X}_b + w_n w_3 \in \mathcal{R}^{5 \times 1}$ , which is the acceleration plus weighted sensor noise. The general structure of the robust control system is shown in Figure 6.4. Where  $P_{cls}$  is the transfer function matrix from external disturbance vector ( $w$ ) to control vector ( $Z_s$ ), and  $\hat{X}_b$  is the estimated states of vehicle body  $X_b$ .  $W_{per}$ ,  $W_{act}$ ,  $W_r$ , and  $W_n$  are the weighting functions used to optimize all aspects of controller performances.

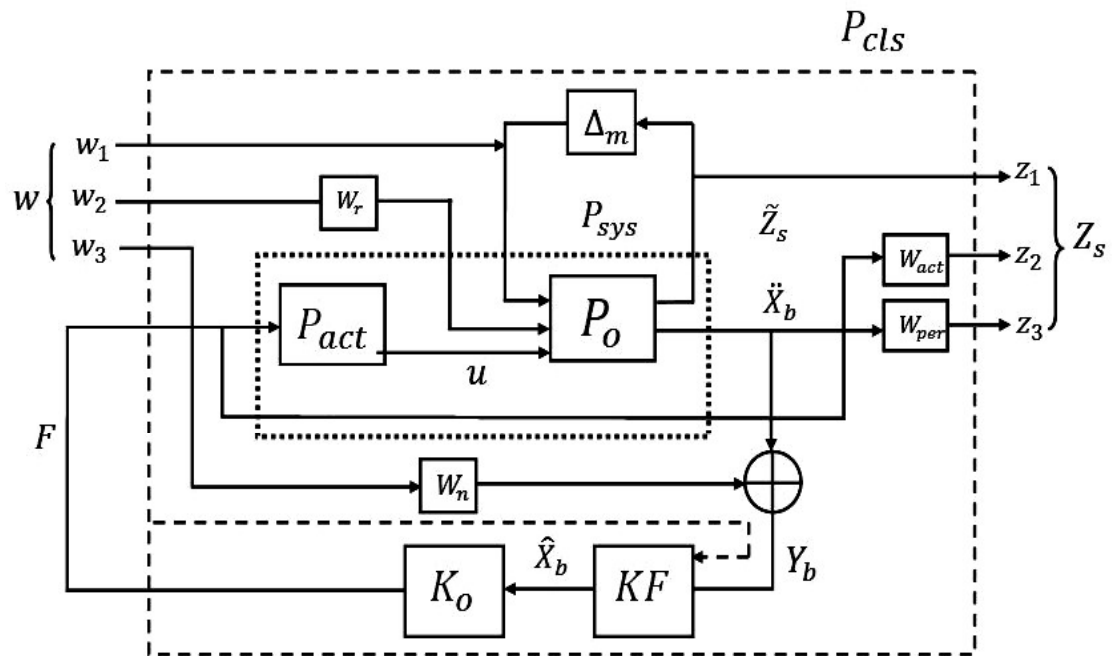


**Figure 6.4** Robust control structure for vibration control of railway vehicles

In matrix form, the above system can also be written as:

$$\begin{bmatrix} Z_s \\ Y_h \end{bmatrix} = [P_{cls}] \begin{bmatrix} W \\ F \end{bmatrix} \quad (6.10)$$

$$F = K_o(s). \hat{X}_b \quad (6.11)$$

$$P_{cls} = F(P_{sys}, K_o) \quad (6.12)$$

where  $\hat{X}_b$  is the estimated state of the nominal plant, and  $K_o$  is the regulator control gain. The main objective of the proposed control scheme is to obtain the gain,  $K_o$ , in such a way that it will provide robust stability and performance. The two controllers employed to achieve the desired performances are described in the next section.

#### 6.4.1 $H_\infty$ Controller

The standard configuration of the  $H_\infty$  controller is shown in Figure 6.4. The control techniques that allow us to incorporate the design specifications (robust stability and performance) in the control framework are based on structured singular values ( $\mu$ ) (Brunton & J. Nathan Kutz, 2019; Dahleh, n.d.). In a closed-loop system, the controller is designed to satisfy the following design specifications:

##### *a. Nominal performance ( $D_{nom-perf}$ )*

The nominal closed-loop stability and the required performance specifications have to be achieved by the controller. These specifications are usually achieved by reducing system gains from the disturbance to desired outputs. In this paper, the weighted  $H_\infty$  norms used for these system gains are expressed as follows:

$$\|P_{cls\ nom}\|_\infty = \left\| \begin{bmatrix} W_{per} S(P_{sys\ nom}) \\ W_{act} KS(P_{sys\ nom}) \end{bmatrix} \right\|_\infty < 1 \quad (6.13)$$

where  $P_{sys\ nom}$  is the system transfer function matrix without uncertainties (*i. e.*,  $\Delta = 0$ ), and  $W_{per}$  and  $W_{act}$  are the weights used to improve performance in a particular frequency range. A description of these weights is given in section 6.3. The matrices  $S(P_{sys\ nom})$  and  $KS(P_{sys\ nom})$  represent the mixed sensitivity functions *w.r.t.* disturbance vector,  $w$ .

##### *b. Robust stability ( $D_{rob-stab}$ )*

The stability of the nominal closed loop system has to be maintained even if the uncertainties perturb the closed loop system. The weighted  $H_\infty$  norms used for this specification are expressed as:

$$\|P_{cls}\|_\infty = \|W_{rob} P_{sys}\|_\infty < 1 \quad (6.14)$$

where  $W_{rob} = \text{diag}(W_a, \delta, \epsilon)$ , are the weights used to normalize the  $H_\infty$  norms of uncertainties  $\Delta$  to 1. The description of  $W_{rob}$  is already presented in section 6.3.1.

*c. Robust performance ( $D_{rob-perf}$ )*

The performance specifications of a closed-loop system have to be satisfied even if the uncertainties perturb the closed-loop system. The  $H_\infty$  norms used for this specification are expressed as follows:

$$\|P_{cls}\|_\infty = \left\| \begin{bmatrix} W_{per} S(P_{cls}) \\ W_{act} K S(P_{cls}) \end{bmatrix} \right\|_\infty < 1 \quad (6.15)$$

where the matrices  $S(P_{cls})$  is the perturbed sensitivity function of  $P_{cls} = F_u(P_{sys}, \Delta)$ .

### 6.4.2 $\mu$ -synthesis controller

The standard configuration for the  $\mu$ -synthesis controller (N. Singh & Bhargal, 2017) is shown in Figure 6.5, where  $M$  is the transfer function matrix with respect to the uncertainties set  $\Delta$ . Let  $M$  be partitioned as:

$$[M] = \begin{bmatrix} M_{11} & M_{12} \\ M_{21} & M_{22} \end{bmatrix} \quad (6.16)$$

$$z = [M_{22} + M_{21} \Delta (I - P_{11} \Delta)^{-1} P_{12}] w = F_u(M, \Delta) w \quad (6.17)$$

where  $F_u$  represents the upper linear fractional transformation (ULFT) matrix.

For robust stability, the following conditions should be satisfied, i.e.,  $\|F_u(M, \Delta)\|_\infty \leq 1$ .

Now, the relationship between  $P_{sys}$  and  $M$  can be represented as:

$$M(P_{sys}, K_o) = F_l(P_{sys}, K_o) \quad (6.18)$$

where  $F_l$  represents the lower linear fractional transformation (LLFT) matrix. For robust stability and robust performance, it is necessary to find a stabilizing controller  $K_o$  such that

$$\sup \mu [M(P_{sys}, K_o)] < 1 \quad (6.19)$$

For optimal robust stability and performance, the aim is to solve for  $K_o$  such that

$$\inf_{K_o} \sup \mu [M(P_{sys}, K_o)] < 1 \quad (6.20)$$

The main idea of the  $\mu$ -synthesis controller is to minimize the largest value ( $\mu$ ) of the LLFT matrix, occurring at a particular frequency (Grimble & Johnson, n.d.). It is an iterative process in which boundary criterion is achieved according to the weighting function applied to the input and output signals of the system. The optimum values of weighting functions considered to achieve robust performance are described in the next section.

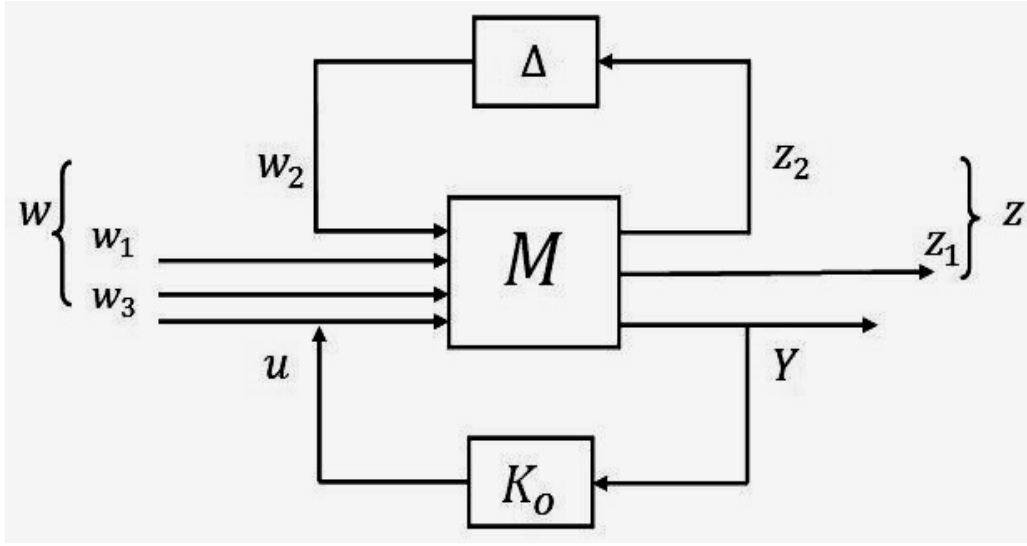


Figure 6.5  $\mu$ -synthesis control configuration

### 6.5 Design of weighting functions

The robust stability and performance of the control system depend upon the choice of appropriate weighting functions. This study aims to improve ride comfort over a particular frequency range, where the impact of vibration on the human body is largest. Therefore, frequency-dependent weighting functions ( $W_{per}$ ) proposed by ISO have been introduced (Fard et al., 2014). These weights were applied to the desired output ( $\tilde{Z}_{s3}$ ) in the frequency range of 0.5-10 Hz. The gain of these weighting functions is set to increase in the frequency range below 8 Hz, where the human body is more sensitive to vibrations. Furthermore, it is imperative to impose penalties on the control effort in the low-frequency range due to the potential difficulty of the E-H actuators in accurately following the control force at high frequencies. Therefore, the actuator performance ( $\tilde{Z}_{s2}$ ), is modified by incorporating a low pass filter transfer function ( $W_{act}$ ), resulting in a



reduction of control effort throughout the frequency range of up to 10 Hz. The values of these frequency-dependent weighting functions for acceleration and control efforts are denoted as follows (Yamashita, 1994):

$$W_{per} = 10^{-6} * \text{diag}(W_{per0}, W_{per0}, W_{per0}, W_{per0}, W_{per0}) \quad (6.21)$$

$$W_{act} = 10^{-2} * \text{diag}(W_{act0}, W_{act0}, W_{act0}, W_{act0}, W_{act0}, W_{act0}) \quad (6.22)$$

Where  $W_{per0} = \frac{108.6}{s^2 + 19s + 400}$  and  $W_{act0} = \frac{0.1s^2 + 13.20s + 40}{20s^2 + 3552s + 400}$ .

The weighting function,  $W_n$ , is the sensor noise, which may corrupt the measurement. The sensor noise has a combination of low and high-frequency components. For five measurements, the  $W_n$  is taken as  $\text{diag}(W_{n0} W_{n0} W_{n0} W_{n0} W_{n0})$ . Where ( $W_{n0}$ ) is designed with the following transfer function (Orvnäs et al., 2011):

$$W_{n0} = \frac{2 \cdot 10^{-5} s^3 + 0.202 s^3 + 20.04 s + 4}{2 \cdot 10^5 s + 400} \quad (6.23)$$

The graphical representation of  $W_{per0}$ ,  $W_{act0}$ , and  $W_{n0}$  is given in Figure 6.6.

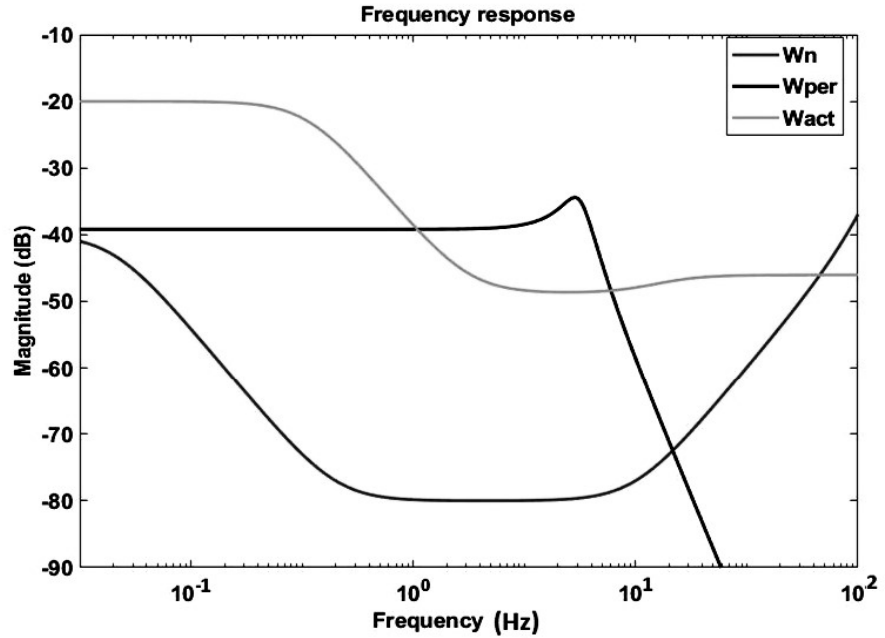


**Figure 6.6** frequency response for  $W_{per0}$ ,  $W_{act0}$ , and  $W_{n0}$

The weighting function,  $W_r$ , represents the track disturbances, a low pass filter expressed in terms of spatial frequency. To express this, the power spectral densities (PSDs) of three

types of track disturbances (Goodwin, 1987): lateral alignment ( $S_a$ ), vertical profile ( $S_v$ ), and cross-level ( $S_{cl}$ ) are considered as:

$$S_a(\Omega) = \frac{A_a \cdot \Omega_c^2}{(\Omega^2 + \Omega_r^2)(\Omega^2 + \Omega_c^2)} \quad (6.24)$$

$$S_v(\Omega) = \frac{A_v \cdot \Omega_c^2}{(\Omega^2 + \Omega_r^2)(\Omega^2 + \Omega_c^2)} \quad (6.25)$$

$$S_{cl}(\Omega) = \frac{A_v \cdot \Omega_c^2 \cdot \Omega^2}{l_r^2 (\Omega^2 + \Omega_r^2)(\Omega^2 + \Omega_c^2)(\Omega^2 + \Omega_s^2)} \quad (6.26)$$

The various symbols and pictorial representations of track PSDs defined in Eqns. (6.24)-(6.26) are already discussed in chapter 3 (section 3.5.2).

Let  $w_2 = [Z_{v1}, Y_{a1}, \theta_{cl1}, \dot{Z}_{v1}, \dot{Y}_{a1}, \dot{\theta}_{cl1}]^T$  implies the track inputs to the first wheelset.

Then,  $Z_{v1} \sim Z_{v4}$ ,  $Y_{a1} \sim Y_{a4}$ , and  $\theta_{cl1} \sim \theta_{cl4}$  are related by the following relation:

$$\begin{bmatrix} Z_{v2} \\ Y_{a2} \\ \theta_{cl2} \\ \dot{Z}_{v2} \\ \dot{Y}_{a2} \\ \dot{\theta}_{cl2} \end{bmatrix} = \begin{bmatrix} Z_{v1} \\ Y_{a1} \\ \theta_{cl1} \\ \dot{Z}_{v1} \\ \dot{Y}_{a1} \\ \dot{\theta}_{cl1} \end{bmatrix} e^{-\tau_2 s}, \quad \begin{bmatrix} Z_{v3} \\ Y_{a3} \\ \theta_{cl3} \\ \dot{Z}_{v3} \\ \dot{Y}_{a3} \\ \dot{\theta}_{cl3} \end{bmatrix} = \begin{bmatrix} Z_{v1} \\ Y_{a1} \\ \theta_{cl1} \\ \dot{Z}_{v1} \\ \dot{Y}_{a1} \\ \dot{\theta}_{cl1} \end{bmatrix} e^{-\tau_3 s}, \quad \begin{bmatrix} Z_{v4} \\ Y_{a4} \\ \theta_{cl4} \\ \dot{Z}_{v4} \\ \dot{Y}_{a4} \\ \dot{\theta}_{cl4} \end{bmatrix} = \begin{bmatrix} Z_{v1} \\ Y_{a1} \\ \theta_{cl1} \\ \dot{Z}_{v1} \\ \dot{Y}_{a1} \\ \dot{\theta}_{cl1} \end{bmatrix} e^{-\tau_4 s} \quad (6.27)$$

where  $\tau_2 = \frac{2L_d}{v}$ ,  $\tau_3 = \frac{2L_b}{v}$ ,  $\tau_4 = \frac{2(L_d+L_b)}{v}$  are the time delays between the wheelsets. The values of  $L_d$  and  $L_b$  are given in Appendix 1.

## 6.6 Results and Discussions

This section evaluates the performance of a robust control-based active suspension system employed to mitigate vibrations in railway vehicles. In the first part, the robustness of the  $H_\infty$  and  $\mu$ -synthesis controller in terms of design specifications is investigated in the frequency domains. Then, in the second part, the closed-loop performances of the regulated system are evaluated in the time and frequency domains, and the results are compared to the passive system. Finally, the ride comfort of rail vehicles is evaluated, and the results are validated with the empirical data reported by RDSO. The various parameters of railway vehicles, tracks, and electro-hydraulic actuators used in the simulation are given in Appendix 1.

### 6.6.1 Robustness analysis

To check the robustness of proposed controllers, the following uncertainties have been considered in the railway vehicle system. Consider the structured uncertainties in the body mass ( $M_c$ ) and moments of inertia ( $I_{zc}, I_{yc}, I_{xc}$ ), which have 10 % and 15 % relative errors to their nominal value, respectively. On the other hand, the unstructured uncertainties in the actuators have a 30 % error in the low-frequency range, around 2 rad/s. The % variation starts increasing and crosses 100 % at 15 rad/sec and reaches 1000% at 1000 rad/sec. With these uncertainties and proposed weighting functions, the  $H_\infty$  and  $\mu$ -synthesis controllers are built in MATLAB® using *hinfsv* and *musyn*, respectively. Then, the robust stability and performance of the proposed controllers is evaluated in term of structured singular value ( $\mu$ ).

The frequency response graphs of the structured singular value with  $H_\infty$  control may be shown in Figure 6.7. Looking at Figure 6.7 (a), we can see that the greatest value of  $\mu$  is 0.828. This indicates that the system remains stable even when subjected to perturbations. The system stays stable as long as the uncertainty levels are less than 120% of the provided values. However, when it comes to analyzing performance in a strong and reliable way, we can see from Figure 6.7 (b) that the highest value of  $\mu$  is 1.613. It seems that the proposed  $H_\infty$  controller does not achieve robust performance in the closed-loop system.

Similarly, Figure 6.8 displays the upper and lower bound plots of the structured singular value with  $\mu$ -synthesis control. Looking at Figure 6.8 (a), we can see that the maximum value of  $\mu$  is 0.729, which meets the robust stability criteria. It also shows that the system remains stable even when it is disturbed by 137% of its nominal values. The frequency response of  $\mu$  for the case of robust performance analysis may be shown in Figure 6.8 (b). Looking at the graphic, it's evident that the closed-loop system performs well in different conditions, as indicated by the maximum value of  $\mu$  being 0.705. In this case, it can be assured that the closed-loop system will stay stable as long as the uncertainty level is less than 141% of the supplied values. Additionally, the values of the performance index will be equal to or less than 0.70.

Hence, it is concluded that both controllers ( $H_\infty$  and  $\mu$ -synthesis) ensure robust stability. But, as far as robust performance is concerned, the  $\mu$ -synthesis controller guarantees robust performance, while the  $H_\infty$  controller does not perform well in the desired frequency range.

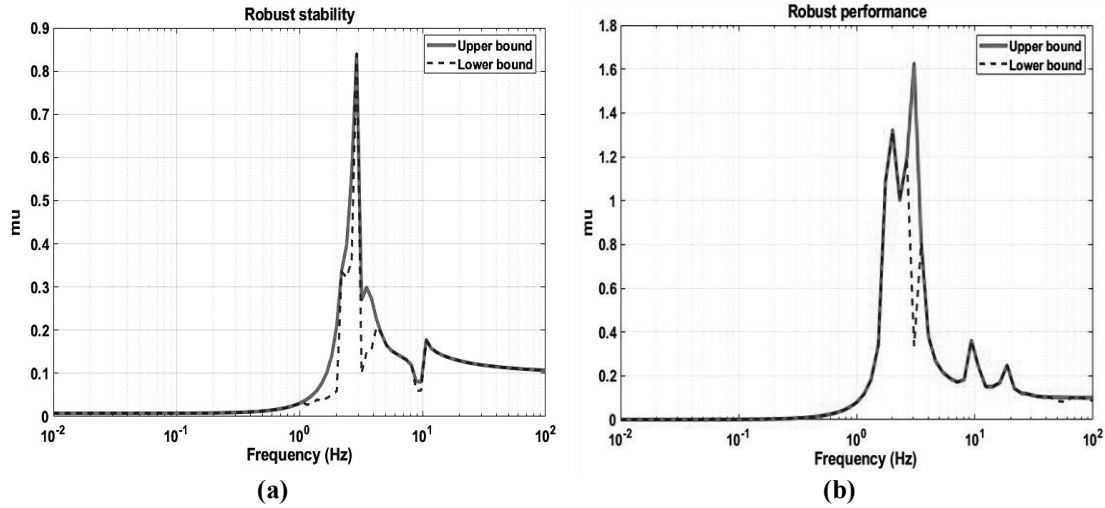


**Figure 6.7** Singular values test of  $H_\infty$  controller for (a) robust stability, (b) robust performance

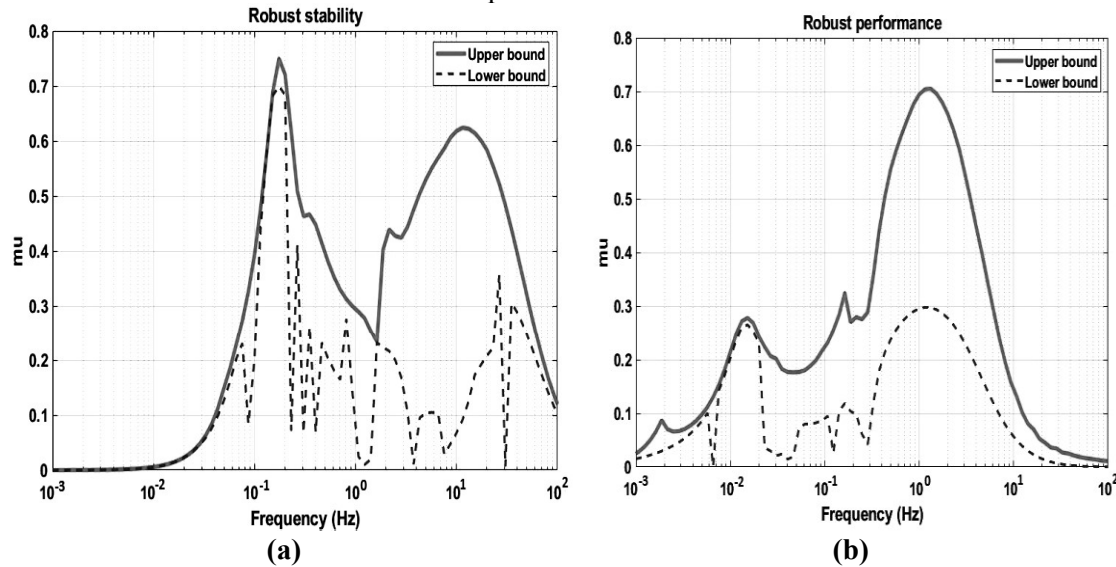


**Figure 6.8** Singular values test of  $\mu$ -synthesis controller for (a) robust stability, (b) robust performance

Now, to investigate the feasibility of the proposed strategy for the vibration mitigation of high-speed railway vehicles, the simulation studies were carried out in the next section. (under different types of uncertainties)

## 6.6.2 Simulation under random track irregularities

### 6.6.2.1 Acceleration responses of the vehicle body

To examine the effect of a robust controlled-active suspension system on the acceleration of the vehicle body, three types of random track irregularities have been used (discussed in chapter 3). A comparison has been made between the  $H_\infty$  controller, the  $\mu$ -synthesis controller, and the passive system. The closed loop perturbed frequency responses of the car body's acceleration with their corresponding time histories are shown in Figure 6.9. Also, the best and worst root mean square (RMS) values and the percentage improvement of RMS values for different control strategies are given in Table 6.1. The percentage improvement of RMS values using robust active control over the passive system has been calculated by using the following equation:

$$\% \text{ reduction} = \frac{p_s - c_s}{p_s} \times 100 \quad (42)$$

where  $p_s$  and  $c_s$  are the RMS values of the passive and active control systems, respectively.

According to Figure 6.9 (a), it is observed that the  $H_\infty$  and  $\mu$ -synthesis controllers successfully suppress the lateral acceleration of the vehicle body. Among them, the  $\mu$ -synthesis controller is more significant in reducing the resonant peaks in the desired frequency range of 1-20 Hz as shown in Figure 6.9 (b). In the case of the  $H_\infty$  controller, there exists some set of uncertainties around the frequency range of 1-5 Hz, where the closed loop frequency response does not behave according to the design specifications. This situation forces the  $H_\infty$  controller to generate a non-robust performance. Moreover, the percentage improvement of RMS values with the  $\mu$ -synthesis controller is 22.79%, more than that of the  $H_\infty$  controller (4.92%) in the worst-case scenario, as given in Table 6.1 (a). However, in the best case, the percentage improvements with both robust controllers are almost the same (approx. 26%).

From Figures 6.9 (c) and (e), in the case of vertical and pitch acceleration, it can be found that the presence of uncertainties does not affect the performance of  $H_\infty$  and  $\mu$ -synthesis controllers by a significant amount. The closed loop frequency responses of both accelerations show smooth behavior in the entire frequency range, as shown in Figures

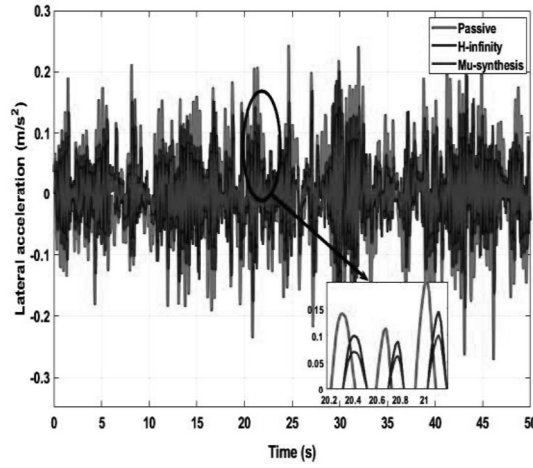
6.9 (d) and (f). However, the active suspension system controlled with  $\mu$ -synthesis control law offers more attenuation power than the passive system and  $H_\infty$  control law. According to Table 6.1 (b) and (c), the percentage improvement of RMS values with the  $\mu$ -synthesis controller is found in the range of 21%-35%, which is more than that of the  $H_\infty$  controller that achieves 21%-24 % improvement.

In case of roll acceleration, from Figure 6.9 (g), it can be seen that the vibration isolation capability of the active suspension system with  $\mu$ -synthesis controller is superior to that of the  $H_\infty$  controller. In the case of the  $H_\infty$  controller, the effects of uncertainties are more prominent in the extensive frequency range, because of which the closed loop frequency response shows very high peaks, as shown in Figure 6.9 (h). These high peaks are the primary cause of instability within the system. In contrast to the  $H_\infty$  controller, the resonant peaks of roll acceleration occurring between 2-12 Hz are effectively reduced by the  $\mu$ -controller. The superiority of the  $\mu$ -synthesis controller over the  $H_\infty$  controller can also be verified from Table 6.1 (d), where the improvement of RMS values with the  $\mu$ -synthesis controller shows a higher percentage as compared to the  $H_\infty$  controller.

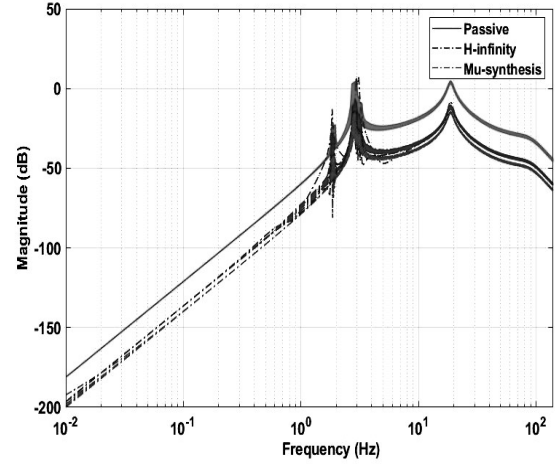
Now, observing Figure 6.9 (i), it can be seen that the behavior of the  $\mu$ -synthesis controller corresponding to yaw acceleration is similar to those of lateral and roll acceleration. In the case of the  $H_\infty$  controller, near 5 Hz frequency, some set of variation in parameters causes the designed controller to perform even worse than the passive suspension system, as shown in Figure 6.9 (j). This behavior can also be verified from Table 6.1 (e), where the percentage reduction of RMS values with  $H_\infty$  controller in the worst-case scenario is -2.73%. However, the percentage reduction of RMS values with the  $\mu$ -synthesis controller is 31.04% in the best case and 26.30% in the worst case, which proves the effectiveness of the  $\mu$ -synthesis controller.

Hence, from the above discussion, it can be concluded that the active suspension system controlled with proposed robust control schemes may enhance the ride comfort of a railway vehicle over the passive suspension system. The presence of uncertain dynamics can deteriorate the performance of the  $H_\infty$  controller, but the performance of the  $\mu$ -synthesis controller is not affected by the uncertainties in the entire frequency range. In

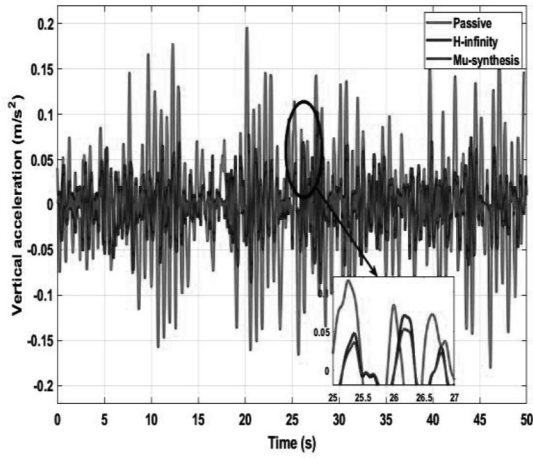
the next section, the simulated results of the proposed control strategies are validated with the experimental data on ride comfort.



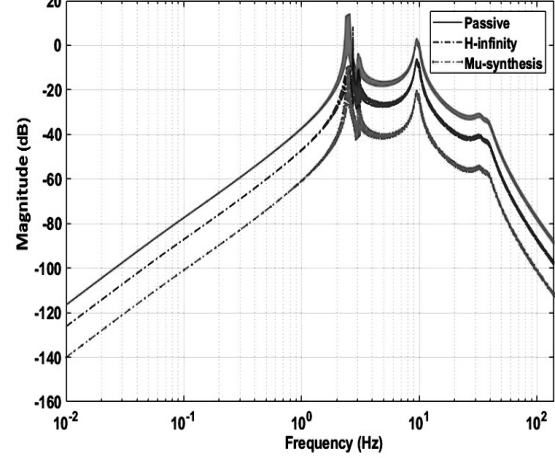
(a)



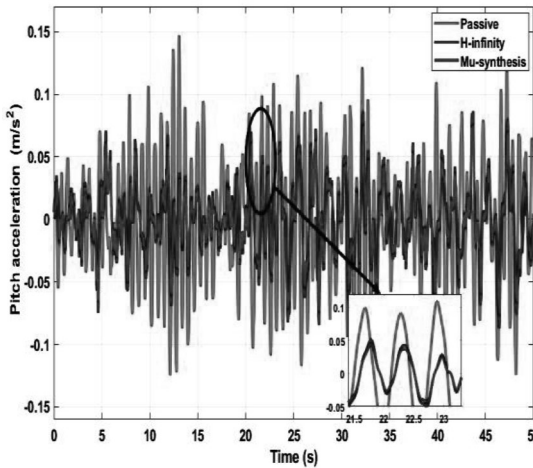
(b)



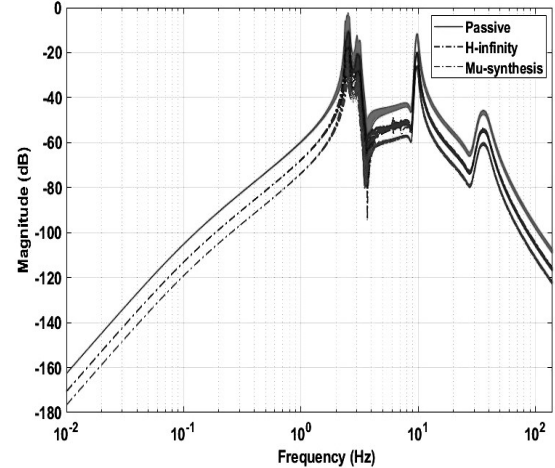
(c)



(d)



(e)



(f)

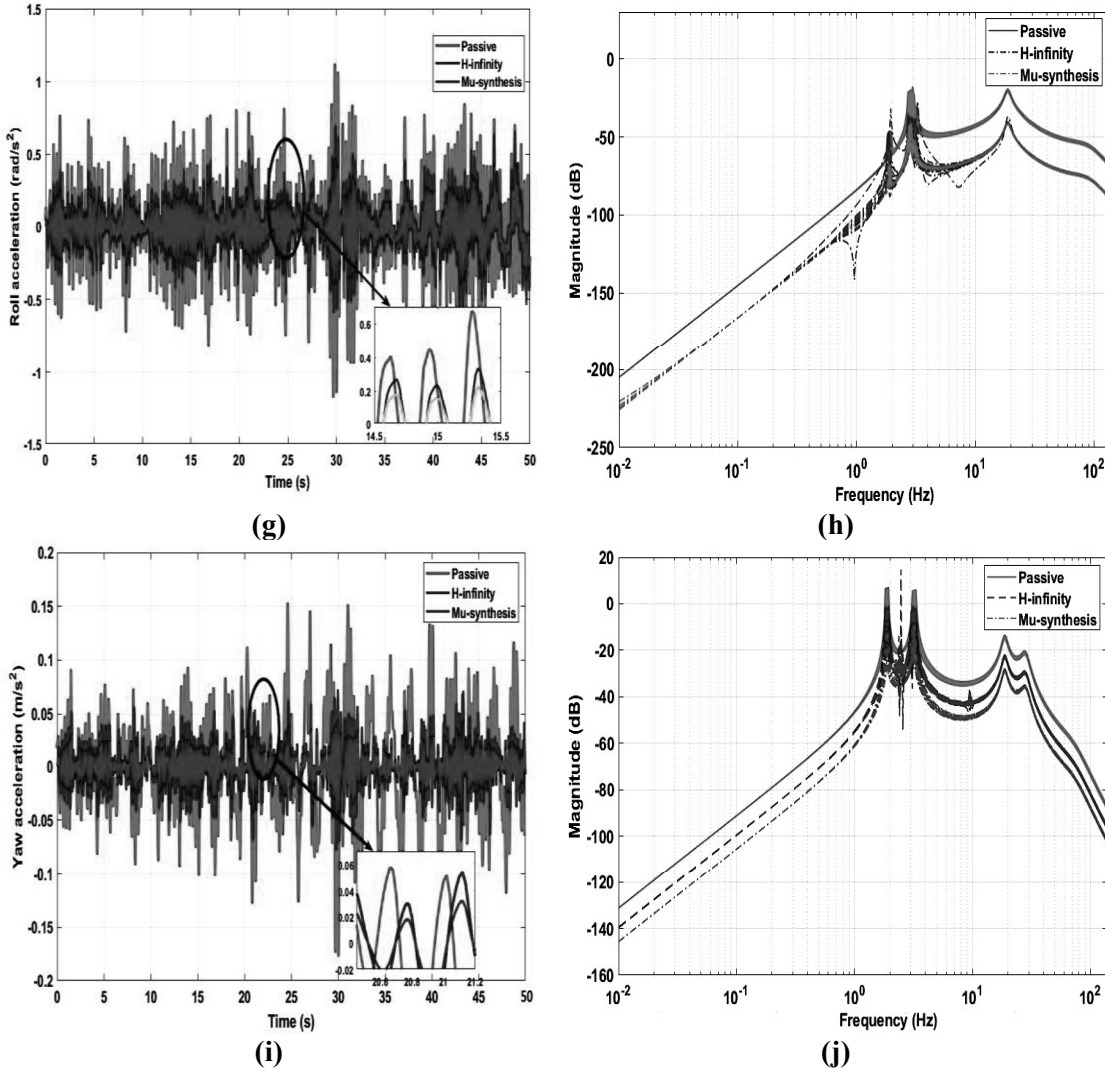


**Figure 6.9** Perturbed frequency responses and time series of vehicle body acceleration under random track disturbances (a,b) lateral acceleration ( $\ddot{Z}_c$ ) (c,d) vertical acceleration ( $\ddot{Y}_c$ ) (e,f) pitch acceleration ( $\ddot{\psi}_c$ ) (g,h) roll acceleration ( $\ddot{\theta}_c$ ), and (i, j) yaw acceleration ( $\ddot{\phi}_c$ )

**Table 6.1** RMS values of car body accelerations and % improvement under random track disturbances

<i>(a) Lateral acceleration</i>				
	<i>Worst case</i>		<i>Best case</i>	
System	RMS Values (m/s <sup>2</sup> )	% improvement	RMS Values (m/s <sup>2</sup> )	% improvement
Passive	5.603e-02	-	5.603e-02	-
H- $\infty$	5.327e-02	4.92 %	4.128e-02	26.32%
$\mu$ -synthesis	4.326e-02	22.79 %	4.104e-02	26.75%
<i>(b) Vertical acceleration</i>				
	<i>Worst case</i>		<i>Best case</i>	
System	RMS Values (m/s <sup>2</sup> )	% improvement	RMS Values (m/s <sup>2</sup> )	% improvement



Passive	5.253e-02	-	5.253e-02	-
H- $\infty$	4.115e-02	21.66 %	4.031e-02	23.26%
$\mu$ - synthesis	<b>3.602e-02</b>	<b>31.42%</b>	<b>3.429e-02</b>	<b>34.72%</b>
<b>(c) Pitch acceleration</b>				
	<i>Worst case</i>		<i>Best case</i>	
System	RMS Values (m/s <sup>2</sup> )	% improvement	RMS Values (m/s <sup>2</sup> )	% improvement
Passive	4.843e-02		4.843e-02	
H- $\infty$	3.995e-02	17.50 %	3.606e-02	25.54%
$\mu$ - synthesis	<b>3.528e-02</b>	<b>27.15%</b>	<b>3.414e-02</b>	<b>29.50%</b>
<b>(d) Roll acceleration</b>				
	<i>Worst case</i>		<i>Best case</i>	
System	RMS Values (m/s <sup>2</sup> )	% improvement	RMS Values (m/s <sup>2</sup> )	% improvement
Passive	6.285e-02		6.285e-02	
H- $\infty$	5.993e-02	4.64 %	5.119e-02	18.55%
$\mu$ - synthesis	<b>4.686e-02</b>	<b>25.44%</b>	<b>4.426e-02</b>	<b>29.57%</b>
<b>(a) Yaw acceleration</b>				
	<i>Worst case</i>		<i>Best case</i>	
System	RMS Values (m/s <sup>2</sup> )	% improvement	RMS Values (m/s <sup>2</sup> )	% improvement
Passive	4.174e-02		4.174e-02	
H- $\infty$	4.288e-02	-2.73 %	3.288e-02	21.22%
$\mu$ - synthesis	<b>3.076e-02</b>	<b>26.30%</b>	<b>2.878e-02</b>	<b>31.04%</b>

## 6.7 Validation of the proposed control schemes with experimental results

The simulated results of the proposed control schemes with active suspension are validated using the oscillations test results (Railways, Audit, 2022). The RDSO carried out the test trials on a prototype LHB chair car (as shown in Figures 3.14 ) to assess ride comfort in a test speed range of 33.33–55 m/s (120–200 Km/h). The accelerometers and displacement sensors are linked by a cable to the data acquisition system in the instrument's cabin for recording the oscillation data. In the course of oscillation test trials, these sensors capture acceleration and displacement signals on the wheelset axle box, the

car body's floor, and the test coach's bogie frame. Here, the RDSO/Sperling's criteria were used to evaluate the ride index of coaches equipped with coil springs in the secondary suspensions. Therefore, the same Sperling's method has been used in this paper to evaluate the ride comfort of railway vehicles integrated with proposed control strategies, and the results are compared with the experimental outcomes.

#### 6.7.1. Evaluation of ride comfort using Sperling's method

To evaluate the ride comfort of passengers,  $W_z$  method discussed in the chapter 3 has been used. The experimental and simulated implementations of ride indices in the lateral and vertical directions under worse and best conditions have been shown in Figure 6.10. The comparison has been made at a speed of 200 Km/h. From Figure 6.10, it can be observed that the values produced using the suggested model show greater agreement with the experimental data, with an error range of 2.36–8.81% for the lateral motion and 2.84–6.30% for the vertical motion, respectively.

Further, from Figure 6.10 (a), it can also be noted that the ride comfort with the  $\mu$ -synthesis controller is less than 2.5 in both worst and best conditions. This value implies that the  $\mu$ -synthesis controller significantly improves the lateral ride of railway vehicles compared to the  $H_\infty$  controller and passive system. Observing Figure 6.10 (b), a similar kind of behavior is found in the case of vertical motion, where the ride indices of railway vehicles using  $\mu$ -controlled active suspension are close to 2.5 in both cases. On the other hand, the ride indices for the passive and worst-case  $H_\infty$  controller are more than 2.5, which may cause an unpleasant ride experience. However, in the case scenario, the  $H_\infty$  controller provides an acceptable level of ride comfort since the value of  $W_z$  is close to 2.5.

Therefore, from the above analysis, it is observed that the active suspension controlled with the  $\mu$ -analysis technique significantly improve the ride comfort of railway vehicle. Even in the presence of uncertainties, the performances of the proposed controller stay robust.

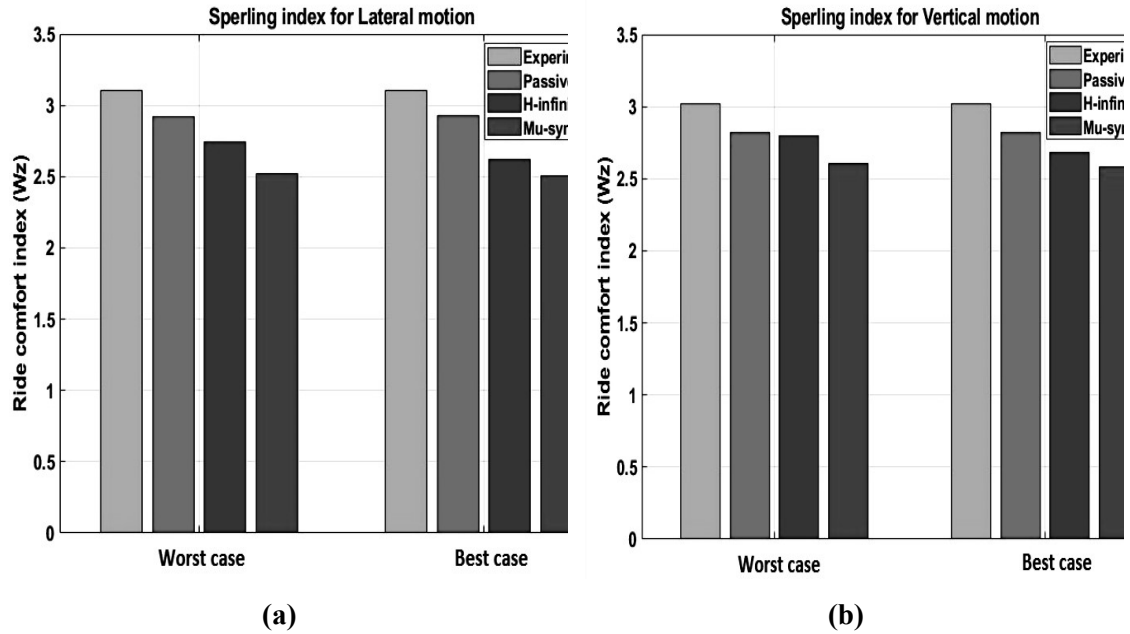


**Figure 6.10** Comparison of ride comfort indices ( $W_z$ ) with different control algorithms for  
(a) lateral motion and (b) vertical motion

## 6.8 Conclusions

This chapter proposed a robust active suspension system to suppress the vibrations of the railway vehicle. For analytical purposes, a 27-DOF uncertain model of railway vehicles integrated with an uncertain actuator model is utilized. Then, two robust controllers based on  $H_\infty$  and  $\mu$ -analysis are successfully implemented using MATLAB<sup>®</sup>. The effectiveness and robust performance of proposed controllers have been investigated in the time and frequency domain under three types of random track irregularities. Furthermore, the ride comfort of the railway vehicle is evaluated using Sperling's method, and the simulated results are validated with the experimental data. According to simulation and analysis, the following outcomes are encased:

- When dealing with uncertainties, both controllers ensure stability. However, when it comes to performance, the  $\mu$ -synthesis controller offers greater robustness compared to the  $H_\infty$  controller.
- The vibration suppression capability of the  $\mu$ -synthesis controller is superior to that of the  $H_\infty$  controller as it can provide 22-35% RMS reduction for the car

body's accelerations. On the other hand, in case of the  $H_\infty$  controller, this percentage is comparatively lesser, even in the best-case scenario.

- The simulated outcomes of the proposed study exhibit a high degree of conformity with the experimental data, showing a minimal margin of error within the range of 2.36–8.81% for the vertical motion and 4.84–5.30% for the lateral motion.
- Also, the ride comfort indices ( $W$ ) for vertical and lateral motion using  $\mu$ -synthesis are found to be less than 2.50 in both the best and worst-case scenarios. These values represent a superior comfort level compared to passive and  $H_\infty$  controller where the value of  $W_z$  is greater than 2.5.
- The robustness issue of the LQG controller is successfully resolved by the implementation of both robust controllers as shown in Figure 6.11 and Table 6.2. The stability margins of both  $H_\infty$  and  $\mu$ -synthesis controllers are significantly higher than that of EO-LQG controller (defined in previous chapter). However, the stability margins of the  $\mu$ -synthesis controller are substantially larger compared to  $H_\infty$  controllers.

Hence, based on the above discussions, it is evident that an active suspension system equipped with a  $\mu$ -synthesis controller exhibits a tremendous capability to mitigate track vibrations. The robust stability and robust performance of the proposed  $\mu$ -synthesis controller are perfectly achieved in the desired frequency range.

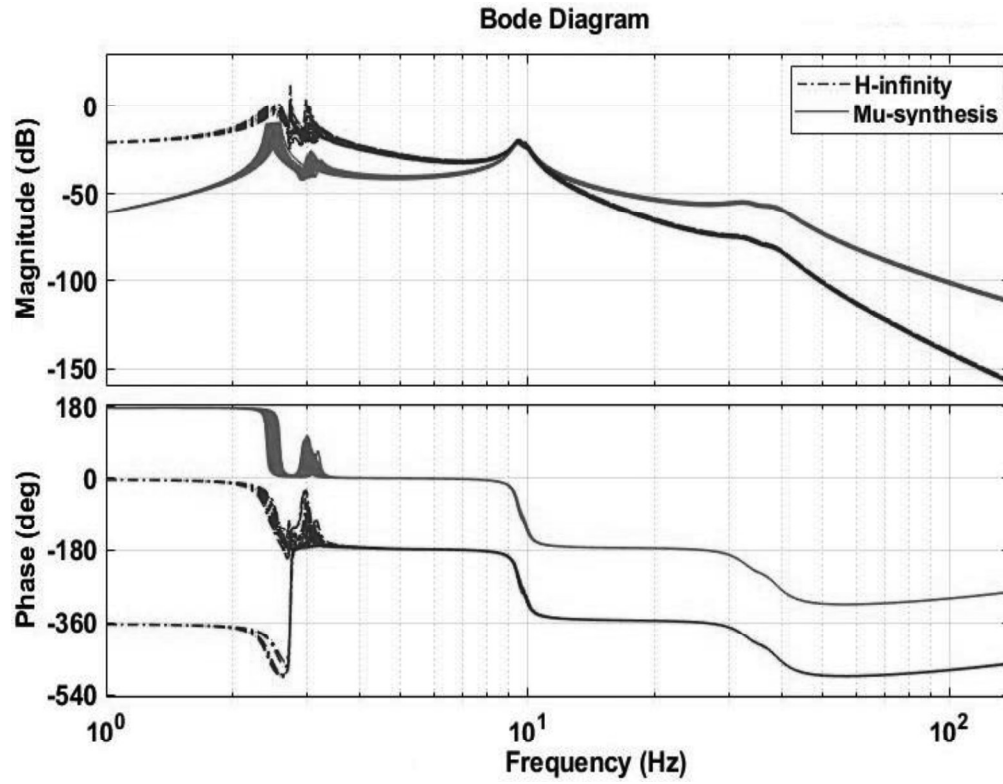


**Figure 6.11** Robustness comparison of  $H_\infty$  and  $\mu$ -synthesis controller

**Table 6.2** Stability margins of proposed robust controller

$H_\infty$	$\mu$ – synthesis
Gain margin: $[0.7617 \ 1.3129]$	Gain margin: $[0.5147 \ 1.9382]$
Phase margin: $[-15.4069 \ 15.4069]$	Phase margin: $[-35.653 \ 35.653]$
Disk margin: $[0.2705]$	Disk margin: $[0.6348]$
Lower bound: $[0.2715]$	Lower bound: $[0.6348]$
Upper bound: $[0.2711]$	Upper bound: $[0.6342]$



## CHAPTER 7

## CONCLUSIONS AND FUTURE SCOPES

---

*This chapter briefly summarizes the research outcomes and the significant contributions of this dissertation. It includes the research findings, highlights the research's limitations, and enlightens the future scope for improving the proposed research works.*

### 7.1 Conclusions

This thesis describes the research's contribution to improving vehicle ride performance for high-speed railway cars by controlling active secondary suspension system. To achieve this, we primarily focus on developing a full-scale vehicle model and intelligent vibration control strategies. The work began with developing a dynamic railway vehicle model combined with wheel-rail contact forces and track irregularities. Then, for the controlling purpose, two types of control structures i.e., centralized and decentralized integrated with classical and metaheuristic optimization algorithms, have been proposed. The performance of the proposed models are evaluated under three types of periodic and random track irregularities. Finally, the railway vehicle ride comfort index with every control scheme is evaluated, and the simulated results are compared with the experimental results. A brief summary of the proposed work, along with dissertation outcomes, is given below:

- A mathematical model with 38 degrees of freedom was created to simulate the motion of a full-scale railway vehicle. This model takes into account the vertical, lateral, roll, yaw, pitch, and yaw motion of the car body, bogies, and wheelsets. The governing equations of motion bring together the physics of railway vehicles with the wheel-rail contact model and rail irregularity model. The contact forces between the wheel and rail were assessed using the Kalker and non-Hertzian contact model. This model used the FASTSIM algorithm to calculate the creep forces. For the case study, a Linke-Hofmann-Busch coach (LHB) based model was employed. Based on pole-zero theory of control system, the critical speed of

the vehicle was evaluated. Then, the effect of various track irregularities and vehicle speed on the ride comfort of railway vehicle has been evaluated. The analysis is done using a 2-D state-space continuous model, and the findings were examined in both the time and frequency domains. The simulation results indicate that the different track imperfections can have different impacts on the dynamic performance of high-speed vehicles. Such as, the relationship between the vertical and pitch acceleration of the body and velocity is linear. In contrast, lateral, roll, and yaw accelerations behave differently as the velocity approaches the critical point. The vehicle's lateral, roll, and yaw motions are more sensitive to cross-level irregularities than lateral and vertical irregularities, which means these motions require extra attention during cross-level type rail irregularities. At specific constant values of vehicle and rail parameters, the operating and critical speeds of the vehicle are found to be different while running on the same track. According to Sperling's criteria, the simulated result suggests an average operating speed of up to 208 km/h, satisfying the human comfort level. In contrast, the critical speed is 223.2 km/h, nearly identical to that reported by the Indian railway board for LHB coaches. Finally, the simulated results of the proposed model demonstrate a remarkable alignment with the experimental data, exhibiting a small error ranging from 2.36–8.81% for vertical motion, 5.84–8.30% for lateral motion under lateral alignment, and 8.68–18.65 % under cross-level rail irregularities. Although the 38-DOF model successfully evaluates the vehicle body's vertical, lateral, pitch, roll and yaw acceleration under various track irregularities. However, the longitudinal acceleration of the car body, bogies and wheelset cannot be affected by the high class of cross-level track irregularities significantly. Therefore, these motions were eliminated in further studies.

- A novel hybrid PSO-GWO-based decentralized control system was developed to suppress the translational and angular vibrations of the car body. This scheme utilizes a 27-DOF dynamic model of a full-scale railway vehicle incorporated with wheel-rail forces and an active suspension system. Three types of periodic and random track irregularities, named vertical profile, lateral alignment, and cross-level, were used as input to the vehicle. To calculate the optimal active force, a



novel hybrid metaheuristic algorithm named hybrid PSO-GWO was proposed, and the simulated results were compared with a passive system as well as classical (ZN) and two metaheuristic tuning algorithms (PSO, GWO). The outcomes of the car body's vertical, lateral, pitch, roll, and yaw acceleration under periodic and random track irregularities were analyzed in both time and frequency domains. According to simulation and analysis, the proposed hybrid algorithm (PSO-GWO) tuned FOPID controller provides the best trade-off between maximum acceleration and control efforts expressed in terms of quadratic cost function compared to PSO and GWO. Apart from this, it is also seen that the PSO and GWO have a trapping issue at the local minimum points with the slower convergence rate as compared to proposed hybrid algorithm. Under periodic track disturbances, the time domain controller performance shows a significant decrement in the translational and angular accelerations of the vehicle body relative to the passive system. It was also noted that the suspension system controlled with a hybrid-tuned FOPID controller has comparatively better attenuation towards the vehicle vibration in terms of the percentage improvement in RMS values. It provides approximately 84.60%, 77.81%, 71.42%, 75.29 %, and 63.74% improvement of RMS values for the vehicle's vertical, lateral, pitch, roll, and yaw motions, respectively. Under random track disturbances, the success of the proposed controller has been tested in the frequency domain, and the results are critically analyzed in terms of PSDs. From the results, it is evident that the FOPID controller using hybrid algorithm provides better suppression results of resonant peaks at the extensive range of frequency. The percentage reduction in RMS values for the vertical, lateral, pitch, roll, and yaw motion were 34.83%, 29.27%, 39.17%, 24.99%, and 33.45%, respectively, as compared to the classical and other metaheuristic (PSO and GWO) techniques. However, it can also be seen that the attenuation ability of the proposed controller is significantly higher in the case of periodic track irregularities compared to the random track. The reason behind this is the configuration of a decentralized controller, which calculates the control force based on the periodic wavelengths of the track. In practical scenarios, a train is more likely to encounter random track irregularities than

periodic ones. Consequently, this point suggests that a centralized control strategy is required to manage such circumstances.

- This research presents a new algorithm-based centralized control system for the suppression of railway vehicle vibrations. An active suspension system controlled with an optimal tuned LQG controller to suppress the translational and angular vibrations of the car body was proposed. Two controllers, termed system controller (LQG) and force tracking controllers (ANFIS) with electro-hydraulic actuators, are adopted to suppress the vibration of the five motions of the car body. To calculate the optimal active force for the suspension system, two metaheuristic algorithms named PSO and EO with one classical method, i.e. Bryson's rule, were used, and the simulated results were compared with a passive system. The time-domain and frequency-domain analyses are performed on the simulated results of the vehicle's acceleration in the presence of randomly generated track imperfections. Furthermore, the ride comfort of the railway vehicle is also evaluated using Sperling's methods. The outcomes prove that the active suspension system controlled with a metaheuristic-based LQG controller provides the best results compared to traditional LQG, as the controller tuned with Bryson's rule and PSO have a slower convergence rate than the proposed equilibrium optimization algorithm. The output of the ANFIS inverse model trained with a hybrid algorithm is closely aligned with the forward dynamics of the electro-hydraulic actuator, indicating the effectiveness of tracking the desired controlling force. The performance of the proposed control scheme has been tested under three types of random track disturbances, and the results are critically analyzed. The results show that the LQG controller tuned with the metaheuristic algorithm (EO) provides better suppression results at the desired frequency range. In the case of EO optimization, the percentage reduction in RMS values for the vertical, lateral, pitch, roll, and yaw acceleration were 35.62%, 24.98%, 38.77%, 27.98%, and 35.68%, respectively. On the other hand, the active suspension system tuned to Bryson's rule, and PSO shows lower reduction capability than the proposed EO optimization technique. Also, the ride comfort indices for vertical motion using EO algorithms are found to be 2.482, and for lateral motion, the indices were

2.528 respectively. These values represent a superior comfort level compared to passive and other tuning algorithms. Although the proposed LQG control scheme exhibits a tremendous capability to mitigate the track vibrations effectively, it has an inherent robustness problem. To check the robustness of the proposed controller, the response of EO-LQG is evaluated considering the 10% variation in vehicle mass, and the results show that the stability margin with a proposed controller is shallow. Therefore, we should move toward robust control that provides better suppression in the presence of various uncertainties.

- Then, finally, this work proposed a robust active suspension system that suppresses the vehicle vibrations even in the uncertain environment of railway system. For this, a 27-DOF uncertain model of railway vehicles integrated with an uncertain actuator model was utilized. Then, two robust controllers based on  $H_\infty$  and  $\mu$ -analysis were successfully implemented using MATLAB®. The effectiveness and robust performance of proposed controllers have been investigated in the time and frequency domain under three types of random track irregularities. Furthermore, the ride comfort of the railway vehicle is evaluated using Sperling's method, and the simulated results are validated with the experimental data. The simulated findings indicate that when encountered with structured and unstructured uncertainty, both controllers demonstrate robust stability. However, in terms of robust performance, the  $\mu$ -synthesis controller outperforms the  $H_\infty$  controller. The vibration suppression capability of the  $\mu$ -synthesis controller is superior to that of the  $H_\infty$  controller as it can provide 22–35% RMS reduction for the car body's accelerations. On the other hand, in the case of the  $H_\infty$  controller, this percentage is comparatively lesser, even in the best-case scenario. The simulated outcomes of the proposed study exhibit a high degree of conformity with the experimental data, showing a minimal margin of error within the range of 2.36–8.81% for the vertical motion and 4.84–5.30% for the lateral motion. Also, the ride comfort indices ( $W$ ) for vertical and lateral motion using  $\mu$ -synthesis are found to be less than 2.50 in both the best and worst-case scenarios. These values represent a superior comfort level compared to passive and  $H_\infty$  controller where the value of  $W_z$  is greater than 2.5. The robustness issue

of the LQG controller is successfully resolved by the implementation of both robust controllers. The stability margins of  $H_\infty$  and  $\mu$ -synthesis controllers are significantly higher than that of EO-LQG controller. However, the stability margins of the  $\mu$ -synthesis controller are considered to be much larger than those of  $H_\infty$  controller.

- Hence, based on the above discussions, it is evident that an active suspension system equipped with EO-LQG and  $\mu$ -synthesis controller exhibits a tremendous capability to mitigate track vibrations. The ride comfort index of railway vehicles with both controllers is significantly improved compared to the passive system, as shown in Figure 7.1. Also, the vibration attenuation ability of the proposed active suspension system with three control strategies is superior as compare to previously reported semi-active or active suspension systems, as rendered in Table 7.1. Therefore, we can say that the ride quality of railway vehicles with active suspension systems controlled with the proposed control schemes is significantly improved in the desired frequency range.

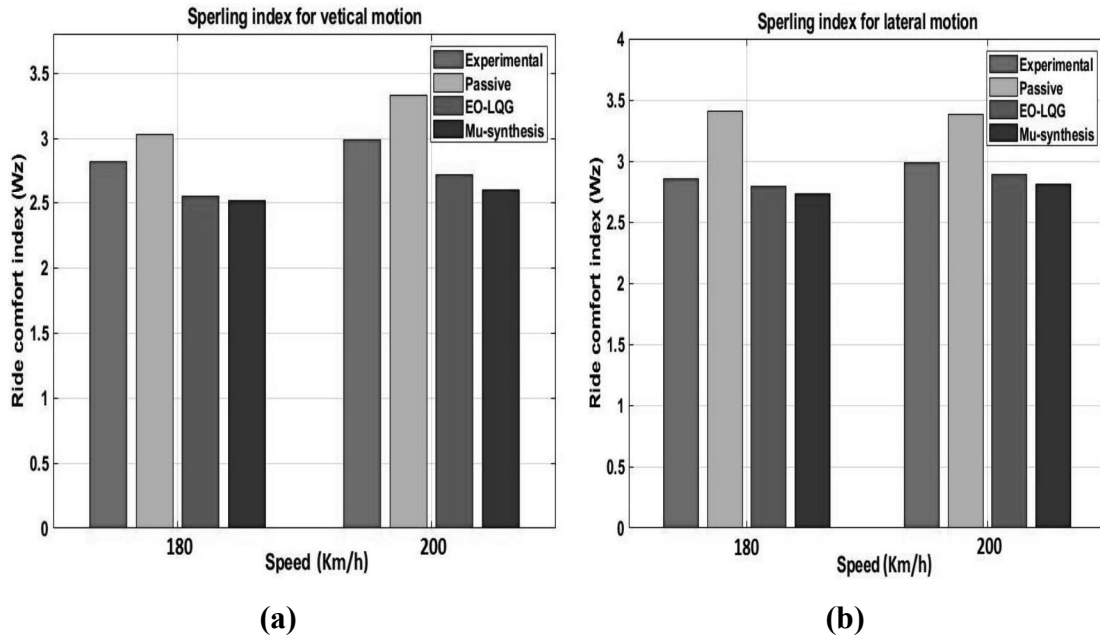


**Figure 7.1** Comparison of ride comfort indices ( $W_z$ ) with different control algorithms for (a) vertical motion and (b) lateral motion

**Table 7.1** Comparison of proposed control scheme with previous control techniques

Techniques	Authors/Year	Ranges of %age reduction
Semi-active	(C. W. Zhang et al., 2006)	Up to 30 %
Semi active	(Zong et al., 2013)	27.4 % – 32.1%
Semi-active	(H. C. Kim et al., 2017)	29.8% – 34.05%
Active	(Ripamonti & Chiarabaglio, 2019)	17.0 % – 22.0 %
Semi-active	(S. Singh & Kumar, 2022)	18.3 % – 25.3%
Active	(H. Cao et al., 2022)	5.0 % – 10.0%
Semi-active	(Jeniš et al., 2023)	28.3% – 33.6%
Fully-active	(Huang et al., 2023)	20.0% – 32.0%
<b>Proposed Active with PSO-GWO tune FOPID controller</b>	—	<b>63.7%– 84.6%</b> <b>(periodic)</b> <b>24.8% – 34.7%</b> <b>(random)</b>
<b>Proposed Active with EO-LQG control</b>	—	<b>24.8% – 38.7%</b>
<b>Proposed Active with robust control</b>	—	<b>24.9% – 39.1%</b>

## 7.2 Future scopes

As with all PhD thesis research, there are constraints on resources and time, which restrict the investigation of every possible aspect, regardless of its level of interest. However, fresh research ideas continue to emerge during the task. Fortunately, these ideas may help other researchers to improve the control scenario in the challenging field of the railway system. The suggested ideas are as follows:

- The 38-degree-of-freedom lumped model of a railway vehicle can be improved by extending it to a distributed model.
- The 2-D continuous state-space model may be further used to investigate the ride quality and comfort level by varying the damping ratio and stiffness values of the suspension system.

- Only a single objective cost function is evaluated in this study. However, the ride quality of railway vehicles could also be enhanced using a hybrid control structure tuned with a multi-objective cost function. The controller parameters could also be finely tuned with advanced metaheuristic optimization techniques that can help to increase ride pleasure.
- Actuator delay and non-linearity may affect the controller's performance. In order to remove these limitations, the proposed control scheme can be integrated with predictive and adaptive control algorithms.
- In the future, the proposed control scheme can be utilized to evaluate the ride comfort in the curved track also. The ride comfort can be evaluated and compared with more standard methods of ride quality.
- The effect of aerodynamics forces on the dynamics of railway vehicle and the human ride comfort can also be studied in the future.

## REFERENCES

---

- A. G. Thompson. (2007). An Active Suspension with Optimal Linear State Feedback. *Vehicle System Dynamics*, 5(4), 37–41.
- Abdelkareem, M. A. A., Xu, L., Ali, M. K. A., Elagouz, A., Mi, J., Guo, S., Liu, Y., & Zuo, L. (2018). Vibration energy harvesting in automotive suspension system: A detailed review. *Applied Energy*, 229(August), 672–699. <https://doi.org/10.1016/j.apenergy.2018.08.030>
- Abdessalem, J., & Abdessalem, H. (2013). *Design and Modeling of Mechanical Systems*. 2003, 549–555. <https://doi.org/10.1007/978-3-642-37143-1>
- Adubi, S. A., & Misra, S. (2014). A comparative study on the ant colony optimization algorithms. *Proceedings of the 11th International Conference on Electronics, Computer and Computation, ICECCO 2014*, 1. <https://doi.org/10.1109/ICECCO.2014.6997567>
- Afshar, K. K., & Javadi, A. (2019). *Constrained H 1 control for a half-car model of an active suspension system with actuator time delay by predictor feedback*. August 2018. <https://doi.org/10.1177/1077546319828457>
- Ahmed, J. M. (2020). Optimal tuning linear quadratic regulator for gas turbine by genetic algorithm using integral time absolute error. *International Journal of Electrical and Computer Engineering*, 10(2), 1367–1375. <https://doi.org/10.11591/ijece.v10i2.pp1367-1375>
- Akers, A., Gassman, M., & Smith, R. (2006). Hydraulic power system analysis. In *Hydraulic Power System Analysis*. <https://doi.org/10.1201/9781420014587>
- Al-Betar, M. A., Awadallah, M. A., Abu Doush, I., Hammouri, A. I., Mafarja, M., & Alyasseri, Z. A. A. (2019). Island flower pollination algorithm for global optimization. *Journal of Supercomputing*, 75(8), 5280–5323. <https://doi.org/10.1007/s11227-019-02776-y>
- Al-Tashi, Q., Abdul Kadir, S. J., Rais, H. M., Mirjalili, S., & Alhussian, H. (2019). Binary Optimization Using Hybrid Grey Wolf Optimization for Feature Selection. *IEEE Access*, 7, 39496–39508. <https://doi.org/10.1109/ACCESS.2019.2906757>
- Alamdar Ravari, M., & Yaghoobi, M. (2019). Optimum Design of Fractional Order Pid Controller Using Chaotic Firefly Algorithms for a Control CSTR System. *Asian Journal of Control*, 21(5), 2245–2255. <https://doi.org/10.1002/asjc.1836>
- Alehashem, S. M. S., Ni, Y. Q., & Liu, X. Z. (2021). A Full-Scale Experimental Investigation on Ride Comfort and Rolling Motion of High-Speed Train Equipped with MR Dampers. *IEEE Access*, 9, 118113–118123. <https://doi.org/10.1109/ACCESS.2021.3106953>
- Alexander, A., Vacca, A., & Cristofori, D. (2017). Active Vibration Damping in

## REFERENCES

- Hydraulic Construction Machinery. *Procedia Engineering*, 176, 514–528. <https://doi.org/10.1016/j.proeng.2017.02.351>
- Alfi, S., Prandi, D., Ward, C., Bruni, S., & Goodall, R. (2019). *Active secondary yaw control to improve curving behaviour of a railway vehicle* © The Japan Society of Mechanical Engineers *Active secondary yaw control to improve curving behaviour of a railway vehicle*. 0–10.
- Ali, M., Obaid, M., Husain, A. R., & Ahmed, Y. (2014). *Intelligent optimal Controller of Active Suspension System Based on Particle Swarm Optimization*. 6(3).
- Arabia, S. (2001). *of Active Controls for*. 1237–1252.
- Arora, M., Raut, N., & Hote, Y. V. (2019). Tuning of PI/PID controllers for MIMO System using Modified Gerschgorin theorem. *2019 IEEE International Conference on Electrical, Control and Instrumentation Engineering, ICECIE 2019 - Proceedings*. <https://doi.org/10.1109/ICECIE47765.2019.8974792>
- Ashokkumar, S., Kaushik, N. K., Han, I., Uhm, H. S., Park, J. S., Cho, G. S., Oh, Y. J., Shin, Y. O., & Choi, E. H. (2023). Persistence of Coronavirus on Surface Materials and Its Control Measures Using Nonthermal Plasma and Other Agents. *International Journal of Molecular Sciences*, 24(18). <https://doi.org/10.3390/ijms241814106>
- Aslam, M. S., Tiwari, P., Pandey, H. M., & Band, S. S. (2023). Observer-Based Control for a New Stochastic Maximum Power Point Tracking for Photovoltaic Systems With Networked Control System. *IEEE Transactions on Fuzzy Systems*, 31(6), 1870–1884. <https://doi.org/10.1109/TFUZZ.2022.3215797>
- Åström, K. J., & Hägglund, T. (2004). Revisiting the Ziegler-Nichols step response method for PID control. *Journal of Process Control*, 14(6), 635–650. <https://doi.org/10.1016/j.jprocont.2004.01.002>
- Auciello, J., Meli, E., Falomi, S., & Malvezzi, M. (2009). Dynamic simulation of railway vehicles: Wheel/rail contact analysis. *Vehicle System Dynamics*, 47(7), 867–899. <https://doi.org/10.1080/00423110802464624>
- Automotive, A. N., & Suspension, A. (1990). 3~40 -. *December*.
- Bailey, J. R., & Hedrick, J. K. (2015). *Rail Vehicle Energy Dissipation Due to Lateral Vehicle / Track Interaction*. 3114(October). <https://doi.org/10.1080/00423118808969238>
- Baranowski, J., Bauer, W., Zagorowska, M., Dziwinski, T., & Piatek, P. (2015). Time-domain Oustaloup approximation. *2015 20th International Conference on Methods and Models in Automation and Robotics, MMAR 2015*, 116–120. <https://doi.org/10.1109/MMAR.2015.7283857>
- Barbosa, R. S., Tenreiro Machado, J. A., & Jesus, I. S. (2010). Effect of fractional orders in the velocity control of a servo system. *Computers and Mathematics with Applications*, 59(5), 1679–1686. <https://doi.org/10.1016/j.camwa.2009.08.009>
- Bartyś, M., & Hryniewicki, B. (2019). The trade-off between the controller effort and



## REFERENCES

- control quality on example of an electro-pneumatic final control element. *Actuators*, 8(1). <https://doi.org/10.3390/act8010023>
- Baumal, A. E., McPhee, J. J., & Calamai, P. H. (1998). Application of genetic algorithms to the design optimization of an active vehicle suspension system. *Computer Methods in Applied Mechanics and Engineering*, 163(1–4), 87–94. [https://doi.org/10.1016/S0045-7825\(98\)00004-8](https://doi.org/10.1016/S0045-7825(98)00004-8)
- Beltran-carbajal, F., Valderrabano-gonzalez, A., Favela-contreras, A., Hernandez-avila, J. L., Lopez-garcia, I., & Tapia-olvera, R. (n.d.). *An Active Vehicle Suspension Control Approach with Electromagnetic and Hydraulic Actuators*. 1–18. <https://doi.org/10.3390/act8020035>
- Ben, L. Z., Hasbullah, F., & Faris, F. W. (2014). A comparative ride performance of passive, semi-active and active suspension systems for off-road vehicles using half car model. *International Journal of Heavy Vehicle Systems*, 21(1), 26–41. <https://doi.org/10.1504/IJHVS.2014.057827>
- Bhardawaj, S., Sharma, R. C., & Sharma, S. K. (2020). Development in the modeling of rail vehicle system for the analysis of lateral stability. *Materials Today: Proceedings*, 25, 610–619. <https://doi.org/10.1016/j.matpr.2019.07.376>
- Bhatt, A., & Kato, H. (2021). High-speed rails and knowledge productivity: A global perspective. *Transport Policy*, 101(April 2020), 174–186. <https://doi.org/10.1016/j.tranpol.2020.12.006>
- Bilgic, H. H., Sen, M. A., Yapici, A., Yavuz, H., & Kalyoncu, M. (2021). Meta-Heuristic Tuning of the LQR Weighting Matrices Using Various Objective Functions on an Experimental Flexible Arm Under the Effects of Disturbance. *Arabian Journal for Science and Engineering*, 46(8), 7323–7336. <https://doi.org/10.1007/s13369-021-05428-7>
- Bingul, Z., & Karahan, O. (2018). Comparison of PID and FOPID controllers tuned by PSO and ABC algorithms for unstable and integrating systems with time delay. *Optimal Control Applications and Methods*, 39(4), 1431–1450. <https://doi.org/10.1002/oca.2419>
- Body, H., & Graph, B. (2018). *IMECE2017-71288. 2001*, 1–8.
- Bogart, D., & Chaudhary, L. (2015). Railways in colonial India: An economic achievement? *A New Economic History of Colonial India, May*, 140–160. <https://doi.org/10.4324/9781315771083>
- Bongardt, B., & Kirchner, F. (2017). *Newton-Euler equations in general coordinates. September*, 1–8. <https://doi.org/10.19124/ima.2015.001.20>
- Bosso, N., Gugliotta, A., Magelli, M., & Zampieri, N. (2019). Monitoring of railway freight vehicles using onboard systems. *Procedia Structural Integrity*, 24, 692–705. <https://doi.org/10.1016/j.prostr.2020.02.061>
- Bousmalis, K., Pfaffmann, J. O., & Hayes, G. M. (2008). Improving evolutionary

## REFERENCES

- algorithms with scouting: High-dimensional problems. *Lecture Notes in Computer Science (Including Subseries Lecture Notes in Artificial Intelligence and Lecture Notes in Bioinformatics)*, 5097 LNAI(c), 365–375. [https://doi.org/10.1007/978-3-540-69731-2\\_36](https://doi.org/10.1007/978-3-540-69731-2_36)
- Brunton, S., & J. Nathan Kutz. (2019). *I Svd* (Issue Dmd).
- Cao, H., Li, G., & Liang, N. (2022). Active Vibration Control of Railway Vehicle Car Body by Secondary Suspension Actuators and Piezoelectric Actuators. *IEEE Access*, 10(October), 105404–105411. <https://doi.org/10.1109/ACCESS.2022.3210968>
- Cao, J. Y., Liang, J., & Cao, B. G. (2005). Optimization of Fractional Order PID controllers based on genetic algorithms. *2005 International Conference on Machine Learning and Cybernetics, ICMLC 2005, August*, 5686–5689. <https://doi.org/10.1109/icmlc.2005.1527950>
- Chachuat, B. (2007). Chapter 3: Optimal Control. *Nonlinear and Dynamic Optimization: From Theory to Practice.*, 105–187.
- Chamorro, R., Escalona, J. L., & Recuero, A. M. (2014). Stability analysis of multibody systems with long flexible bodies using the moving modes method and its application to railroad dynamics. *Journal of Computational and Nonlinear Dynamics*, 9(1), 1–10. <https://doi.org/10.1115/1.4025284>
- Chang, C.-C., & Zhou, L. (2002). Neural Network Emulation of Inverse Dynamics for a Magnetorheological Damper. *Journal of Structural Engineering*, 128(2), 231–239. [https://doi.org/10.1061/\(asce\)0733-9445\(2002\)128:2\(231\)](https://doi.org/10.1061/(asce)0733-9445(2002)128:2(231))
- Chang, W. Der, & Chen, C. Y. (2014). PID controller design for MIMO processes using improved particle swarm optimization. *Circuits, Systems, and Signal Processing*, 33(5), 1473–1490. <https://doi.org/10.1007/s00034-013-9710-4>
- Chauhan, U., Kumar, B., Rani, A., & Singh, V. (2019). Optimal Perturbation MPPT Technique for Solar PV System using Grey Wolf Optimization. *2019 International Conference on Computing, Power and Communication Technologies, GUCON 2019*, 589–592.
- Chauhan, Y., Sharma, B. B., & Ranjan, R. K. (2021). Synchronization of Nonlinear Systems in Chain Network Configuration with Parametric Uncertainty. *Proceedings of the 2021 IEEE 18th India Council International Conference, INDICON 2021*, 1–6. <https://doi.org/10.1109/INDICON52576.2021.9691586>
- Chen, C. J., Fang, C., Qu, G. Q., & He, Z. Y. (2021). Vertical vibration modelling and vibration response analysis of Chinese high-speed train passengers at different locations of a high-speed train. *Proceedings of the Institution of Mechanical Engineers, Part F: Journal of Rail and Rapid Transit*, 235(1), 35–46. <https://doi.org/10.1177/0954409720901882>
- Chen, Z. H., & Ni, Y. Q. (2017). Adaptive Semiactive Cable Vibration Control: A Frequency Domain Perspective. *Shock and Vibration*, 2017, 14–25.

## REFERENCES

- <https://doi.org/10.1155/2017/2593503>
- Chentit, H. (2003). *A multi-objective control design for active suspensions with hard constraints*. 2–7.
- Chevrie, M., Farges, C., & Sabatier, J. (2019). Linear quadratic control law design for commensurate fractional order models. *2019 18th European Control Conference, ECC 2019*, 4122–4127. <https://doi.org/10.23919/ECC.2019.8796136>
- Chevrie, M., Sabatier, J., Farges, C., & Malti, R. (2015). H2-norm of a class of fractional transfer functions suited for modeling diffusive phenomena. *Proceedings of the American Control Conference, 2015-July*, 2199–2204. <https://doi.org/10.1109/ACC.2015.7171059>
- Chhabra, H., Mohan, V., Rani, A., & Singh, V. (2019). Multi-objective cuckoo search algorithm-based 2-DOF FOPD controller for robotic manipulator. In *Lecture Notes in Electrical Engineering* (Vol. 526). Springer Singapore. [https://doi.org/10.1007/978-981-13-2553-3\\_33](https://doi.org/10.1007/978-981-13-2553-3_33)
- Choi, S. B., Choi, J. H., Nam, M. H., Cheong, C. C., & Lee, H. G. (1998). A semi-active suspension using ER fluids for a commercial vehicle seat. *Journal of Intelligent Material Systems and Structures*, 9(8), 601–606. <https://doi.org/10.1177/1045389X9800900803>
- Chudzikiewicz, A. (2000). Simulation of rail vehicle dynamics in MATLAB environment. *Vehicle System Dynamics*, 33(2), 107–119. [https://doi.org/10.1076/0042-3114\(200002\)33:2;1-1;FT107](https://doi.org/10.1076/0042-3114(200002)33:2;1-1;FT107)
- Da Fonseca Neto, J. V., Abreu, I. S., & Da Silva, F. N. (2010). Neural-genetic synthesis for state-space controllers based on linear quadratic regulator design for eigenstructure assignment. *IEEE Transactions on Systems, Man, and Cybernetics, Part B: Cybernetics*, 40(2), 266–285. <https://doi.org/10.1109/TSMCB.2009.2013722>
- Dahleh, M. (n.d.). Lectures on Dynamic Systems and Control Robust Performance and Introduction to the Structured Singular Value Function. *Electrical Engineering*.
- Dahunsi, O. A., Dangor, M., Pedro, J. O., & Ali, M. M. (2020). Proportional + integral + derivative control of nonlinear full-car electrohydraulic suspensions using global and evolutionary optimization techniques. *Journal of Low Frequency Noise Vibration and Active Control*, 39(2), 393–415. <https://doi.org/10.1177/1461348419842676>
- Dai, L., & Singh, M. C. (1997). An analytical and numerical method for solving linear and nonlinear vibration problems. *International Journal of Solids and Structures*, 34(21), 2709–2731. [https://doi.org/10.1016/S0020-7683\(96\)00169-2](https://doi.org/10.1016/S0020-7683(96)00169-2)
- Daniyan, I. A., Mpofu, K., Daniyan, O. L., & Adeodu, A. O. (2019). Dynamic modelling and simulation of rail car suspension systems using classic controls. *Cogent Engineering*, 6(1), 1–20. <https://doi.org/10.1080/23311916.2019.1602927>

## REFERENCES

- Das, S., Saha, S., Das, S., & Gupta, A. (2011). On the selection of tuning methodology of FOPID controllers for the control of higher order processes. *ISA Transactions*, 50(3), 376–388. <https://doi.org/10.1016/j.isatra.2011.02.003>
- Dastranj, M. R., Rouhani, M., & Hajipoor, A. (2012). Design of Optimal Fractional Order PID Controller Using PSO Algorithm. *International Journal of Computer Theory and Engineering*, January 2016, 429–432. <https://doi.org/10.7763/ijcte.2012.v4.499>
- Davies, R., & Clarke, T. (1995). Parallel implementation of a genetic algorithm. *Control Engineering Practice*, 3(1), 11–19. [https://doi.org/10.1016/0967-0661\(94\)00059-P](https://doi.org/10.1016/0967-0661(94)00059-P)
- Davis, B. R., & Thompson, A. G. (1988). Optimal Linear Active Suspensions with Integral Constraint. *Vehicle System Dynamics*, 17(6), 357–366. <https://doi.org/10.1080/00423118808968911>
- Debnath, M. K. (2016). Technique for Automatic Generation control of a multi- source Power System. *IEEE Uttar Pradesh Section International Conference on Electrical, Computer and Electronics Engineering (UPCON)*, 531–536.
- Debnath, S., & Biswas, P. K. (2021). Design, analysis, and testing of I-type electromagnetic actuator used in single-coil active magnetic bearing. *Electrical Engineering*, 103(1), 183–194. <https://doi.org/10.1007/s00202-020-01071-x>
- Delavari, H., Lanusse, P., & Sabatier, J. (2013). Fractional order controller design for a flexible link manipulator robot. *Asian Journal of Control*, 15(3), 783–795. <https://doi.org/10.1002/asjc.677>
- Dorato, P. D. (1987). A Historical Review of Robust Control. *IEEE Control Systems Magazine*, 7(2), 44–47. <https://doi.org/10.1109/MCS.1987.1105273>
- Du, H., Lam, J., & Sze, K. Y. (2003). Non-fragile output feedback  $H_{\infty}$  vehicle suspension control using genetic algorithm. *Engineering Applications of Artificial Intelligence*, 16(7–8), 667–680. <https://doi.org/10.1016/j.engappai.2003.09.008>
- Duan, Z., & Xiang, Z. (2017). Finite frequency  $H_{\infty}$  control of 2-D continuous systems in Roesser model. *Multidimensional Systems and Signal Processing*, 28(4), 1481–1497. <https://doi.org/10.1007/s11045-016-0430-3>
- Dumitriu, M., & Fologea, D. (2019). Numerical analysis on the correlation between bogie dynamic response and vertical track irregularities. *UPB Scientific Bulletin, Series D: Mechanical Engineering*, 81(4), 99–110.
- Dumitriu, M., & Stănică, D. I. (2021). Study on the evaluation methods of the vertical ride comfort of railway vehicle—mean comfort method and sperling’s method. *Applied Sciences (Switzerland)*, 11(9). <https://doi.org/10.3390/app11093953>
- Dyke, S. J., Spencer, B. F., Sain, M. K., & Carlson, J. D. (1996). Modeling and control of magnetorheological dampers for seismic response reduction. *Smart Materials and Structures*, 5(5), 565–575. <https://doi.org/10.1088/0964-1726/5/5/006>
- Eiben, A. E. (1997). Genetic algorithms + data structures = evolution programs. In *Artificial Intelligence in Medicine* (Vol. 9, Issue 3, pp. 283–286).

## REFERENCES

- [https://doi.org/10.1016/s0933-3657\(96\)00378-8](https://doi.org/10.1016/s0933-3657(96)00378-8)
- Eickhoff, B. M., Evans, J. R., & Minnis, A. J. (1995). A Review of Modelling Methods for Railway Vehicle Suspension Components. *Vehicle System Dynamics*, 24(6–7), 469–496. <https://doi.org/10.1080/00423119508969105>
- El-Deen, A. T., Hakim Mahmoud, A. A., & El-Sawi, A. R. (2015). Optimal PID tuning for DC motor speed controller based on genetic algorithm. *International Review of Automatic Control*, 8(1), 80–85. <https://doi.org/10.15866/ireaco.v8i1.4839>
- El Beshbichi, O., Wan, C., Bruni, S., & Kassa, E. (2020). Complex eigenvalue analysis and parameters analysis to investigate the formation of railhead corrugation in sharp curves. *Wear*, 450–451(December 2019), 203150. <https://doi.org/10.1016/j.wear.2019.203150>
- Elmadany, M. M. (1990). Optimal Linear Active Suspensions with Multivariable Integral Control. *Vehicle System Dynamics*, 19(6), 313–329. <https://doi.org/10.1080/00423119008968950>
- Elmadany, M. M. (1991). Integral and state variable feedback controllers for improved performance in automotive vehicles. *Proceedings of the ASME Design Engineering Technical Conference, Part F1684(2)*, 339–346. <https://doi.org/10.1115/DETC1991-0266>
- Elmadany, M. M., & Qarmoush, A. O. (2011). Dynamic analysis of a slow-active suspension system based on a full car model. *JVC/Journal of Vibration and Control*, 17(1), 39–53. <https://doi.org/10.1177/1077546309352828>
- ElMadany, M. M., & Samaha, M. E. (1992). On the optimum ride control of a stochastic model of a tractor-semitrailer vehicle. *Journal of Sound and Vibration*, 156(2), 269–281. [https://doi.org/10.1016/0022-460X\(92\)90697-V](https://doi.org/10.1016/0022-460X(92)90697-V)
- Emary, E., Zawbaa, H. M., & Hassanien, A. E. (2016). Binary grey wolf optimization approaches for feature selection. *Neurocomputing*, 172, 371–381. <https://doi.org/10.1016/j.neucom.2015.06.083>
- Escalona, J. L., Chamorro, R., & Recuero, A. M. (2012). Description of methods for the eigenvalue analysis of railroad vehicles including track flexibility. *Journal of Computational and Nonlinear Dynamics*, 7(4). <https://doi.org/10.1115/1.4006729>
- Eshtay, M., Faris, H., & Obeid, N. (2018). Improving Extreme Learning Machine by Competitive Swarm Optimization and its application for medical diagnosis problems. *Expert Systems with Applications*, 104, 134–152. <https://doi.org/10.1016/j.eswa.2018.03.024>
- Eski, I., & Yildirim, Ş. (2009). Vibration control of vehicle active suspension system using a new robust neural network control system. *Simulation Modelling Practice and Theory*, 17(5), 778–793. <https://doi.org/10.1016/j.simpat.2009.01.004>
- Esmailzadeh, E., & Taghirad, H. D. (1998). Active vehicle suspensions with optimal state-feedback control. *International Journal of Modelling and Simulation*, 18(3),

## REFERENCES

- 228–237. <https://doi.org/10.1080/02286203.1998.11760383>
- Fadiga, L., Farges, C., Sabatier, J., & Santugini, K. (2013).  $H_\infty$  output feedback control of commensurate fractional order systems. *2013 European Control Conference, ECC 2013*, 2, 4538–4543. <https://doi.org/10.23919/ecc.2013.6669646>
- Faramarzi, A., Heidarinejad, M., Stephens, B., & Mirjalili, S. (2020). Equilibrium optimizer: A novel optimization algorithm. *Knowledge-Based Systems*, 191, 105190. <https://doi.org/10.1016/j.knosys.2019.105190>
- Fard, M., Lo, L., Subic, A., & Jazar, R. (2014). Effects of seat structural dynamics on current ride comfort criteria. *Ergonomics*, 57(10), 1549–1561. <https://doi.org/10.1080/00140139.2014.934300>
- Farges, C., Fadiga, L., & Sabatier, J. (2013).  $\mathcal{H}_\infty$  Analysis and Control of Commensurate Fractional Order Systems. *Mechatronics*, 23(7), 772–780. <https://doi.org/10.1016/j.mechatronics.2013.06.005>
- Fessi, R., & Bouallègue, S. (2019). LQG controller design for a quadrotor UAV based on particle swarm optimisation. *International Journal of Automation and Control*, 13(5), 569–594. <https://doi.org/10.1504/IJAAC.2019.101910>
- Fourie, D. J., Gräbe, P. J., Heyns, P. S., & Fröhling, R. D. (2019). Frequency domain model for railway wheel squeal resulting from unsteady longitudinal creepage. *Journal of Sound and Vibration*, 445, 228–246. <https://doi.org/10.1016/j.jsv.2018.12.014>
- Frequency Domain Analysis of Mechanical Vibrations in Automatic Rolling Systems*. (1997). 0032(4).
- Fu, B., & Bruni, S. (2022a). An examination of alternative schemes for active and semi-active control of vertical car-body vibration to improve ride comfort. *Proceedings of the Institution of Mechanical Engineers, Part F: Journal of Rail and Rapid Transit*, 236(4), 386–405. <https://doi.org/10.1177/09544097211022108>
- Fu, B., & Bruni, S. (2022b). *An examination of alternative schemes for active and semi-active control of vertical car-body vibration to improve ride comfort*. <https://doi.org/10.1177/09544097211022108>
- Fu, B., Di Gialleonardo, E., Liu, B., & Bruni, S. (2023). Modelling, hardware-in-the-loop tests and numerical simulation of magneto-rheological semi-active primary suspensions in a railway vehicle. *Vehicle System Dynamics*. <https://doi.org/10.1080/00423114.2023.2239391>
- Fu, B., Giossi, R. L., Persson, R., Stichel, S., Bruni, S., & Goodall, R. (2020). Active suspension in railway vehicles: a literature survey. *Railway Engineering Science*, 28(1), 3–35. <https://doi.org/10.1007/s40534-020-00207-w>
- Ganguly, S., Sahoo, N. C., & Das, D. (2010). A novel multi-objective PSO for electrical distribution system planning incorporating distributed generation. *Energy Systems*, 1(3), 291–337. <https://doi.org/10.1007/s12667-010-0014-5>

## REFERENCES

- Gao, H., Lam, J., & Wang, C. (2006). *ARTICLE IN PRESS Multi-objective control of vehicle active suspension systems via load-dependent controllers*. 290, 654–675. <https://doi.org/10.1016/j.jsv.2005.04.007>
- Garivaltis, D. S., Garg, V. K., & D'Souza, A. F. (1980). Dynamic Response of a Six-axle Locomotive to Random Track Inputs. *Vehicle System Dynamics*, 9(3), 117–147. <https://doi.org/10.1080/00423118008968620>
- Gaspar, P., Szaszi, I., & Bokor, J. (2010). *Design of Robust Controllers for Active Vehicle Suspension Using the Mixed  $\mu$  Synthesis*. 3114. <https://doi.org/10.1076/vesd.40.2.193.16541>
- Ghith, E. S., & Tolba, F. A. A. (2022). Design and Optimization of PID Controller using Various Algorithms for Micro-Robotics System. *Journal of Robotics and Control (JRC)*, 3(3), 244–256. <https://doi.org/10.18196/jrc.v3i3.14827>
- Gomonwattanapanich, O., Pannucharoenwong, N., Rattanadecho, P., Echaroj, S., & Hemathulin, S. (2020). Vibration control of vehicle by active suspension with LQG algorithm. *International Journal of Automotive and Mechanical Engineering*, 17(2), 8011–8018. <https://doi.org/10.15282/ijame.17.2.2020.19.0600>
- Gong, D., Liu, G., & Zhou, J. (2021). Research on mechanism and control methods of carbody chattering of an electric multiple-unit train. *Multibody System Dynamics*, 53(2), 135–172. <https://doi.org/10.1007/s11044-021-09779-9>
- Gong, D., Wang, Z., Liu, G., & Zhou, J. (2020). A modal frequency optimization approach for a fully-equipped car body of high-speed trains. *Journal of Mechanical Science and Technology*, 34(1), 11–21. <https://doi.org/10.1007/s12206-019-1202-4>
- Gong, D., Zhao, K., Liu, G., Wang, Z., You, T., & Zhou, J. (2022). Modal vibration decomposition method and its application on multi-mode vibration control of high-speed railway car bodies. *Journal of the Franklin Institute*, 359(10), 4699–4726. <https://doi.org/10.1016/j.jfranklin.2022.05.002>
- Goodall, R. (2007). *Active Railway Suspensions: Implementation Status and Technological Trends Active Railway Suspensions: Implementation Status*. 3114. <https://doi.org/10.1080/00423119708969351>
- Goodall, R. M., & Kortüm, W. (1983). Active Controls in Ground Transportation—Review of the State-of-the-Art and Future Potential. *Vehicle System Dynamics*, 12(4–5), 225–257. <https://doi.org/10.1080/00423118308968755>
- Goodall, R. M., & Mei, T. X. (2006). Active suspensions. In *Handbook of Railway Vehicle Dynamics* (Issue 25014). <https://doi.org/10.1201/9780429469398-15>
- Goodwin, M. J. (1987). Dynamics of railway vehicle systems. *Journal of Mechanical Working Technology*, 14(2), 245–247. [https://doi.org/10.1016/0378-3804\(87\)90070-2](https://doi.org/10.1016/0378-3804(87)90070-2)
- Graa, M., Nejlaoui, M., Houidi, A., Affi, Z., & Romdhane, L. (2018). Modeling and control of rail vehicle suspensions: A comparative study based on the passenger

## REFERENCES

- comfort. *Proceedings of the Institution of Mechanical Engineers, Part C: Journal of Mechanical Engineering Science*, 232(2), 260–274. <https://doi.org/10.1177/0954406216682542>
- Grimble, M. J., & Johnson, M. A. (n.d.). *Advanced Textbooks in Control and Signal*.
- Guclu, R., & Metin, M. (2009). Fuzzy logic control of vibrations of a light rail transport vehicle in use in Istanbul traffic. *JVC/Journal of Vibration and Control*, 15(9), 1423–1440. <https://doi.org/10.1177/1077546309102664>
- Guizani, A., Hammadi, M., Choley, J., Soriano, T., Abbes, M. S., & Haddar, M. (2015). Multiphysics Modelling and Simulation for Systems Design and Monitoring. *Multiphysics Modelling and Simulation for Systems Design and Monitoring*, 189–198. <https://doi.org/10.1007/978-3-319-14532-7>
- Guo, D., Wang, X., Gao, K., Jin, Y., Ding, J., & Chai, T. (2022). Evolutionary Optimization of High-Dimensional Multiobjective and Many-Objective Expensive Problems Assisted by a Dropout Neural Network. *IEEE Transactions on Systems, Man, and Cybernetics: Systems*, 52(4), 2084–2097. <https://doi.org/10.1109/TSMC.2020.3044418>
- Hać, A. (1992). Optimal Linear Preview Control of Active Vehicle Suspension. *Vehicle System Dynamics*, 21(1), 167–195. <https://doi.org/10.1080/00423119208969008>
- Hajihassani, M., Jahed Armaghani, D., & Kalatehjari, R. (2018). Applications of Particle Swarm Optimization in Geotechnical Engineering: A Comprehensive Review. *Geotechnical and Geological Engineering*, 36(2), 705–722. <https://doi.org/10.1007/s10706-017-0356-z>
- Handbook, I., & Bogie, F. (2012). *Introduction Handbook on FIAT Bogie, Foreword. July*.
- Hanta, V., & Procházka, A. (2014). *Rational approximation of time delay. May*.
- Haq, I. U., Khan, Q., Khan, I., Akmeliawati, R., Nisar, K. S., & Khan, I. (2020). Maximum Power Extraction Strategy for Variable Speed Wind Turbine System via Neuro-Adaptive Generalized Global Sliding Mode Controller. *IEEE Access*, 8, 128536–128547. <https://doi.org/10.1109/ACCESS.2020.2966053>
- Harun, M. H., Mohd Zailimi, W., Abdullah, W., Jamaluddin, H., Rahman, R. A., & Hudha, K. (2014). Analysis of primary and secondary lateral suspension system of railway vehicle. *Journal of Mechanical Engineering*, 11(2), 19–40.
- He, H., Li, Y., Jiang, J. Z., Burrow, S., Neild, S., & Conn, A. (2023). Enhancing the trade-off between ride comfort and active actuation requirements via an inerter-based passive-active-combined automotive suspension. *Vehicle System Dynamics*. <https://doi.org/10.1080/00423114.2023.2184703>
- He, J., Liu, Z., & Zhang, C. (2020). Sliding mode control of lateral semi-active suspension of high-speed train. *Journal of Advanced Computational Intelligence and Intelligent Informatics*, 24(7), 925–933. <https://doi.org/10.20965/JACIII.2020.P0925>



## REFERENCES

- Howimanporn, S., Thanok, S., Chookaew, S., & Sootkaneung, W. (2017). Design and implementation of PSO based LQR control for inverted pendulum through PLC. *SII 2016 - 2016 IEEE/SICE International Symposium on System Integration*, 664–669. <https://doi.org/10.1109/SII.2016.7844075>
- Hrovat, D. (1990). Optimal active suspension structures for quarter-car vehicle models. *Automatica*, 26(5), 845–860. [https://doi.org/10.1016/0005-1098\(90\)90002-Y](https://doi.org/10.1016/0005-1098(90)90002-Y)
- Hrovat, D. (1993). Applications of optimal control to advanced automotive suspension design. *Journal of Dynamic Systems, Measurement and Control, Transactions of the ASME*, 115(2B), 328–342. <https://doi.org/10.1115/1.2899073>
- Huang, W., Ahmadian, M., Rahimi, A., & Steiginga, L. (2023). Dynamics performance of long combination vehicles with active control systems. *Vehicle System Dynamics*, 61(7), 1829–1878. <https://doi.org/10.1080/00423114.2023.2194545>
- Hurtado-Hurtado, G., Morales-Velazquez, L., Valtierra-Rodríguez, M., Otremba, F., & Jáuregui-Correa, J. C. (2022). Frequency by the Hunting Analysis Phenomenon of the Railway Track under Loads Caused by the Hunting Phenomenon. *Mathematics*, 10(13). <https://doi.org/10.3390/math10132286>
- Introduction, I. (2021). *Design And Analysis Of Lqr Controller Using Bees Colony And Particle Swarm Algorithm*. 8(5), 3242–3256.
- Indian railway technical bulletin, volume LXX , November 2013, 2557; 4:88–1002557;4:88–100.
- Iwnicki, S. (2006). Handbook of railway vehicle dynamics. In *Handbook of Railway Vehicle Dynamics*. <https://doi.org/10.1201/9781420004892>
- Jain, N., & Mathur, M. (2017). Technology : Transforming Railway Transportation. *AT Kearney*.
- Jain, S., & Hote, Y. V. (2020). Design of FOPID Controller Using BBBC via ZN Tuning Approach: Simulation and Experimental Validation. *IETE Journal of Research*, 0(0), 1–15. <https://doi.org/10.1080/03772063.2020.1756937>
- Jain, S., Hote, Y. V., & Saxena, S. (2022). Fractional Order PID Design Using Big Bang–Big Crunch Algorithm and Order Reduction: Application to Load Frequency Control. *Electric Power Components and Systems*, 49(6–7), 624–636. <https://doi.org/10.1080/15325008.2021.2011482>
- Jalili, M. M., & Salehi, H. (2011). Wheel/rail contact model for rail vehicle dynamics. *Comptes Rendus - Mécanique*, 339(11), 700–707. <https://doi.org/10.1016/j.crme.2011.07.006>
- Jawahar, P. M., Gupta, K. N., & Raghu, E. (1990). Mathematical modelling for lateral dynamic simulation of a railway vehicle with conventional and unconventional wheelset. *Mathematical and Computer Modelling*, 14(C), 989–994. [https://doi.org/10.1016/0895-7177\(90\)90326-I](https://doi.org/10.1016/0895-7177(90)90326-I)

## REFERENCES

- Jeniš, F., Kubík, M., Michálek, T., Strecker, Z., Žáček, J., & Mazurek, I. (2023). Effect of the Magnetorheological Damper Dynamic Behaviour on the Rail Vehicle Comfort: Hardware-in-the-Loop Simulation. *Actuators*, 12(2), 1–13. <https://doi.org/10.3390/act12020047>
- Jezequel, L., Roberti, V., Ouyahia, B., & Toutain, Y. (1992). Improvement of very high speed trains comfort with preview semi-active suspensions. *Vehicle System Dynamics*, 20(sup1), 299–313. <https://doi.org/10.1080/00423119208969405>
- Jiang, J. Z., Matamoros-Sanchez, A. Z., Goodall, R. M., & Smith, M. C. (2012). Passive suspensions incorporating inerters for railway vehicles. *Vehicle System Dynamics*, 50(SUPPL. 1), 263–276. <https://doi.org/10.1080/00423114.2012.665166>
- Jiang, J. Z., Matamoros-Sanchez, A. Z., Zolotas, A., Goodall, R. M., & Smith, M. C. (2015). Passive suspensions for ride quality improvement of two-axle railway vehicles. *Proceedings of the Institution of Mechanical Engineers, Part F: Journal of Rail and Rapid Transit*, 229(3), 315–329. <https://doi.org/10.1177/0954409713511592>
- Jiang, Y., Chen, B. K., & Thompson, C. (2019). A comparison study of ride comfort indices between Sperling's method and EN 12299. *International Journal of Rail Transportation*, 7(4), 279–296. <https://doi.org/10.1080/23248378.2019.1616329>
- Jin, T., Liu, Z., Sun, S., Ren, Z., Deng, L., Yang, B., Christie, M. D., & Li, W. (2020). Development and evaluation of a versatile semi-active suspension system for high-speed railway vehicles. *Mechanical Systems and Signal Processing*, 135, 106338. <https://doi.org/10.1016/j.ymssp.2019.106338>
- Jing, L., Wang, K., & Zhai, W. (2021). Impact vibration behavior of railway vehicles: a state-of-the-art overview. *Acta Mechanica Sinica/Lixue Xuebao*, 37(8), 1193–1221. <https://doi.org/10.1007/s10409-021-01140-9>
- Joseph, S. B and Dada, E. . (2018). Mml. *Proportional-Integral-Derivative (PID) Controller Tuning for an Inverted Pendulum Using Particle Swarm Optimisation (PSO) Algorithm*, 2(2), 72–78.
- Joseph, S. B., Dada, E. G., Abidemi, A., Oyewola, D. O., & Khammas, B. M. (2022). Metaheuristic algorithms for PID controller parameters tuning: review, approaches and open problems. *Heliyon*, 8(5), e09399. <https://doi.org/10.1016/j.heliyon.2022.e09399>
- Kalker, J. J. (1991). *Wheel-rail*. 144, 243–261.
- Kalker, J. J. (1973). *on the Rolling Contact of Two Elastic Bodies in the Presence of Dry Friction*. (AUGUST, 1973). [https://doi.org/10.1016/0043-1648\(68\)90178-6](https://doi.org/10.1016/0043-1648(68)90178-6)
- Kamada, T., Fujita, T., & Hatayama, T. (1997). *Active vibration control of frame structures with smart structures using piezoelectric actuators ( Vibration control by control of bending moments of columns )*. 448.
- Kamada, T., & Karaki, T. (2023). *Active vertical vibration suppression of high-speed*

## REFERENCES

- railway vehicles by controlling internal pressure of the air spring using  $\mu$ -synthesis control.* <https://doi.org/10.1080/00423114.2023.2250024>
- Kang, C., Yu, X., Wang, S. H., Guttery, D. S., Pandey, H. M., Tian, Y., & Zhang, Y. D. (2021). A Heuristic Neural Network Structure Relying on Fuzzy Logic for Images Scoring. *IEEE Transactions on Fuzzy Systems*, 29(1), 34–45. <https://doi.org/10.1109/TFUZZ.2020.2966163>
- Karkoub, M. A., & Zribi, M. (2006). Active/semi-active suspension control using magnetorheological actuators. *International Journal of Systems Science*, 37(1), 35–44. <https://doi.org/10.1080/00207720500436344>
- Kashani, R., & Kiriczi, S. (1992). Robust Stability Analysis of LQG-Controlled Active Suspension with Model Uncertainty Using Structured Singular Value,  $\mu$ , Method. *Vehicle System Dynamics*, 21(1), 361–384. <https://doi.org/10.1080/00423119208969016>
- Kaur, R., & Ohri, J. (2022). Novel Approach to Optimal Preview Control of DC Motor using Evolutionary Algorithms. *IETE Journal of Research*, 68(2), 883–901. <https://doi.org/10.1080/03772063.2019.1627914>
- Kim, D. H., & Park, J. (2005). Intelligent PID controller tuning of AVR system using GA and PSO. *Lecture Notes in Computer Science*, 3645(PART II), 366–375. [https://doi.org/10.1007/11538356\\_38](https://doi.org/10.1007/11538356_38)
- Kim, H. C., Shin, Y. J., You, W., Jung, K. C., Oh, J. S., & Choi, S. B. (2017). A ride quality evaluation of a semi-active railway vehicle suspension system with MR damper: Railway field tests. *Proceedings of the Institution of Mechanical Engineers, Part F: Journal of Rail and Rapid Transit*, 231(3), 306–316. <https://doi.org/10.1177/0954409716629706>
- Kim, Y., Kwon, H., Kim, S., Park, C., & Park, T. (2015). Correlation of ride comfort evaluation methods for. *Journal of Rail and Rapid Transit*, 217, 73–88.
- Kim, Y. S., Lim, T. K., Park, S. H., & Jeong, R. G. (2008). Dynamic model for ride comfort evaluations of the rubber-tired light rail vehicle. *Vehicle System Dynamics*, 46(11), 1061–1082. <https://doi.org/10.1080/00423110701759637>
- Kouroussis, G., Connolly, D. P., & Verlinden, O. (2014). Railway-induced ground vibrations – a review of vehicle effects. *International Journal of Rail Transportation*, 2(2), 69–110. <https://doi.org/10.1080/23248378.2014.897791>
- Kumar, A., & Suhag, S. (2017). Multiverse optimized fuzzy-PID controller with a derivative filter for load frequency control of multisource hydrothermal power system. *Turkish Journal of Electrical Engineering and Computer Sciences*, 25(5), 4187–4199. <https://doi.org/10.3906/elk-1612-176>
- Kumar, H., Kumar, R., Yadav, J., Rani, A., & Singh, V. (2017). Genetic Algorithm based PID controller for blood pressure and Cardiac Output regulation. *1st IEEE International Conference on Power Electronics, Intelligent Control and Energy Systems, ICPEICES 2016*, 1–6. <https://doi.org/10.1109/ICPEICES.2016.7853680>

## REFERENCES

- Kumar, M., & Hote, Y. V. (2022). Comments and further results on “Optimal design of non-fragile PID controller.” *Asian Journal of Control*, 24(6), 3601–3602. <https://doi.org/10.1002/asjc.2694>
- Kumar, S., Shukla, A., Tiwari, K., & Mohan, H. (n.d.). *An Efficient Deep Convolutional Neural Network Model For Yoga Pose Recognition Using Single Images*.
- Kwok, N. M., Ha, Q. P., Nguyen, T. H., Li, J., & Samali, B. (2006). A novel hysteretic model for magnetorheological fluid dampers and parameter identification using particle swarm optimization. *Sensors and Actuators, A: Physical*, 132(2), 441–451. <https://doi.org/10.1016/j.sna.2006.03.015>
- Laiton-Bonadiez, C., Branch-Bedoya, J. W., Zapata-Cortes, J., Paipa-Sanabria, E., & Arango-Serna, M. (2022). Industry 4.0 Technologies Applied to the Rail Transportation Industry: A Systematic Review. *Sensors*, 22(7). <https://doi.org/10.3390/s22072491>
- Lanusse, P., Sabatier, J., & Oustaloup, A. (2015). Fractional order pid and first generation crone control system design. In *Intelligent Systems, Control and Automation: Science and Engineering* (Vol. 77). [https://doi.org/10.1007/978-94-017-9807-5\\_2](https://doi.org/10.1007/978-94-017-9807-5_2)
- Lauriks, G., Evans, J., Forstberg, J., Balli, M., & Barron De Angoit, I. (2003). *Investigation of ride comfort and comfort disturbance on transition and circular curves*. 130.
- Leblebici, A. S., & Türkay, S. (2016). Track Modelling and Control of a Railway Vehicle. *IFAC-PapersOnLine*, 49(21), 274–281. <https://doi.org/10.1016/j.ifacol.2016.10.566>
- Lei, S., Ge, Y., Li, Q., & Thompson, D. J. (2023). Frequency-domain method for non-stationary stochastic vibrations of train-bridge coupled system with time-varying characteristics. *Mechanical Systems and Signal Processing*, 183(January 2022), 1–18. <https://doi.org/10.1016/j.ymssp.2022.109637>
- Lei, X., & Noda, N. A. (2002). Analyses of dynamic response of vehicle and track coupling system with random irregularity of track vertical profile. *Journal of Sound and Vibration*, 258(1), 147–165. <https://doi.org/10.1006/jsvi.2002.5107>
- Lei, Y., & Wu, D. T. (2011). A new decentralized control approach for the benchmark problem. *Procedia Engineering*, 14, 1229–1236. <https://doi.org/10.1016/j.proeng.2011.07.154>
- Lengare, M. J., Chile, R. H., & Waghmare, L. M. (2012). Design of decentralized controllers for MIMO processes. *Computers and Electrical Engineering*, 38(1), 140–147. <https://doi.org/10.1016/j.compeleceng.2011.11.027>
- Lewis, R., & Olofsson, U. (2006). Chapter 5: Tribology of the Wheel–Rail Contact. *Handbook of Railway Vehicle Dynamics*, 131.
- Li, H., Liu, H., Hand, S., & Hilton, C. (2013). *Design of robust  $H_\infty$  controller for a half-vehicle active suspension system with input delay*. 7721. <https://doi.org/10.1080/00207721.2011.617895>

## REFERENCES

- Li, H., Liu, H., Hilton, C., & Hand, S. (2013). Non-fragile  $H_{\infty}$  control for half-vehicle active suspension systems with actuator uncertainties. *JVC/Journal of Vibration and Control*, 19(4), 560–575. <https://doi.org/10.1177/1077546311434972>
- Li, L., Sun, L., Guo, J., Qi, J., Xu, B., & Li, S. (2017). Modified Discrete Grey Wolf Optimizer Algorithm for Multilevel Image Thresholding. *Computational Intelligence and Neuroscience*, 2017. <https://doi.org/10.1155/2017/3295769>
- Li, P., Goodall, R., Weston, P., Seng Ling, C., Goodman, C., & Roberts, C. (2007). Estimation of railway vehicle suspension parameters for condition monitoring. *Control Engineering Practice*, 15(1), 43–55. <https://doi.org/10.1016/j.conengprac.2006.02.021>
- Li, S. X., & Wang, J. S. (2015). Dynamic modeling of steam condenser and design of pi controller based on grey Wolf optimizer. *Mathematical Problems in Engineering*, 2015. <https://doi.org/10.1155/2015/120975>
- Likaj, R., Shala, A., & Bajrami, X. (2017). Optimal Control of quarter car vehicle suspensions. *International Scientific Journal Trans & MotAuto World*, 2(5), 184–186. <https://doi.org/http://www.stumejournals.com/tm/2017/5-2017.pdf>
- Lin, F., Muthuraman, K., & Lawley, M. (2010). An optimal control theory approach to non-pharmaceutical interventions. *BMC Infectious Diseases*, 10. <https://doi.org/10.1186/1471-2334-10-32>
- Lin, X., & Chen, S. (2016). Optimal inverse magnetorheological damper modeling using shuffled frog-leaping algorithm-based adaptive neuro-fuzzy inference system approach. *Advances in Mechanical Engineering*, 8(8), 1–18. <https://doi.org/10.1177/1687814016662770>
- Liu, B., & Bruni, S. (2022). Comparison of wheel–rail contact models in the context of multibody system simulation: Hertzian versus non-Hertzian. *Vehicle System Dynamics*, 60(3), 1076–1096. <https://doi.org/10.1080/00423114.2020.1847297>
- Liu, B., Vollebregt, E., & Bruni, S. (2023). Review of conformal wheel/rail contact modelling approaches: towards the application in rail vehicle dynamics simulation. *Vehicle System Dynamics*. <https://doi.org/10.1080/00423114.2023.2228438>
- Liu, C., Thompson, D., Griffin, M. J., & Entezami, M. (2020). Effect of train speed and track geometry on the ride comfort in high-speed railways based on ISO 2631-1. *Proceedings of the Institution of Mechanical Engineers, Part F: Journal of Rail and Rapid Transit*, 234(7), 765–778. <https://doi.org/10.1177/0954409719868050>
- Liu, S., Zheng, T., Zhao, D., Hao, R., & Yang, M. (2022). Strongly perturbed sliding mode adaptive control of vehicle active suspension system considering actuator nonlinearity. *Vehicle System Dynamics*, 60(2), 597–616. <https://doi.org/10.1080/00423114.2020.1840598>
- Livesey, D. A. (1986). Optimal control theory and grants in aid. *Environment & Planning C: Government & Policy*, 4(2), 121–129. <https://doi.org/10.1068/c040121>

## REFERENCES

- Lu, H., Rui, X., Ding, Y., Chang, Y., Chen, Y., Ding, J., & Zhang, X. (2022). A hybrid numerical method for vibration analysis of linear multibody systems with flexible components. *Applied Mathematical Modelling*, 101, 748–771. <https://doi.org/10.1016/j.apm.2021.09.015>
- Luo, Y., Liu, H., Jia, L., & Cai, W. (2011). A practical guideline to control structure selection for MIMO processes. *IEEE International Conference on Automation and Logistics, ICAL, August*, 405–410. <https://doi.org/10.1109/ICAL.2011.6024752>
- Maghfiroh, H., Nizam, M., Anwar, M., & Ma'Arif, A. (2022). Improved LQR Control Using PSO Optimization and Kalman Filter Estimator. *IEEE Access*, 10, 18330–18337. <https://doi.org/10.1109/ACCESS.2022.3149951>
- Mathur, S., & Sharma, B. B. (2017). EKF and UKF based synchronization of hyperchaotic systems. *International Conference on Automatic Control and Dynamic Optimization Techniques, ICACDOT 2016*, 743–749. <https://doi.org/10.1109/ICACDOT.2016.7877685>
- Mech, J. (2018). “ To develop safe , modern and cost effective Railway Technology complying with Statutory and Regulatory requirements , through excellence in Research , Designs and Standards and Continual improvements in Quality Management System to cater to growing dema. 474005.
- Metin, M., & Guclu, R. (2011). Active vibration control with comparative algorithms of half rail vehicle model under various track irregularities. *JVC/Journal of Vibration and Control*, 17(10), 1525–1539. <https://doi.org/10.1177/1077546310381099>
- Metin, M., & Guclu, R. (2014a). Rail vehicle vibrations control using parameters adaptive PID controller. *Mathematical Problems in Engineering*, 2014. <https://doi.org/10.1155/2014/728946>
- Metin, M., & Guclu, R. (2014b). Rail vehicle vibrations control using parameters adaptive PID controller. *Mathematical Problems in Engineering*, 2014(October 2010). <https://doi.org/10.1155/2014/728946>
- Meymand, S. Z., Keylin, A., & Ahmadian, M. (2016a). A survey of wheel-rail contact models for rail vehicles. *Vehicle System Dynamics*, 54(3), 386–428. <https://doi.org/10.1080/00423114.2015.1137956>
- Meymand, S. Z., Keylin, A., & Ahmadian, M. (2016b). A survey of wheel-rail contact models for rail vehicles. *Vehicle System Dynamics*, 54(3), 386–428. <https://doi.org/10.1080/00423114.2015.1137956>
- Mirjalili, S. (2019). Ant colony optimisation. *Studies in Computational Intelligence*, 780(November), 33–42. [https://doi.org/10.1007/978-3-319-93025-1\\_3](https://doi.org/10.1007/978-3-319-93025-1_3)
- Mirjalili, S., Mirjalili, S. M., & Lewis, A. (2014). Grey Wolf Optimizer. *Advances in Engineering Software*, 69, 46–61. <https://doi.org/10.1016/j.advengsoft.2013.12.007>
- Mitra, A. C., Patil, M. V., & Banerjee, N. (2015). Optimization of Vehicle Suspension Parameters for Ride Comfort Based on RSM. *Journal of The Institution of Engineers*

## REFERENCES

- (India): *Series C*, 96(2), 165–173. <https://doi.org/10.1007/s40032-014-0156-7>
- Mitra, S., Nguyen, L. N., Akter, M., & Park, G. (2019). Impact of ROS Generated by Chemical , Physical ,. *Cancers*, 11(7), 1–31.
- Mobayen, S., Rabiei, A., Moradi, M., & Mohammady, B. (2011). Linear quadratic optimal control system design using particle swarm optimization algorithm. *International Journal of Physical Sciences*, 6(30), 6958–6966. <https://doi.org/10.5897/IJPS11.726>
- Mohammed, N. F., Song, E., Ma, X., & Hayat, Q. (2014). Tuning of PID controller of synchronous generators using genetic algorithm. *2014 IEEE International Conference on Mechatronics and Automation, IEEE ICMA 2014*, 4, 1544–1548. <https://doi.org/10.1109/ICMA.2014.6885929>
- Mohan, V., Chhabra, H., Rani, A., & Singh, V. (2019). An expert 2DOF fractional order fuzzy PID controller for nonlinear systems. *Neural Computing and Applications*, 31(8), 4253–4270. <https://doi.org/10.1007/s00521-017-3330-z>
- Mohan, V., Rani, A., & Singh, V. (2017). Robust adaptive fuzzy controller applied to double inverted pendulum. *Journal of Intelligent and Fuzzy Systems*, 32(5), 3669–3687. <https://doi.org/10.3233/JIFS-169301>
- Molatefi, H., Hecht, M., & Bokaeian, V. (2017). Stability and safety analysis of an active steering bogie according to EN 14363 standard. *Journal of the Brazilian Society of Mechanical Sciences and Engineering*, 39(8), 2945–2956. <https://doi.org/10.1007/s40430-017-0758-0>
- Mosaad, M. I., Osama abed el-Raouf, M., Al-Ahmar, M. A., & Banakher, F. A. (2019). Maximum power point tracking of PV system based cuckoo search algorithm; review and comparison. *Energy Procedia*, 162, 117–126. <https://doi.org/10.1016/j.egypro.2019.04.013>
- Mršnik, M., Slavič, J., & Boltežar, M. (2013). Frequency-domain methods for a vibration-fatigue-life estimation - Application to real data. *International Journal of Fatigue*, 47, 8–17. <https://doi.org/10.1016/j.ijfatigue.2012.07.005>
- Muñoz, S., Aceituno, J. F., Urda, P., & Escalona, J. L. (2019). Multibody model of railway vehicles with weakly coupled vertical and lateral dynamics. *Mechanical Systems and Signal Processing*, 115, 570–592. <https://doi.org/10.1016/j.ymssp.2018.06.019>
- Nagarkar, M. P., & Vikhe Patil, G. J. (2012). Performance analysis of quarter car active suspension system: LQR and  $H_{\infty}$  control strategies. *2012 3rd International Conference on Computing, Communication and Networking Technologies, ICCCNT 2012*, 1–6. <https://doi.org/10.1109/ICCCNT.2012.6396067>
- Nagarkar, M. P., & VikhePatil, G. J. (2016). Optimization of the linear quadratic regulator (LQR) control quarter car suspension system using genetic algorithm. *Ingenieria e Investigacion*, 36(1), 23–30. <https://doi.org/10.15446/ing.investig.v36n1.49253>

## REFERENCES

- Nayak, B. P., Nayak, P. C., & Prusty, R. C. (2020). Application of FPA based on PID controller for LFC of two-Area multi-source hydrothermal Power system. *Proceedings of the 2020 International Conference on Renewable Energy Integration into Smart Grids: A Multidisciplinary Approach to Technology Modelling and Simulation, ICREISG*, 2020, 228–233. <https://doi.org/10.1109/ICREISG49226.2020.9174197>
- Ngigi, R. W., Pislaru, C., Ball, A., & Gu, F. (2012). Modern techniques for condition monitoring of railway vehicle dynamics. *Journal of Physics: Conference Series*, 364(1). <https://doi.org/10.1088/1742-6596/364/1/012016>
- Nisar, K. S., Baleanu, D., & Qurashi, M. M. Al. (2016). Fractional calculus and application of generalized Struve function. *SpringerPlus*, 5(1). <https://doi.org/10.1186/s40064-016-2560-3>
- Nitish, & Kumar Singh, A. (2023). Active control of railway vehicle suspension using PID controller with pole placement technique. *Materials Today: Proceedings*, 80, 278–284. <https://doi.org/10.1016/j.matpr.2023.01.188>
- Nor, A. S. M., Selamat, H., & Alimin, A. J. (2011). Optimal controller design for a railway vehicle suspension system using particle swarm optimization. *Jurnal Teknologi*, 54, 71–84. <https://doi.org/10.11113/jt.v54.92>
- Nyarko, E. K., Cupec, R., & Filko, D. (2014). A Comparison of several heuristic algorithms for solving high dimensional optimization Problems. *International Journal of Electrical and Computer Engineering Systems.*, 5(1), 1–8.
- Omar, M., & Abdelghaffar, W. (2018). Parametric numerical study of electrohydraulic active suspension performance against passive suspension. *Alexandria Engineering Journal*, 57(4), 3609–3614. <https://doi.org/10.1016/j.aej.2018.05.007>
- Organisation, S., Engineering, M., & No, R. P.122. '.
- Orvnäs, A., Stichel, S., & Persson, R. (2011). *Active lateral secondary suspension with  $H_{\infty}$  control to improve ride comfort: simulations on a full-scale model*. 3114. <https://doi.org/10.1080/00423114.2010.527011>
- Pacchioni, A., Goodall, R. M., & Bruni, S. (2010). Active suspension for a two-axle railway vehicle. *Vehicle System Dynamics*, 48(SUPPL. 1), 105–120. <https://doi.org/10.1080/00423111003668252>
- Pandey, H. M. (2017). Genetic Algorithm and Particle Swarm Optimization: Analysis and Remedial Suggestions. *Lecture Notes in Networks and Systems*, 5, 437–441. [https://doi.org/10.1007/978-981-10-3226-4\\_44](https://doi.org/10.1007/978-981-10-3226-4_44)
- Pang, H., Chen, Y., Chen, J. N., & Liu, X. (2017). Design of LQG Controller for Active Suspension without Considering Road Input Signals. *Shock and Vibration*, 2017. <https://doi.org/10.1155/2017/6573567>
- Park, J. H., & Kim, Y. S. (1999). *An  $H_{\infty}$  Controller for Active Suspensions and its Robustness Based on a Full-Car Model*. 8178–8183.



## REFERENCES

- Patel, P., Nandi, A., Verma, S. K., Kaushik, N., Suar, M., Choi, E. H., & Kaushik, N. K. (2023). Zebrafish-based platform for emerging bio-contaminants and virus inactivation research. *Science of the Total Environment*, 872(January), 162197. <https://doi.org/10.1016/j.scitotenv.2023.162197>
- Peram, M., Mishra, S., Vemulapaty, M., Verma, B., & Padhy, P. K. (2018). Optimal PI-PD and I-PD Controller Design Using Cuckoo Search Algorithm. *2018 5th International Conference on Signal Processing and Integrated Networks, SPIN 2018*, 643–646. <https://doi.org/10.1109/SPIN.2018.8474214>
- Piotrowski, J., & Chollet, H. (2007). *Wheel – rail contact models for vehicle system dynamics including multi-point contact*. 3114. <https://doi.org/10.1080/00423110500141144>
- Piotrowski, J., & Kik, W. (2008). A simplified model of wheel/rail contact mechanics for non-Hertzian problems and its application in rail vehicle dynamic simulations. *Vehicle System Dynamics*, 46(1–2), 27–48. <https://doi.org/10.1080/00423110701586444>
- Rabinow, J. (1948). The Magnetic Fluid Clutch. *Transactions of the American Institute of Electrical Engineers*, 67, 1308–1315. <https://doi.org/10.1109/T-AIEE.1948.5059821>
- Rajakumar, R., Amudhavel, J., Dhavachelvan, P., & Vengattaraman, T. (2017). GWO-LPWSN: Grey Wolf Optimization Algorithm for Node Localization Problem in Wireless Sensor Networks. *Journal of Computer Networks and Communications*, 2017. <https://doi.org/10.1155/2017/7348141>
- Rajesh, R. J., & Ananda, C. M. (2015). PSO tuned PID controller for controlling camera position in UAV using 2-axis gimbal. *Proceedings of the 2015 IEEE International Conference on Power and Advanced Control Engineering, ICPACE 2015*, 128–133. <https://doi.org/10.1109/ICPACE.2015.7274930>
- Ranjan, R., Kumar, V., & Ganapathy, R. (2018). Adaptive predator – prey optimization for tuning of infinite horizon LQR applied to vehicle suspension system. *Applied Soft Computing Journal*, 72, 518–526. <https://doi.org/10.1016/j.asoc.2018.06.044>
- Rawool, S. M., & Mohan, V. M. (2022). *Design of Active Suspension System for Quarter-Car Model using Linear Quadratic Regulator (LQR)*. 11(04), 37–43. [www.ijert.org](http://www.ijert.org)
- Ray, L. R. (2016). *Robust Linear-Optimal Control Laws for Active Suspension Systems*. 114(December 1992).
- Redfield, R. C. (1988). *Performance Sensitivity of an Actively Damped*.
- Ren, Z., Iwnicki, S. D., & Xie, G. (2011). A new method for determining wheel-rail multi-point contact. *Vehicle System Dynamics*, 49(10), 1533–1551. <https://doi.org/10.1080/00423114.2010.539237>
- Ren, Z., Sun, S., & Zhai, W. (2005). Study on lateral dynamic characteristics of vehicle/turnout system. *Vehicle System Dynamics*, 43(4), 285–303.

## REFERENCES

- <https://doi.org/10.1080/00423110500083262>
- Ripamonti, F., & Chiarabaglio, A. (2019). A smart solution for improving ride comfort in high-speed railway vehicles. *JVC/Journal of Vibration and Control*, 25(13), 1958–1973. <https://doi.org/10.1177/1077546319843377>
- Robandi, I., Nishimori, K., Nishimura, R., & Ishihara, N. (2001). Optimal feedback control design using genetic algorithm in multimachine power system. *International Journal of Electrical Power and Energy Systems*, 23(4), 263–271. [https://doi.org/10.1016/S0142-0615\(00\)00062-4](https://doi.org/10.1016/S0142-0615(00)00062-4)
- Ronasi, H., & Nielsen, J. C. O. (2013). Inverse identification of wheel-rail contact forces based on observation of wheel disc strains: An evaluation of three numerical algorithms. *Vehicle System Dynamics*, 51(1), 74–90. <https://doi.org/10.1080/00423114.2012.713498>
- Rovira, A., Roda, A., Marshall, M. B., Brunskill, H., & Lewis, R. (2011). Experimental and numerical modelling of wheel-rail contact and wear. *Wear*, 271(5–6), 911–924. <https://doi.org/10.1016/j.wear.2011.03.024>
- Sakalo, L., Sakalo, L., Rodikov, L., & Yazykov, L. (2016). Fast algorithm for wheel and rail conformal contact modeling. *Proceedings of 2015 International Conference on Mechanical Engineering, Automation and Control Systems, MEACS 2015*, 2, 1–6. <https://doi.org/10.1109/MEACS.2015.7414915>
- Sammier, D., Sename, O., Dugard, L., Sammier, D., Sename, O., & Dugard, L. (2000). *H<sub>∞</sub> CONTROL OF ACTIVE VEHICLE SUSPENSIONS*. 1–6.
- Samuel, O. D., Kaveh, M., Oyejide, O. J., Elumalai, P. V., Verma, T. N., Nisar, K. S., Saleel, C. A., Afzal, A., Fayomi, O. S. I., Owamah, H. I., Sarikoç, S., & Enweremadu, C. C. (2022). Performance comparison of empirical model and Particle Swarm Optimization & its boiling point prediction models for waste sunflower oil biodiesel. *Case Studies in Thermal Engineering*, 33(March), 101947. <https://doi.org/10.1016/j.csite.2022.101947>
- Satapathy, S. C., Biswal, B. N., Udgata, S. K., & Mandal, J. K. (2014). Proceedings of the 3rd International Conference on Frontiers of Intelligent Computing: Theory and Applications (FICTA) 2014. *Advances in Intelligent Systems and Computing*, 327, 441–442. <https://doi.org/10.1007/978-3-319-11933-5>
- Sathans, & Swarup, A. (2011). Intelligent load frequency control of two-area interconnected power system and comparative analysis. *Proceedings - 2011 International Conference on Communication Systems and Network Technologies, CSNT 2011*, 360–365. <https://doi.org/10.1109/CSNT.2011.81>
- Satyanarayana, V. S. V., Gopala Rao, L. V. V., Sateesh, B., & Mohan Rao, N. (2021). Computation of passive suspension parameters for improvement of vehicle ride quality based on stochastic optimal controller with a look-ahead preview. *Noise and Vibration Worldwide*, 52(9), 233–242. <https://doi.org/10.1177/09574565211000390>
- Saxena, S., & Hote, Y. V. (2016). Decentralized PID load frequency control for perturbed

## REFERENCES

- multi-area power systems. *International Journal of Electrical Power and Energy Systems*, 81, 405–415. <https://doi.org/10.1016/j.ijepes.2016.02.041>
- Schurter, K. C., & Roschke, P. N. (2000). Fuzzy modeling of a magnetorheological damper using ANFIS. *IEEE International Conference on Fuzzy Systems*, 1, 122–127. <https://doi.org/10.1109/fuzzy.2000.838645>
- Sedighi, H. M., & Shirazi, K. H. (2012). Bifurcation analysis in hunting dynamical behavior in a railway bogie: Using novel exact equivalent functions for discontinuous nonlinearities. *Scientia Iranica*, 19(6), 1493–1501. <https://doi.org/10.1016/j.scient.2012.10.028>
- Sezer, S., & Atalay, A. E. (2011). Dynamic modeling and fuzzy logic control of vibrations of a railway vehicle for different track irregularities. *Simulation Modelling Practice and Theory*, 19(9), 1873–1894. <https://doi.org/10.1016/j.simpat.2011.04.009>
- Sh. Sichani, M., Enblom, R., & Berg, M. (2016). A fast wheel–rail contact model for application to damage analysis in vehicle dynamics simulation. *Wear*, 366–367, 123–130. <https://doi.org/10.1016/j.wear.2016.06.015>
- Shabana, A. A., Zaazaa, K. E., Escalona, J. L., & Sany, J. R. (2004). Development of elastic force model for wheel/rail contact problems. *Journal of Sound and Vibration*, 269(1–2), 295–325. [https://doi.org/10.1016/S0022-460X\(03\)00074-9](https://doi.org/10.1016/S0022-460X(03)00074-9)
- Sharma, P., Gupta, A., Aggarwal, A., Gupta, D., Khanna, A., Hassanien, A. E., & de Albuquerque, V. H. C. (2020). The health of things for classification of protein structure using improved grey wolf optimization. *Journal of Supercomputing*, 76(2), 1226–1241. <https://doi.org/10.1007/s11227-018-2639-4>
- Sharma, P., Sundaram, S., Sharma, M., Sharma, A., & Gupta, D. (2019). Diagnosis of Parkinson's disease using modified grey wolf optimization. *Cognitive Systems Research*, 54, 100–115. <https://doi.org/10.1016/j.cogsys.2018.12.002>
- Sharma, S. K., & Kumar, A. (2016). Dynamics Analysis of Wheel Rail Contact Using FEA. *Procedia Engineering*, 144, 1119–1128. <https://doi.org/10.1016/j.proeng.2016.05.076>
- Sharma, V., Sharma, B. B., & Nath, R. (2017). Digital image chaotic encryption and transmission using UIO. *2017 International Conference on Computer, Communications and Electronics, COMPTHELIX 2017*, 32–37. <https://doi.org/10.1109/COMPTHELIX.2017.8003933>
- Sharp, R. S., & Hassan, S. A. (1986). An Evaluation of Passive Automotive Suspension Systems with Variable Stiffness and Damping Parameters. *Vehicle System Dynamics*, 15(6), 335–350. <https://doi.org/10.1080/00423118608968859>
- Shen, Y., Jia, M., Yang, X., Liu, Y., & Chen, L. (2023). Vibration suppression using a mechatronic PDD-ISD-combined vehicle suspension system. *International Journal of Mechanical Sciences*, 250(February), 108277. <https://doi.org/10.1016/j.ijmecsci.2023.108277>

## REFERENCES

- Shie, F. S., Chen, M. Y., & Liu, Y. S. (2012). Prediction of corporate financial distress: An application of the America banking industry. *Neural Computing and Applications*, 21(7), 1687–1696. <https://doi.org/10.1007/s00521-011-0765-5>
- Shieh, N. C., Lin, C. L., Lin, Y. C., & Liang, K. Z. (2005). Optimal design for passive suspension of a light rail vehicle using constrained multiobjective evolutionary search. *Journal of Sound and Vibration*, 285(1–2), 407–424. <https://doi.org/10.1016/j.jsv.2004.08.014>
- Shim, J., Kim, G., Cho, B., & Koo, J. (2021). Application of vibration signal processing methods to detect and diagnose wheel flats in railway vehicles. *Applied Sciences (Switzerland)*, 11(5), 1–18. <https://doi.org/10.3390/app11052151>
- Shukla, A., Pandey, H. M., & Mehrotra, D. (2015). Comparative review of selection techniques in genetic algorithm. *2015 1st International Conference on Futuristic Trends in Computational Analysis and Knowledge Management, ABLAZE 2015*, 515–519. <https://doi.org/10.1109/ABLAZE.2015.7154916>
- Sichani, M. S. (2016). *On efficient modelling of wheel-rail contact in vehicle dynamic simulation*. <https://www.diva-portal.org/smash/get/diva2:899731/FULLTEXT01.pdf>
- Sikander, A., Verma, P., Patel, N., & Nair, N. K. C. (2018). Design of controller using reduced order modeling for LED driver circuit. *2017 IEEE Innovative Smart Grid Technologies - Asia: Smart Grid for Smart Community, ISGT-Asia 2017*, 1–5. <https://doi.org/10.1109/ISGT-Asia.2017.8378455>
- Sims, N. D., & Stanway, R. (2003). Semi-active vehicle suspension using smart fluid dampers: A modelling and control study. *International Journal of Vehicle Design*, 33(1–3), 76–102. <https://doi.org/10.1504/ijvd.2003.003568>
- Singh, A., & Sathans. (2017). ANFIS based control strategy for frequency regulation in AC microgrid. *Proceedings on 5th International Conference on Eco-Friendly Computing and Communication Systems, ICECCS 2016, Mc*, 38–42. <https://doi.org/10.1109/Eco-friendly.2016.7893238>
- Singh, H., Srivastava, H. M., Hammouch, Z., & Sooppy Nisar, K. (2021). Numerical simulation and stability analysis for the fractional-order dynamics of COVID-19. *Results in Physics*, 20, 103722. <https://doi.org/10.1016/j.rinp.2020.103722>
- Singh, N., & Bhangal, K. (2017). Robust Control of Double Inverted Pendulum System. *Journal of Automation and Control Engineering*, 5(1), 14–20. <https://doi.org/10.18178/joace.5.1.14-20>
- Singh, S. (2021). *Introduction to Optimal Control ORF523 Convex And Conic Optimization*.
- Singh, S. D., Mathur, R., & Srivastava, R. K. (2017). Dynamic Response of Linke Hofmann Busch (LHB) Rail Coach Considering Suspended Equipments. *Indian Journal of Science and Technology*, 10(38), 1–20. <https://doi.org/10.17485/ijst/2017/v10i38/112223>

## REFERENCES

- Singh, S., & Kumar, A. (2022). Modelling and Analysis of a Passenger Train for Enhancing the Ride Performance Using MR-Based Semi-active Suspension. *Journal of Vibration Engineering and Technologies*, 10(5), 1737–1751. <https://doi.org/10.1007/s42417-022-00479-y>
- Singh, S., Tayal, V. K., Singh, H. P., & Yadav, V. K. (2022). Optimal Design of Fractional Order PID Controllers for Solid Oxide Fuel Cell System Employing PSO Algorithm. *AIUB Journal of Science and Engineering*, 21(1), 7–15. <https://doi.org/10.53799/ajse.v21i1.225>
- Singh, S., Tayal, V. K., Singh, H. P., & Yadav, V. K. (2023). Dynamic performance improvement of proton exchange membrane fuel cell system by robust loop shaping and artificial intelligence optimized fractional order PI controllers. *Energy Sources, Part A: Recovery, Utilization and Environmental Effects*, 45(3), 9308–9324. <https://doi.org/10.1080/15567036.2023.2236081>
- Slowik, A. (2011). Particle Swarm Optimization. *The Industrial Electronics Handbook - Five Volume Set*, 1942–1948. [https://doi.org/10.1007/978-3-319-46173-1\\_2](https://doi.org/10.1007/978-3-319-46173-1_2)
- Smith, R. A. (2001). Railway Technology—The Last 50 Years and Future Prospects. *Japan Railway & Transport Review*, 27(june 2001), 16–24.
- Soni, R., & Sathans. (2018). Optimal control of a ball and beam system through LQR and LQG. *Proceedings of the 2nd International Conference on Inventive Systems and Control, ICISC 2018, Icisc*, 179–184. <https://doi.org/10.1109/ICISC.2018.8399060>
- Sonoda, T., & Nakata, M. (2022). Multiple Classifiers-Assisted Evolutionary Algorithm Based on Decomposition for High-Dimensional Multiobjective Problems. *IEEE Transactions on Evolutionary Computation*, 26(6), 1581–1595. <https://doi.org/10.1109/TEVC.2022.3159000>
- Spencer, B. F., Dyke, S. J., Sain, M. K., & Carlson, J. D. (1997). Phenomenological Model for Magnetorheological Dampers. *Journal of Engineering Mechanics*, 123(3), 230–238. [https://doi.org/10.1061/\(asce\)0733-9399\(1997\)123:3\(230\)](https://doi.org/10.1061/(asce)0733-9399(1997)123:3(230))
- Spiryagin, M., Shrestha, S., Persson, I., Wu, Q., Arango, E. B., & Cole, C. (2022). Adaptive simulation and integration method for wheel-rail contact problems in locomotive traction studies. *Vehicle System Dynamics*, 60(12), 4206–4225. <https://doi.org/10.1080/00423114.2021.2000624>
- Spring, L. M., Marshall, M. R., & Warner, E. T. (2011). *K. L. Johnson - Contact Mechanics-Cambridge University Press (1985)*. 123(3), 401–409.
- Srihari, P., & Ramji, K. (2018). Eigenvalue Analysis of Railway Coach Using Finite Element Method. *International Journal For Technological Research In Engineering*, 5(9), 3728–3734.
- Srivastava, J. P., Sarkar, P. K., Kiran, M. R., & Ranjan, V. (2019). A numerical study on effects of friction-induced thermal load for rail under varied wheel slip conditions. *Simulation*, 95(4), 351–362. <https://doi.org/10.1177/0037549718782629>

## REFERENCES

- Srivastava, J. P., Sarkar, P. K., Meesala, V. R. K., & Ranjan, V. (2017). Rolling contact fatigue life of rail for different slip conditions. *Latin American Journal of Solids and Structures*, 14(12), 2243–2264. <https://doi.org/10.1590/1679-78254161>
- Srivastava, J. P., Sarkar, P. K., & Ranjan, V. (2013). An approximate analysis for hertzian elliptical wheel-rail contact problem. *1st International and 16th National Conference on Machines and Mechanisms, INaCoMM 2013*, 249–253.
- Srivastava, J. P., Sarkar, P. K., & Ranjan, V. (2014). Contact Stress Analysis in Wheel–Rail by Hertzian Method and Finite Element Method. *Journal of The Institution of Engineers (India): Series C*, 95(4), 319–325. <https://doi.org/10.1007/s40032-014-0145-x>
- Srivastava, J. P., Sarkar, P. K., & Ranjan, V. (2015). Analytical modeling of rail track system. *Proceedings of India International Science Festival – Young Scientists’ Meet, December*, 1–6.
- Standard, I. (2009). *Railway applications - Ride comfort for passengers - Measurement and evaluation*.
- Stanway, R., Sproston, J. L., & Stevens, N. G. (1987). Non-linear modelling of an electro-rheological vibration damper. *Journal of Electrostatics*, 20(2), 167–184. [https://doi.org/10.1016/0304-3886\(87\)90056-8](https://doi.org/10.1016/0304-3886(87)90056-8)
- Steenbergen, M. (2006). Modelling of wheels and rail discontinuities in dynamic wheel-rail contact analysis. *Vehicle System Dynamics*, 44(10), 763–787. <https://doi.org/10.1080/00423110600648535>
- Stribersky, A., Kienberger, A., Wagner, G., & Müller, H. (1998). Design and evaluation of a semi-active damping system for rail vehicles. *Vehicle System Dynamics*, 29(SUPPL.), 669–681. <https://doi.org/10.1080/00423119808969594>
- SUGAHARA, Y., TAKIGAMI, T., KAZATO, A., KOGANEI, R., & SAMPEI, M. (2008). Suppression of Vertical Vibration in Railway Vehicles by Damping Force Control of Primary Suspension Using an LQG Controller. *Journal of System Design and Dynamics*, 2(1), 251–262. <https://doi.org/10.1299/jsdd.2.251>
- Sugiyama, H., & Suda, Y. (2009). On the contact search algorithms for wheel/rail contact problems. *Journal of Computational and Nonlinear Dynamics*, 4(4), 1–7. <https://doi.org/10.1115/1.3187211>
- Sule, A. H., Mokhtar, A. S., Jamian, J. J. Bin, Khidrani, A., & Larik, R. M. (2020). Optimal tuning of proportional integral controller for fixed-speed wind turbine using grey Wolf optimizer. *International Journal of Electrical and Computer Engineering*, 10(5), 5251–5261. <https://doi.org/10.11591/IJECE.V10I5.PP5251-5261>
- Sun, J., Chi, M., Cai, W., Gao, H., & Liang, S. (2021). An investigation into evaluation methods for ride comfort of railway vehicles in the case of carbody hunting instability. *Proceedings of the Institution of Mechanical Engineers, Part F: Journal of Rail and Rapid Transit*, 235(5), 586–597.

## REFERENCES

- <https://doi.org/10.1177/0954409720949116>
- Sun, J., Chi, M., Cai, W., & Jin, X. (2019). Numerical Investigation into the Critical Speed and Frequency of the Hunting Motion in Railway Vehicle System. *Mathematical Problems in Engineering*, 2019. <https://doi.org/10.1155/2019/7163732>
- Sun, W., Zhou, J., Gong, D., & You, T. (2016). Analysis of modal frequency optimization of railway vehicle car body. *Advances in Mechanical Engineering*, 8(4), 1–12. <https://doi.org/10.1177/1687814016643640>
- Sun, Y., & Ling, L. (2022). An optimal tangential contact model for wheel-rail non-Hertzian contact analysis and its application in railway vehicle dynamics simulation. *Vehicle System Dynamics*, 60(9), 3240–3268. <https://doi.org/10.1080/00423114.2021.1942078>
- Taghirad, H. D., & Esmailzadeh, E. (1998). Automobile passenger comfort assured through LQG/LQR active suspension. *JVC/Journal of Vibration and Control*, 4(5), 603–618. <https://doi.org/10.1177/107754639800400504>
- Tang, J. S. (1996). Passive and semi-active airspring suspensions for rail passenger vehicles - theory and practice. *Proceedings of the Institution of Mechanical Engineers, Part F: Journal of Rail and Rapid Transit*, 210(2), 103–116. [https://doi.org/10.1243/pime\\_proc\\_1996\\_210\\_333\\_02](https://doi.org/10.1243/pime_proc_1996_210_333_02)
- Tao, G., Wen, Z., Zhao, X., & Jin, X. (2016). Effects of wheel–rail contact modelling on wheel wear simulation. *Wear*, 366–367, 146–156. <https://doi.org/10.1016/j.wear.2016.05.010>
- Taylor, P., Bailey, J. R., & Hedrick, J. K. (2007). *Vehicle System Dynamics : International Journal of Vehicle Mechanics and Mobility Rail Vehicle Energy Dissipation Due to Lateral Vehicle / Track Interaction*. April 2013, 37–41.
- Taylor, P., Piotrowski, J., & Chollet, H. (n.d.). *Vehicle System Dynamics : International Journal of Vehicle Mechanics and Wheel – rail contact models for vehicle system dynamics including multi-point contact*. November 2012, 37–41.
- Taylor, P., Torstensson, P. T., & Nielsen, J. C. O. (2010). *Vehicle System Dynamics : International Journal of Vehicle Mechanics and Simulation of dynamic vehicle – track interaction on small radius curves Simulation of dynamic vehicle – track interaction*. April 2013, 37–41.
- Taylor, P., Williamson, C., Lee, S., & Ivantysynova, M. (n.d.). *International Journal of Fluid Power Active Vibration Damping for an Off-Road Vehicle with Displacement Controlled Actuators*. December 2014, 37–41. <https://doi.org/10.1080/14399776.2009.10780984>
- Theunissen, J., Tota, A., Gruber, P., Dhaens, M., & Sorniotti, A. (2021). Preview-based techniques for vehicle suspension control: a state-of-the-art review. *Annual Reviews in Control*, 51, 206–235. <https://doi.org/10.1016/j.arcontrol.2021.03.010>

## REFERENCES

- Tilahun, S. L., & Ong, H. C. (2012). Modified firefly algorithm. *Journal of Applied Mathematics*, 2012. <https://doi.org/10.1155/2012/467631>
- Tiwari, V., Sharma, S. C., & Harsha, S. P. (2023). Ride comfort analysis of high-speed rail vehicle using laminated rubber isolator based secondary suspension. *Vehicle System Dynamics*, 61(10), 2689–2715. <https://doi.org/10.1080/00423114.2022.2131584>
- Trials, O., Broad, O. F., Covered, G., Carrier, A., & Railway, N. (2013).
- Tronic, M., For, S., Speed, H., Vehicles, R., Nagyt, Z., Goodaut, R. M., & Wickens, A. H. (2000). *Mechatronic Solutions For High Speed Railway Vehicle T. X. Mei*. 265–270. [https://doi.org/10.1016/S1474-6670\(17\)39155-3](https://doi.org/10.1016/S1474-6670(17)39155-3)
- Tsai, S. J., Huo, C. L., Yang, Y. K., & Sun, T. Y. (2013). Variable feedback gain control design based on particle swarm optimizer for automatic fighter tracking problems. *Applied Soft Computing Journal*, 13(1), 58–75. <https://doi.org/10.1016/j.asoc.2012.07.032>
- Tsang, H. H., Su, R. K. L., & Chandler, A. M. (2006). Simplified inverse dynamics models for MR fluid dampers. *Engineering Structures*, 28(3), 327–341. <https://doi.org/10.1016/j.engstruct.2005.06.013>
- Tyler, J., & Tuteur, F. (1966).pp, 84–92.
- Valério, D., & da Costa, J. S. (2006). Tuning of fractional PID controllers with Ziegler-Nichols-type rules. *Signal Processing*, 86(10), 2771–2784. <https://doi.org/10.1016/j.sigpro.2006.02.020>
- Verma, S. K., Yadav, S., & Nagar, S. K. (2017). Optimization of Fractional Order PID Controller Using Grey Wolf Optimizer. *Journal of Control, Automation and Electrical Systems*, 28(3), 314–322. <https://doi.org/10.1007/s40313-017-0305-3>
- Vinodh Kumar, E., Raaja, G. S., & Jerome, J. (2016). Adaptive PSO for optimal LQR tracking control of 2 DoF laboratory helicopter. *Applied Soft Computing Journal*, 41, 77–90. <https://doi.org/10.1016/j.asoc.2015.12.023>
- Vollebregt, E. A. H. (2014). Numerical modeling of measured railway creep versus creep-force curves with CONTACT. *Wear*, 314(1–2), 87–95. <https://doi.org/10.1016/j.wear.2013.11.030>
- Volume : LXX Number :pp. 348..*
- Wahab, R., Kaushik, N. K., Verma, A. K., Mishra, A., Hwang, I. H., Yang, Y. B., Shin, H. S., & Kim, Y. S. (2011). Fabrication and growth mechanism of ZnO nanostructures and their cytotoxic effect on human brain tumor U87, cervical cancer HeLa, and normal HEK cells. *Journal of Biological Inorganic Chemistry*, 16(3), 431–442. <https://doi.org/10.1007/s00775-010-0740-0>
- Wang, D. H., & Liao, W. H. (2009a). Semi-active suspension systems for railway vehicles using magnetorheological dampers. Part I: System integration and modelling. *Vehicle System Dynamics*, 47(11), 1305–1325.



## REFERENCES

- <https://doi.org/10.1080/00423110802538328>
- Wang, D. H., & Liao, W. H. (2009b). Semi-active suspension systems for railway vehicles using magnetorheological dampers. Part II: Simulation and analysis. *Vehicle System Dynamics*, 47(12), 1439–1471. <https://doi.org/10.1080/00423110802538336>
- Wang, G., Chen, C., & Yu, S. (2016). Optimization and static output-feedback control for half-car active suspensions with constrained information. *Journal of Sound and Vibration*, 378, 1–13. <https://doi.org/10.1016/j.jsv.2016.05.033>
- Wang, P., Li, H., Zhang, J., & Mei, T. (2015). An analytical design approach for self-powered active lateral secondary suspensions for railway vehicles. *Vehicle System Dynamics*, 53(10), 1439–1454. <https://doi.org/10.1080/00423114.2015.1050964>
- Wang, Q., Zeng, J., Shi, H., & Jiang, X. (2023). Parameter optimization of multi-suspended equipment to suppress carbody vibration of high-speed railway vehicles: a comparative study. *International Journal of Rail Transportation*, 00(00), 1–20. <https://doi.org/10.1080/23248378.2023.2291202>
- Watson, M. J. (2014). *A System Engineering Approach to Electro-mechanical Actuator*. November.
- Wei, W., Li, Q., Xu, F., Zhang, X., Jin, J., Jin, J., & Sun, F. (2020). Research on an electromagnetic actuator for vibration suppression and energy regeneration. *Actuators*, 9(2). <https://doi.org/10.3390/ACT9020042>
- Wei, X., Zhu, M., & Jia, L. (2016). A semi-active control suspension system for railway vehicles with magnetorheological fluid dampers. *Vehicle System Dynamics*, 54(7), 982–1003. <https://doi.org/10.1080/00423114.2016.1177189>
- Welcome to Rail Coach Factory Kapurthala Official Website. (n.d.). Retrieved December 7, 2021, from <https://rcf.indianrailways.gov.in/index.jsp>
- Williamson, C., Lee, S., & Ivantysynova, M. (2009). Active vibration damping for an off-road vehicle with displacement controlled actuators. *International Journal of Fluid Power*, 10(3), 5–16. <https://doi.org/10.1080/14399776.2009.10780984>
- Willumeit, & Kalker, J. J. (2018). Survey of Wheel-Rail Rolling Contact Theory. *The Dynamics of Vehicles on Roads and on Tracks*, May 2013, 13–13. <https://doi.org/10.1201/9780203736845-4>
- Wilson, D. A., Sharp, R. S., & Hassan, S. A. (1986). The Application of Linear Optimal Control Theory to the Design of Active Automotive Suspensions. *Vehicle System Dynamics*, 15(2), 105–118. <https://doi.org/10.1080/00423118608968846>
- Winslow, W. (1947). Method and means for translating electrical impulses into mechanical force. *US Patent* 2,417,850, 6. <http://www.freepatentsonline.com/2417850.html>
- Wu, H., Zeng, X. H., Lai, J., & Yu, Y. (2019). Nonlinear hunting stability of high-speed railway vehicle on a curved track under steady aerodynamic load. *Vehicle System*

## REFERENCES

- Dynamics*, 0(0), 1–23. <https://doi.org/10.1080/00423114.2019.1572202>
- Wu, J. S. (2015). Analytical and Numerical Methods for Vibration Analyses. *Analytical and Numerical Methods for Vibration Analyses*, 1–706. <https://doi.org/10.1002/9781119137207>
- Wu, K., Liu, J., Li, M., Liu, J., & Wang, Y. (2021). Multi-mode active suspension control based on a genetic k-means clustering linear quadratic algorithm. *Applied Sciences (Switzerland)*, 11(21). <https://doi.org/10.3390/app112110493>
- Wu, X., & Griffin, M. J. (1997). A semi-active control policy to reduce the occurrence and severity of end-stop impacts in a suspension seat with an electrorheological fluid damper. *Journal of Sound and Vibration*, 203(5), 781–793. <https://doi.org/10.1006/jsvi.1996.0901>
- Xiao, F., & Lin, J. J. (2021). High-speed rail and high-tech industry evolution: Empirical evidence from China. *Transportation Research Interdisciplinary Perspectives*, 10(March), 100358. <https://doi.org/10.1016/j.trip.2021.100358>
- Xu, Y., Xie, Z., Zhao, J., Li, W., Li, P., & Wong, P. K. (2021). Robust non-fragile finite frequency  $H_\infty$  control for uncertain active suspension systems with time-delay using T-S fuzzy approach. *Journal of the Franklin Institute*, 358(8), 4209–4238. <https://doi.org/10.1016/j.jfranklin.2021.03.019>
- Yadav, S., Verma, S. K., & Nagar, S. K. (2016). Optimized PID controller for magnetic levitation system. *IFAC-PapersOnLine*, 49(1), 778–782. <https://doi.org/10.1016/j.ifacol.2016.03.151>
- Yamashita, M. (1994). *Application of Control to Active Suspension Systems* 30(11), 1717–1729.
- Yan, Z., Li, G., Luo, J., Zeng, J., Zhang, W., Wang, Y., Yang, W., & Ma, G. (2022). Vibration control of superconducting electro-dynamic suspension train with electromagnetic and sky-hook damping methods. *Vehicle System Dynamics*, 60(10), 3375–3397. <https://doi.org/10.1080/00423114.2021.1948080>
- Yang, X. S., & Deb, S. (2009). Cuckoo search via Lévy flights. *2009 World Congress on Nature and Biologically Inspired Computing, NABIC 2009 - Proceedings*, 210–214. <https://doi.org/10.1109/NABIC.2009.5393690>
- Yang, Y., Wang, G., Tiwari, P., Pandey, H. M., & Lei, Z. (2021). Pixel and Feature Transfer Fusion for Unsupervised Cross-Dataset Person Reidentification. *IEEE Transactions on Neural Networks and Learning Systems*, PP, 1–13. <https://doi.org/10.1109/TNNLS.2021.3128269>
- Yang, Z., Chen, Y., Tang, Z., & Zhang, N. (2013). A subjective evaluation system for high-speed trains ride comfort. *Proceedings - 6th International Symposium on Computational Intelligence and Design, ISCID 2013*, 2, 88–91. <https://doi.org/10.1109/ISCID.2013.136>
- Yang, Z., Li, Z., & Dollevoet, R. (2016). Modelling of non-steady-state transition from

## REFERENCES

- single-point to two-point rolling contact. *Tribology International*, 101, 152–163. <https://doi.org/10.1016/j.triboint.2016.04.023>
- Yao, Y., Wu, G., Sardahi, Y., & Sun, J. Q. (2018). Hunting stability analysis of high-speed train bogie under the frame lateral vibration active control. *Vehicle System Dynamics*, 56(2), 297–318. <https://doi.org/10.1080/00423114.2017.1375128>
- Yi-Xuan, W., En-Li, C., Peng-Fei, L., Zhuang, Q., & Lin, Z. (2018). A simplification of railway vehicle lateral vibration model based on LQG control strategy. *Australian Journal of Mechanical Engineering*, 16(2), 147–161. <https://doi.org/10.1080/14484846.2018.1486793>
- Yin, Y., Luo, B., Ren, H., Fang, Q., & Zhang, C. (2022). Robust control design for active suspension system with uncertain dynamics and actuator time delay. 36(12), 6319–6327. <https://doi.org/10.1007/s12206-022-1143-1>
- Yoshimura, T., Edokoro, K., & Ananthanarayana, N. (1993). An active suspension model for rail/vehicle systems with preview and stochastic optimal control. In *Journal of Sound and Vibration* (Vol. 166, Issue 3, pp. 507–519). <https://doi.org/10.1006/jsvi.1993.1309>
- Yu, M., Evangelou, S., & Dini, D. (2023). Advances in Active Suspension Systems for Road Vehicles. *ENGINEERING*. <https://doi.org/10.1016/j.eng.2023.06.014>
- Yu, X., Liu, X., Wang, X., Wang, X., & Wang, Y. (2021). Vibration control of improved LQG for wheel drive electric vehicle based on uncertain parameters. *Proceedings of the Institution of Mechanical Engineers, Part D: Journal of Automobile Engineering*, 235(8), 2253–2264. <https://doi.org/10.1177/0954407020983150>
- Zaazaa, K. E., & Schwab, A. L. (2016). DETC-87655. pp. 1–12.
- Zboinski, K., & Dusza, M. (2017). Bifurcation analysis of 4-axle rail vehicle models in a curved track. *Nonlinear Dynamics*, 89(2), 863–885. <https://doi.org/10.1007/s11071-017-3489-y>
- Zeng, Y. C., Zhang, W. H., & Song, D. L. (2022). Lateral-vertical coupled active suspension on railway vehicle and optimal control methods. *Vehicle System Dynamics*, 60(1), 258–280. <https://doi.org/10.1080/00423114.2020.1814358>
- Zhai, W. (n.d.). *Vehicle – Track Coupled Dynamics*.
- Zhai, W., & Sun, X. (1994). A Detailed Model for Investigating Vertical Interaction between Railway Vehicle and Track. *Vehicle System Dynamics*, 23(sup1), 603–615. <https://doi.org/10.1080/00423119308969544>
- Zhai, W., & Sun, X. (2008). *Vehicle System Dynamics : International Journal of Vehicle Mechanics and Mobility A Detailed Model for Investigating Vertical Interaction between Railway Vehicle and Track*. March 2013, 37–41.
- Zhang, C., Kordestani, H., & Shadabfar, M. (2023). A combined review of vibration control strategies for high-speed trains and railway infrastructures: Challenges and solutions. *Journal of Low Frequency Noise Vibration and Active Control*, 42(1),

## REFERENCES

- 272–291. <https://doi.org/10.1177/14613484221128682>
- Zhang, C. W., Ou, J. P., & Zhang, J. Q. (2006). Parameter optimization and analysis of a vehicle suspension system controlled by magnetorheological fluid dampers. *Structural Control and Health Monitoring*, 13(5), 885–896. <https://doi.org/10.1002/stc.63>
- Zhang, S., Cheng, G., Sheng, X., & Thompson, D. J. (2020). Dynamic wheel-rail interaction at high speed based on time-domain moving Green's functions. *Journal of Sound and Vibration*, 488. <https://doi.org/10.1016/j.jsv.2020.115632>
- Zheng, X., Zolotas, A., & Goodall, R. (2020a). Combined active suspension and structural damping control for suppression of flexible bodied railway vehicle vibration. 3114. <https://doi.org/10.1080/00423114.2019.1572902>
- Zheng, X., Zolotas, A., & Goodall, R. (2020b). Combined active suspension and structural damping control for suppression of flexible bodied railway vehicle vibration. *Vehicle System Dynamics*, 58(2), 198–228. <https://doi.org/10.1080/00423114.2019.1572902>
- Zhou, R., Zolotas, A., & Goodall, R. (2014). Robust system state estimation for active suspension control in high-speed tilting trains. *Vehicle System Dynamics*, 52(SUPPL. 1), 355–369. <https://doi.org/10.1080/00423114.2014.901540>
- Zhu, Q., Ding, J. J., & Yang, M. L. (2018). LQG control based lateral active secondary and primary suspensions of high-speed train for ride quality and hunting stability. *IET Control Theory and Applications*, 12(10). <https://doi.org/10.1049/iet-cta.2017.0529>
- Zhu, Q., Li, L., Chen, C. J., Liu, C. Z., & Hu, G. Di. (2018). A Low-Cost Lateral Active Suspension System of the High-Speed Train for Ride Quality Based on the Resonant Control Method. *IEEE Transactions on Industrial Electronics*, 65(5), 4187–4196. <https://doi.org/10.1109/TIE.2017.2767547>
- Zhu, T., Wang, X. rui, Fan, Y. wei, Wang, M. meng, Zhang, J. ke, Xiao, S. ne, Yang, G. wu, & Yang, B. (2022). A time domain method for wheel-rail force identification of rail vehicles. *Vehicle System Dynamics*, 60(3), 790–809. <https://doi.org/10.1080/00423114.2020.1838562>
- Zong, L. H., Gong, X. L., Xuan, S. H., & Guo, C. Y. (2013). Semi-active  $H_{\infty}$  control of high-speed railway vehicle suspension with magnetorheological dampers. *Vehicle System Dynamics*, 51(5), 600–626. <https://doi.org/10.1080/00423114.2012.758858>

Parameters of railway vehicle and track

Symbols	Values	Symbols	Values
$M_c$	32,000 kg	$C_{2y}$	$5.2 \times 10^4$ N.s/m
$J_{cx}$	$7.50 \times 10^4$ kg.m <sup>2</sup>	$C_{2z}$	$1.6 \times 10^4$ N.s/m
$J_{cy}$	$2.48 \times 10^6$ kg.m <sup>2</sup>	$C_{1y}$	0
$J_{cz}$	$2.24 \times 10^6$ kg.m <sup>2</sup>	$C_{1z}$	$3 \times 10^4$ N.s/m
$M_t$	3296 kg	$h_3$	0.78 m
$J_{tx}$	1900 kg.m <sup>2</sup>	$h_2$	0.22 m
$J_{ty}$	2100 kg.m <sup>2</sup>	$h_1$	-0.2085 m
$J_{tz}$	2200 kg.m <sup>2</sup>	$l_b$	9 m
$M_w$	1750 kg	$l_d$	1.28 m
$J_{wz}$	1400 kg.m <sup>2</sup>	$\lambda_e$	0.05 m
$W$	$1.117 \times 10^5$ N	$\sigma$	0.05
$K_{2x}$	$3.4 \times 10^5$ N/m	$a$	0.8751m
$K_{2y}$	$3.5 \times 10^5$ N/m	$b_1$	1 m
$K_{2z}$	$6.8 \times 10^5$ N/m	$b_2$	1 m
$K_{1x}$	$2.90 \times 10^7$ N/m	$d_p$	1 m
$K_{1y}$	$1.50 \times 10^7$ N/m	$d_s$	1 m
$K_{1z}$	$1.33 \times 10^6$ N/m	$R_1$	0.4575 m
$K_{Gz}$	$1.25 \times 10^5$ N/m	$V$	55.55 m/s
$K_{Gy}$	$7.5 \times 10^3$ N/m	$f_{11}$	$1.12 \times 10^7$
$C_{2x}$	$4.5 \times 10^5$ N.s/m	$f_{22}$	$9.98 \times 10^6$
$\Omega_c$	0.8246 rad/m	$A_v$	$1.08 \times 10^{-6}$ m <sup>2</sup> .m/rad
$\Omega_s$	0.438 rad/m	$A_a$	$6.125 \times 10^{-7}$ m <sup>2</sup> .m/ rad

Roughness coefficients and cut-off frequencies for German track irregularities PSDs

Track class	$\Omega_c$ (rad/m)	$\Omega_c$ (rad/m)	$\Omega_c$ (rad/m)	$A_a$ ( m <sup>2</sup> . rad/m)	$A_v$ ( m <sup>2</sup> . rad/m)
Low	0.8246	0.0206	0.4380	$2.119 \times 10^{-7}$	$4.032 \times 10^{-7}$

## APPENDIX 1

Ride evaluation scale

Ride index ( $W_z$ )	Comfort (vibration sensitivity)
1	Just noticeable
2	Noticeable
2.5	More pronounced but not unpleasant
3	Strong, irregular, but still tolerable
3.25	Very irregular
3.5	Extremely irregular, unpleasant, annoying; prolonged exposure intolerable
4	Extremely unpleasant; prolonged exposure intolerable

Parameters of electro-hydraulic actuator

Symbols	Values
$m_s$	0.075 Kg
$k_s$	185000 N/m
$c_s$	471 Ns/m
$k_i$	142 Nm/A
$p_s$	$2 \times 10^7 \text{ N/m}^2$
$\frac{dq_a}{dx_v}$	0.00935
$\frac{dq_b}{dx_v}$	0.01218
$\frac{dq_a}{dp_a}$	$2.022 \times 10^{-12}$
$\frac{dq_b}{dp_b}$	$-1.9232 \times 10^{-12}$
$\beta$	$1.38 \times 10^9$
$V_a$	$5.063 \times 10^{-6} \text{ m}^3$
$V_b$	$9.093 \times 10^{-4} \text{ m}^3$
$a_a$	$2.25 \times 10^{-4} \text{ m}^2$
$a_b$	$4.02 \times 10^{-4} \text{ m}^2$
$c_d$	$1.20 \times 10^3 \text{ Ns/m}$

## Pseudo-code of PSO and GWO for tuning of FOPID controller

PSO	GWO
<p>Define objective function <math>J(x_1, x_2) = \int w_1 \cdot x_1 + w_2 \cdot x_2</math> //using Eqn.(32)</p> <p>Set known parameters of railway vehicle// <i>Appendix 1</i></p> <p>Parameter setting</p> <p>Lower Bound &amp; Upper Bound</p> <p><math>[K_P, K_I, K_D] = [10 - 10^5]</math></p> <p><math>[\lambda, \mu] = [0 - 2]</math></p> <p>Population size (<math>N=100</math>)</p> <p>Inertial weight, <math>w</math>, (<math>w_{max} = 0.9</math> and, <math>w_{min} = 0.4</math>)</p> <p>Acceleration factors (<math>c_1</math> and, <math>c_2 = 2</math>)</p> <p>Maximum iteration (<math>T=100</math>)</p> <p>Initialization</p> <p>Generate <math>N</math> particles with random velocities(<math>v_i</math>) and particles(<math>z_i</math>)</p> <p>Calculate the fitness of each particle in the swarm</p> <p>Set iteration = 0</p> <p>Update the <math>pBest</math> and <math>gBest</math> values</p> <p>Update the position and velocity of each particle</p> <p>Set iteration=1</p> <p>While <math>t &lt; T</math></p> <p><math>w = w_{max} - [(w_{max} - w_{min}) \frac{iteration}{T}]</math></p> <p>for <math>i = 1:N</math></p> <p>Calculate the fitness value <math>f_{i,j}^k</math></p> <p>Update the velocity and position</p> $v_{i,j}^{k+1} = w \cdot v_{i,j}^k + c_1 r_1 (pBest_{i,j}^k - z_{i,j}^k) + c_2 r_1 (gBest_{i,j}^k - z_{i,j}^k)$ $z_{i,j}^{k+1} = z_{i,j}^k + v_{i,j}^k$ <p>Calculate the fitness <math>F_i^{k+1} = J(z_i^{k+1})</math>, find the index of best particle</p> <p>end for</p> <p>If the fitness increases then update the <math>pBest</math> and <math>gBest</math> value</p> <p>end while</p>	<p>Define objective function <math>J(x_1, x_2) = \int w_1 \cdot x_1 + w_2 \cdot x_2</math> //using Eqn.(32)</p> <p>Set known parameters of railway vehicle// <i>Appendix 1</i></p> <p>Parameter setting</p> <p>Lower Bound &amp; Upper Bound</p> <p><math>[K_P, K_I, K_D] = [10 - 10^5]</math></p> <p><math>[\lambda, \mu] = [0 - 2]</math></p> <p>Population size (<math>N=100</math>)</p> <p>Maximum iteration (<math>T=100</math>)</p> <p>Initialization</p> <p>Randomly initialize Grey wolf population <math>P</math></p> <p>Initialize <math>a</math>, <math>A</math> and <math>C</math></p> <p><math>a</math> linearly decreasing from 2 to 0</p> <p><math>A = 2ar_1 - a</math>, <math>C = 2r_2</math> // <math>r_1</math> and <math>r_2</math> are random vectors <math>[0, 1]</math></p> <p>Calculate the fitness of each search agent</p> <p><math>X_\alpha</math> = Best search agent</p> <p><math>X_\beta</math> = Second Best search agent</p> <p><math>X_\delta</math> = Third Best search agent</p> <p>While <math>t &lt; T</math></p> <p>for <math>i = 1:N</math></p> <p>Update the distance and position of each search agent</p> $Dist =  C \cdot X_p(t) - X(t) , X_i$ $= X_p(t) - A \cdot Dist, p$ $= \alpha, \beta, \delta \text{ and } i = 1, 2, 3$ $X(t+1) = \frac{X_1 + X_2 + X_3}{3}$ <p>end for</p> <p>Update <math>a</math>, <math>A</math> and <math>C</math></p> <p>Calculate the fitness value <math>f</math></p> <p>Update <math>X_\alpha</math>, <math>X_\beta</math>, and <math>X_\delta</math></p> <p><math>t = t + 1</math></p> <p>end while</p> <p>Display the optimum solution</p>

Display the optimum solution <i>Guest</i>	
<b>Pseudo-code of PSO and EO for tuning of LQG controller</b>	
<b>PSO</b>	<b>EO</b>
<p>Define the objective function  Set known parameters of railway vehicle//  <i>Appendix 1</i>  Set the parameters of algorithms  Fix the lower and upper Bound  <math>[Q]=[0 - 1000]</math>, <math>[R]=[0-0.01]</math>, <math>[S]=0</math>  Set the size of population (<math>N=100</math>)  Set the inertial weight, <math>w</math>, (<math>w_{max} = 0.9</math> and, <math>w_{min} = 0.4</math>)  Fix the acceleration factors (<math>c_1</math> and, <math>c_2 = 2</math>)  Se the maximum no. of iterations (<math>T=100</math>)  Initialization phase  Generate the <math>N</math> particles with random velocities(<math>v_i</math>) and particles(<math>z_i</math>)  Then, calculate the fitness of each particle in the swarm  Set iteration = 0  Update the <math>pBest</math> and <math>gBest</math> values  Update the position and velocity of each particle  Set iteration=1</p> <p><b>while</b> <math>t &lt; T</math>  <math>w = w_{max} - [(w_{max} - w_{min}) \frac{iteration}{T}]</math>  <b>for</b> <math>i = 1:N</math>  Calculate the fitness value <math>f_{i,j}^k</math>  Update the velocity and position  <math display="block">v_{i,j}^{k+1} = w \cdot v_{i,j}^k + c_1 r_1 (pBest_{i,j}^k - z_{i,j}^k) + c_2 r_2 (gBest_{i,j}^k - z_{i,j}^k)</math> <math display="block">z_{i,j}^{k+1} = z_{i,j}^k + v_{i,j}^{k+1}</math> Calculate the fitness <math>F_i^{k+1} = J(z_i^{k+1})</math>, find the index of best particle  <b>end for</b>  If the fitness increases then update the <math>pBest</math> and <math>gBest</math> value  <b>end while</b>  Display the optimum solution <i>Guest</i></p>	<p>Define the objective function  Set known parameters of railway vehicle//  <i>Appendix 1</i>  Set the parameters of algorithms  Fix the lower and upper Bound  <math>[Q]=[0 - 1000]</math>, <math>[R]=[0-0.01]</math>, <math>[S]=0</math>  Initialize the particle's populations (<math>i = 1</math> to <math>n</math>)  Assign equilibrium candidates' fitness a large number  Assign free parameters <math>a_1 = 0.9</math>; <math>a_2 = 0.4</math>; <math>GP = 0.5</math>  <b>While</b> <math>iter &lt; Max\_iter</math>  <b>for</b> <math>t=1: no. of particle (n)</math>  Calculate fitness of <math>i^{th}</math> particle  <b>if</b> <math>fit(\vec{C}_i) &lt; fit(\vec{C}_{eq1})</math>  Replace <math>\vec{C}_{eq1}</math> with <math>\vec{C}_i</math> and <math>fit(\vec{C}_{eq1})</math> with <math>fit(\vec{C}_i)</math>  <b>Else if</b> <math>fit(\vec{C}_i) &gt; fit(\vec{C}_{eq1})</math> &amp; <math>fit(\vec{C}_i) &lt; fit(\vec{C}_{eq2})</math>  Replace <math>\vec{C}_{eq2}</math> with <math>\vec{C}_i</math> and <math>fit(\vec{C}_{eq2})</math> with <math>fit(\vec{C}_i)</math>  <b>Else if</b> <math>fit(\vec{C}_i) &gt; fit(\vec{C}_{eq1})</math> &amp; <math>fit(\vec{C}_i) &gt; fit(\vec{C}_{eq2})</math> &amp; <math>fit(\vec{C}_i) &lt; fit(\vec{C}_{eq3})</math>  Replace <math>\vec{C}_{eq3}</math> with <math>\vec{C}_i</math> and <math>fit(\vec{C}_{eq3})</math> with <math>fit(\vec{C}_i)</math>  <b>Else if</b> <math>fit(\vec{C}_i) &gt; fit(\vec{C}_{eq1})</math> &amp; <math>fit(\vec{C}_i) &gt; fit(\vec{C}_{eq2})</math> &amp; <math>fit(\vec{C}_i) &lt; fit(\vec{C}_{eq3})</math> &amp; <math>fit(\vec{C}_i) &lt; fit(\vec{C}_{eq4})</math>  Replace <math>\vec{C}_{eq4}</math> with <math>\vec{C}_i</math> and <math>fit(\vec{C}_{eq4})</math> with <math>fit(\vec{C}_i)</math>  <b>End (if)</b>  <b>End (for)</b>  <math display="block">C_{avg} = \frac{(C_{eq1} + C_{eq2} + C_{eq3} + C_{eq4})}{4}</math></p>



	<p>Construct the equilibrium pool</p> $C_{avg} = \{ \vec{C}_{eq\ 1}, \vec{C}_{eq\ 2}, \vec{C}_{eq\ 3}, \vec{C}_{eq\ 4}, \vec{C}_{eq\ (avg)} \}$ <p>Accomplish memory saving (<i>if iter &gt; I</i>)</p> <p>Assign <math>t = (1 - \frac{iter}{Max\_iter})^{a_2 \frac{iter}{Max\_iter}}</math></p> <p><b>For <math>i = no. of particle (n)</math></b></p> <p>Randomly choose one candidate from the equilibrium pool (vector)</p> <p>Generate random vectors of <math>\vec{\lambda}, \vec{r}</math> from Eqn. (1b)</p> <p>Construct <math>\vec{F} = a_1 sign(\vec{r} - 0.5)[e^{-\vec{\lambda}t} - 1]</math> (1b)</p> <p>Construct <math>\overrightarrow{GCP} = \begin{cases} 0.5 r_1 &amp; r_2 \geq GP \\ 0 &amp; r_2 &lt; GP \end{cases}</math></p> <p>Construct <math>\vec{G}_o = \overrightarrow{GCP}(\vec{C}_{eq} - \vec{\lambda} \vec{C})</math></p> <p>Construct <math>\vec{G} = \vec{G}_o \cdot \vec{F}</math></p> <p>Update concentration <math>\vec{F} = \vec{C}_{eq} + (\vec{C} - \vec{C}_{eq}) \cdot F + \frac{\vec{G}}{\vec{\lambda}V} (1 - \vec{F})]</math></p> <p><b>End (For)</b></p> <p><b>Iter = iter + 1</b></p> <p><b>End while</b></p>
--	--

# Nitish part 1

## ORIGINALITY REPORT

17%

SIMILARITY INDEX

12%

INTERNET SOURCES

16%

PUBLICATIONS

%

STUDENT PAPERS

## PRIMARY SOURCES

1	www.researchgate.net Internet Source	2%
2	www.cse.dmu.ac.uk Internet Source	1%
3	link.springer.com Internet Source	1%
4	usir.salford.ac.uk Internet Source	1%
5	www.tandfonline.com Internet Source	1%
6	"Advances in Dynamics of Vehicles on Roads and Tracks", Springer Science and Business Media LLC, 2020 Publication	1%
7	Stephen Bassi Joseph, Emmanuel Gbenga Dada, Afeez Abidemi, David Opeoluwa Oyewola, Ban Mohammed Khammas. "Metaheuristic Algorithms for PID Controller Parameters Tuning: Review, Approaches and Open Problems", Heliyon, 2022	<1%

Nitish

AK Singh

# Thesis second part updated

## ORIGINALITY REPORT

10%

SIMILARITY INDEX

3%

INTERNET SOURCES

9%

PUBLICATIONS

1%

STUDENT PAPERS

## PRIMARY SOURCES

- 1

Lu-Hang Zong, Xing-Long Gong, Shou-Hu Xuan, Chao-Yang Guo. "Semi-active  $H^\infty$  control of high-speed railway vehicle suspension with magnetorheological dampers", Vehicle System Dynamics, 2013  
Publication

1%
- 2

D. H. Wang, W. H. Liao. "Semi-active suspension systems for railway vehicles using magnetorheological dampers. Part II: simulation and analysis", Vehicle System Dynamics, 2009  
Publication

1%
- 3

Wang, Dai-Hua, and Wei-Hsin Liao. "", Smart Structures and Materials 2003 Smart Structures and Integrated Systems, 2003.  
Publication

<1%
- 4

[www.uodiyala.edu.iq](http://www.uodiyala.edu.iq)  
Internet Source

<1%
- 5

P. Shambhu Prasad, Aivelu M. Parimi, L. Renuka. "Control of hybrid AC/DC microgrids", Elsevier BV, 2022

<1%

with

Abdullah